



**Politecnico
di Torino**



**UNIVERSITÀ
DI TORINO**

Doctoral Dissertation
PhD Program in Bioengineering and Medical-surgical Sciences
(35th Cycle)

A wearable multi-sensor array for the home prevention of acute heart failure

From conceptualization to pre-clinical validation

By

Noemi Giordano

Supervisors:

Prof. Marco Knaflitz, Supervisor
Prof. Gabriella Balestra, Co-Supervisor

Doctoral Examination Committee:

Prof. Laura Burattini, Referee, Università Politecnica delle Marche
Prof. Samuel Emil Schmidt, Referee, Aalborg University
Prof. Francesco Renna, University of Porto

Politecnico di Torino
2023

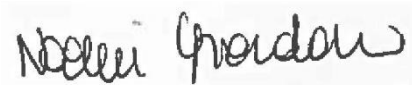
Declaration

This thesis is licensed under a Creative Commons License, Attribution - Noncommercial - No Derivative Works 4.0 International: see www.creativecommons.org. The text may be reproduced for non-commercial purposes, provided that credit is given to the original author.

I hereby declare that the contents and organization of this dissertation constitute my own original work and does not compromise in any way the rights of third parties, including those relating to the security of personal data.

Noemi Giordano

7th September 2023

A handwritten signature in black ink that reads "Noemi Giordano". The signature is written in a cursive style and is placed on a light gray rectangular background.

Acknowledgements

The three years resulting in this Doctoral Dissertation were, at the same time, inspiring, tough, satisfying, stressful, cheerful, insightful. They were full, and deep. Nothing would have been the same without sharing them.

I thank my Supervisors, Prof. Marco Knaflitz and Prof. Gabriella Balestra, who provided me with insightful guidance, passionate support, and generously shared their skills and knowledge with me while letting me develop my own research path.

I thank my fellow researchers at the Biolab laboratory, who shared this path with me at a close distance and witnessed the best and the worst of it, always helping me to dream big but also keep my feet rooted to the ground. More than colleagues!

I thank Prof. Samuel Emil Schmidt and the whole CardioTech group at Aalborg University, who warmly welcomed me in Denmark and gifted me with great skills and the opportunity of sharing their own research world.

I thank my friends outside the Politecnico di Torino, who always immensely valued my work but, at the same time, offered me the best opportunities to recharge my batteries and enjoy life outside of the lab.

I thank my family, who cheered up for my smallest success and suffered with me when things were tougher. And who love me unconditionally and always offer me a safe comfort zone where to find joy and appreciation.

I thank everyone who gifted me with a moment of share, of joy, of laugh, of talk, of emotion. You need a village to survive a PhD, and I have the best.

Abstract

The home monitoring of patients affected by chronic heart failure (CHF) is of key importance to prevent acute episodes, the main contributors to hospitalization and mortality. The most effective biomarker in this sense is the intracardiac pressure, whose changes start weeks before the acute episode occurs. Nevertheless, no wearable technological solution currently exists to monitor them. A possibility could be offered by Cardiac Time Intervals (CTIs), which provide a temporal description of the phases of the cardiac cycle from an electro-mechanical perspective and can be extracted from simultaneous recordings of electrocardiography (ECG) and of phonocardiography (PCG). In fact, PCG is the digital recording of the heart sounds, that are generated by the closure of the four cardiac valves. This approach offers many benefits in terms of applicability to homecare: low cost, portability, noninvasivity. Nevertheless, the applicability of PCG in home care is limited at this time by the need for an expert examiner: the recording of a good-quality PCG signal requires an accurate positioning of the stethoscope over the chest, which is unfeasible for a naïve user as the patient or a caregiver.

The goal of this work is to propose a wearable multi-sensor array to enable the noninvasive monitoring of the time of closure of the cardiac valves in a domicile context by naïve users. The design of the system spans from its conceptualization to the design of the hardware and mechanical aspects of the device, to the design and implementation of the signal processing algorithms to extract the clinical features of interest, to the pre-clinical validation.

The multi-sensor array was designed in the form of a flexible pad consisting of a flexible PCB mounting the sensors and a 3D-printed biocompatible case. The

sensors consist of 48 microphones, distributed over the pad with a high spatial resolution, 3 electrodes to record an ECG in a nonstandard precordial lead, and a Magneto-Inertial Measurement Unit (MIMU) to detect motion and posture. The array was designed to cover the left hemithorax of the subject: in this way, the problem of finding the best auscultation area for the specific valve is shifted from the recording phase, when the user is in charge for, to the processing phase.

The proposed signal processing pipeline includes four main steps. First, an algorithm for the estimation of the time of closure of the four cardiac valves based on the Shannon Energy envelope of the heart sounds was designed. Second, the automated assessment of the quality of the PCG signals was carried out and thresholds were determined depending on the acceptable error on the estimate. Third, a method to divide the multiple available channels into consistent groups representing potential auscultation areas was proposed. And fourth, the automatic selection of the best auscultation area was investigated, testing multiple criteria and their combination.

In the end, two distinct pre-clinical validation studies were carried out. On one side, the physiological hypothesis of the project, i.e., that changes in the intracardiac pressures reflect in changes of the timing of heart sounds, was validated on a porcine model. Preliminary results show that a positive correlation exists between the split of the second heart sound and the pressure in the pulmonary artery and open to novel possibilities of analysis on the effect of different physiological variables on the timing of heart sounds. On the other side, the technical hypothesis of the project, i.e., that multi-source PCG enables inexperienced users to record heart sounds in a domiciliary setting, was validated on a population of 42 healthy volunteers. Extremely promising results were obtained concerning the usability of the device by inexperienced users, regardless of their anatomical characteristics. A consistent comparison between the CTIs estimated using the proposed multi-sensor array positioned by naïve users and the CTIs estimated using a traditional single-

source system located by an expert user suggests that the primary goal of the project was fulfilled.

In the overall, this work shows the benefits of the use of multi-source PCG not only to enable inexperienced users to record heart sounds without the help of clinical staff, but also to gain access to a novel insight into the hemodynamic behavior of the heart. The presented multi-sensor array is expected to find a straightforward clinical application in the near future and to move a step further towards the noninvasive monitoring of patients affected by HF to prevent acute episodes.

Contents

1. Introduction.....	1
1.1 An innovative solution to an established clinical problem.....	1
1.2 Goal of the project	2
1.3 Structure of the thesis	3
2. Clinical and Technical Background.....	5
2.1 The clinical problem: Acute Heart Failure	5
2.1.1 Brief pathophysiology of heart failure	5
2.1.2 Management of heart failure in the clinical practice	8
2.1.3 Heart failure in numbers	11
2.1.4 Importance of the prevention of acute episodes	13
2.2 Monitoring of heart failure patients: state of the art.....	15
2.2.1 Current clinical guidelines for the follow-up of HF patients.....	15
2.2.2 Literature review	17
2.2.3 Technological benchmark.....	26
2.3 The promise of electro-phonocardiography	28
2.3.1 The Cardiac Time Intervals and how to find them	29
2.3.2 Cardiac Time Intervals and Heart Failure.....	37
2.3.3 The perks of multi-source Phonocardiography.....	43
3. Design of the multi-sensor array.....	47
3.1 Conceptualization of the array.....	47
3.2 Electronic design	53
3.2.1 PCG sensing.....	56
3.2.2 ECG sensing	60
3.2.3 Management of the signal recording	65

3.2.4 Implementation: realization of the Printed Circuit Boards	67
3.3 Mechanical design	70
3.3.1 Dimensions, shape and distribution of the sensors	71
3.3.2 Design of the case	73
3.4 Testing of the complete system	75
3.4.1 Complete system and setup.....	76
4. Algorithms for Signal Processing	79
4.1 Introduction	79
4.2 Estimation of the time of closure of the cardiac valves.....	80
4.3 Assessment of the quality of PCG signals.....	88
4.3.1 Materials and methods	90
4.3.2 Experimental results	96
4.3.3 Discussion	100
4.4 Spatial clustering of the signals	102
4.4.1 Materials and methods	104
4.4.2 Experimental results	109
4.4.3 Discussion	112
4.5 Automatic identification of the best auscultation area	113
4.5.1 Materials and methods	115
4.5.2 Experimental results	117
4.5.3 Discussion	120
4.6 Signal selection or signal combination?	122
5. Pre-clinical validation	127
5.1 Introduction	127
5.2 Validation on animal model	128
5.2.1 Motivation for the animal model	129
5.2.2 Experimental protocol.....	130
5.2.3 Sample population and efficacy of the model	133

5.2.4 Correlation between S2 split and PAP.....	135
5.3 Validation on healthy subjects.....	142
5.3.1 Experimental protocol.....	143
5.3.2 Validation of usability	146
5.3.3 Validation against single-source PCG	155
5.3.4 Final remarks	165
6. Conclusions.....	167
6.1 Resume of the project	167
6.2 Take-home messages	168
6.3 Limitations of the work	169
6.4 Future developments	170
7. List of publications	173
List of Publications.....	173
8. References.....	177
References	177

List of Abbreviations

The following abbreviations are used in the manuscript:

A2	Aortic component of the second heart sound
ACC	American College of Cardiology
ADC	Analog-to-Digital Amplifier
AGC	Automatic gain control
AIMD	Active implantable medical device
AHA	American Heart Association
AHF	Acute heart failure
ANOVA	Analysis of Variance
BMI	Body Mass Index
BNP	B-type natriuretic peptide
BSS	Blind Source Separation
CHF	Chronic heart failure
CTI	Cardiac Time Interval
CVD	Cardiovascular disease
DBP	Diastolic blood pressure
DistInter	Inter-cluster distance
DRL	Driven Right Leg
ECG	Electrocardiography
ECM	Electret condenser microphone
EF	Ejection Fraction
EMAT	Electro-mechanical activation time
ESC	European Society of Cardiology
FIR	Finite Impulse Response
HF	Heart failure
HFmrEF	Heart failure with mid-range Ejection Fraction
HFpEF	Heart failure with preserved Ejection Fraction
HFrEF	Heart failure with reduced Ejection Fraction
HR	Heart rate
HRV	Heart rate variability
ICA	Independent Component Analysis
ICG	Impedance cardiography
IIR	Infinite Impulse Response
IVCP	Isovolumic Contraction Period
JADE	Joint Approximation of Diagonalization of Eigenmatrices
LA	Left atrium
LAP	Left atrium pressure
LV	Left ventricle

LVEF	Left ventricular Ejection Fraction
LVET	Left ventricular ejection time
LVST	Left ventricular systolic time
MCDA	Multi-criteria Decision Analysis
MEMS	Micro-electro-mechanical system
MIMU	Magneto-inertial measurement unit
ML	Machine Learning
NRMSE	Normalized root-mean-square error
NP	Natriuretic peptide
NT-proBNP	N-terminal pro-B-type natriuretic peptide
NYHA	New York Heart Association
P2	Pulmonary component of the second heart sound
PA	Pulmonary artery
PAP	Pulmonary artery pressure
PCB	Printed circuit board
PCG	Phonocardiography
PEP	Pre-ejection period
PH	Pulmonary hypertension
QS2	Total electromechanical systole
R-S _{1,M}	Delay between the R-wave and the mitral component in S1
R-S _{1,T}	Delay between the R-wave and the tricuspid component in S1
R-S _{2,A}	Delay between the R-wave and the aortic component in S2
R-S _{2,P}	Delay between the R-wave and the pulmonary component in S2
RA	Right atrium
RCT	Randomized Clinical Trial
RI	Rand Index
RV	Right ventricle
RVP	Right ventricular pressure
S1	First heart sound
S2	Second heart sound
S3	Third heart sound
S4	Fourth heart sound
SBP	Systolic blood pressure
SC	Silhouette coefficient
SCG	Seismocardiography
SE	Shannon energy
SNR	Signal-to-noise ratio
SpO2	Blood oxygen saturation
TST	Total systolic time
VarIntra	Intra-cluster variability
VGA	Variable gain amplifier

List of Figures

Figure 1: The two major classification systems for HF, namely ACC/AHA based on the progression of the disease and the NYHA, based on the disability caused by the symptoms [5,6].....	6
Figure 2: Effect of the acute episodes of HF on the deterioration of the myocardial function. From [7].....	8
Figure 3: Diagnostic algorithm for HF proposed by the ESC and accepted by the main clinical guidelines worldwide [2]. At date, the HF diagnosis is mainly based on BNP and echocardiography.	9
Figure 4: Phases of the process of decompensation in AHF. Adapted from [32]	14
Figure 5: Main existing approaches for HF monitoring and phase of the decompensation process where they act. Partially adapted from [32].....	18
Figure 6: Technological benchmark, along with commercially available and under development devices.....	27
Figure 7: Visual definition of the main Cardiac Time Intervals, in relation to the LV intracardiac pressures and to the main biomedical signals used for their estimation (ECG and heart sounds), in a modified version of the Wiggers diagram. M_C represents the instant of closure of the mitral valve, A_O and A_C represent respectively the opening and closure of the aortic valve. Adapted from [93,94]. .	30
Figure 8: Representation of a typical PCG signal and the main heart sounds [97].....	33
Figure 9: Definition of the fiducial points of the SCG signal according to Sørensen et al. [99].	34
Figure 10: Definition of the fiducial points of the ICG signal [103].	36
Figure 11: Differences in the CTIs due to the presence of Systolic Heart Failure with respect to a normal subject. The same definitions as in Figure 7 apply. Adapted from [93,94].	40
Figure 12: Visual representation of the variability of the quality of signal and of the latency of the closure of the mitral valve with respect to the ventricular depolarization. Each circle represents a microphone. The diameter of the colored	

circle represents the Signal-to-Noise Ratio of the signal recorded from that point of the chest. The color represents the estimated latency according to the colorbar on the right.....	44
Figure 13: Correlation between the traditional auscultation areas (panel A) and the design of shape of the array (panel B).	49
Figure 14: Distribution of the microphone sensors over the surface of the array, in two options: A) homogenously distributed; B) higher concentration over the traditional auscultation area.	50
Figure 15: Comparison between the anatomical position of the heart (panel A) and the positioning of the electrodes in the designed device (panel B).....	51
Figure 16: Graphical representation of the multi-sensor array and the embedded sensors.....	52
Figure 17: Architecture of the designed system.....	55
Figure 18: Electrical circuit of the PCG sensing block, comprising the microphone sensor TOM-1537L-HD-R by Pui Audio™ and the analog front-end MAX9814 by Maxim Integrated™.	56
Figure 19: Cross-sectional design of the three categories of microphone sensors. Adapted from [158].....	58
Figure 20: Block diagram of the MAX9814 by Maxim Integrated™. From the datasheet.....	60
Figure 21: Electrical circuit of the ECG sensing block, comprising the custom-made stainless-steel electrodes and the conditioning circuit, based on a DRL technique.....	61
Figure 22: Graphical representation of the electrode-skin interface and its electrical model for respectively A) wet conductive electrodes, B) dry conductive electrodes and C) capacitive electrodes. Adapted from [162].	63
Figure 23: Temporal diagram of the digital control signals generated by the microcontroller to define the sampling frequency, the multiplexing of the PCG signals and the conversion of the signals from analog to digital performed by the internal ADC of the NI DAQ USB 6210.	66
Figure 24: Implementation of the designed architecture in two PCBs, a flexible PCB with the sensors and the conditioning circuit to be placed on the thorax and a rigid PCB with the remaining electronics.	68

Figure 25: Dimensioned drawings of the flexible PCBs in the version with homogeneously distributed microphones (panel A) and in the version with the microphones concentrated over the traditional auscultation areas (panel B). All dimensions are expressed in millimeters.	72
Figure 26: Dimensioned drawings of the case of the flexible PCBs in the “cluster” version. Panel A: housing, where the flexible PCB is inserted. Panel B: cover. All dimensions are expressed in millimeters.	74
Figure 27: Pictures of the array in its case (without the cover). Version "homogenous" - chest side (A) and top side (B). Version "cluster" - chest side (C) and top side (D).....	75
Figure 28: Block diagram of the complete setup. Relative dimensions are not meant to be realistic.	76
Figure 29: Interface of the designed application devolved to perform the recordings with the multi-sensor array.	77
Figure 30: Flowchart of the algorithm for the estimation of the time of closure of the cardiac valves.	83
Figure 31: Graphical representation of the defined temporal parameters on the ECG, PCG, and PCG envelope signals.....	87
Figure 32: Comparison between a good-quality signal (A, with SNR = 31 dB) and a poor-quality signal (B, with SNR = 4 dB).	88
Figure 33: Definition of the intervals of the heartbeat corresponding to S1, S2 and the noise.	91
Figure 34: flowchart of the methodology for the assessment of the effect of the signal quality on the estimate of the time of closure of the cardiac valves.	92
Figure 35: Variation of the time of closure of the tricuspid valve for one subject (10 experiments) in function of the SNR. The vertical line represents the minimum acceptable SNR value to obtain an estimate not significantly different from the reference.....	94
Figure 36: Recording system for the single-source recordings: A) ReMotus™, B) the custom realized microphone probe, C) the positioning of three electrodes and of the microphone probe over the chest.....	96
Figure 37: Time of closure of each cardiac valve in function of the SNR. The values are normalized with respect to the reference estimate for the purposes of	

comparison. Each line represents a different subject in the testing population. The black vertical lines represent the computed minimum acceptable SNR value.97

Figure 38: Minimum acceptable SNR in function of the acceptable measurement uncertainty for the four cardiac valves.98

Figure 39: Sensitivity of the computed minimum acceptable SNR values over the validation population for the four cardiac valves.99

Figure 40: Single-heartbeat segments recorded by the 48 microphones of the multi-sensor array. The grey signals were classified as poor-quality (SNR < 10 dB) and discarded.105

Figure 41: Comparison between the morphology of the same heartbeat recorded by different microphones. If the heartbeat a) is taken as reference, the heartbeat b) has a high similarity and therefore a low distance whereas the heartbeat c) has a low similarity and thus a high distance.106

Figure 42: Example of comparison between the clustering obtained by agglomerative hierarchical clustering (dendrogram) and k-means over 10 different repetitions on the same heartbeat. Each circle represents a microphone, and the colors of the circles highlight the clusters. The white circles represent microphones whose signal's SNR was below threshold.110

Figure 43: Example of the contingency matrix and the corresponding Rand Index for the clustering shown on the maps.111

Figure 44: Comparison between the distribution of respectively a) the inter-cluster distance, b) the intra-cluster variability and c) the Silhouette Coefficient using hierarchical clustering (dendrogram) and k-means.112

Figure 45: Results of the various phases of the proposed pipeline on a randomly selected heartbeat for the mitral valve: A) dendrogram, B) map of the signals divided in clusters, C) evaluation matrix, D) outranking matrix and E) distillation graph generated by Electre III.118

Figure 46: Maps of the hits for the mitral valve obtained on the recording performed on day 1 using the three approaches: A) minimum time of closure, B) maximum quality, C) MCDA.119

Figure 47: Comparison of the time of closure obtained through: A) the simulated single-source approach, B) the MCDA approach, C) the minimum time of closure approach, D) the maximum quality approach. The dots represent the mean value, the dashed area represents the standard deviation band over each recording.121

Figure 48: Rationale of the tested 3-channel BSS approach devoted to separate the contribution of the left and right sides of the heart to better identify the heart sounds components.....	124
Figure 49: Comparison between the heart sounds components identified on a single-source signal against on separated source signals.....	125
Figure 50: Graphical presentation of the experimental setup, in its original conceptualization (A) and adapted for the validation of the multi-sensor array (B).	132
Figure 51: Changes produced in the monitored physiological parameters when the hypoxemic trigger (A) or the hypercapnic trigger (B) is applied.	134
Figure 52: Example for a single experiment. Representation by images of the S2 segments, before and after alignment, and their envelope. Comparison between the resulting S2 split and the monitored RVPs.	138
Figure 53: Correlation coefficient between S2 split and RVPs of each recording. The red circles represent the estimated R, whereas the blue lines represent the confidence interval.	139
Figure 54: Pig-by-pig comparison between the S2 split and the RVPs over time. Each panel represents the physiological variables of a different pig.....	140
Figure 55: Instructions provided to the volunteer-caregiver on how to locate the multi-sensor array on the chest of the volunteer-patient.....	144
Figure 56: Comparison between the traditional auscultation areas (A) and the positioning of the sensors in the three phases of the experimental protocol (B-D).	146
Figure 57: Violin plots of the distributions of respectively BMI and thoracic circumference, differentiating the biological sex, over the sample population...	147
Figure 58: Boxplots of the distributions of the SNR of S1 and S2 over the sample population, before and after filtering.....	150
Figure 59: Maps of the percentage of recordings belonging to the sample population with respectively A) the SNR of S1 higher than the SNR of S2 and B) the SNR of S2 higher than the SNR of S1. Each circle represents a microphone, the color represents the percentage according to the colorbar.....	151
Figure 60: Scatter plots of the SNR of S1 and S2, in function of the BMI, the thoracic circumference and the biological sex, respectively.	153

Figure 61: Comparison between the positioning of the single-source stethoscope over the four auscultation areas (A, C, E, G) and the corresponding microphones in the multi-sensor array (B, D, F, H). 157

Figure 62: Boxplots of the distribution of the SNR of respectively the single-source and the multi-source recordings for each cardiac valve. 159

Figure 63: Plots of the time of closure of each cardiac valve estimated by single-source PCG recordings performed by an expert user in the traditional auscultation areas and by multi-source PCG recordings performed by inexperienced users through the described multi-sensors array. 161

Figure 64: Boxplots of the CTIs estimated by the single-source and multi-source PCG recordings. The horizontal lines represent the thresholds proposed in the literature to distinguish a normal vs abnormal cardiac functionality. The green area represents the normality area. 163

List of Tables

Table 1: Correction equations for each CTI [91,95].	31
Table 2: CTIs' thresholds that were found discriminative for patients with an impaired cardiac function.	41
Table 3: Characteristics of the PCG signal (S1 and S2) [96,156,157].	57
Table 4: Characteristics of the selected microphone sensor (TOM-1537L-HD-R by Pui Audio™).	59
Table 5: Minimum acceptable SNR value for each cardiac valve.	97
Table 6: Distribution of the Rand Index over the sample population. ...	111
Table 7: Comparison of the baseline and peak values of the monitored physiological variables, both in hypoxemic and hypercapnic experiments.	135
Table 8: Correlation coefficient obtained in the three phases of analysis.	139
Table 9: Correlation coefficients between the SNR of S1 and S2 and the descriptors of the body type.	152
Table 10: Linear regression of the SNR of S2 against BMI and thoracic circumference.	152
Table 11: Average SNR of the signals obtained by the two systems optimized for each auscultation area. ...	159
Table 12: Results of the statistical comparison between the time of closure of each cardiac valve obtained through single-source and multi-source PCG.	160

Chapter 1

Introduction

1.1 An innovative solution to an established clinical problem

Every biomedical engineering project strives to propose an answer to a clinical problem. The object of this PhD thesis finds its motivation in the cardiological field. To date, cardiovascular diseases (CVDs) are the first cause of death globally, and thus they are object of wide research. Among CVDs, heart failure (HF) is the one that poses the highest challenges to the clinicians, given the non-specific nature of its symptoms, its pervasiveness in the elderly population worldwide and the typical severity of the prognosis following an acute episode. Although some effective pharmacological solutions exist to treat heart failure patients if a worsening of their status is detected, how to effectively predict the occurrence of an acute episode is still an open problem.

The problem implicitly resides in finding a suitable biomarker that correlates with the status of decompensation of an HF-patient and that could be monitored in a homecare setting. This issue is not naïve: the earliest changes in the pathophysiological pathway of AHF occur in terms of changes in the intracardiac pressures, which can only be monitored invasively, thus limiting the target population. Therefore, even though some technological solutions exist in the literature and on the market, they are either invasive or ineffective, because they act in a late stage of the decompensation process.

A novel way to tackle the problem consists of grounding the monitoring of HF-patients on the time relationships between electrical and mechanical events in the cardiac cycle. In fact, the time interval between the ventricular depolarization (electrical event) and the closure of the cardiac valves (mechanical event) is determined by the intracardiac pressures. This approach could enable the monitoring of the intracardiac pressures in a noninvasive way: the biomarkers of interest can be extracted from a combined recording of an electrocardiographic signal (ECG) and heart sounds, i.e., the acoustic waves generated by the closure of the cardiac valves.

Even if promising, the applicability of acoustic cardiography to a homecare context is not straightforward and a number of technological challenges need to be solved. First and foremost, the positioning of the electronic stethoscope: the latter requires an expert user to find the most appropriate location over the patient's chest, depending on the application of interest. A possible solution resides in multi-source phonocardiography (PCG) at high spatial resolution: instead of recording a single signal from a well-determined point on the chest, we could record multiple signals from multiple points on the chest and devolve the identification of the best auscultation area to the processing phase. In this way, recordings could be performed even by an unexperienced user in a homecare setting.

What if a system existed, suitable to be used by an unexperienced user in a domiciliary context, capable of recording combined ECG and multi-source PCG signals and extract from them biomarkers that correlate with the worsening of HF patients?

1.2 Goal of the project

The goal of this PhD project is to design and validate a wearable multi-sensor array for the monitoring of at-risk patients for HF, devolved to predict and prevent acute episodes. The final goal, from a clinical perspective, is to integrate the system in a telemedicine clinical pathway with the scope of reducing the HF-related hospitalization rate and mortality.

Given the complex nature of the task, the project was articulated in three main objectives, that can be described as follows.

Objective 1. Design, development, and testing of a wearable multi-sensor device for the simultaneous recording of ECG and multi-source PCG from a hardware perspective.

Objective 2. Design, development, and testing of the algorithms for processing the signals recorded by the device and extracting the features of clinical interest.

Objective 3. Validate the functionality and usability of the system in a pre-clinical setting.

1.3 Structure of the thesis

The present chapter is aimed at introducing the goal of the thesis. The remaining of the thesis is structured as follows.

Chapter 2 provides the reader with some background about HF from a clinical perspective, along with a summary of the monitoring approaches that have been tested in the literature, of the commercially available devices, and of the current guidelines for the diseases management. The existing know-how about electrophonocardiography for HF monitoring is included with the scope of understanding the rationale of the proposed approach.

Chapter 3 presents the design and implementation of the hardware and mechanical aspects of the multi-sensors array. Details about the architecture, the electrical circuits, the microcontroller firmware and the interface with the computer are provided, along with the mechanical design.

Chapter 4 focuses on the design and implementation of the algorithms for the processing of the recorded signals and the extraction of the clinically relevant features. In particular, details about algorithms for the assessment of the quality of PCG signals, for the estimation of the time of closure of the cardiac valves, for the identification of the best auscultation area are provided, along with the results of their testing on real-life recordings.

Chapter 5 shows the results of the pre-clinical validation phase. The pre-clinical validation is two-fold. On one side the assumption of the relationship between the time of closure of the cardiac valves and the intracardiac pressure was tested on an animal model. On the other side, the usability of the device was tested on a population of healthy volunteers and its functionality against a single-source PCG system was assessed. The results are discussed from a clinical perspective.

Chapter 6 concludes the work and highlights the most important findings as well as the limitations of the present work, with the scope of giving hints for future developments.

Chapter 2

Clinical and Technical Background

2.1 The clinical problem: Acute Heart Failure

As anticipated in the Introduction, every bioengineering project is driven by a clinical problem: fully understanding the nature of the problem and the implications for the patients, the healthcare system, and the society is a first essential step to solve it. In the next paragraphs a brief pathophysiology of heart failure is proposed, followed by a summary of the current management of the disease in the clinical practice and of its impact on the public health and society. The goal of this paragraph is to gather all the elements necessary to understand why the prevention of acute episodes of HF is of key importance.

2.1.1 Brief pathophysiology of heart failure

Heart failure is not a disease in the strict sense, but a complex clinical syndrome. Clinically, heart failure refers to every pathological condition involving an impairment of the ability of the heart of fulfilling its main function, i.e., pumping blood. The reduced cardiac output results in an incapability of the heart of providing a sufficient blood flow to meet the metabolic requirements of the body tissues and organs. In this sense, heart failure is not a disorder of the heart, but a disorder of the circulating system in its overall.

The pathophysiology of heart failure is heterogeneous, due to the heterogeneous nature of its underlying cardiac cause [1]. In fact, a structural or

functional cardiac condition is a prerequisite for the development of HF and the identification of its etiology provides significant clues towards the diagnosis and treatment [2]. The most typical causes of HF are coronary artery diseases, which are responsible for reducing the oxygen delivery to the myocardium and thus its functionality; and myocardial infarction, where infarcted myocardial regions cannot contribute to the contraction. Other pathological conditions that can lead to HF are valvular diseases, cardiomyopathies, infective and noninfective myocarditis and chronic arrhythmias [3]. The large variety of pathological conditions leading to HF already gives a hint about its pervasiveness in the population.

Depending on the pre-existing cardiac condition, different pathophysiological pathways are activated to counter the effects of a reduced oxygen delivery to the tissues. The signs and symptoms characterizing the clinical presentation of AHF are highly non-specific: reduced exercise capability, exertional dyspnea, fluid retention, pulmonary or systemic edema [3,4]. Mostly, they can be traced back to systemic congestion: the filling pressure of the ventricular chambers of the heart increases to try to compensate the reduced cardiac output, causing extracellular fluid accumulation [1]. In the clinical practice, the presence of signs and symptoms is a prerequisite for a HF diagnosis, but it is not sufficient alone [2].

Two classification systems of HF patients are most widely accepted at date. The New York Heart Association (NYHA) classification divides HF patients in 4 classes based on the functional disability caused by their symptoms [5]. The American Heart Association and American College of Cardiology (AHA/ACC)

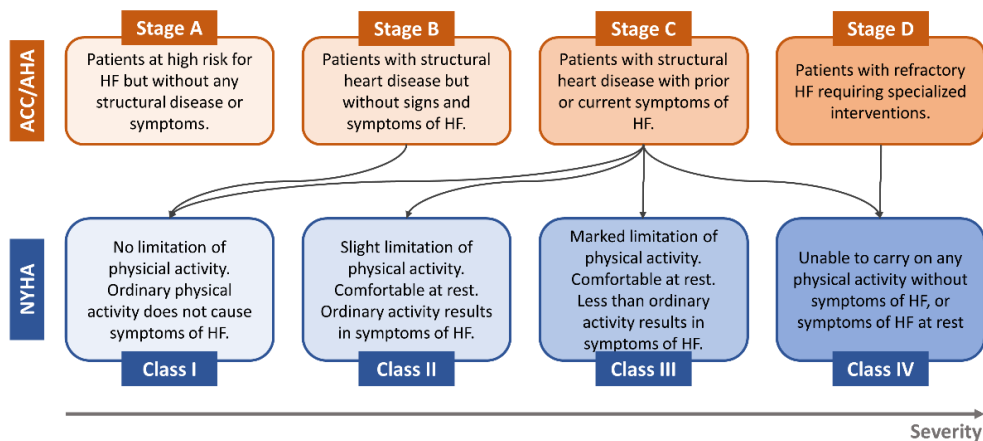


Figure 1: The two major classification systems for HF, namely ACC/AHA based on the progression of the disease and the NYHA, based on the disability caused by the symptoms [5,6].

classification defines 4 stages based on the progression of the disease [6]. Figure 1 shows the two classification systems and how they can be integrated.

Systolic and diastolic HF

The functional impairment of the cardiac function can result from either impaired contractility (systolic failure) or impaired filling ability (diastolic failure) [3]. The two conditions may also be simultaneously present.

In systolic HF, the impaired contractility of the heart causes a reduced stroke volume, which is compensated by an increase in the preload (i.e., the ventricular end-diastolic pressure) for the Frank-Starling mechanism [3]. The compensatory effect has a limit, though, given by the maximum length of the sarcomeres' fibers. This may even lead to ventricular remodeling, devolved to enlarge its volume and increase its compliance [3]. A decrease in the stroke volume and a simultaneous increase in the end-diastolic volume produce a decrease in the ejection fraction (EF), which can fall to below 20% in severe cases.

In diastolic HF, the impaired ventricular filling ability can be caused by either decreased ventricular compliance, typically produced by the hypertrophic effect of prolonged hypertension, or impaired relaxation [3]. An impaired ventricular filling results in a higher preload combined to a lower ventricular end-diastolic volume [3]. Therefore, contrarily to systolic HF, diastolic HF may or may not be associated with a decreased ejection fraction, depending on the relative decrease of stroke volume with respect to ventricular end-diastolic volume.

Both types of HF feature a decrease in the cardiac output and an increase in the preload. The first is typically responsible for a decrease in the arterial pressure and the consequent fatigue and dyspnea experienced by HF patients. The second is mainly responsible for an increase in the venous pressure and thus for the most serious clinical consequences anticipated above. In fact, an increase in the left ventricular pressure reflects back in the pulmonary capillaries causing pulmonary congestion and edema, whereas an increase in the right ventricular pressure is reflected back into the right atrium and the systemic venous vasculature, leading to a systemic congestion and peripheral edema [3,4].

Chronic and Acute HF

Heart failure is a chronic and progressive syndrome [1]. In patients diagnosed with chronic HF, acute heart failure (AHF) is defined as a sudden exacerbation of the symptoms which follows an acute decompensation of the heart. Precipitating

factors are highly heterogeneous and are typically related to sudden changes in the body demands to the heart: increased afterload (e.g., due to uncontrolled hypertension), increased stroke volume (e.g., due to arterial-venous shunts), increased body demands (e.g., due to physical activity) [3].

A chronic patient diagnosed with HF, if carefully compliant to the prescribed therapy and in absence of huge physical efforts, can live a relatively normal life. The occurrence of an acute episode, though, often leads to hospitalization with a poor prognosis. Moreover, as shown in Figure 2, each subsequent acute episode further reduces the myocardial functionality, and therefore the patient's prognosis [7,8]. The importance of timing in the management of AHF has been progressively recognized in the literature and stressed in the clinical practice: AHF episodes should be considered as much emergencies as myocardial infarction or cerebrovascular accidents [1].

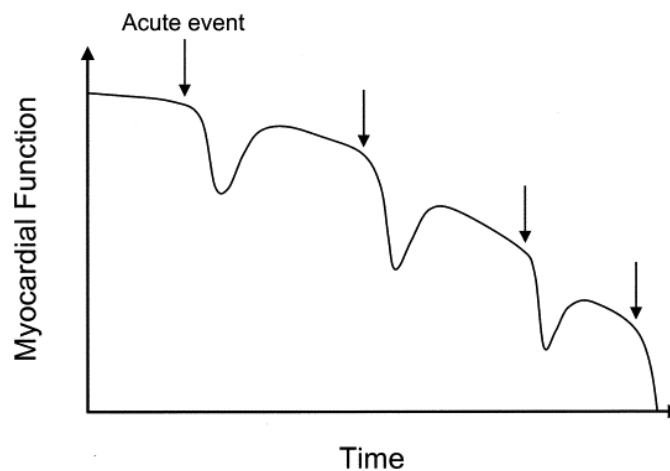


Figure 2: Effect of the acute episodes of HF on the deterioration of the myocardial function. From [7].

2.1.2 Management of heart failure in the clinical practice

The first assessment of a patient with suspected HF relies on the physical examination and the clinical history. Indeed, suspect of HF grounds on the presence of signs and symptoms, even though non-specific, combined with the presence of risk factors and a history of CVDs. If suspect is confirmed, diagnostics tests are run to confirm or exclude the HF diagnosis. Figure 3 presents the diagnostic algorithm first proposed by the European Society of Cardiology (ESC) in the “2021 ESC Guidelines for the diagnosis and treatment of acute and chronic heart failure” [2].

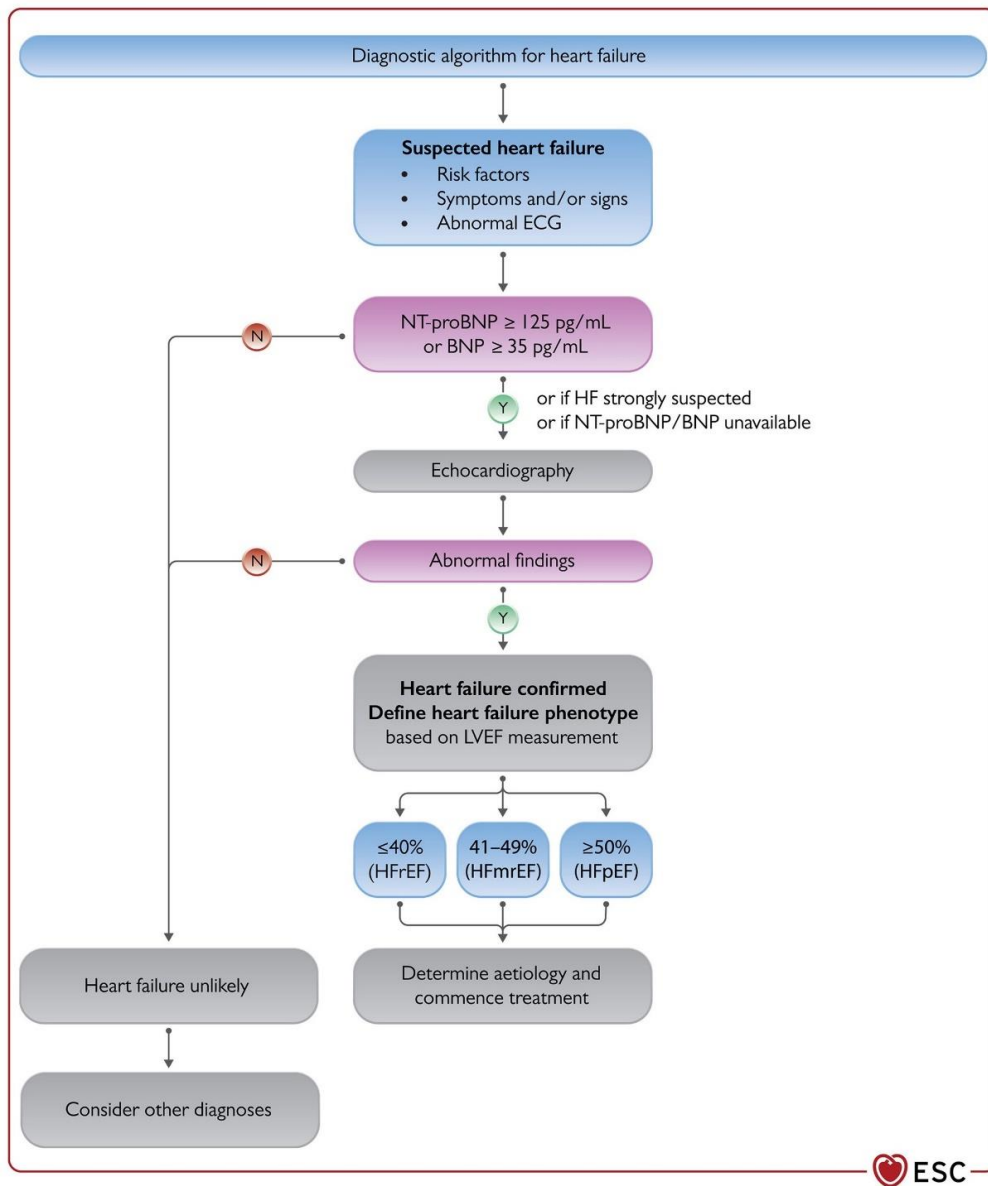


Figure 3: Diagnostic algorithm for HF proposed by the ESC and accepted by the main clinical guidelines worldwide [2]. At date, the HF diagnosis is mainly based on BNP and echocardiography.

At date, the algorithm is the most widely recognized diagnostic pathway worldwide, since it was transposed by the American Heart Association (AHA) and the American College of Cardiology (ACC) in their “2022 AHA/ACC/HFSA Guideline for the management of Heart Failure”.

According to current guidelines [2,6], two diagnostic tests are fundamental to confirm or exclude the HF diagnosis, namely the measurement of the plasma concentration of natriuretic peptides (NPs) and transthoracic echocardiography. Ancillary recommended tests include chest X-ray, routine blood tests and 12-lead electrocardiography (ECG), with the scope of identifying the underlying cardiac condition, if unknown.

Natriuretic peptides are biomarkers released by cardiomyocytes in response to stretch [9]. In other words, the secretion of NPs is triggered by a hemodynamic stimulus, such as pressure overload or volume expansion, which produces a stress in the cardiac wall, as happens in HF [10,11]. In particular, B-type natriuretic peptides (BNP) and N-terminal pro-B-type natriuretic peptides (NT-proBNP) are secreted by the ventricular tissue, therefore they are useful to analyze ventricular dysfunctions [10]. A plasma concentration of BNP lower than 35 pg/mL, or a concentration of NT-proBNP lower than 125 pg/mL rule out a HF diagnosis, as recommended by clinical guidelines [2].

Echocardiography is a key diagnostic test in many clinical situations because it allows for studying the cardiac structure and functionality. Other imaging modalities such as cardiac MR, cardiac CT, PET, SPECT and coronary angiography may provide additional information [6]. Right heart catheterization is recommended only in cases where the echocardiography results are uncertain, or in acute settings.

Besides providing clues about the possible underlying cause, echocardiography is used to extract indices associated to the heart functionality and in particular to its hemodynamics. One of those indices is the Ejection Fraction (EF). Clinical guidelines currently classify HF phenotypes depending on the measured left ventricular ejection fraction (LVEF): HF with reduced EF (HFrEF) if $LVEF \leq 40\%$, HF with mid-range EF (HFmrEF) if $40\% < LVEF \leq 50\%$, and HF with preserved EF (HFpEF) if $LVEF > 50\%$ (and raised NPs confirm the diagnosis) [2,6]. It was often documented that a progressive decrease in the EF is commonly expected in chronic HF patients and a significant reduction is a poor prognostic factor [2,6].

As shown, the diagnostic pathway for HF is quite complex and requires tests and skills that are not always readily available in an Emergency Department. Clearly, the consequence is a delay in treatment and an increase in mortality [12].

After diagnosis, HF is typically addressed by means of a pharmacological treatment with a three-fold goal: reducing the mortality, improving the cardiac

output to guarantee organ perfusion and reducing the symptoms, particularly edema and dyspnea [3]. In chronic patients, guidelines recommend the use of diuretics, to counter edema, and vasodilators, to decrease the high filling pressures [1]. In addition, in acute states and in case of cardiogenic shock, positive inotropic medicaments are used to improve the cardiac output [8].

Even though the guidelines recommend a variety of therapeutic patterns depending on the etiology of the patient [2,6,13], no established pharmacological pattern exists due to the high heterogeneity of HF presentation in cardiological patients. On the contrary, the treatment must be frequently adjusted to meet the specific patient's needs and the specific development of the disease. Increasing body of evidence confirms that delayed treatment is associated with poor outcomes [1,14], whereas prompt therapy adjustments can increase the survival rate.

2.1.3 Heart failure in numbers

Heart failure has often been referred to as a global burden, both in the scientific literature and in common speech. It was first described as a pandemic in 1997 [15] and it has indeed all the characteristics of one.

Worldwide, 64 million people living with HF were estimated in 2017 – 42 million people live with cancer, for the sake of the comparison [16]. The incidence has been estimated to 3/1000 person-years in all age groups, but the number is strongly dependent on the age [17]. Studies show a slow decline in the incidence over the latest 20 years, which reflects, to some extent, a slowly increasing effectiveness of the preventive measures [17,18]. Nevertheless, the absolute number of new cases per year is steadily increasing, due to population ageing [17] and it is expected to keep on raising in the next decades. A larger and larger fraction of the yearly new HF cases presents a preserved EF: this is interesting from a clinical point of view since the patients affected by HFpEF proved to poorly respond to the treatment [18].

Prevalence provides the best indication of the burden of HF for the society and the healthcare system. Recent studies estimate HF prevalence between 1% and 2% in developed countries [2,18]. It should be highlighted that even if incidence is slowly decreasing, prevalence is steadily increasing due to population ageing, but also to the increasing survival rate to cardiovascular events such as myocardial infarction [19]. Moreover, the real prevalence may be significantly higher than what stated because an impressive number of cases are still undiagnosed: a meta-analysis

study reports a prevalence estimated from systematic echocardiographic screening as high as 11.8% [20]. The prevalence was found significantly correlated to age, as shown by the age-specific prevalence which was found as high as [21]:

- 1.36% in the 25-49 years-old group
- 2.93% in the 50-59 years-old group
- 7.63% in the 60-69 years-old group
- 12.67% in the 70-79 years-old group
- 16.14% in the over 80 years-old group

The lifetime risk for HF was estimated around 21% at the age of 40, 28% in the presence of hypertension: one out of five people is expected to develop HF at some point of their life [22,23]. These numbers give real perspective on the pervasiveness of HF syndrome in the population.

Hospital admissions after HF diagnosis occur averagely once a year, and are expected to raise by 50% in the future because of population growth, population ageing and increase of the prevalence of comorbidities [2]. AHF due to the decompensation of a chronic HF patient accounts for the vast majority (approximately 70%) of hospital admissions [24]. In-hospital mortality after an acute episode ranges from 4% to 11% [24,25]. It was proved that each further hospitalization provides a deterioration of the life expectancy of the patient: average life expectancy decreases from 2.5 years after the first hospitalization to 0.5 years after the fourth [24].

Mortality rates impressively high and stable, regardless the efforts and progresses made in the management of HF patients in the latest years, confirm that the prognosis is still poor [2]. A 1-year mortality between 20% and 30%, and a 5-year mortality as high as 50% were found in recent studies [18,26]. High mortality rates make evident that there is room for improvement both in the prevention and in the treatment phase.

Heart failure is not only a clinical problem in its strict sense, but also a severe cost for the society and for the healthcare system. It was reported that 1 to 3% of the overall healthcare expenditure in developed countries is related to HF management [22]. The main contributor to HF-related expenses is hospitalization [24]. Typically, an hospital stay following an acute episode of HF lasts between 4 and 11 days [25]. In the US, the total HF-related cost was estimated at \$31 billion in 2012, accounting for 1% to 2% of the overall healthcare expenditure [27].

Nevertheless, projections indicate that it will increase by 127% by 2030, reaching almost \$70 billion [28,29]. In 2013, the global overall expenditure for HF was estimated around \$108 billion [27].

More difficult to quantify, but worth of being mentioned, HF strongly reduces the quality of life of affected patients (and also their family and caregivers). Symptoms such as extreme fatigue and shortness of breath most often prevent HF patients to work and perform even the most normal daily activities, with a consequent psychological, social and financial distress [22]. Anxiety and depression, often undiagnosed, characterize chronic HF patients, even when treated at their domicile [30].

2.1.4 Importance of the prevention of acute episodes

Prevention of HF can be distinguished in two phases. Primary prevention concerns the prevention of chronic HF and is strictly related to the prevention, early diagnosis, and treatment of HF underlying causes [25]. It can be highly stratified due to the high heterogeneity of possible underlying causes. Secondary prevention concerns the prevention of AHF, i.e., of the episodes of decompensation of chronic HF patients leading to hospitalization [25].

Because of the high impact of hospitalization on mortality, expected quality of life and cost for the healthcare system, secondary prevention is of key importance, both from the medical and the socioeconomical point of view.

In chronic patients, personalized and timed therapy adjustments are capable of avoiding heart decompensation and thus AHF. Nevertheless, accurate and effective treatment adjustments are possible only if a frequent assessment of the status of compensation of the heart is possible. In other words, the prevention of AHF episodes is possible from a therapeutic point of view but requires a reliable method to monitor the status of compensation of the heart of the patient and promptly detect its worsening. According to guidelines, the latter is still an open problem [2,6].

Even though the onset of AHF may look abrupt from a clinical perspective, because signs and symptoms appear in the latest stages, the process of decompensation typically takes several days to weeks [1,31]. Therefore, from the physiopathology perspective, there is room for prompt intervention. The challenge is to find a biomarker, i.e., a measurable indicator of the status of compensation of the heart, with two characteristics:

1. is correlated with changes in a physiological variable involved in the earliest stages of the process of decompensation;
2. is suitable for a frequent, domiciliary follow-up of HF patients.

Figure 4 proposes a graphical representation of the phases of the process of decompensation and their timeline. This interpretation of decompensation as a process was first proposed by Adamson et al. in 2009 [32] and adopted by all the major players in the field. The first detectable variations in the physiological status of a decompensating patient are expected in the intracardiac pressures (phase A). In fact, the first compensatory mechanism of the body to reduced cardiac output consists of increasing the ventricles' filling pressure. Over the days, the downside of this compensatory effect is an autonomic adaptation (phase B), followed by an increasingly higher fluid retention (phase C). It is important to highlight that such increase in tissue fluid could be easily counteracted with an appropriate diuretic adjustment, if detected. If no intervention is carried out, the fluid retention continues and, at some point, it becomes so relevant that an abrupt change in body weight occurs (phase D). Shortly after, symptoms appear (phase E) and hospitalization is most often required, with a poor prognosis.

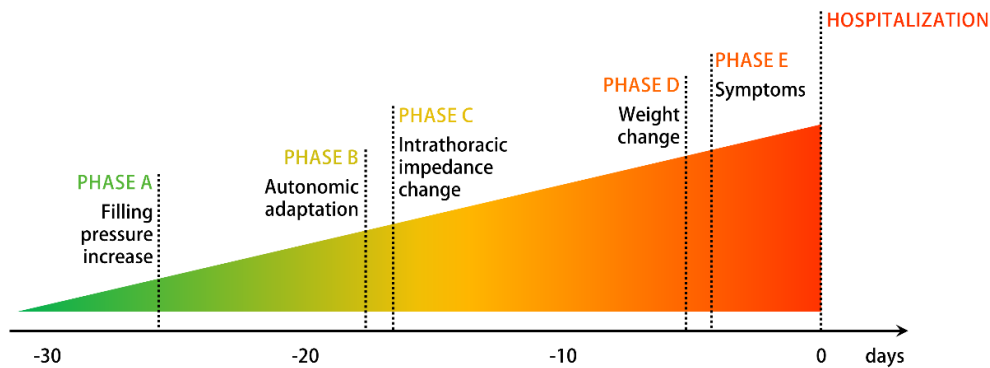


Figure 4: Phases of the process of decompensation in AHF. Adapted from [32]

If small changes in the hemodynamics could be detected, i.e., at the stage of filling pressure increase, changes in the medications could be sufficient to reestablish the status of compensation. Nevertheless, if changes can be detected only at the latest change, i.e., when symptoms occur, as it is to date, important therapy modifications are needed, and they are seldom sufficient to prevent the decompensation [32].

It is clear that the challenge is on the technological side: the availability of novel technological means capable of detecting the earliest changes in physiological variables would allow for a prompt and easy intervention and a reverse of the decompensation process in its earlier phases, with a dramatic impact on HF patients' life expectancy and quality of life.

2.2 Monitoring of heart failure patients: state of the art

Admittedly, the follow-up of patients diagnosed with heart failure is a relatively understudied area, compared to its fundamental importance to optimize the therapy and recognize exacerbation of the syndrome before it reaches the symptomatic level [2].

Nevertheless, a wide new interest in the area has been raised in the latest years, particularly driven by the COVID-19 pandemics. In 2021, the “Guidelines for the diagnosis and treatment of acute and chronic heart failure” by the European Society of Cardiology inserted “The role of remote monitoring strategies in HF in the post COVID-19 era” among the issues that deserve to be addressed in future clinical research [2].

The traditional approach for HF-patient monitoring after a diagnosis or an hospital discharge was based on the monitoring of body weight and symptoms [33]. Until recently, clinical guidelines recommended an intervention in case of worsening of the symptoms or in case of an abrupt increase in body weight, index of liquid retention. Nevertheless, as shown in Figure 4, such intervention corresponds to a very late phase in the process of decompensation, and typically proves ineffective.

At date, novel technological approaches, aiming at tackling the problem at an earlier stage, are under trial. The goal of the following paragraphs is to review the current clinical guidelines, the novel technological approaches proposed in the literature and the devices already on the market.

2.2.1 Current clinical guidelines for the follow-up of HF patients

At date, clinical guidelines ground the follow-up of HF-patients on a periodic repetition of the main diagnostic tests for HF. The recommended interval before the repetition of the tests is 6 months, with a higher frequency being recommended after hospitalization [2]. The scope of the tests is to detect a worsening of the HF status

even if this is not associated with a worsening of patient's symptoms. In fact, at date, treatment is devolved to improve the symptoms. Therefore, variations in the therapeutic plan are mostly guided by symptoms rather than on their effect on the cardiac output or other hemodynamic variables [6].

The plasma concentration of BNP and NT-proBNP is not recommended by either of the main clinical guidelines for the monitoring of the severity of the pathology due to lack of evidence and controversial results of clinical trials [2,6]. On the other side, echocardiogram is often repeated to assess changes in the EF, structural remodeling and valvular function [6]. More hemodynamic indices can be extracted from echocardiography to describe the cardiac structure and function, which can be helpful in identifying worsening of the overall condition of the patient's heart. Nevertheless, this is not recommended by guidelines today.

This follow-up strategy has proved ineffective in reducing the rate of decompensation episodes [6]. Moreover, it is challenging for the logistics of the healthcare system. From an organizational point of view, follow-up should be performed in primary care, but several studies even confirmed that improved outcomes can be obtained if the follow-up is performed by a HF specialist instead [2].

Another aspect to be considered is the frequency of the follow-up. Recent studies show that a more frequent follow-up would improve the survival chances of patients after hospital discharge [34]. Nonetheless, given the burden the healthcare system is already subjected to, a high-frequency follow-up would be feasible only in a domiciliary context. From this point of view, it should be highlighted that the two main diagnostic tests for HF are both unfeasible in a domiciliary context because they rely either on blood tests or on echocardiography, which must be performed by an experienced clinician.

In the latest years, some home telemonitoring approaches have been proposed in the literature, with a high variety of levels of effectiveness. Nevertheless, official recommendations from clinical guidelines are still quite conservative. In the latest version, both ESC and AHA/ACC state that invasive hemodynamic monitors for the measurement of the pulmonary artery pressure "may be considered" in selected symptomatic patients [2,6]. In the overall, the trust in technology in the field of monitoring of HF patients is still quite poor in the clinical practice: at date, device-based care is proposed to less than 40% of the patients who have a class 1 indication with a level of evidence A [32].

2.2.2 Literature review

Many attempts have been made over the last decade to find a suitable biomarker for monitoring the status of compensation of a HF patient. The objective of this literature review is to provide a synthetic yet exhaustive overview of the studies which analyzed the effectiveness of the proposed systems for the monitoring of HF patients.

This literature review grounds on the integration of the results of two systematic reviews published in 2022 on “Heart Failure Reviews” journal. Mhanna et al. [35] reviewed the efficacy of remote physiological monitoring-guided care for CHF. Hafkamp et al. [36] proposed an umbrella review of the effectiveness of heart failure management, and in particular the effectiveness of interventions to reduce the rehospitalization of HF patients. Both systematic reviews followed the PRISMA guidelines [37]. In this analysis were included only the studies involving a device-based monitoring of the status of HF patients. Studies involving telephone-based approaches, educational approaches and pharmacological-based approaches were excluded.

Currently available systems can be grouped into invasive and noninvasive systems. Noninvasive systems are typically based on the monitoring on some traditional physiological parameters. A wide number of parameters and their combinations has been tried out over the years, including weight, blood pressure, heart rate, heart rate variability, blood oxygen saturation (SpO₂) [32,33]. Invasive systems rely either on an active implantable medical device (AIMD), such as pacemakers and CRT-Ds, or a hemodynamic monitor based on an invasive pressure sensor.

The stages of the process of decompensation provide a good track on where to search for a suitable biomarker. Therefore, existing methodologies for HF monitoring were classified according to the phase of the decompensation process where they intervene. Figure 5 shows the correspondence between the existing methodologies, described below, and the stage of the process of decompensation where they act.

According to the stage of the process of decompensation where they intervene, monitoring approaches can be divided into [38]:

1. Monitoring of vital signs

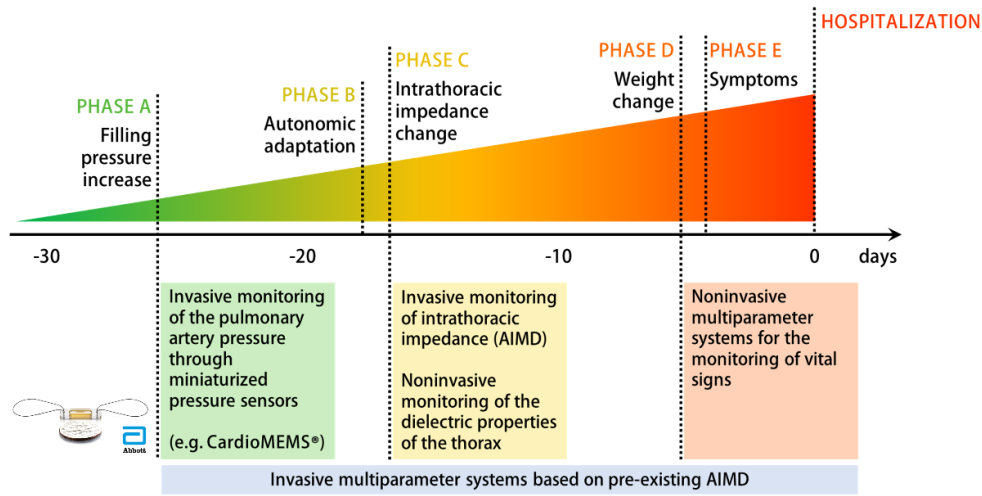


Figure 5: Main existing approaches for HF monitoring and phase of the decompensation process where they act. Partially adapted from [32].

2. Monitoring of lung congestion
3. Monitoring of hemodynamic parameters

A fourth category of systems, not strictly related to the phase of the process of decompensation, has been object of several studies: multiparameter systems based on an existing AIMD. The rationale for the study of such systems is that a relevant percentage of HF patients are implanted with an AIMD following an indication related to an underlying cardiac cause. Therefore, it may be of interest to use the already existing AIMD for monitoring, even though the monitoring parameters are not directly related to the decompensation phase.

The following paragraphs provide details about the studies conducted for each of the four mentioned categories of systems, with particular emphasis on their effectiveness to reduce mortality and hospitalization.

Monitoring of vital signs

Among vital signs, weight monitoring is preferred by clinical practitioners. A change in weight higher than 2 kg over 48 to 72 hours, or a 2% gain, triggers the alarm [39]. Nevertheless, besides occurring in a late phase of decompensation, previous studies found that many HF worsening episodes are not necessarily associated with a detectable weight increase [40]. The credibility of the latter as a AHF predictor was thus questioned and current guidelines do not recommend its monitoring as they did in the past. Clinical trials showed that a raise of 2 kg over

48 hours has a specificity as high as 97%, but a sensitivity of just 9% [39]. A 2% weight gain has a sensitivity of 17% [39]. These numbers prove that the weight changes are an insufficient predictor of decompensation. Accordingly, the WHARF-HF clinical trial showed no reduction in readmission rates, mortality and emergency visits [41]. Consistent results were found in the WISH clinical trial [42].

The value of other physiological parameters measurable through wearables as predictors of AHF is still under analysis. At date, though, evidence about their benefits in reducing hospitalizations and/or mortality is still highly controversial [38]. In fact, a high number of randomized clinical trials analyzed the influence of telemonitoring performed using a combination of vital signs on the clinical outcomes: TENS-HMS [43], HOME-HF [44], HHH [45], MOBITEL [46], SPAN-CHF2 [47], TIM-HF [48], Seto et al. [49], Blum et al. [50], TEMA-HF [51], Vuorinen et al. [52], IN TOUCH [53], BEAT-HF [54], SUPPORT-HF2 [55]. Results concerning readmission rates, mortality, adherence to therapy, quality of life are highly controversial, and most studies report them to be not significant or based on small sample populations. More promising results were found in the TIM-HF2 clinical trial [56]. 1571 patients with HF were provided with a multiparameter monitoring system, involving the daily measurement of weight, heart rate, heart rate variability, blood pressure, and oxygen saturation. The experimental group showed a reduced hospitalization rate (18 days vs 24 days) and a reduced mortality (7.9% person-year vs 11.3% person-year) with respect to the control group. Even though the results are not particularly outstanding they may lay the foundations for further analysis [56].

An important observation about the mentioned studies is that the decision-making process is based on the monitored parameter, but it's still performed by human specialists: no automatic alarm is triggered by the daily values of the parameters. Therefore, it is difficult to assess the actual correlation between the monitored vital signs and the reported clinical outcomes in an objective way. This also strongly limits the real-life applicability of such systems, even if working, since an intensive effort for the healthcare practitioners is decisive for their use.

A special mention concerning the monitoring of vital signs should be made about the monitoring of heart rate variability (HRV). From a theoretical point of view, HRV may be more relevant than the other mentioned vital signs because it reflects the behavior of the parasympathetic nervous system. Thus, it may allow to detect the autonomic adaptation, which occurs at an earlier stage in the process of decompensation [32]. Two studies show that features extracted from the tachogram

present a high predictive power with respect to episodes of AHF [57,58]. Nevertheless, albeit its promising correlation with an early stage of the decompensation process, HRV was never used in the clinical practice.

At date, a single study on vital signs recorded through a stand-alone wearable device exists and is currently enrolling. The observational Nanowear Heart Failure Management Multisensor Algorithm (NanoSense) clinical trial is based on the SimpleSense device by Nanowear Inc. (New York, New York, US). SimpleSense is an undergarment designed to continuously monitor a number of vital signs such as heart rate and sounds, respiration rate, lung volume, and physical activity. The algorithm recently proved effective for the cuffless measurement of blood pressure from a combination ECG and heart sounds [59]. It should be highlighted that this is the first study on a wearable device for AHF prediction. Moreover, SimpleSense is the first wearable device for HF monitoring embedding heart sounds. Nevertheless, the method still has to prove its effectiveness [60].

In the end, the Evaluating Mobile Health Tool Use for Capturing Patient-Centered Outcomes Measures in HF Patients clinical trial is also currently enrolling. The study is funded by Biofourmis (Boston, Massachusetts, US) and will explore the possibility of using smart devices such as their own Everion™ or Apple Watch™ for HF monitoring. The trial is a small feasibility study involving 150 patients and no further information are currently available.

Monitoring of lung congestion

The second category of systems aims at tackling the decompensation at stage of the lung congestion. Lung congestion causes a higher concentration of liquids in the thorax, decreasing its impedance and changing its dielectric properties. Two approaches have been experimented to assess lung congestions, namely thoracic impedance through AIMD and remote dielectric sensing [38].

Thoracic impedance is typically measured between an intracardiac catheter and the case of an AIMD [61,62]. The principle behind the use of thoracic impedance monitoring is that the impedance of a fluid is significantly lower than the impedance of biological tissues. Therefore, a consistent decrease in the measured impedance corresponds to an increase in the interstitial fluid, and was found to happen over a month before hospitalization for HF [61]. Besides its invasiveness, two main limitations affect the usability of the thoracic impedance method: its low sensitivity, found little over 30%, and the high rate of false alarms, found both in DEFEAT-PE and DOT-HF clinical trials [62,63].

The only solution available on the market for thoracic impedance monitoring is OptiVol™ by Medtronic Inc. (Minneapolis, Minnesota). Its efficacy has been object of several studies. Nevertheless, the results are controversial. The FAST-HF study found a sensitivity of 76% in predicting AHF episodes, against 23% obtained with weight monitoring [64]. On the contrary, the DOT-HF, CONNECT-OptiVol, OptiLink-HF and LIMIT-CHF trials all found that thoracic impedance monitoring through OptiVol™ had no significant impact on the clinical outcomes, hospitalization and mortality rate [63,65–67]. The SENSE-HF trial found a maximum sensitivity of 65% for OptiVol™ to predict AHF episodes, which they legitimately declare as unsatisfying from a clinical perspective [68]. Even though the monitoring of thoracic impedance did not show impressive results alone, it may prove its usefulness when combined with other parameters.

Remote dielectric sensing is more interesting, from a certain point of view, because it can be performed using wearables. At date, a single device implementing this technology is available on the market: ReDS™ by Sensible Medical Innovations Ltd. (Netanya, Israel). The principle is similar to thoracic impedance, but it relies on low-power electromagnetic fields emitted run through the thorax using an emitter and receiver located respectively on the chest and the back of the patient [69]. The lung congestion is assessed through the measurement of the dielectric properties of the thorax [69]. Remote dielectric sensing showed more encouraging results with respect to thoracic impedance monitoring: the SMILE-HF trial showed that patients discharged with a remote dielectric sensing system presented a reduction of 50% in hospital readmissions [69].

Monitoring of hemodynamic parameters

The third category of systems intervene in the earliest stage of the decompensation process, since they are based on the monitoring of the intracardiac pressures. It must be highlighted that, traditionally, intracardiac pressures are measured by means of intracardiac catheterization. The latter is an invasive procedure, with a number of associated risks, and is definitely not adequate for domiciliary monitoring. The systems object of this paragraph are implantable hemodynamic monitors based on a pressure sensor located in one of the cardiac chambers.

In the first developed systems, the target of the monitoring was typically the left atrium (LA) or the right ventricle (RV) and the intracardiac pressure was continuously monitored by means of an implantable sensor lead equipped with a

miniaturized pressure sensor. Even though the approach sounds promising from a theoretical point of view, results of clinical trials on both devices are quite controversial at date.

The trials LAPTOP-HF and HOMOSTASIS-HF analyzed the efficacy of HeartPod™, an implantable sensor lead by the late St. Jude Medical Inc. (Sylmar, California) for the monitoring the Left Atrial Pressure (LAP). The LAPTOP-HF clinical trial was suspended because of severe implant-related complications [38,70], suggesting that the approach is not naïve from a surgical perspective. The HOMEOSTASIS study showed moderately promising results on a small population of 40 patients [71], but this was not considered sufficient to organize an appropriate RCT, and the project was not further carried out.

The efficacy of Chronicle™ by Medtronic Inc. (Minneapolis, Minnesota), measuring the pressure in the Right Ventricle, was the object of the COMPASS-HF clinical trial. COMPASS-HF reported a reduction by 21% of the HF-related emergency visits and rehospitalizations, but the difference towards the control group was not found significant [72]. On the other hand, in the hindsight, a 36% reduction in the hospitalization rate was found over NYHA class III patients (against NYHA class IV) [70]. In the overall, the results of COMPASS-HF, the first RCT on hemodynamics monitoring of HF patients, provided the first proof of the importance of PAP monitoring and laid the foundations for the design of the next generation devices [70]. The REDUCE-HF clinical trial further analyzed the efficacy of Chronicle™ in combination with an ICD, but was prematurely suspended due to a device failure [73].

A novel approach for intracardiac pressure monitoring has recently gained the attention of the scientific community, namely the hemodynamic monitoring through implantable pulmonary artery sensors [31]. CardioMEMS™ by Abbott (Chicago, Illinois, US) is the only device currently on the market. It is a miniaturized pressure sensor based on MEMS technology placed in the PA. The CHAMPION-HF clinical trial analyzed its safety and effectiveness in reducing rehospitalization and mortality of HF patients. CHAMPION-HF showed that the daily monitoring of the pulmonary artery pressure (PAP) through CardioMEMS reduced by 80.4% the HF admissions and by 69% the all-cause admissions of HF patients with NYHA III [74]. A new clinical trial with the goal of studying the effectiveness of CardioMEMS in patients with no indication but with future risk (GUIDE-HF) is currently in the recruitment phase.

At date, CardioMEMS is regarded by the scientific community as the most promising technology for the prevention of AHF. The reason of its high effectiveness is to be searched for in the phase of development of the decompensation it acts on: monitoring the PAP, CardioMEMS is capable of detecting the very first changes of the heart physiology, enabling a prompt intervention. Given the high effectiveness of CardioMEMS to reduce the hospitalization of at-risk patients, the only drawback of CardioMEMS is its invasiveness.

A quite unique approach, combining invasive and noninvasive monitoring, is currently under evaluation in the SIRONA clinical trial, based on the Cordella™ system by Endotronix (Lisle, Illinois, US) [60]. Cordella™ is a multiparameter system that combines the information about the PAP recorded through an invasive hemodynamic monitor with a variety of other vital signs (blood pressure, heart rate, blood oxygen, weight), recorded through wearables [75]. The SIRONA study showed that the system is safe and accurate, and ready to undergo an RCT to prove its clinical efficacy. The PROACTIVE-HF study is thus currently enrolling.

Most recently (June 2022), the first results of the VECTOR-HF clinical trial on the efficacy of V-LAP by Vectorious Medical Technologies (Tel Aviv, Israel) were presented. V-LAP is a novel, still under development, LAP-monitoring device consisting of a miniaturized lead-less and battery-less implantable sensor. In synthesis, V-LAP has similar characteristics to CardioMEMS, but is implanted in the LA. Preliminary results showed a 40% reduction in the NYHA class after 6 months, but the study was not powered to assess clinical endpoints [76].

AIMD-based multiparameter systems

The role of AIMD-based multiparameter systems in HF monitoring is not straightforward. The rationale for research on this topic is that a high percentage of chronic HF patients have an underlying cardiac cause, such as arrhythmias or branch blocks, that benefit from the implant of an ICD or CRT-D. Therefore, since many HF patients already have an AIMD implanted, a fair amount of effort has been made over the last decade to benefit from the device for the monitoring of the patient and the prevention of acute episodes. It should be highlighted, though, that the implant of AIMDs in HF patients is not recommended by guidelines unless they have an indication due to another cardiac condition [2,6].

The first documented RCT aimed at analyzing the effectiveness of ICDs to reduce hospitalization of chronic HF patients is the TRUST-HF clinical trial, in

2010. The monitoring relied on commercial ICDs by Medtronic (Minneapolis, Minnesota) and involved a range of typical ICD features, (such as the rate of VT, VF, SVT episodes) combined with thoracic impedance. The results of the study were quite promising, showing a reduction of in-hospital follow-up visits by 45% with a preserved adverse events' rate [77]. Similar conclusions were drawn in the EVOLVO study [78], in the MORE-CARE study [79]. Nevertheless, the impact of the ICD use on the prevention of acute episodes was beyond the objectives of either of these studies.

On the contrary, the PARTNERS-HF trial aimed at answering this question. The investigators still used ICDs by Medtronic (Minneapolis, Minnesota), equipped with the Optivol™ module for thoracic impedance monitoring. A diagnostic algorithm was developed, based on the following features: atrial fibrillation (AF) duration, ventricular rate during AF, fluid index (Optivol™), patient activity, night heart rate, HRV, percentage of pacing CRT, ICD shock for potentially lethal VT/VF [80]. The results are very interesting: the diagnostic algorithm was found capable of stratifying the patients for the risk of an acute episode, and, in particular, patients with a positive diagnostic result were found 4.8 more likely to incur in a HF-related hospitalization in the following month than patients with a negative result [80]. The results of the PARTNERS-HF trial show how the integration of multiple HF-related parameters can lead to a positive result, even though the single parameters did not prove very effective for HF monitoring when considered alone (as HRV or thoracic impedance).

Similarly, the IN-TIME clinical trial studied the efficacy of an analogue ICD-based system developed by Biotronik (Berlin, Germany), relying on the Biotronik Home Monitoring function. The study found a decrease in 1-year mortality from 8.7% in the control group to 3.4% in the group of patients subjected to telemonitoring [81]. The Authors claim that the efficacy of the ICD-based telemonitoring is based on three factors: early detection of ventricular and atrial tachyarrhythmias, early detection of suboptimal functioning of the device, better recognition of the patient's symptoms due to interviews prompted by the device's alarms [81].

The RESULT-HF study was even more relevant for a real life scenario, since it involved all the available AIMD-based systems for HF monitoring: CareLink™ by Medtronic (Minneapolis, Minnesota), Merlin@home™ by Abbott (Chicago, Illinois), Home Monitoring™ by Biotronik (Berlin, Germany) and Latitude™ by Boston Scientific (Marlborough, Massachusetts) [82]. Results show a significant

reduction in the hospitalization rate of the remote monitoring group from 45.5% to 37.1% [82].

It should be highlighted that other RCTs found less optimistic results. The TELECARD study found that telemonitoring based on CRT-D could effectively predict the hospitalization rate of HF patients but showed no reduction in either all-cause or cardiovascular-related mortality [83]. The REM-HF study grounded the monitoring of 1650 HF patients on a variety of commercial CRT devices (by Medtronic, Boston Scientific or Abbott) and on a variety of features (including percentage of bi-ventricular pacing, nocturnal HR, thoracic impedance, activity levels, AT/AF burden, HRV). Even though the study design reminds the one from the PARTNERS-HF study, they found no significant difference between experimental and control groups on either mortality or hospitalization [84]. The INCONTACT study, using the Merlin@home system by Abbott (Chicago, Illinois), found comparable clinical outcomes between in-person follow-up and telemonitoring [85].

Two studies aimed at developing a predictor index for AHF based on AIMD-derived parameters, i.e., the TRIAGE-HF study [86] and the MultiSENSE study [87].

The TRIAGE-HF study developed and validated a HF risk status (HFRS) based on parameters recorded using the CareLink™ system by Medtronic (Minneapolis, Minnesota). The score uses the same parameters as the PARTNERS-HF trial, which already proved their value [80]. A validation over 971 patients showed that patients who were characterized by an above-threshold value for the HFRS were found 10 times more likely to be admitted for HF in the following 30 days [86]. A further study analyzed the predictive value of the HFRS towards mortality, and found that a day with HFRS corresponded to a three times higher risk of mortality [88].

The MultiSENSE study aggregates data from the Latitude™ system by Boston Scientific (Marlborough, Massachusetts) in a composite index of clinical relevance, through a multisensory alert algorithm named HeartLogic™. Features are extracted from physiological parameters such as heart sounds (S1 and S3), lung impedance, respiratory rate and volume, activity, and night-time heart rate [87]. The study involved 974 HF patients, divided into a development set and a test set. The HeartLogic index was found to have a sensitivity of 70% for the prediction of HF acute episodes, with a median advance of 34 days [87]. The results are very encouraging to obtain a sensitive and timely prediction of AHF. The actual

effectiveness of HeartLogic from a clinical perspective is object of the MANAGE-HF clinical trial, currently enrolling [60]. It should be highlighted that, at date, HeartLogic™ is the only technological solution involving features extracted from heart sounds, even though recorded invasively.

In the overall, it can be concluded that AIMD-based multiparameter systems can be quite promising in flanking CardioMEMS™ and other hemodynamics monitors for the prevention of AHF. It should be highlighted, though, that given the risks associated with the implant, AIMDs are not used on HF patients full-scale, but they are implanted only when there is an indication based on the underlying cardiological cause.

2.2.3 Technological benchmark

After having reviewed all the monitoring possibilities explored in the literature in the last decades, the goal of this paragraph is to synthesize the currently available systems in a more market-oriented way. The goal is to provide a link between research and clinical practice: among all the above-described approaches that were tested from a scientific perspective, what methodologies could actually reach the market and be used in clinics?

It should be highlighted that all the mentioned approaches for remote monitoring of HF patients are effective only if integrated in an appropriate care service. In fact, the benefits of the use of each of the abovementioned systems were produced by a therapy adjustment triggered by changes in the monitored physiological features. The COMPASS-HF clinical trial on hemodynamic monitoring showed that the therapy was adjusted 28% more times in the group of patients with the implanted hemodynamic monitor [72]. No system can really be effective without being integrated in an appropriate telemonitoring clinical pathways.

Figure 6 resumes the main characteristics of the technological solutions proposed in the literature, along with the commercially available devices exploiting each technology and the devices currently in the validation phase.

Some important considerations can be derived from the analysis of the technological benchmark.

	Vital signs monitoring (weight)	Thoracic impedance monitoring (invasive)	Thoracic impedance monitoring (invasive)	Vital signs monitoring (heart rate variability)	Intracardiac pressure monitoring	AIMD-based multi-parametric systems
Phase of the decompensation	Phase D	Phase C	Phase C	Phase B	Phase A	Various
Prediction timing						
Prediction accuracy						
Non-invasiveness						
Usability						
Commercially available	-	* <i>Optimol</i> [®] (Medtronic)	* <i>ReDS</i> [®] (Sensible Medical Innovations)	-	* <i>CardioMEMS</i> [®] (Abbott)	* <i>TriageHF</i> [®] (Medtronic) * <i>Merlin@home</i> [®] (Abbott) * <i>Home Monitoring</i> [®] (Biotronik) * <i>Latitude</i> [®] (Boston Scientific)
Under development	-	-	-	* <i>SimpleSense</i> [®] (Nanowear Inc.)	* <i>Cordella</i> [®] (Endotronix) * <i>V-LAP</i> [®] (Vectorius Medical Technologies)	-

Figure 6: Technological benchmark, along with commercially available and under development devices.

At date, no system based on vital signs monitoring is available on the market. This is fundamentally due to the fact that no noninvasive technology proved effective enough to reach the market and the clinical environment. The only exception is ReDS[®], based on remote dielectric sensing. Nevertheless, the latter acts in a mid-term phase of the decompensation process: there is room for improvement, in terms of time promptness as well as efficacy.

The technological benchmark highlights a high number of commercially available AIMD-based systems. Basically, all the main players in the AIMD market proposed a solution for HF monitoring based on their device. Even though controversial results emerged from the literature analysis, the efficacy of some systems looks particularly promising. It must be underlined that each system grounds its monitoring on different physiological features: on one side, this may strongly affect their efficacy, on the other side it makes it difficult to localize their intervention in the process of decompensation. Research in this sense is surely

worth continuing, since many patients affected by HF are implanted with an AIMD on an indication for some comorbidity. The AIMD-implanted HF-patients is a rather small population compared to the entire population of patients affected by HF: the proportion of patients living with HF implanted with an ICD was estimated between 2% and 8% [89]. A more pervasive technology is required to have a larger impact.

Invasive hemodynamic monitoring is nowadays the only technology cardiologists really rely on for the prediction of AHF. A fair amount of research is still ongoing, but the results presented by Abbott about CardioMEMS™ undeniably confirm the efficacy of the method. The presence of two more systems based on the same approach in the validation phase confirms the trend and the interest of the scientific population as well as the clinical environment. The main limitation to the use of CardioMEMS™, or potential similar devices, resides in the implant phase: even though its safety was demonstrated in the CHAMPION-HF clinical trial [74], the need for an implant limits the use of the device to patients already diagnosed with HF. At-risk patients are unlikely to get a hemodynamic monitor implanted, therefore a huge proportion of patients who could benefit from the monitoring of their status of compensation are excluded.

It is evident from the technological benchmark that there is a gap in the market (and therefore in the clinical practice) for a noninvasive system capable of monitoring hemodynamic variables, as CardioMEMS™ already does in an invasive way.

2.3 The promise of electro-phonocardiography

As shown in the previous paragraphs, there is a clinical need for a biomarker, that could be monitored noninvasively, whose changes are related to changes in the intracardiac pressures. Such a biomarker would enable the domiciliary monitoring of HF patients with the scope of preventing AHF episodes.

The idea of using electro-phonocardiography (or acoustic cardiography) grounds on the assumption that AHF is associated with changes in the timing of the mechanical events in the heart, which reflect the changes in the intracardiac pressures. Those changes reflect, for example, in the electromechanical coupling of the heart, i.e., the latency between the electrical depolarization of the ventricles and their mechanical contraction. The first is clearly visible in the ECG, the second

causes the closure of the cardiac valves, which generates the main vibrations of the heart sounds.

The time intervals between electrical and mechanical events in the cardiac cycle go under the name of Cardiac Time Intervals. The goal of this paragraph is to propose an analysis on the Cardiac Time Intervals, how to estimate them from biomedical signals and their relationship to AHF. In the end, a summary of the technical challenges to bring electro-phonocardiography to homecare will be presented along with the proposed solution.

2.3.1 The Cardiac Time Intervals and how to find them

The Cardiac Time Intervals (CTIs) provide a temporal description of the phases of the cardiac cycle from an electro-mechanical perspective, and are therefore important hemodynamic indices [90]. For this reason, they have been object of wide research over the last decades. Most often, they are referred to as Systolic Time Intervals (STIs) since they mainly describe the systolic phase of the cardiac cycle [91]. The CTIs can typically be measured by means of echocardiography, but researchers are focusing on finding alternative ways based on some biomedical signals, with the scope of making the methodology suitable for domiciliary monitoring [90].

Figure 7 illustrates the main CTIs described in the literature. As reported, they can be described as follows [90,92]:

- **Electromechanical Activation Time (EMAT) – or Delay (EMD):** time between the onset of the ventricular depolarization and the closure of the mitral valve.
- **Pre-ejection Period (PEP):** time between the onset of the ventricular depolarization and the opening of the aortic valve.
- **Isovolumic Contraction Period (IVCP):** time between the closure of the mitral valve and the opening of the aortic valve.
- **Left Ventricular Ejection Time (LVET):** time between the opening and the closure of the aortic valve.
- **Left Ventricular Systolic Time (LVST):** time between the closure of the mitral valve and the closure of the aortic valve.
- **Total Systolic Time (TST) or Total Electromechanical Systole (QS2):** time between the onset of the ventricular depolarization and the closure of the aortic valve.

Figure 7 proposes a definition of the CTIs on an extended version of the famous Wiggers diagram including the relevant biomedical signals.

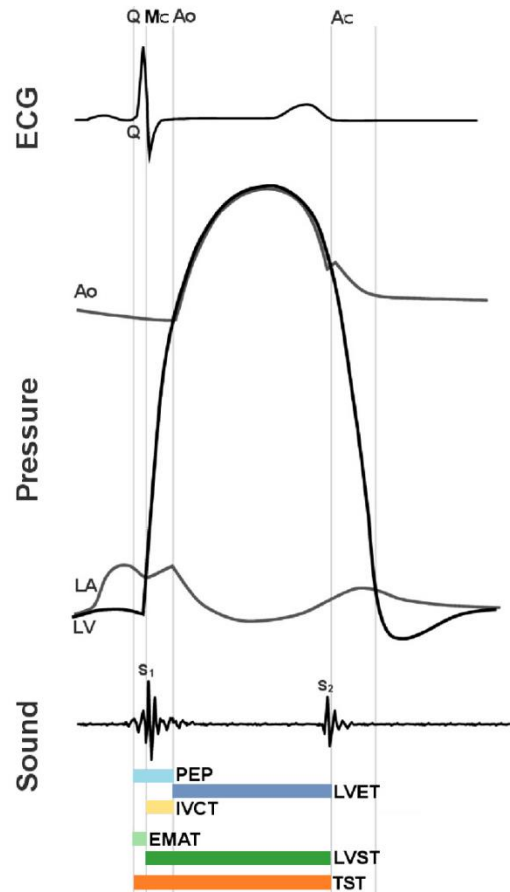


Figure 7: Visual definition of the main Cardiac Time Intervals, in relation to the LV intracardiac pressures and to the main biomedical signals used for their estimation (ECG and heart sounds), in a modified version of the Wiggers diagram. M_C represents the instant of closure of the mitral valve, A_O and A_c represent respectively the opening and closure of the aortic valve. Adapted from [93,94].

As shown in Figure 7, the CTIs are defined according to the opening and closure of the cardiac valves, but these events correspond to specific points in the curves of the intracardiac pressures. In other words, a change in the intracardiac pressures produces a change in the CTIs. Therefore, the latter may be a suitable biomarker for the monitoring of the status of decompensation of the heart, from a theoretical point of view.

It should be highlighted that all the CTIs are traditionally described for the left side of the heart, because the assessment of the left ventricular performance is

typically most used in clinics. Nevertheless, the same parameters could be described for the right side of the heart. In that case, the opening and closure of the tricuspid and pulmonary valves would substitute the opening and closure of the mitral and aortic valves in the definitions above.

Reasonably, the CTIs are influenced by the length of the cardiac cycle, i.e., they vary inversely with the heart rate. Therefore, it is well established that the variations of the CTIs need to be compensated for variations in the heart rate to be correctly interpreted from a clinical perspective [91]. Back in 1968, Weissler et al. studied the regression between the heart rate and each CTI and proposed correction equations [95], which are presented in Table 1.

The normality indexes represent the normal value of the corresponding CTI at a theoretical heart rate (HR) of 0 bpm, as found by the Authors in 211 normal subjects [95].

Table 1: **Correction equations for each CTI [91,95].**

CTI	Sex	Correction equation	Normality index
EMAT	M	$cEMAT = - 0.4 * HR + EMAT$	EMAT = 90 ms
	F	$cEMAT = - 0.3 * HR + EMAT$	EMAT = 89 ms
PEP	M	$cPEP = - 0.4 * HR + PEP$	PEP = 131 ms
	F	$cPEP = - 0.4 * HR + PEP$	PEP = 133 ms
IVCP	M	Independent on HR	IVCP = 38 ms
	F	Independent on HR	IVCP = 39 ms
LVET	M	$cLVET = - 1.7 * HR + LVET$	LVET = 413 ms
	F	$cLVET = - 1.6 * HR + LVET$	LVET = 418 ms
LVST	M	$cLVST = - 1.8 * HR + LVST$	LVST = 456 ms
	F	$cLVST = -1.6 * HR + LVST$	LVST = 461 ms

TST	M	$cTST = - 2.1 * HR + TST$	TST = 546 ms
	F	$cTST = - 2.0 * HR + TST$	TST = 549 ms

The equations show that the dependence of the CTIs on the heart rate is linear and that the coefficients slightly differ for males and females.

Even though the correction equations remain valid at date, most Authors compute the corrected CTIs by simply dividing the CTI value by the RR interval (e.g., $cEMAT = EMAT/RR$). Moreover, considering the fact that relative values are more important than absolute values, two more CTIs were defined as the ratio of other timing interval, namely:

- **EMAT/LVST**: ratio between the electromechanical delay and the left ventricular systolic time (based on the closure of the mitral and aortic valves).
- **PEP/LVET**: ratio between the pre-ejection period and the left ventricular ejection time (based on the opening and closure of the aortic valve).

CTIs are typically expressed in milliseconds. Corrected CTIs are expressed as a percentage of the cardiac cycle. Ratios are dimensionless.

In the overall, the definition of the CTIs grounds on the identification of the time of occurrence of three events: the onset of the ventricular depolarization, the opening of some cardiac valves, the closure of some cardiac valves.

The onset of the ventricular depolarization can easily be identified as the beginning of the QRS complex in the ECG. Some Authors reported the use of the R-wave peak as reference, instead of the Q-wave, because of its easier identification.

The identification of the time of opening and closure of the cardiac valves is more critical. The two mechanical events can be easily identified in the echocardiogram, but, as already highlighted, the latter is not an option if the application is in a homecare context. The first noninvasive way to extract the CTIs from biomedical signals grounded on simultaneous recordings of ECG, heart sounds and carotid pulse wave in 1977 [91]. Since then, a variety of biomedical

signals were used: a brief description of their characteristics and potentiality is proposed below.

Phonocardiography

Phonocardiography (PCG) is the recording by means of a microphone of the acoustic vibrations generated by the closure of the cardiac valves (heart sounds) and the blood flow in the heart [90]. Sometimes, when used in combination with ECG, it is also referred to as acoustic cardiography [92].

In a healthy subject, two main heart sounds are recognizable: the first heart sound (S1), generated by the closure of the atrioventricular valves (mitral and tricuspid); and the second heart sound (S2), generated by the closure of the semilunar valves (aortic and pulmonary). Physiologically, the acoustic waves are produced by the vibration of the taut valves, and consequently of the adjacent cardiac wall, occurring immediately after the closing because of the blood backflow [96]. In pathophysiological situations, a third heart sound (S3), may occur at the beginning of the middle third of the diastole, possibly due to the blood reverberation inside the ventricles during their filling. A fourth heart sound (S4), occurring during the atrial contraction and caused by the vibration of blood rushing into the ventricles, may appear in even rarer cases [96]. Figure 8 presents a plot of a typical PCG signal with S1, S2 and S3 highlighted, in relation to a simultaneous ECG.

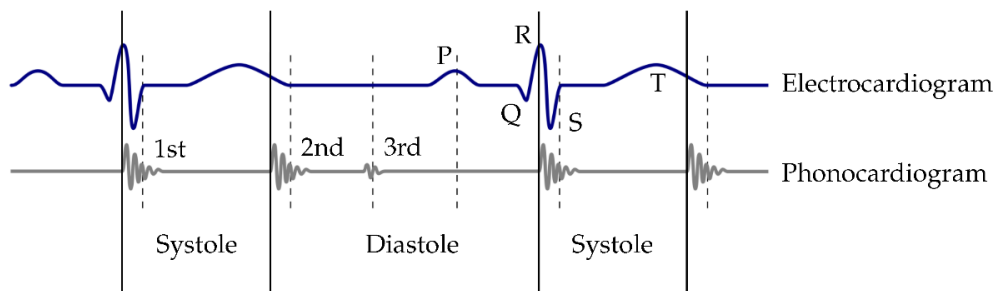


Figure 8: Representation of a typical PCG signal and the main heart sounds [97].

Given the nature of the signal, the PCG has traditionally been used to estimate the EMAT and the LVST, but it's considered unsuitable for the estimation of the PEP and the LVET, because it does not contain any information about the opening of the cardiac valves. Nevertheless, Paiva et al. proposed a Bayesian approach to estimate the PEP and LVET from PCG recordings [98]. Their approach reached an estimation error of 9.97% and 4.26% respectively for PEP and LVET. The TST was

successfully estimated through PCG with an error of 2.1% against echocardiography by Dehkordi et al [90]. A higher percentage error (28.5%) was found for EMAT, but it could admittedly be due to the echocardiography device [90]. In the overall, PCG can be reliably used to estimate the EMAT, the LVST, the ratio EMAT/LVST and the TST.

Seismocardiography

Seismocardiography (SCG) uses an accelerometer to record the chest vibrations generated by the motion of the myocardium. The accelerometer is typically located in the lower part of the sternum [90].

The SCG is a deterministic signal with a repeatable morphology. Nevertheless, the correlation of the waves of the signal with respect to the physiological events in the heart was unclear until recently. In 2018, Sørensen et al. formalized the

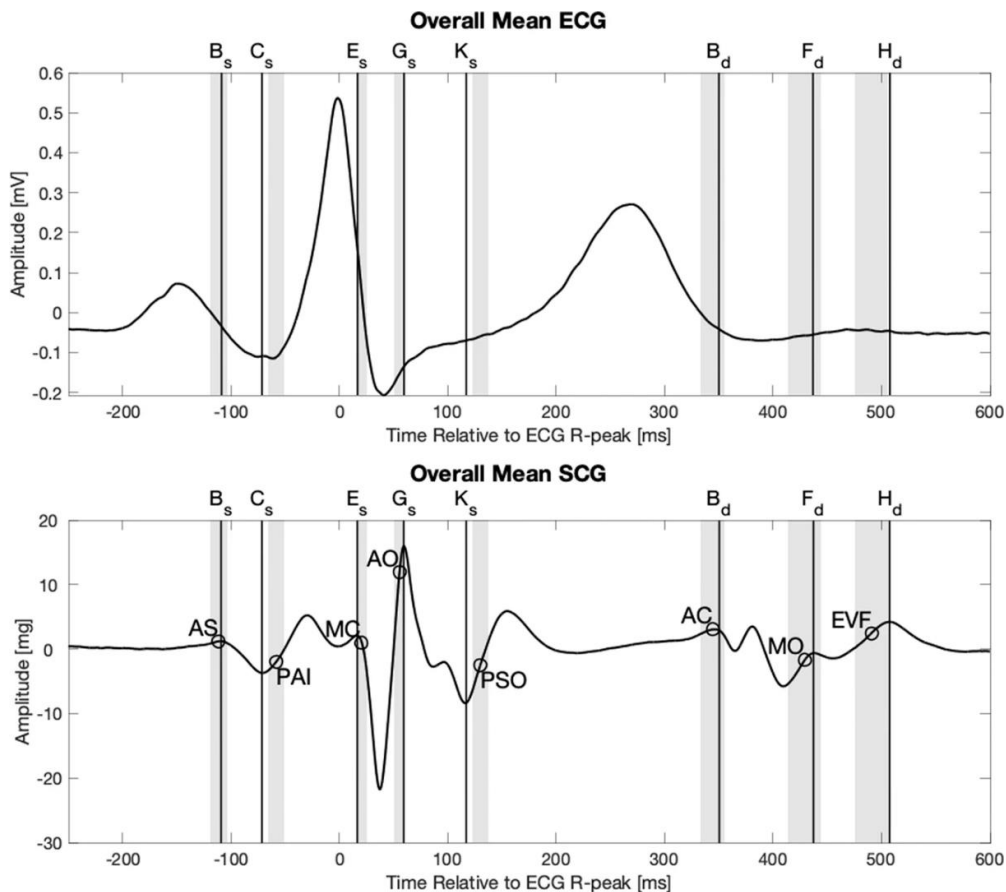


Figure 9: Definition of the fiducial points of the SCG signal according to Sørensen et al. [99].

definition of the SCG fiducial points and their significance with respect to the events of the cardiac cycle [99]. Their definitions are proposed in Figure 9. It should be underlined that the most important fiducial points for the definition of the CTIs are present, namely:

- The closure of the mitral valve (MC)
- The opening of the aortic valve (AO)
- The closure of the aortic valve (AC)
- The opening of the mitral valve (MO)

Nevertheless, all fiducial points refer to the left side of the heart and the opening and closure of the tricuspid and pulmonary valves have not been determined in the SCG signal so far.

Since both the opening and the closure of the mitral and the aortic valves are visible in the SCG, the latter was found suitable for the estimation of every CTI. Dehkordi et al. found SCG suitable for estimating TST with a 1.4% error and PEP with a 12.8% error against echocardiography (best of the tested methodologies) [90]. As for PCG, a higher percentage error (24.0%) was found for EMAT [90]. In the overall, PCG can be reliably used to estimate all CTIs.

It should be highlighted that a morphological analysis of the SCG signal, based on the identification of its fiducial points, may not be used to obtain the CTIs in case of pathology, as investigated by Işilay Zeybek et al. [100]. In fact, the morphology of the signal may be distorted and the fiducial points are not recognizable. Moreover, even in healthy cases, the morphology of the signal presents a high inter-subject variability [101]. It was proposed that combining the information from the accelerometer with the information from a co-located gyroscope helps in improving the estimate of the PEP [102].

Impedance Cardiography

Impedance Cardiography (ICG) is the measure of the changes in the thorax impedance generated by the changes in blood volume and velocity in the aorta within the cardiac cycle [90].

As highlighted in Figure 10, which proposes a representation of the ICG signal and its main fiducial points, the opening and closure of the aortic valves can be identified in the ICG as the B and X fiducial points respectively. In this way, the LVET and the PEP can be estimated. Even though ICG is suitable for estimating

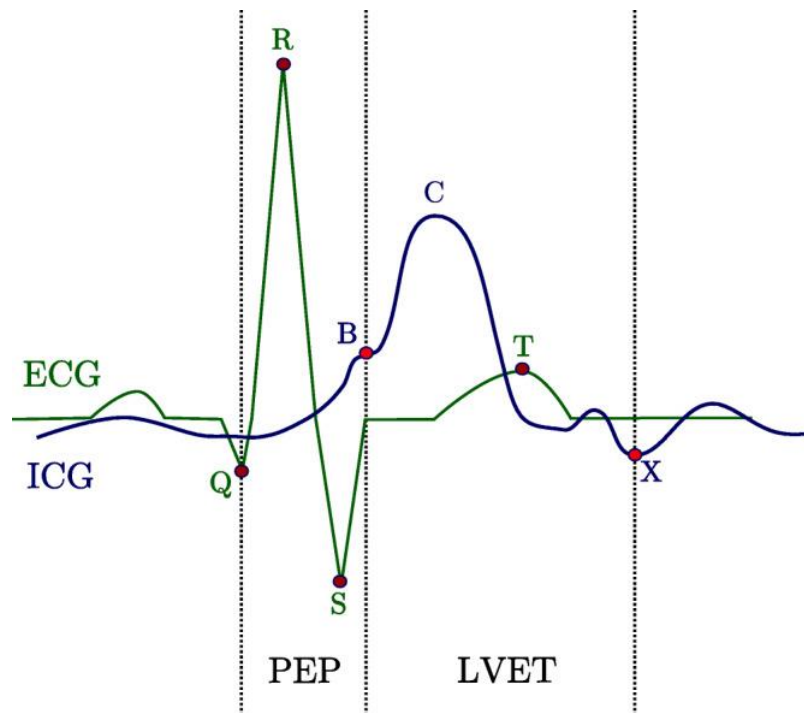


Figure 10: Definition of the fiducial points of the ICG signal [103].

every CTI, it was found severely sub-optimal in terms of accuracy and precision of the estimate with respect to PCG, SCG and even photoplethysmography [90,104]. This is mainly due to the technical difficulties in reliably detecting the fiducial points in the ICG signal [104].

Other signals

A variety of other signals have been proposed in the literature with the purpose of estimating the CTIs in a noninvasive way, even though their validity has not been yet extensively verified as in the case of PCG, SCG and ICG. Promising results were obtained from the analysis of the carotid pressure waveform [105], continuous wave radar signal [106], ballistocardiography [107,108] and photoplethysmography [104,109].

The wide number of signals that were exploited over the years to obtain a noninvasive assessment of CTIs proves that: 1) the potentiality of obtaining CTIs from biomedical signals is high; and 2) a noninvasive estimate of the CTIs would be extremely valuable for ambulatory and domicile applications.

2.3.2 Cardiac Time Intervals and Heart Failure

The possibility of using the CTIs to assess the status of HF-patients is considered highly appealing by the experts in the field. In the latest decades, several Authors investigated the correlation of one or more CTIs with respect to:

1. The intracardiac pressures, whose changes represent the first signal of an upcoming episode of decompensation.
2. The systolic and/or diastolic function of the heart, measured by means of some echocardiographic marker, which is directly correlated with the worsening of the condition of HF-patients.
3. Some clinical outcome related to the disease, such as the mortality or hospitalization rate.

In other words, three levels of analysis of the problem are possible: the intracardiac level of analysis, the functional level of analysis and the clinical level of analysis. In the next paragraphs the results of the main studies involving the analysis of the CTIs extracted from biomedical signals on one of the three mentioned levels are discussed. It should be underlined that a many studies exist that aim at correlating echocardiography-based CTIs with cardiac functionality and HF, but they are outside the purposes of this review.

Few works focused on the relationship between the CTIs and the intracardiac pressures in the state of the art. This is mainly due to the technical difficulties of performing this kind of studies, which involve invasive cardiac catheterization. In particular, right heart catheterization is required to obtain the Pulmonary Artery Pressure (PAP), which is particularly fascinating due to the tremendously positive results invasively obtained by CardioMEMS™. Some previous works highlighted that various characteristics of the heart sounds showed a positive correlation with the PAP, namely the S2 complexity and the ratio between the S2 complexity and the S1 complexity [110]; the S2 width and S3 strength [111]; the S1 and S2 energy [112]. In this sense, PCG could potentially provide the most complete information for the assessment of the cardiac function in patients affected by HF.

Concerning the timing relationships, Wang et al. experimentally found a strong correlation between the cEMAT and the right ventricular systolic blood pressure ($R = 0.81$) in four beagle dogs subjected to right ventricular catheterization and pharmacologically induced in a pulmonary hypertensive state [112]. The result is definitely promising, even though a wider study would be required to draw

conclusions. On the other hand, Shapiro et al. [113] and Efstratiadis et al. [114] found no direct correlation between the cEMAT and the left ventricular end-diastolic pressure. It can be concluded that the literature is still lacking robust evidence on this point.

The large majority of previous works focused on the correlation between CTIs and some metrics of the cardiac function. Moyers et al. investigated the relationship between CTIs extracted from PCG and the left ventricular dysfunction, defined as the presence of a left ventricular end-diastolic pressure higher than 15 mmHg together with an Ejection Fraction lower than 50%. They found that patients presenting left ventricular dysfunction were characterized by a significantly higher EMAT and EMAT/LVST [115]. Similarly, a higher EMAT and a lower LVST have been found to be associated with an impaired LV performance [116], with a lower LVEF [93,114,117,118] and with a lower maximum LV dP/dt [119]. Also TST was found to be inversely correlated with LVEF [93]. Kosmicki et al. found that CTIs extracted from heart sounds were better predictors of a lower EF than BNP, which is the gold standard at date (AUC = 0.88 vs 0.67) [117].

EMAT, cEMAT and EMAT/LVST can be extracted from heart sounds and were the object of the large majority of previous works. As described above, their correlation with metrics of the cardiac function is very promising. Nevertheless, a few Authors checked the correlation between the other CTIs, extracted from different biomedical signals, and the cardiac performance. It should be highlighted that Shah et al. found a moderate yet significant correlation between the ratios EMAT/LVST (extracted from electro-phonocardiography) and PEP/LVET (estimated through echocardiography) [93]. Therefore, since they are correlated, it's expected that the set of CTIs using the closure of mitral and aortic valves (EMAT, LVST and their ratio) and the set of CTIs using the opening and closure of the aortic valve (PEP, LVET and their ratio) should be suitable to reach the same clinical goals.

Cheng et al. used combined recordings of ECG, PCG and pulse volume signal and found that the ratio PEP/LVET is significantly associated with the ratio of effective arterial elastance (Ea) to ventricular end-diastolic elastance (Ees), which is an echocardiographic biomarker indicating the status of the ventriculo-arterial coupling [120]. The same Authors had previously demonstrated that NT-proBNP was linearly correlated to both PEP and PEP/LVET [121]. The PEP/LVET ratio was also proved to be inversely correlated with LVEF in ICG recordings by Thompson et al. [122].

Some very recent studies (from 2020 on) explored the influence of a CTIs-based monitoring on the clinical outcomes in patients affected by HF. Already in 2013, Constantino et al. highlighted that EMAT is significantly higher in HF patients and proposed a relevant mechanistic insight [123]. Later, Burkhoff et al. characterized the normality ranges for EMAT, cEMAT, LVST and cLVST in patients affected by HF, for the sake of comparison against a normal population [124]. Trabelsi et al. explored the diagnostic potentiality of EMAT, LVST and EMAT/LVST on 855 patients with suspected HF. They found that EMAT/LVST has the highest correlation with LVEF and they obtained sensitivity and specificity as high as 72% and 88% respectively with a threshold of 40% [12]. Similar results were achieved by Orter et al. using oscillometric brachial blood pressure measurements in a head-tilt condition used to simulate the physiological effects of HF: a significant reduction of cLVET and cTST along with a significant increase of cPEP and PEP/LVET was found [125]. Moreover, they found that the parameters went back to their baseline values after the end of the experiment, showing that the method may be valuable for monitoring purposes [125].

Wang et al. moved a step further and demonstrated that CTIs are meaningful not only to distinguish normal vs HF patients, but also HF phenotypes, i.e., HF with reduced EF against HF with preserved EF (more difficult to discriminate than the other). They found that a cEMAT higher than 11.54% differentiated patients with HF with preserved EF from patients with hypertension with the same accuracy as echocardiography (AUC = 0.83) [126].

More recently, other studies focused their effort on analyzing the effects of a CTI-based management of HF-patients on their long-term clinical outcomes. Zhang et al. found that a cEMAT higher than 13.8% is an independent predictive factor for Major Cardiac Adverse Events (MACEs) in HF-patients [127] and a cEMAT higher than 15% is predictive for cardiogenic death [128]. A similar result was obtained by Chao et al., who found that cPEP and cEMAT at discharge could both predict an adverse event (rehospitalization or death) within one year [129]. Shitara et al. prospectively enrolled patients hospitalized for AHF and followed up the variation of the CTIs during their treatment until discharge. They found that cEMAT progressively decreased over the recovery, whereas TST increased [130]. Lastly, Sung et al. conducted a prospective single-blind study and found that EMAT-based management of HF patients resulted in lower hospitalization rate and mortality at the 1-year follow-up than traditional symptoms-driven management [131].

In the overall, there is a great agreement among the experts in the field concerning the qualitative relationship between CTIs and cardiac function, and even with the clinical outcome of HF patients. To summarize, the following modifications occur in the CTIs in case of a worsening cardiac functionality due to HF:

- cEMAT and cPEP increase.
- cLVST and cLVET decrease.
- EMAT/LVST and PEP/LVET increase.

Figure 11 proposes a graphical representation of the changes occurring on the CTIs due to systolic HF, in relation to the intracardiac pressures and the main signals of interest (ECG and heart sounds).

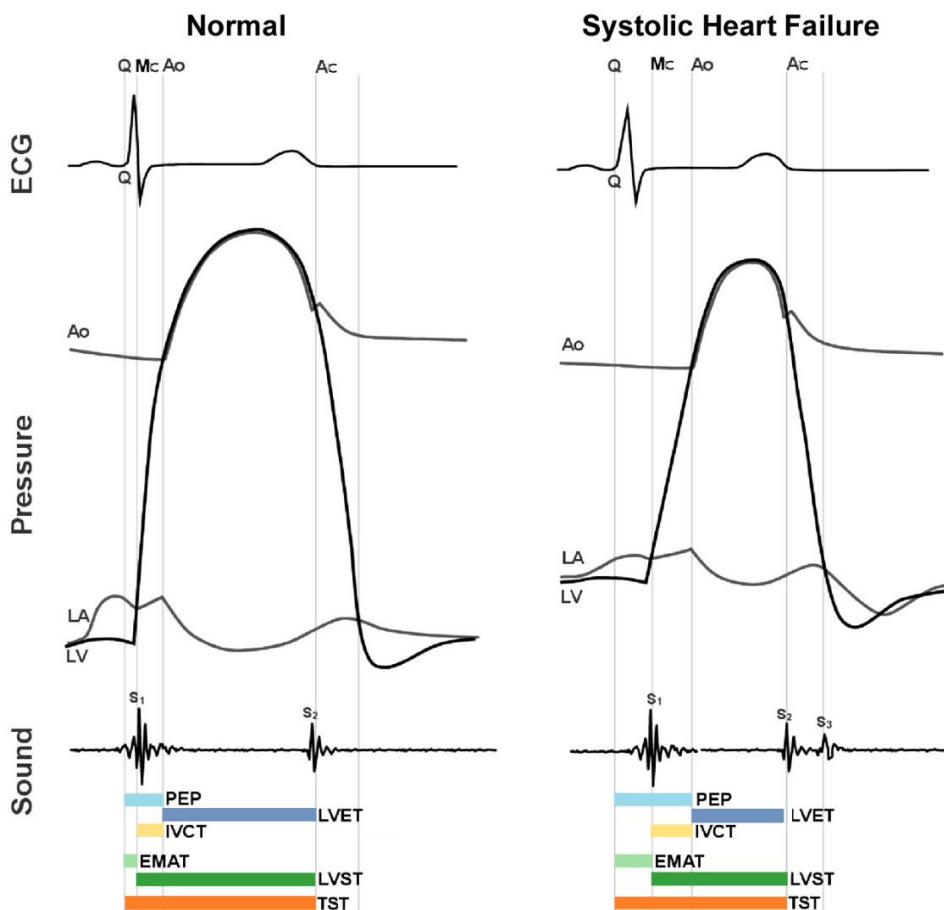


Figure 11: Differences in the CTIs due to the presence of Systolic Heart Failure with respect to a normal subject. The same definitions as in Figure 7 apply. Adapted from [93,94].

Some Authors tried to move a step further and analyze the problem from a quantitative perspective. In fact, for the method to be useful in the clinical practice, thresholds are needed to distinguish patients with an impaired functionality of the heart from healthy subjects.

The thresholds which were found discriminative for patients with an impaired cardiac function are reported in Table 2.

Table 2: CTIs' thresholds that were found discriminative for patients with an impaired cardiac function.

CTI	Threshold	Sensitivity and specificity	Reference
EMAT	> 100 ms	Se: 63%, Sp: 89%	[94,119]
	> 110 ms	Se: 64%, Sp: 86%	[12]
	> 120 ms	N/A	[132]
cEMAT	> 11.54%	Se: 55%, Sp: 90%	[126]
	> 13.8%	Se: 81.8%, Sp: 65.9%	[127]
	> 15%	Se: 44%, Sp: 94%	[115,128,129]
		Se: 54%, Sp: 92%	[114]
LVST	< 270 ms	Se: 71%, Sp: 82%	[12]
EMAT/LVST	> 40%	Se: 55%, Sp: 95%	[115]
		Se: 72%, Sp: 88%	[12]
PEP	> 89 ms	Se: 60%, Sp: 60%	[121]
LVET	< 272 ms, > 310 ms	Se: 63%, Sp: 60%	[121]

PEP/LVET	> 31%	Se: 60%, Sp: 62%	[121]
	> 42.3%	Se: 85.7%, Sp: 84.3%	[120]

It should be highlighted that most quantitative studies are grounded on the EMAT. This is reasonable because in HF the electrical behavior of the heart is not necessarily compromised, but its mechanical function is. Moreover, most studies rely on PCG to estimate the CTIs, therefore they can only rely on the CTIs involving the closure of the cardiac valves (and not the opening).

Many works propose thresholds that are suboptimal in terms of sensitivity but achieve a very high specificity. Even though the accuracy is not impressive, given the low sensitivity, a very high specificity confirms the suitability of some CTIs as biomarkers for the prevention of AHF. In fact, a positive result in a CTI-based test could be followed by further diagnostic investigations if needed, but it is of utmost importance that no decompensation episode is missed.

As already highlighted, an increased intracardiac pressure is not only associated with changes in the CTIs, but also with other variations in the heart sounds, like an increase in the energy of S1 and S2, the presence of S3 and sometimes of S4. CTIs are considered more reliable than the other biomarkers to monitor HF patients on a long-term basis because they were proved to show lower circadian variation besides a lower correlation with the age of the subject [133]. Nevertheless, using a combination of different biomarkers extracted from heart sounds may result in an even better prediction capability.

In fact, some works attempted to put together various information extracted from combined recording of ECG and heart sounds into a multivariate index capable of discriminating HF patients from healthy patients. Collins et al. grounded their multivariate model on LVST, strength of S3, maximum negative area on the P-wave and QTc interval in the ECG and used it to predict an increase in LV filling pressure in HF patients. They obtained an AUC of 0.83 even considering cases where the BNP was indeterminate [134]. Shapiro et al. used an index based on EMAT/LVST and S3, which was found to have an AUC of 0.89 for the diagnosis of LV dysfunction [113]. Shah et al. proposed an index based on the product of QRS duration, QR interval, S3 strength and cEMAT with an AUC of 0.89 for the detection of LV dysfunction [93]. The latter index was formally defined as Systolic

Dysfunction Index (SDI) by Dillier et al. and it was found that a SDI higher than 5 indicated a systolic dysfunction, and a SDI higher than 7.5 a severe systolic dysfunction [133]. Wang et al. found that a SDI higher than 5.43 yielded a sensitivity of 53% and a specificity of 91% [126]. Burkhoff et al. confirmed that SDI is higher in patients affected by HF [124]. In the end, Erath et al. developed an algorithm combining cEMAT, S3 strength and heart rate and proved that their model could detect HF-patients in phase of decompensation better than the traditional NYHA classification, with a median advance of 32 days with respect to the event [135]. The latter result is compatible to what obtained invasively in the MultiSENSE study [87].

2.3.3 The perks of multi-source Phonocardiography

As shown in the previous paragraph, the evidence supporting the value of various CTIs for the assessment of the cardiac function and thus for the prevention of AHF is, at date, pretty robust. Nevertheless, the technological benchmark highlighted that no real-life application currently exists that exploits this approach for the purposes of domiciliary monitoring. The reasons for this should be searched for in the easy-of-use of current technologies: as a matter of fact, none of the biomedical signals suitable for the extraction of the CTIs can be easily recorded at the patient's domicile by the patient himself or by an inexperienced caregiver. So far.

Among all techniques, the combination of ECG and PCG for CTI estimation and HF monitoring was studied the most over the last 20 years and most data are present showing the correlation between the extracted CTIs and the clinical outcomes in HF patients. For this reason, electro-phonocardiography was chosen as object of the present project.

Even though PCG has largely been considered a suitable signal for homecare applications, as a matter of fact, some technical issues still limit its applicability in a domiciliary context. One of them is the need for a careful positioning of the digital stethoscope over the chest of the patient. It was previously demonstrated that the quality of the PCG signal strongly varies over different recording points [136]. Also the time of closure of heart valves is different when measured at different recording points, due to the inhomogeneity of the acoustic response of biological tissues [137,138]. Figure 12 shows an example of what stated above.

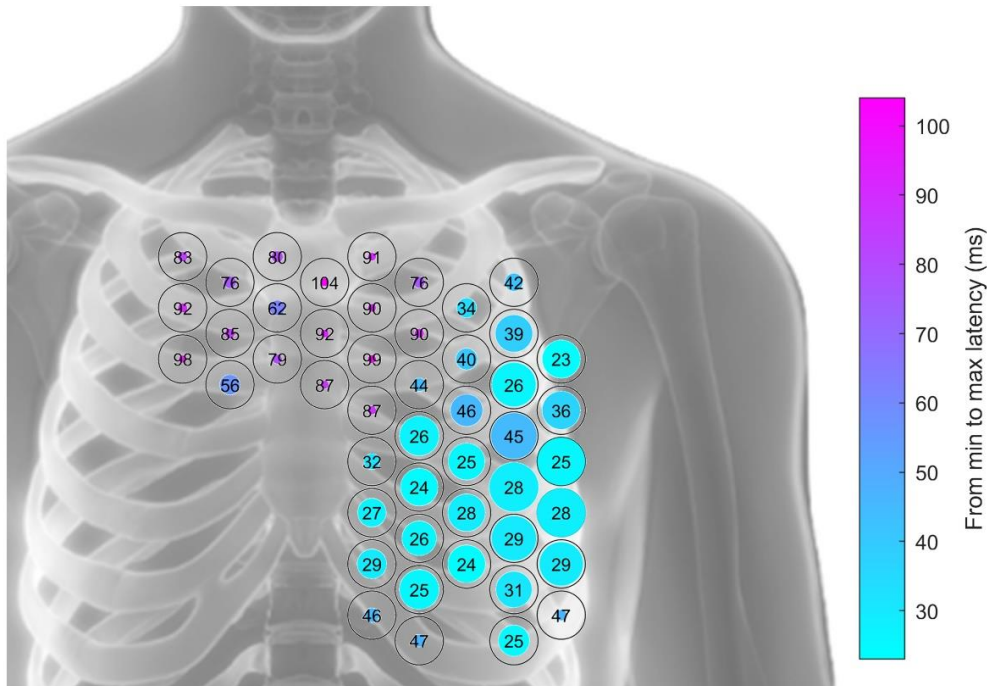


Figure 12: Visual representation of the variability of the quality of signal and of the latency of the closure of the mitral valve with respect to the ventricular depolarization. Each circle represents a microphone. The diameter of the colored circle represents the Signal-to-Noise Ratio of the signal recorded from that point of the chest. The color represents the estimated latency according to the colorbar on the right.

Moreover, the most suitable auscultation point depends on the application, as in traditional auscultation: the clinician knows *where* to locate the head of the stethoscope depending on *what* he/she wants to auscultate. A naïve user does not. Therefore, the positioning of the stethoscope by a naïve user cannot be trusted to obtain reliable results.

Theoretically, multi-source PCG is expected to provide a possible solution to this problem. By simultaneously recording multiple PCG signals from different points over the chest of the patient, the selection of the best auscultation point is shifted from the recording phase (i.e., from the user) to the processing phase (i.e., to the algorithm).

Even though it is a quite innovative methodology, multi-source PCG was already used in the past for different scopes. On one side, it proved a valuable tool for technical aspects, like signal compression [139], noise detection [140] or signal quality improvement [136,141]. On the other side, it sometimes proved more

efficient than its single-channel counterpart in clinical classification tasks. Features extracted from both single-channel and multi-channel recordings were successfully employed for the classification of subjects suffering from coronary artery disease against normal subjects [142–144], for the classification of cardiac murmurs [145,146], and for the estimation of the LVEF [147]. In the context of the estimation of features related to the heart timing, Paiva et al. [148] used a two-channel approach to improve the accuracy of their estimation of the PEP. They selected the best channel according to a feature related to the signal contrast and reduced the estimation error from 10.1 to 9.2 milliseconds [148].

All above-mentioned works rely on 2 to 6 microphones, positioned over the patient's chest by an expert user over the traditional auscultation areas using anatomical landmarks. Their focus is rather research than real-life domiciliary applications. A few exceptions exist. Radzievsky et al. [147] used a 36-microphone array which was originally developed for lung sound recordings and must be placed on the back. Zhang et al. [149] proposed a multi-channel device embedding 16 microphones in a memory foam pad to be located over the subject's chest. Nevertheless, the device is optimized in terms of shape, dimensions, and distribution of the sensors for the recording of lung sounds rather than heart sounds. In the end, Guo et al. [150] designed a vest embedding 72 microphone sensors covering the entire thorax to record heart sounds and map their propagation. Their approach is definitely inspiring, but the resulting product is more suitable for research than to a real-life use due to its bulkiness.

To my best knowledge, no previous examples of the usage of a pad embedding a large number of microphones with a high spatial resolution optimized for the recording of heart sounds exist in the literature. Moreover, no previous work explores the use of multi-source PCG at a high spatial resolution for the estimation of CTIs.

This PhD project aims at filling this gap and at proposing to the scientific community a multi-sensor device for the simultaneous recording of ECG and multiple PCG signals at a high spatial resolution along with the algorithms to estimate some of the main CTIs from recordings performed by inexperienced users through the device in a simulated homecare setting.

Chapter 3

Design of the multi-sensor array

3.1 Conceptualization of the array

The design of a wearable device always involves peculiar challenges that need to be faced to make the device usable by the common population and suitable for the use on the widest possible range of patients, regardless their body shape or other physical characteristics. Since the proposed device is unique and little previous experience was available to ground the project on, a first phase of conceptualization was carried out.

The goal of this paragraph is to present the reasoning behind the main design decisions that led from the idea to the architecture of the array.

The array must be suitable to record two types of signals: ECG and PCG. The two signals have different characteristics and different roles for the estimation of the features of interest. The ECG signal has a repeatable and well-known waveform, suitable for a morphological analysis. For the estimation of the CTIs, the information to be extracted from the ECG signal is the time of occurrence of the depolarization of the ventricles. Even though the shape of the waveform varies depending on the positioning of the electrodes, a morphological analysis is besides the scopes of the application of interest. Therefore, the recording of the ECG signal is not particularly critical, and the positioning of the electrodes can be interpreted as secondary with respect to the other requirements.

The main challenge resides in the recording of the PCG signals. The latter is a quasi-periodic signal whose morphology has not been considered interpretable so far. It is generated by the closure of four different cardiac structures (the heart valves), whose contribution to the waveform of the two main heart sounds is yet to be properly understood. Nevertheless, it is well known that the signal presents different characteristics depending on the point of auscultation.

Traditionally, four auscultation points (or areas, according to a more modern interpretation) are defined, one for each heart valve [96]:

- Mitral area: fifth left intercostal space, along the midclavicular line
- Tricuspid area: fourth left intercostal space next to the sternum
- Aortic area: second right intercostal space next to the sternum
- Pulmonary area: second left intercostal space next to the sternum

The location of the auscultation areas is presented in Figure 13. It should be highlighted that the auscultation points are not necessarily placed right over the cardiac valve of interest, but mainly depend on their blood flow [151] and were identified thanks to decades of clinical experience. All the traditional auscultation areas are located in the left hemithorax, except for the aortic area, which is located on the right margin of the sternum. All the auscultation areas are defined using the intercostal spaces as fiducial points, that are not easily identifiable by an inexperienced user.

The idea of developing a multi-sensor array has the main objective of guaranteeing that, even if the device is positioned by a naïve user, unaware of any knowledge about the cardiovascular system or auscultation, the traditional auscultation areas are covered. Therefore, an L-shaped pad was designed, with the largest area covering the left hemithorax and the smallest area covering the right side of the sternum where the aortic area is expected to fall. Figure 13 presents a graphical representation of the shape of the array in its optimal position over the chest.

As Figure 13 shows, the device is suitable for covering all the four traditional auscultation areas. For the sake of comparison, an average male thorax is presented: the relative spatial relationships among the shape of the array and the four auscultation areas may differ in case of a smaller or wider chest. The suitability of a single device for all body shapes was object of analysis in the pre-clinical validation phase.

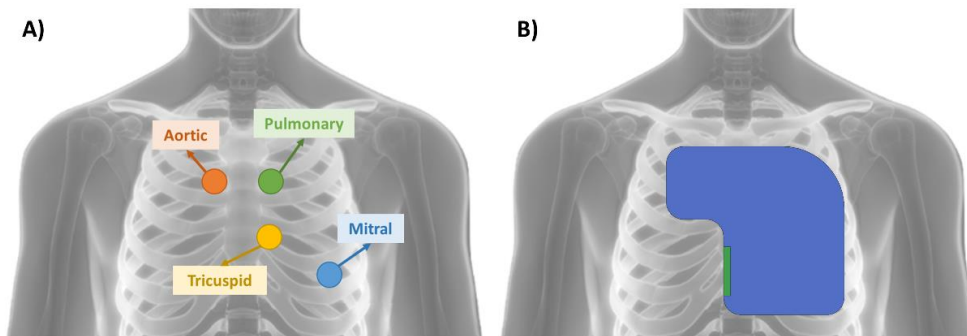


Figure 13: Correlation between the traditional auscultation areas (panel A) and the design of shape of the array (panel B).

The next challenge consists in how to distribute the microphones over the thorax. The main constraint in this sense is posed by the intercostal spaces: in fact, the traditional definition of the auscultation points is grounded on the positioning of the stethoscope in specific intercostal spaces. Such constraint is dictated by the difference in sound propagation properties across different biological tissues [152]: the filtering effect of the bone tissue would affect the quality of the recordings, and therefore it should be avoided.

As anticipated, a naïve user cannot be relied on autonomously finding the intercostal spaces correctly. Therefore, the distribution of the microphones should guarantee that at least some of the microphones fall within the intercostal spaces, regardless the positioning performed by the user. To achieve this, the distance between closest neighboring microphones should be lower than the distance between consecutive intercostal spaces. In other words, the microphones are required to be located on a grid with a sufficiently high spatial resolution. Considering the size of an average rib, a distance between neighboring microphones lower than 20 mm should be considered as sufficient. It can be derived that some tens of microphones are required to cover the area of interest with a sufficient spatial resolution. Forty-eight microphones were used in this work.

On the available surface, microphones can be distributed in different ways. Among the infinite possibilities, two options were hypothesized:

1. **“Homogeneous” array**: microphones are distributed homogeneously over the surface of the array.
2. **“Cluster” array**: the concentration of microphones is higher in correspondence of the expected traditional auscultation areas.

Figure 14 proposes a graphical representation of the above-described distributions of the microphone sensors over the array surface. Accordingly, two versions of the multi-sensor array were designed and implemented.

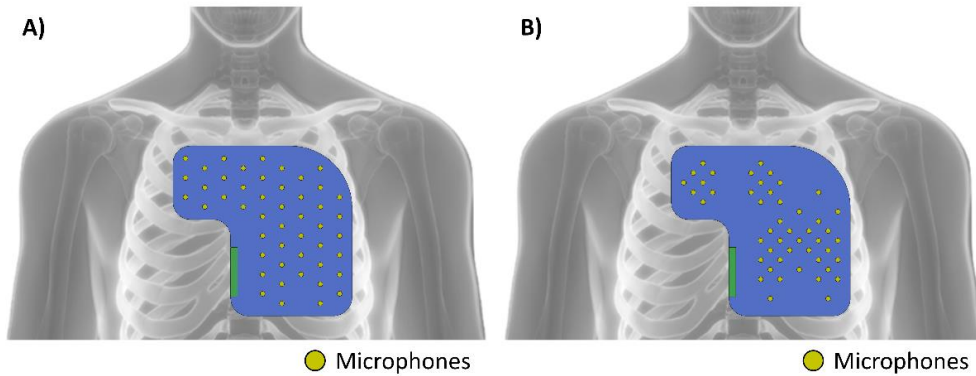


Figure 14: Distribution of the microphone sensors over the surface of the array, in two options: A) homogeneously distributed; B) higher concentration over the traditional auscultation area.

As anticipated, the positioning of the electrodes could be considered secondary to the distribution of the microphones. The best electrodes' positioning to correctly identify the time of occurrence of the ventricular depolarization would be the first standard lead, with an active electrode on each wrist and the reference electrode on the right ankle. The same lead could be recreated on the chest by placing the active electrodes in the subclavian areas and the reference electrode on the right side of the thorax. Nevertheless, even such adaptation would require to severely increase the area of the pad, which would increase its bulkiness and possibly limit its usability in domiciliary setting.

A different solution was pursued by identifying a custom non-standard lead which exploits the available space and does not require to modify the shape or the size of the pad. The defined custom lead involves the positioning of three electrodes as follows:

- A first recording electrode is located over the second intercostal space, along the mid-clavicular line.
- A second recording electrode is located over the fifth intercostal space, along the mid-clavicular line.
- The reference electrode is located over the sternum, at approximately the same distance from the two recording electrodes.

A differential configuration was preferred to a single-ended one to reduce the effect of the common mode interference. The references based on the intercostal spaces are meant to give an approximate idea of the positioning on the chest: in fact, the location of the electrodes is fixed on the array, therefore their location with respect to the fiducial points of the chest depends on the body shape, as happens with the microphones. Moreover, it should be highlighted that the positioning of the electrodes on or off a rib is not relevant. Figure 15 proposes a graphical representation of the positioning of the electrodes with respect to the typical anatomical positioning of the heart in the chest.

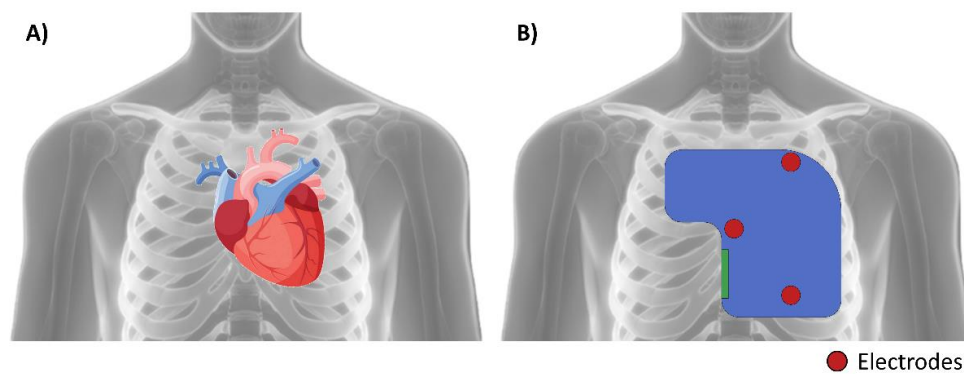


Figure 15: Comparison between the anatomical position of the heart (panel A) and the positioning of the electrodes in the designed device (panel B).

As highlighted by Figure 15, the proposed positioning of the electrodes is dictated by the need for having the two recording electrodes on opposite sides of the heart and of the reference electrode, to obtain a signal of sufficient amplitude. The main drawback of this approach resides in the fact that the morphology of the signal is strongly dependent on the orientation of the electrical axis of the subject. Since the device is expected to be used by a single subject for monitoring purposes, the latter may not be a problem, but the identification of an appropriate time reference, invariant with respect to the orientation of the electrical axis, was investigated in the signal processing phase.

Besides microphones and electrodes, which constitute the core of the proposed approach, a Magneto-Inertial Measurement Unite (MIMU) completes the set of sensors embedded in the array. The purpose of the MIMU is twofold. On one side, it was previously demonstrated that the posture of the subject influences the intracardiac pressures [153–155]. Its influence on the Cardiac Time Intervals was never investigated, but due to their correlation with the intracardiac pressures, it can

be hypothesized. Therefore, the availability of a MIMU would enable an assessment of the posture of the subject and, if necessary, an appropriate compensation of the clinical features of interest. On the other side, the MIMU would allow a simple detection of the motion artifacts. Sudden movements of the patient can decrease the quality of the signal and affect the estimation of the CTIs: if motion could be accurately detected, affected signal segments could be removed from the analysis.

Following the presented considerations, the multi-sensor array was equipped with three types of sensors:

1. Three electrodes, aimed at recording an ECG signal.
2. Forty-eight microphones, aimed at recording 48 PCG signals from different points of the chest with a sufficiently high spatial resolution.
3. A MIMU, aimed at sensing the subject's posture and motion that could influence the quality of the recording.

Figure 16 shows a graphical representation of the array with the embedded sensors.

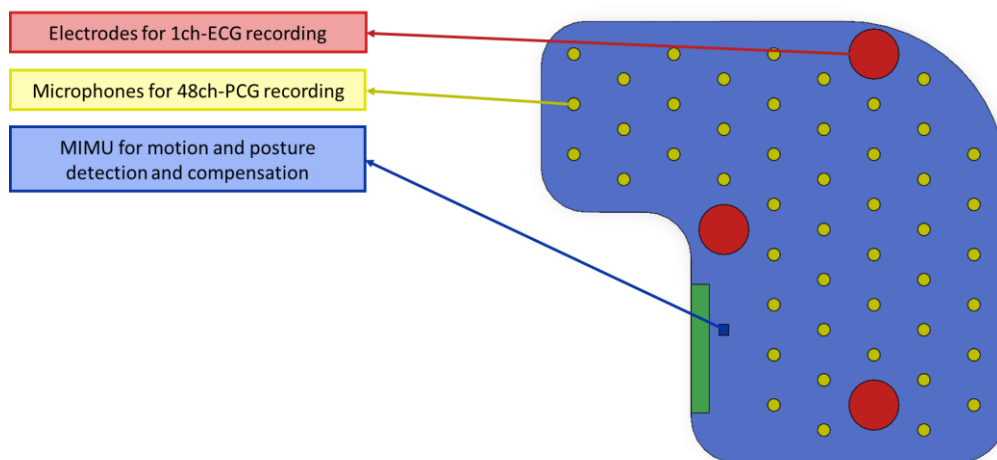


Figure 16: Graphical representation of the multi-sensor array and the embedded sensors.

Besides the sensors, a further characteristic is required to make the multi-sensor array apt for use by inexperienced users on the widest possible range of body shapes: a sufficient flexibility. In fact, both the microphones and the electrodes need to contact the skin of the subject to work properly, for different reasons. In the case of the microphones, the acoustic vibrations on the chest are quite weak and the filtering effect of the air would further diminish the quality of the signal. In the case

of the electrodes, the contact is fundamental to ensure conductivity. The flexibility of the array can be achieved by mounting the sensors on a flexible Printed Circuit Board (PCB) and designing a custom case to be 3D printed with an elastomeric material.

Given the innovative nature of the proposed device, the latter was patented in Italy (Patent ID 102020000014428 – “Multi-sensor device for the prevention of heart failure”, 17/06/2020). The project was realized thanks to a Proof of Concept funding (PoC Instrument 2020-2022) awarded by Compagnia di Sanpaolo.

3.2 Electronic design

In its final conceptualization, the device is expected to be used by a naïve user in a domiciliary context. For this purpose, the device should be microcontroller-based, embed the algorithms to extract the parameters of interest and communicate the results of the analysis to the smartphone of the patient. Nevertheless, given the novelty of the sensor side, a first prototyping phase was carried on with the double-sided scope of validating the concept from a technical and clinical perspective and gathering sufficient real-life data to design and optimize the algorithms. In this phase, a multi-sensor array has been designed and developed that is completely analogous to the final device, with the exception that the signal processing does not take place on board the microcontroller: instead, the array is connected to a commercial I/O device and the signals are processed on a computer.

The architecture of the system was designed considering that the array was meant to be used in connection with a commercial I/O device by National Instrument™ – the multifunction I/O device DAQ USB 6210. The latter offers 8 differential analog input channels and is equipped with a 16-bit Analog-to-Digital Converter (ADC), suitable for the biomedical signals of interest. The electronic design of the device is grounded on four main requirements:

1. The signals need to be acquired using up to 8 differential analog channels and hence they need to be multiplexed.
2. All the signals must be sampled simultaneously, not to artificially modify the temporal relationships among them, which is a key point for the application to AHF monitoring.
3. The sampling frequency must guarantee a temporal resolution of at least 1 millisecond to guarantee a sufficient resolution on the estimated CTIs.

4. The amplitude of the signals input to the commercial I/O device must be balanced properly using the entire dynamics of the ADC and not cause saturation.

Figure 17 proposes a graphical representation of the architecture of the designed system.

The architecture involves three main blocks:

1. **PCG sensing.** The block is devoted to the sensing and conditioning of the acoustic waves on the thorax. It consists of 48 microphones and 48 front-end circuits.
2. **ECG sensing.** The block is devoted to the sensing and conditioning of the electrical signal on the subject's skin. It consists of 3 custom conductive electrodes. The conditioning is performed using a traditional front-end, involving a differential amplifier, and the reference is obtained as a traditional Driven Right Leg (DRL) circuit.
3. **Signal recording.** The block is devolved to the sampling, multiplexing and acquisition of the signals. A microcontroller is in charge for defining the control signals and defining their timing.

At this stage, the MIMU was not connected. Each block is described in detail in the next paragraphs, along with the design decisions that were taken.

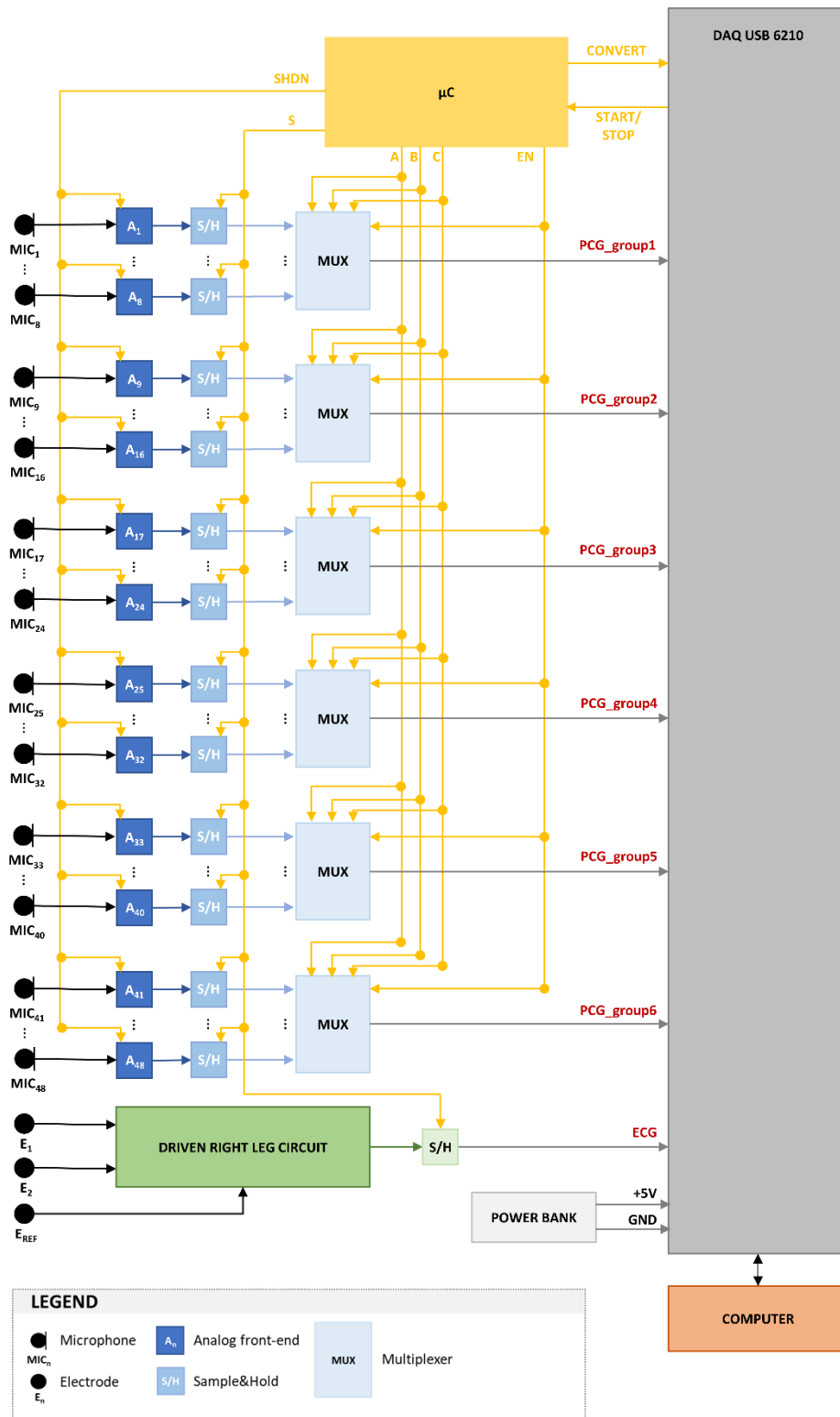


Figure 17: Architecture of the designed system.

3.2.1 PCG sensing

The PCG sensing block is based on three sub-blocks, namely:

- A microphone sensor
- A low-noise amplifier with a gain of 50 dB
- A high-pass filter with a cut-off frequency of 2 Hz

The microphone sensor is responsible for transducing the acoustic vibrations into an electric signal. The amplifier and filter constitute an analog front-end block which is responsible for amplifying the signal by 50 dB and removing the baseline wandering. Figure 18 presents the electrical circuit of the PCG sensing block and identifies its sub-blocks: 48 identical blocks are embedded in the array.

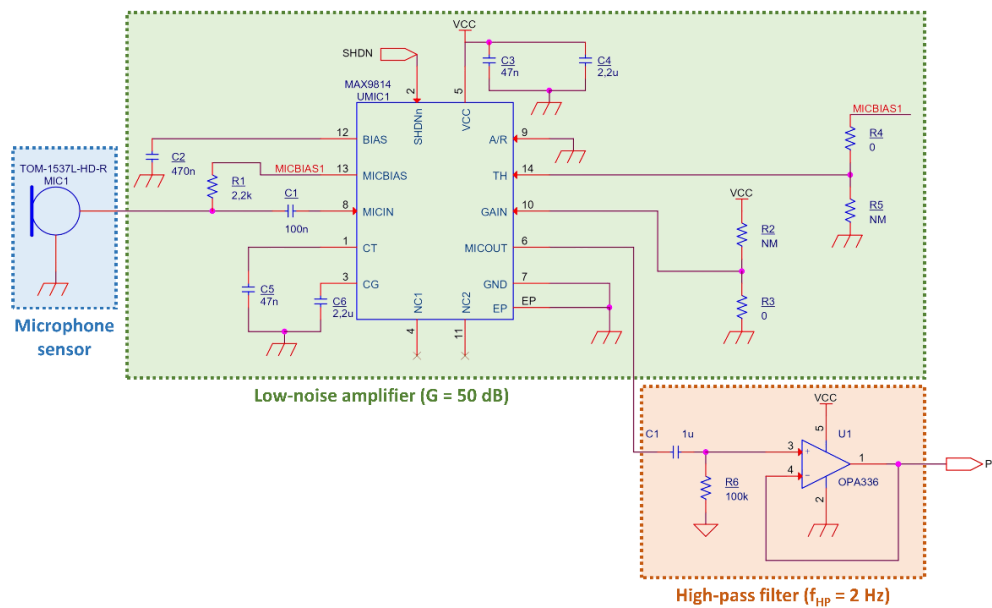


Figure 18: Electrical circuit of the PCG sensing block, comprising the microphone sensor TOM-1537L-HD-R by Pui Audio™ and the analog front-end MAX9814 by Maxim Integrated™.

Microphone sensor

A microphone sensor is a transducer that converts mechanical vibrations (audio) into an electrical signal. The choice of the microphone sensor is particularly critical for the application of interest and is driven by the characteristics of the acoustic signal to be acquired. Table 3 summarizes the main characteristics of the first and second heart sounds, that are the focus of the application of interest.

Table 3: **Characteristics of the PCG signal (S1 and S2)** [96,156,157].

Sound	Intensity	Frequency	Duration	Split
S1	< 20 mPa	20 Hz – 100 Hz	~ 140 ms	20 ms – 30 ms
S2	< 20 mPa	20 Hz – 150 Hz	~ 110 ms	20 ms – 80 ms

As shown, the frequency content of the two main heart sounds is focused on the lowest frequencies of the audible spectrum. The second heart sound is slightly shorter in duration and higher pitched than the first. Typically, microphone sensors on the market cover the large majority of the audible range but they are optimized for higher frequencies and might be suboptimal in the low-frequency region. Also, the weak intensity of S1 and S2 makes the choice of a highly sensitive microphone sensor mandatory.

Two families of microphone sensors suitable to this application exist on the market, namely the electret condenser microphones (ECM) and the microphones based on Micro-Electro-Mechanical Systems (MEMS microphones). ECM is the most consolidate technology and is based on a capacitive operating principle: a capacitor is created between a moving thin metallic membrane (called diaphragm) and a static metallic backplate. The pressure on the diaphragm caused by the acoustic vibrations triggers a variation in the distance between diaphragm and backplate which reflects in a variation in the capacitance. MEMS microphones can be either capacitive or piezoelectric. Capacitive MEMS microphones are dominant at date and are based on a similar operating principle to ECMs, but the pressure-sensitive diaphragm is etched into a silicon wafer via MEMS processing. On the contrary, in piezoelectric MEMS microphones the membrane is realized using a piezoelectric material, capable of directly converting the mechanical changes in electrical charge changes without the need of a metallic backplate [158]. Figure 19 proposes a graphical representation of the structure of the three categories of microphone sensors.

Even though capacitive MEMS microphones have the largest share of the market at date, both families are widely used in various electronic devices for

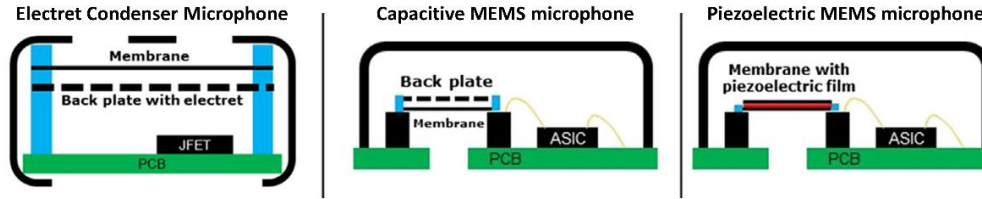


Figure 19: Cross-sectional design of the three categories of microphone sensors. Adapted from [158].

capturing sound, because they have different benefits and drawbacks. MEMS microphones can typically provide better performances at smaller size, but this comes at cost of the low-frequency cut-off, which is typically higher. On the other side, ECM proved more resilient in difficult environments.

For the application of interest, three characteristics of the microphones are fundamental:

- The frequency bandwidth, which should be suitable for acquiring low-frequency acoustic waves, as the heart sounds have frequency components as low as 20 Hz.
- The sensitivity, which should be maximized given the small amplitude of the signal of interest.
- The dimensions, which should be minimized to ensure the required spatial resolution without affecting the array flexibility and thus its capability of adapting to the chest surface.

As anticipated, size and frequency bandwidth are partially correlated, since the dimension of the diaphragm influences the high-pass cut-off frequency of the sensor: a diaphragm with a smaller diameter can physically not transmit low-frequency components without attenuation, regardless its manufacturing principle. In this scenario, condenser microphones and MEMS microphones offer complementary solutions to the problem: MEMS microphone smaller size is preferable, but the higher sensitivity offered by condenser microphones is appealing.

In this work, the best trade-off was found in the TOM-1537L-HD-R by Pui Audio™. Table 4 presents the main characteristics of the selected microphone.

Table 4: Characteristics of the selected microphone sensor (TOM-1537L-HD-R by Pui Audio™).

Parameter	Value
Diameter	4 mm
Sensitivity	-37 dB \pm 3 dB
Signal-to-Noise Ratio (SNR)	68 dB
Frequency range	20 Hz – 20 kHz
Output load impedance	2.2 k Ω
Directivity	Omnidirectional

The selected microphone sensor is an ECM. Accordingly, its performances in terms of sensitivity and SNR are among the highest available on the market. Moreover, it provides a good trade-off between size and frequency bandwidth: even with a diameter as small as 4 mm, the producer guarantees a high-pass cut-off frequency as low as 20 Hz, suitable for recording the two main heart sounds without sensible phase shift. To date, no commercially available MEMS-microphone could guarantee an equally low high-pass cut-off frequency.

Analog front-end

As anticipated, the amplitude of the signal output of the microphone is low. Therefore, to improve the amplitude of the signal and exploit the dynamics of the ADC, analog amplification is carried out. The latter was grounded on a commercial high-quality microphone amplifier: the MAX9814 by Maxim Integrated™. Figure 20 presents a simplified block diagram extracted from its datasheet.

The MAX9814 is a high-quality amplifier optimized for microphone sensors. It provides a low-noise bias to the microphone and is characterized by an Input-Referred Noise Density as low as 30 nV/ $\sqrt{\text{Hz}}$, suitable for small amplitude signals. The gain of the amplifier is achieved through three stages:

1. A low-noise pre-amplifier (gain: 12 dB)

2. A variable gain amplifier (VGA), controlled by a programmable automatic gain control (AGC) circuitry (gain: 0 dB to 20 dB, with 20 dB when the AGC is deactivated)
3. An output amplifier with a selectable gain (gain: 8 dB, 18 dB, 28 dB)

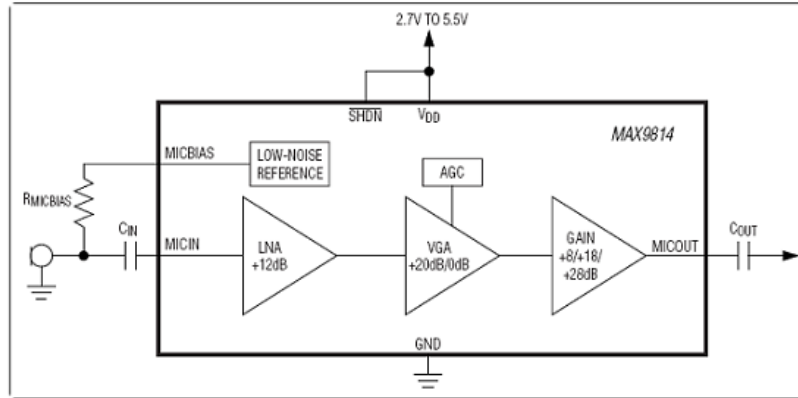


Figure 20: Block diagram of the MAX9814 by Maxim Integrated™. From the datasheet.

In this work, the AGC was deactivated to avoid differences in gain between different channels and the gain of the output amplifier was set to 18 dB (mid-range). The final overall amplification was thus set to 50 dB. Nevertheless, the availability of multiple gain options could help in obtaining a custom amplification depending on the subject's body shape in the future. It should be highlighted that saturation due to DC components is avoided by means of a 100 nF input capacitor.

The output of the MAX9814 is subjected to a passive first-order high-pass filter with a cut-off frequency of 2 Hz. The latter decreases the effect of baseline wandering and removes the bias inserted by the MAX9814. In the end, a buffer is introduced to decrease the impedance of the PCG sensing block with respect to the next block, i.e., the sample and hold.

3.2.2 ECG sensing

Figure 21 presents the electric circuit of the ECG sensing blocks and the sub-blocks, each provided with the corresponding gain and/or cut-off frequency. In the overall, a gain of 380 is achieved along with the filtering of frequency components below 6 Hz on the differential mode, and the reduction of the effect of the common mode by means of the DRL circuit.

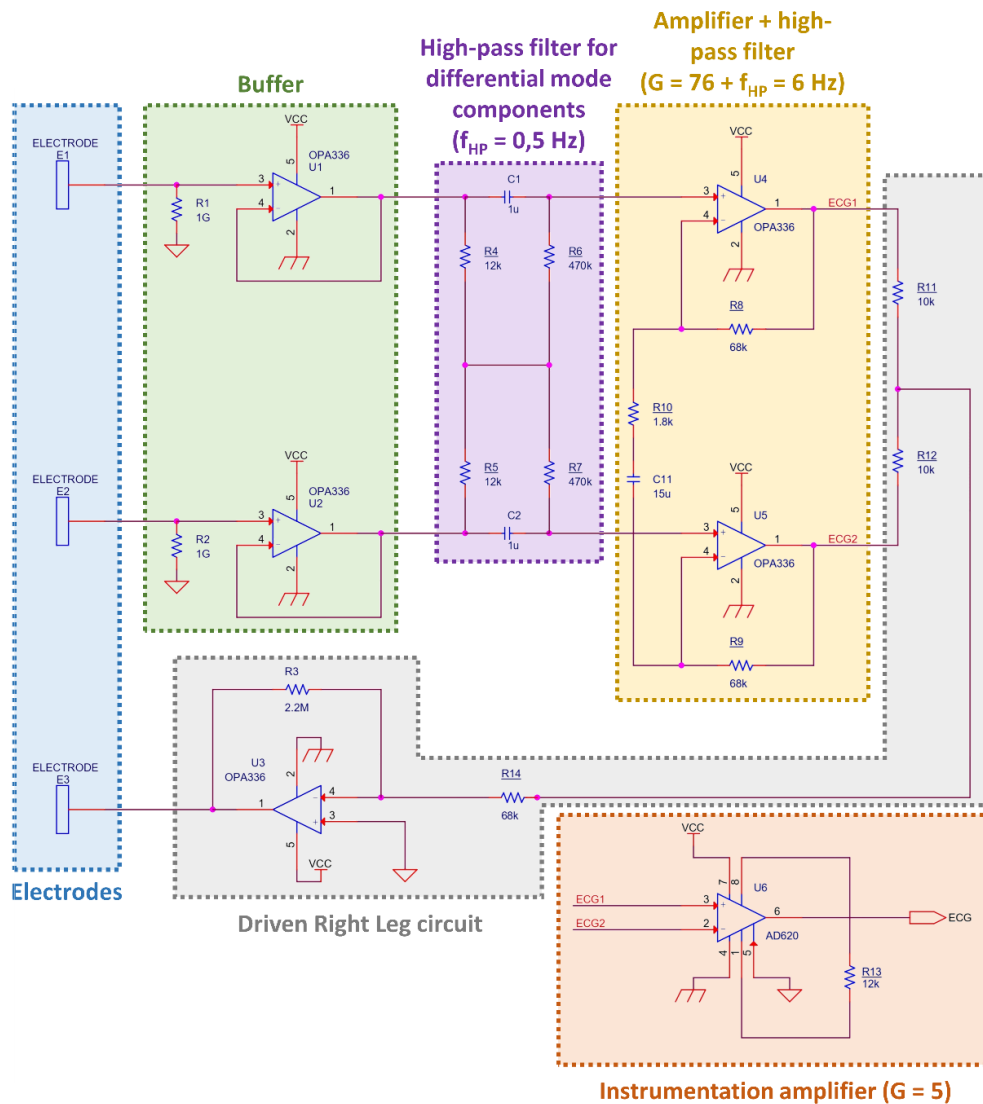


Figure 21: Electrical circuit of the ECG sensing block, comprising the custom-made stainless-steel electrodes and the conditioning circuit, based on a DRL technique.

Electrodes

The sensing and acquisition of the ECG is a consolidated clinical problem with a number of consolidated technological solutions. In the clinical practice, ECG is typically sensed by means of disposable wet electrodes with an Ag/AgCl skin interface. Even if this technology has optimal performances for short-term recordings in an ambulatory or hospital setting, it is not apt for use in a domiciliary setting by inexperienced users. In fact, the disposable electrodes need to be changed

and correctly re-positioned at each use of the device, which definitely limits its usability.

The mentioned issue is not novel and is common to every wearable device involving the recording of an ECG signal. Given the impressive trend in the use of wearables for home monitoring, particularly in the cardiological field, many different solutions have been tested in the literature over the past decade. Among the various possible solutions, three main families of reusable electrodes can be identified, namely wet electrodes, dry conductive electrodes, and capacitive electrodes [159–161].

Wet electrodes involve the use of a liquid or hydrogel electrolyte to be placed at the interface between the skin and the sensing area of the electrode, with the scope of improving the conductivity properties [161]. They are the go-to choice in a clinical setting, they are considered suboptimal in domiciliary applications, where solutions requiring no maintenance are preferred.

Dry conductive electrodes still work on a conductive operating principle but, contrarily to wet electrodes, do not need to have any gel interposed [161]. Their use in wearables is object of wide research and multiple materials were explored including metals, polymers, and carbon-based materials [160]. Nevertheless, the use of dry electrodes poses new challenges, since the avoidance of a liquid electrolyte increases the skin-electrode contact impedance by several orders of magnitude, thus worsening the effect of noise and motion artifacts [161].

Capacitive electrodes work on a different operating principle: the electrode and the skin are separated by a layer of a dielectric material, as to recreate a capacitor. The concept of capacitive electrodes is very appealing for the use in wearables, because they would avoid any direct contact between the patient and a part subjected to a voltage. Nevertheless, their use in ECG monitoring has often proved critical and the design of the conditioning circuit rather complicated [160].

Figure 22 presents a graphical interpretation of the operating principle of the three families of electrodes and a model of their contact with the skin.

In this work, the choice fell on dry conductive electrodes due to the combination of ease of use and performances. Concerning the material, among the many available options, stainless-steel disks with a diameter of 16 millimeters were

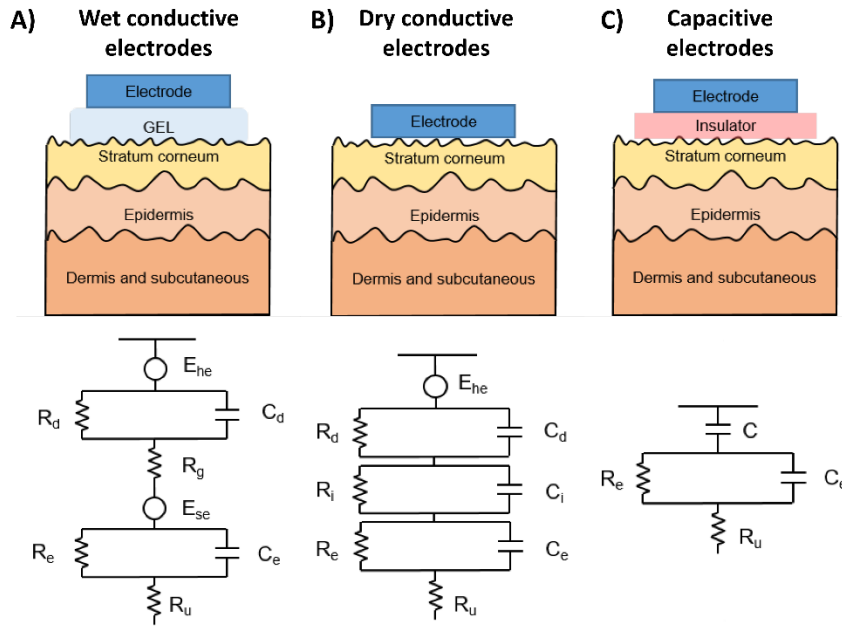


Figure 22: Graphical representation of the electrode-skin interface and its electrical model for respectively A) wet conductive electrodes, B) dry conductive electrodes and C) capacitive electrodes. Adapted from [162].

selected. In fact, stainless steel proved a great candidate because of its good electrical properties at a low price and high availability [163–165]. Moreover, a diameter of 16 mm was previously proved to be sufficient to obtain a comparable quality of the signal to disposable Ag/AgCl electrodes when ECG is recorded at rest [166].

Conditioning circuit

The conditioning circuit is based on a typical differential ECG front-end, with the reference generated by means of the well-known DRL circuit. Figure 22 presents the electric circuit diagram. In this paragraph, the identified sub-blocks are presented, along with their utility for the recording of a good-quality ECG signal.

Buffer. As already highlighted, dry conductive electrodes show an equivalent impedance 10 to 100 times higher than traditional wet electrodes. To deal with this, a first buffering stage with a high input impedance (1 G Ω) is inserted. The buffer has the scope of decoupling the high impedance of the sensing block from the rest of the circuit.

High-pass filter for differential mode components. In a differential acquisition modality, as the one proposed, the ECG signal is typically subjected to two types of noise contributions, which ought to be treated differently: a differential mode noise contribution and a common mode noise contribution. It is of utmost importance not to translate the common mode components into differential mode components: in this way, their effect would be much more difficult to deal with. With this scope, the high-pass filtering stage is designed to act on differential mode components only. The value of the passive components is defined to ensure a high-pass cutoff frequency of 0.5 Hz, suitable to remove the baseline wandering and avoid it to cause saturation in the amplifying stage.

Amplifier + high-pass filter. Each of the two active channels is pre-amplified. The amplification block relies on a rail-to-rail operational amplifier (OPA336 by Texas Instruments) in a non-inverting configuration. The gain is set to 38 for each channel. The amplification block is also provided with a high-pass filtering effect, active on differential components only, thanks to the use of the capacitor C11. The high-pass cut-off frequency is set to 6 Hz, suitable for the application of interest (QRS-complex components start from 10 Hz).

Driven Right Leg circuit. Until this point, no reduction was applied to the effect of common mode noise contributions. Nevertheless, common mode components may be important in the ECG acquisition and are mainly related to the effect of the electric interference due to the power line. A well-known and widely used method to deal with common mode rejection in ECG acquisition is the DRL circuit, first described by Winter and Webster in 1983 [167]. The technique works on negative feedback: the common mode from the patient is sampled through two averaging resistors, inverted, amplified and actively delivered back to the patient, through the reference electrode, with the scope of reducing the interference on the patient himself [167].

Instrumentation amplifier. In the end, the two signals from the two active channels are fed to an instrumentation amplifier (AD620 by Analog Devices), which amplifies the difference between the inputs. The gain is set to 5, which was considered a good trade-off between exploiting the dynamics of the DAQ USB 6210 analog input channels and not cause saturation of the AD620.

3.2.3 Management of the signal recording

Paragraphs “3.2.1 PCG sensing” and “3.2.2 ECG sensing” showed how the variations of physiological variables were converted into biomedical signals and how those signals were amplified and filtered according to the characteristics of the physiological variable and the application of interest. All the described processing was carried on analog signals. Once the analog signals are conveniently conditioned, they can be sampled, converted into their digital version and recorded.

As anticipated, in the first prototyping phase, the recording system is based on the commercial I/O device DAQ USB 6210 by National Instruments. The recording of the signals relies on three different steps:

1. **Sampling**, i.e., the conversion of a continuous-time signal into a discrete-time signal. It is performed independently on all 49 signals (48 PCG + one ECG), using 49 sample-and-hold chips, but the same control signal (S/H) is used for all channels. In this way, all signals are sampled at exactly the same time instant, and no temporal difference is inserted by the sampling operation.
2. **Multiplexing**, i.e., the combination of multiple different signals into a single one on a shared line. Here, 48 PCG signals are combined 8-by-8 to obtain 6 signals to be acquired by the USB 6210. This step is required due to the USB 6210 technical specifications, since the latter is equipped with 8 analog input lines, which are not sufficient to record all 48 channels independently. Six 8-to-1 multiplexers are used. Multiplexers are controlled by three control signals (A, B and C) forming up a 3-bit counter. Moreover, the multiplexer can be enabled using a further control signal (EN).
3. **Analog-to-digital conversion and acquisition on a computer**. This step is performed by the I/O device DAQ USB 6210, which embeds a 16-bit ADC with a maximum conversion frequency of 250 kSa/s with a time resolution of 50 ns. Two control signals need to be used to properly control the DAQ USB 6210, namely a START/STOP signal to define when the acquisition should begin and end, and a CONVERT signal determining the time instants when the conversion of the analog input signals is performed by the ADC.

The recording is controlled by the user using a custom-designed application running on a Windows computer. The user can set the duration of the recording and pressing a button he/she can start the recording. In that moment, the START/STOP control signal is set to 1.

The management of the control signals, which are mainly responsible to define the timing of the sampling, multiplexing and conversion of the signals, is a task of the microcontroller embedded in the device. An 8-bit ATmega8 microcontroller was used for this purpose. The firmware of the microcontroller was programmed in Assembly language to ensure the highest control on the counters and on the timing intervals. The microcontroller periodically checks if the START/STOP signal is set to 1, and if so, it starts sets to 0 the EN signal to enable the multiplexers and starts generating the S/H, CONVERT and A/B/C signals. Figure 23 presents the temporal diagram of the control signals.

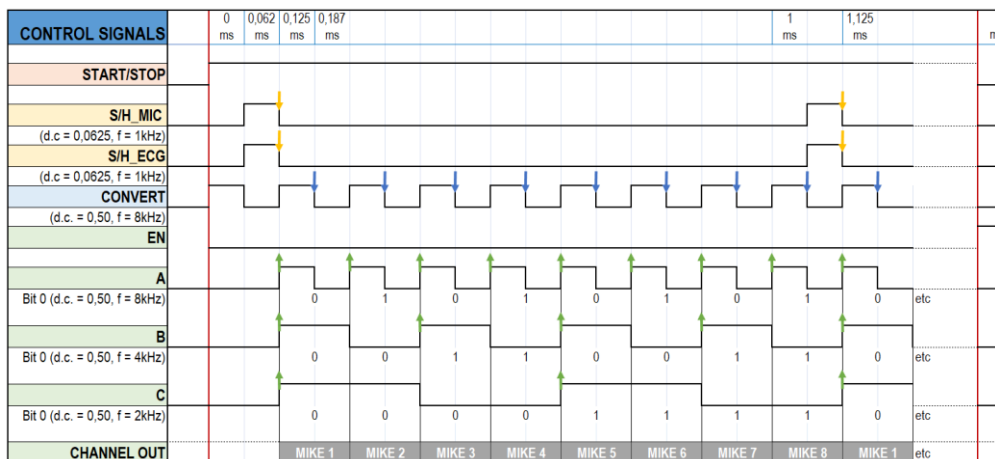


Figure 23: Temporal diagram of the digital control signals generated by the microcontroller to define the sampling frequency, the multiplexing of the PCG signals and the conversion of the signals from analog to digital performed by the internal ADC of the NI DAQ USB 6210.

As shown, the sampling frequency is set to 1 kHz for both the ECG and the PCG channels. Accordingly, the conversion of all 48 channels must take place within a 1 ms time interval.

The selected sample&hold (SMP04 by Analog Devices) holds the last sample at the falling edge of the S/H control signal. As soon as the first sample is kept in hold mode, the counter starts counting. This is achieved by means of three control signals (A, B and C, where A is the Least Significant Bit of the counter). At each combination of the A, B and C control signals, the multiplexers switch: when A =

0, $B = 0$ and $C = 0$ the input corresponding to the first channel is set to the output; when $A = 1$, $B = 0$ and $C = 0$ the input corresponding to the second channel is set to the output; and so on. When the counter reaches the $A = 1$, $B = 1$, $C = 1$ combination, i.e., a 1-ms time interval has gone, a new sample is sampled, and the counter starts again.

The conversion by the ADC is controlled by the control signal CONVERT, generated by the microcontroller and transmitted to the NI DAQ USB 6210. Each multiplexed signal contains samples from 8 different channels within the 1-ms time interval defined by the sampling frequency. Accordingly, the CONVERT signal must have an 8-times higher frequency (8 kHz) with a duty cycle of 50%. The conversion was set to take place at the falling edge of the CONVERT signal, so that the output of the multiplexer is stable.

As a result of the signal recording chain, the ECG and the 48 PCG channels are all sampled simultaneously at a 1 kHz sampling frequency and they are acquired as multiplexed 8-by-8 by the computer. The demultiplexing takes place on the computer.

3.2.4 Implementation: realization of the Printed Circuit Boards

The above-described electrical circuits were implemented in the form of two distinct Printed Circuit Boards (PCBs). The rationale for dividing the circuit into two PCBs is two-sided. On one side, the array to be located on the thorax should be characterized by a high level of flexibility to adapt to the chest thorax, so the minimum possible electronics ought to be located on board. On the other side, as anticipated, the use of the NI DAQ USB 6210 is temporary, and a re-engineering of the signal recording stage can be forecasted. The separation of the circuit into two PCBs will allow for redesigning the front-end PCB only, while the multi-sensor array could be preserved.

Figure 24 presents a graphical illustration of how the designed architecture was divided into the two PCBs. Details about the two PCBs and their realization are provided in the following paragraphs.

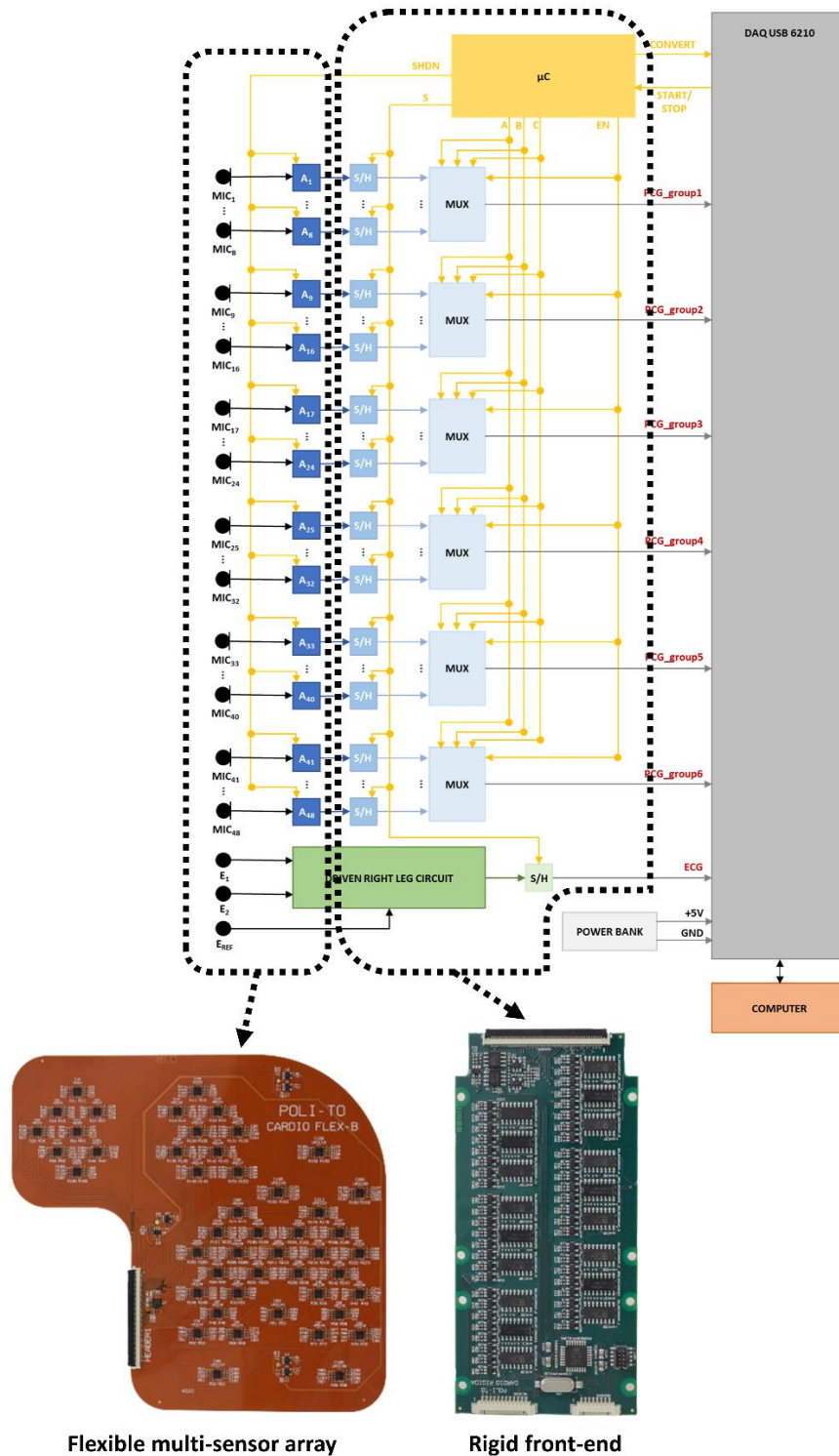


Figure 24: Implementation of the designed architecture in two PCBs, a flexible PCB with the sensors and the conditioning circuit to be placed on the thorax and a rigid PCB with the remaining

Flexible multi-sensor array

The sensors and their conditioning circuits are mounted on a flexible PCB. The PCB was realized in Kapton, a polyimide film typically used in flexible electronics applications. The PCB was realized in 4 layers, organized as follows:

- Top layer: electronic components (MIMU, MAX9814, part of the ECG conditioning circuits), connectors, electrical connections
- Inner layer 1: ground
- Inner layer 2: positive supply
- Bottom layer: microphones, pads for electrodes

The PCB presents a total thickness of 353 μm . The obtained flexibility is more than sufficient to best adapt to the conformation of the chest of the subject. The PCB realization and mounting was contracted to a specialized company. Only the mounting of microphones and electrodes was conducted internally, since it required manual soldering instead of industrial soldering.

A fundamental aspect of the realization of the flexible array was the distribution of the sensors. The latter followed specific mechanics and ergonomics considerations which will be described in paragraph “3.3 Mechanical design”.

As shown in Figure 24, the output of the flexible PCB are 3 ECG signals, 48 PCG signals and the power supply. Therefore, the PCB was equipped with a 70-pin connector to communicate with the front-end.

Rigid front-end

The rigid front-end mounts the remaining electronics, i.e., the sample-and-hold chips, the multiplexers, the microcontroller, and part of the ECG conditioning circuit. The mentioned components do not require to be located on the chest of the patient and occupy a rather large space which would unnecessarily increase the rigidity of the flexible array. Therefore, they were conveniently separated from the latter and located on a traditional rigid PCB to be connected with the array by a flat cable and located next to the subject.

The rigid front-end was implemented in the form of a 4-layer FR4 board and was realized and mounted by a specialized company. The four layers are organized as follows:

- Top layer: electronic components, connectors, electrical connections

- Inner layer 1: ground, electrical connections
- Inner layer 2: positive supply, electrical connections
- Bottom layer: electrical connections

It should be highlighted that whereas the flexible PCB is mostly traversed by analog signals, a number of digital control signals run through the rigid PCB. For the best management of the digital signals, which are characterized by fast transitions, some of the electrical connections were located in the inner layers as buried connections.

The rigid PCBs is equipped with 3 connectors to provide the required interface to the array, on one side, and to the NI DAQ USB 6210, on the other side. The interface with the flexible array is ensured by means of a 70-pin connector, as described above. The interface with the NI DAQ USB 6210 is made up of two connectors, one for the analog signals (ECG, 6 multiplexed PCGs, ground and power supply) and one for the digital signals (START/STOP and CONVERT).

3.3 Mechanical design

In the realization of a wearable device, the design of the mechanical aspects is not secondary to the design of the electrical circuits. In fact, the ergonomics of the device and its usability are strongly influenced by the choice of its dimensions, shape, and material.

In the case of interest, the design of the mechanics of the wearable multi-sensor array followed the considerations presented in the paragraph “3.1 Conceptualization of the array”. To resume, the multi-sensor array should fulfill the following requirements:

- The pad should cover the four traditional auscultation areas.
- The distribution of the microphone sensors should have a sufficiently high spatial resolution to ensure that some microphones fall within the intercostal spaces regardless the exact positioning of the device.
- The pad should be flexible enough to adapt to the conformation of the thorax of the subject to ensure a good contact between the sensors and the skin.

The goal of this paragraph is to present further details about the mechanical design of the multi-sensor array, according to the proposed conceptualization. In

particular, the distribution of the sensors over the array is proposed and some insight about the design of the flexible case are presented.

3.3.1 Dimensions, shape and distribution of the sensors

As anticipated, two versions of the array were designed, which differ in terms of distribution of the microphones. Figure 25 proposes the drawing of the two versions of the flexible PCB. Only the most relevant dimensions are reported for readability reasons. All dimensions are expressed in millimeters. The CAD design of the PCBs was carried on through SolidWorks™.

The drawings in Figure 25 represent the bottom side of the array, where the sensors are located. In other words, the array is looked at from the chest side. It can be observed that the array is L-shaped and covers a surface of approximately 149 mm x 141 mm. In the optimal forecasted positioning, the right side of the L, with an area of 101 mm x 141 mm, covers the left hemithorax from the second to the fifth intercostal spaces and from the left border of the sternum (which the 70-pin header border should be aligned to) until the midclavicular line. The left side of the L, with an area of 61 mm x 48 mm, should cover the aortic area on the right hemithorax. The dimensions were designed considering the dimensions of the chest of a wide-chested male subject (worst case scenario): the array will cover a wider portion of the chest in case of a thinner subject.

Both the MIMU and the reference electrode were located approximately over the sternum, separating them from the left border by approximately 10 mm. The positioning of the MIMU over the vertical axis was not critical. The positioning of the reference electrode, instead, was guided by the positioning of the two recording electrodes: it was located at the same distance from both.

The distribution of the microphones was expected to cover the four auscultation areas while creating a grid of sufficient spatial resolution to ensure that at least some of the microphone sensors could always cover every intercostal spaces. In the “homogenous” version, the microphones were organized in 9 columns distanced by 16 mm. The microphones over the same column were also distanced by 16 mm, but the columns were shifted by 8 mm from each other on the vertical axis to increase the spatial resolution. In the “cluster” version, the microphones were located focusing on the areas where the auscultation areas should fall in case of optimal positioning. In those areas, the spatial resolution of the microphones is higher than in the “homogeneous” version since each microphone is distanced from its closest

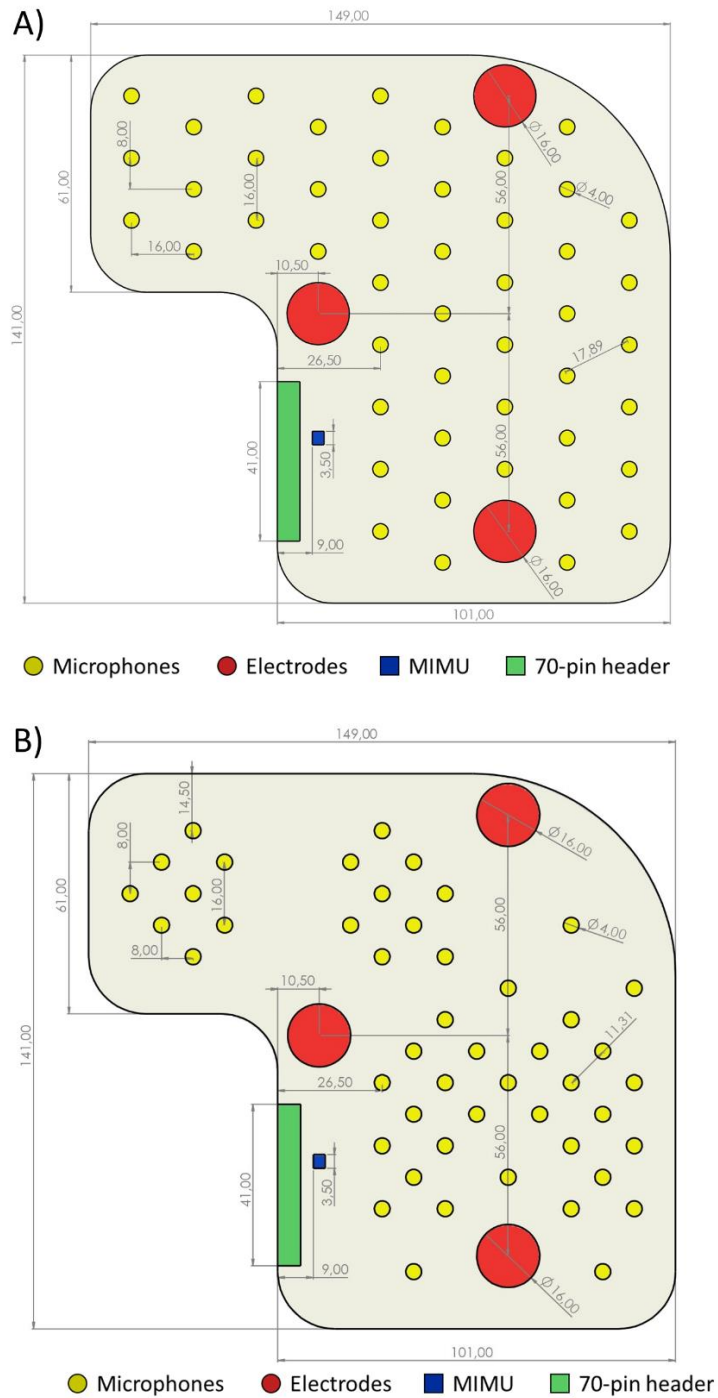


Figure 25: Dimensioned drawings of the flexible PCBs in the version with homogeneously distributed microphones (panel A) and in the version with the microphones concentrated over the traditional auscultation areas (panel B). All dimensions are expressed in millimeters.

neighbors by 8 mm both on the horizontal and on the vertical axis. Nevertheless, some microphones are located outside the expected auscultation areas, even if with a lower spatial resolution: they are meant to ensure a good covering of the auscultation areas even in case of suboptimal positioning of the array.

The 70-pin header was located on the left border of the wide side of the L for convenience. Nevertheless, it may help in providing a good reference for the positioning performed by a naïve user.

3.3.2 Design of the case

The design of the case is particularly important in the application of interest. In fact, on one side, the case is the part of the system in contact with the human body: an appropriate case is needed to ensure biocompatibility and patient safety throughout the life cycle of the device. On the other side, the case must not worsen the properties of the device, particularly its flexibility.

The particular shape of the array and the presence of distributed sensors makes it evident that a complete customization is needed. Figure 26 shows the CAD design of the case for the “cluster” version of the device, developed using SolidWorks™.

As it can be observed, the case is composed by two parts: a hollow housing, to host the flexible PCB, provided with appropriate holes in correspondence of the sensors, to allow their contact with the skin of the subject; and a cover, to be placed on top of the PCB and secured by means of double-sided tape.

The realization of the case was planned to ensure the maximum flexibility at a sufficient robustness and durability. Among multiple possibilities, the choice fell on a 3D-print approach. In particular, the VisiJet® M2E-BK70 elastomeric resin by 3D Systems™ was used for the purpose. The selected material is characterized by a 70 Shore A hardness (similar to an automotive tire) and by an elongation at break of 42%, which give an idea of the achieved flexibility and of the good resilience to break. Moreover, the material was declared biocompatible by the producer (USP Class VI testing).

Figure 27 presents pictures of the array in its case, without the cover to allow for a proper understanding of how the PCB fits into the housing.

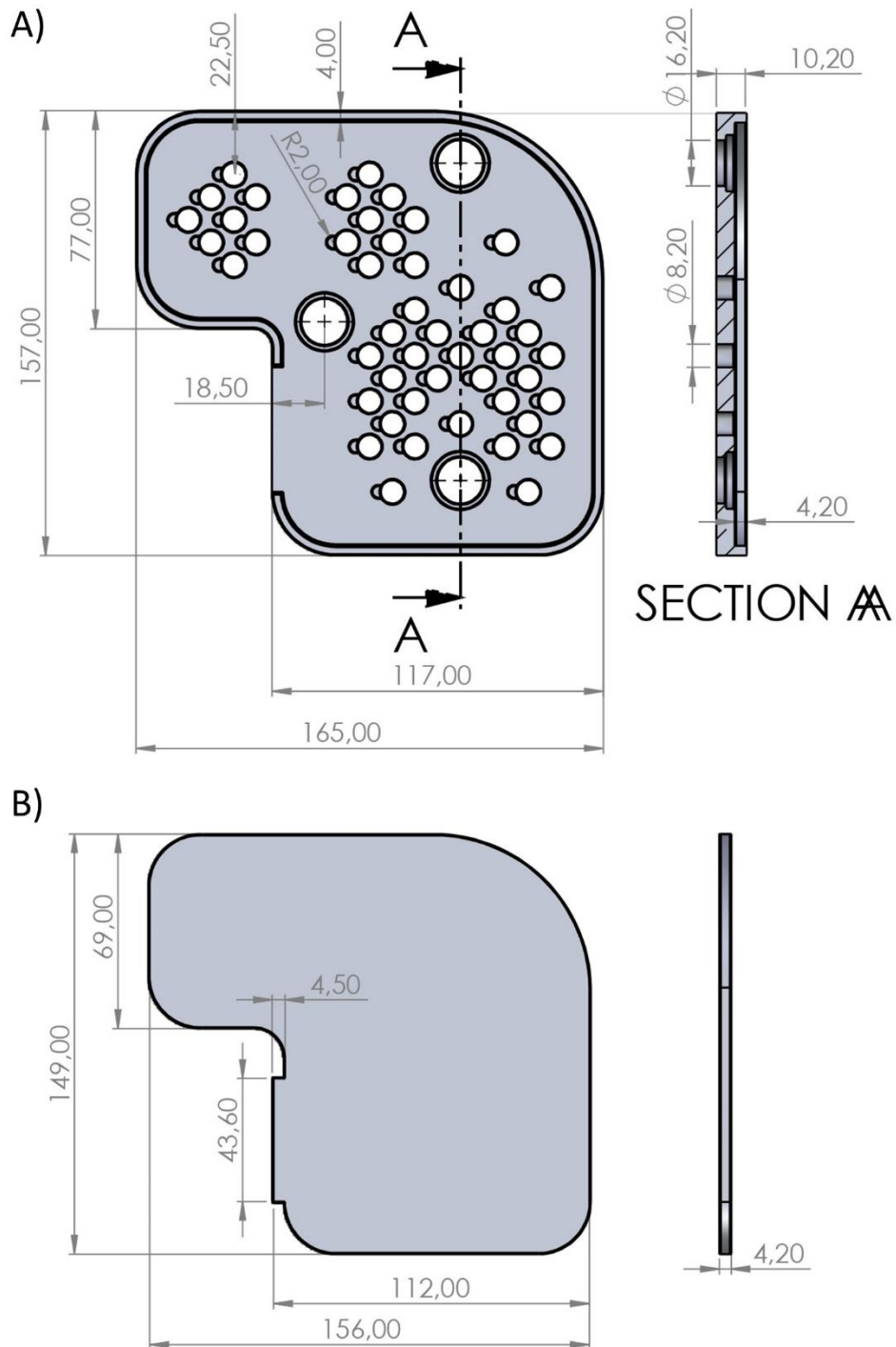


Figure 26: Dimensioned drawings of the case of the flexible PCBs in the “cluster” version. Panel A: housing, where the flexible PCB is inserted. Panel B: cover. All dimensions are expressed in millimeters.

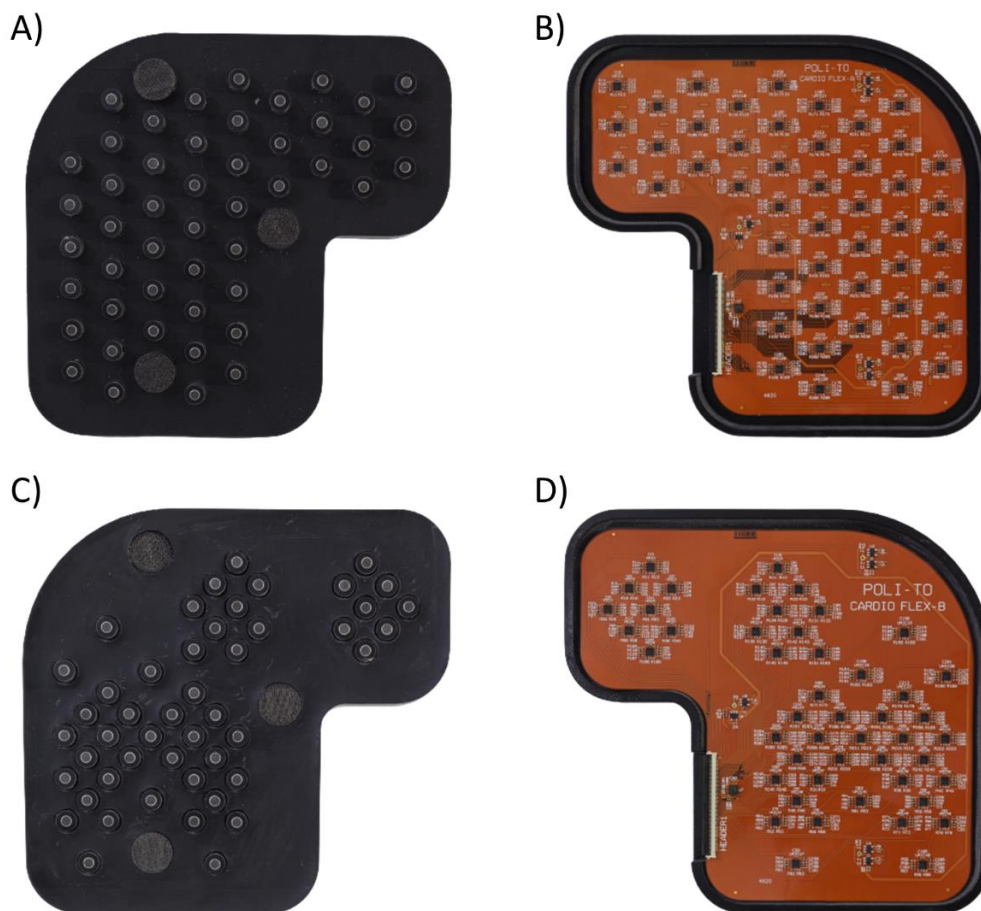


Figure 27: Pictures of the array in its case (without the cover). Version "homogenous" - chest side (A) and top side (B). Version "cluster" - chest side (C) and top side (D).

3.4 Testing of the complete system

In the previous paragraphs, the idea behind the multi-sensor array was presented, along with details about its design and realization. It was also highlighted that, given the novelty of the approach, the multi-sensor array was realized in a prototype version to validate the idea behind its design and its usability in a real-life monitoring scenario.

Following these considerations, the multi-sensor array is not, in its first version, a stand-alone device but must be connected to a computer by means of other devices to work.

The goal of this paragraph is to summarize the components of the system and to define the setup to be used to perform the recordings using the designed multi-sensor array.

3.4.1 Complete system and setup

The complete setup involves five fundamental elements:

1. The flexible array
2. The rigid front-end
3. The NI DAQ USB 6210 device
4. A computer with a custom application installed
5. A 5 V power bank

To perform the recordings, the subject is expected to lay supine and bare-chested on a bed or examination table. The flexible array is located on the chest of the subject and connected by means of a 70-pin flex cable to the rigid front-end, which can be located next to the subject on the examination table. On the other side, the front end is connected to the NI DAQ USB 6210 device by means of two custom flat cables, one for the analog signals and one for the digital signals. The power supply is provided by means of a power bank to decouple the subject from the power line and increase the safety of the system with respect to the macroshock

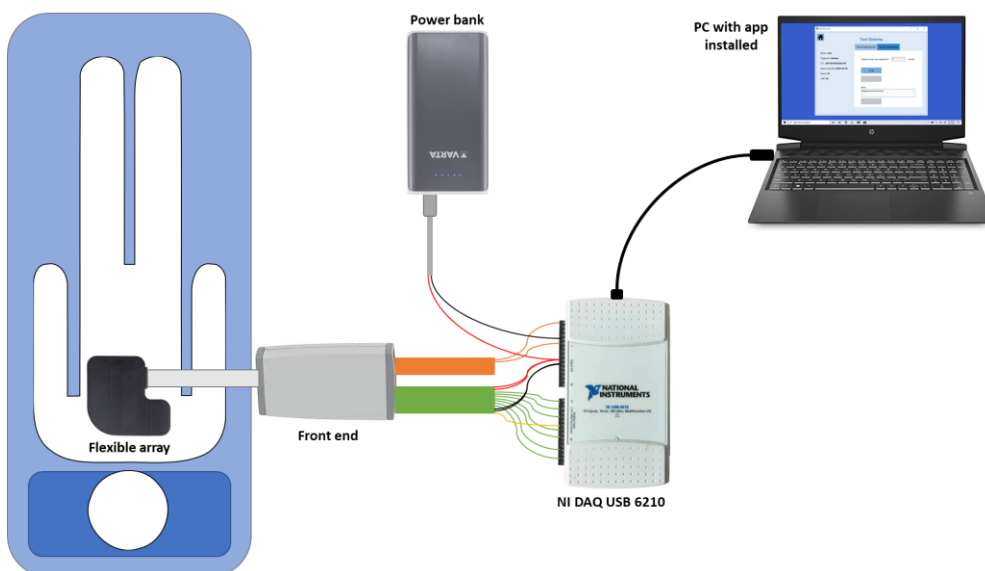
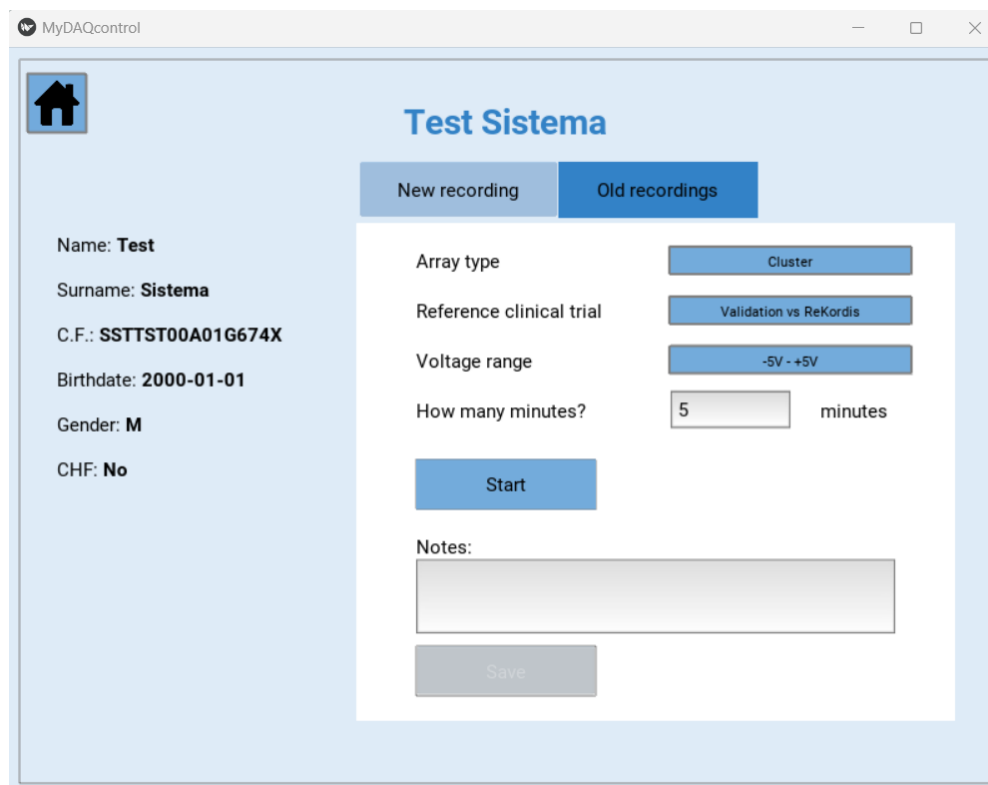


Figure 28: Block diagram of the complete setup. Relative dimensions are not meant to be realistic.

hazard. The power bank works at a 5 V voltage and can provide up to 2.4 A of current. The NI DAQ USB 6210 is connected to a computer by means of a USB cable. Figure 28 proposes a graphical representation of the block diagram of the complete setup.

The recording is managed using an application installed on a Windows computer, programmed in Python for the purpose. The application allows the user to define:

1. The type of array used for the recording (“homogenous” or “cluster”).
2. The duration of the recording (in minutes).
3. The dynamics of the NI DAQ USB 6210, among the ± 1 V or the ± 5 V options. This helps in partially customizing the dynamics depending on the characteristics of the subject.
4. Optionally, the clinical trial the recording belongs to.
5. Optionally, experimental notes in the form of plain text.



The screenshot shows a Windows application window titled "MyDAQcontrol". The main interface is titled "Test Sistema" and features a home icon in the top left. On the left side, there is a form for user information: Name: Test, Surname: Sistema, C.F.: STTST00A01G674X, Birthdate: 2000-01-01, Gender: M, and CHF: No. The main area has two tabs: "New recording" (selected) and "Old recordings". Below the tabs, there are several configuration options: "Array type" set to "Cluster", "Reference clinical trial" set to "Validation vs ReKordis", "Voltage range" set to "-5V -- +5V", and "How many minutes?" set to "5" minutes. There is a "Start" button below these options. At the bottom, there is a "Notes:" field with a text input area and a "Save" button.

Figure 29: Interface of the designed application devolved to perform the recordings with the multi-sensor array.

Figure 29 shows a sample of the interface for a fictitious patient “Test Sistema”.

When the user presses the Start button the START/STOP signal is set to 1 and transmitted to the entire system. The recording starts, a plot window is shown to the user with the goal of allowing a monitoring of the signals throughout the recording time. In the plot window the ECG and the 6 multiplexed PCG channels are visualized over a 10-second running window. The user can wait until the end of the recording or terminate it whenever needed by pressing the combination Shift+C. Then, the user can decide whether to save the recording or not. When the recording is saved, a JSON file is created containing a matrix of size N-by-7 (where N is the length of the recording in samples), along with the parameters set by the user.

At this point, the recording is ready for signal processing, to extract the clinical features of interest. The signal processing is performed on the computer using Matlab™.

Chapter 4

Algorithms for Signal Processing

4.1 Introduction

The proposed multi-sensor array outputs an ECG signal, 48 PCG signals and 3-axial accelerometer, 3-axial gyroscope, and 3-axial magnetometer signals. The signals from the MIMU were not used in this phase. The ECG signal and the 48 PCG signals were used for the estimation of the CTIs.

An accurate and robust method for the estimation of the CTIs from simultaneous ECG-PCG recordings is not fully described in the literature. In fact, most previous works describing the use of CTIs for the monitoring of the cardiac functionality, reported in paragraph “2.3.2 Cardiac Time Intervals and Heart Failure”, do not describe the method they used to extract the time of closure of the cardiac valves from the PCG signal. The task is not naïve from a processing viewpoint, since it involves differentiating the two components which make up each heart sound. In fact, the estimate of the time of closure of the valve should be valve-specific to improve the accuracy and robustness of the estimate, even in cases where a single side of the heart is of interest. Even though multiple algorithms exist for the segmentation of the two main heart sounds within the PCG signal, with or without a simultaneous ECG as reference, few previous works tackled the problem of identifying the two components separately.

Our research group proposed an envelope-based method to identify the components of the two main heart sounds in simultaneous ECG-PCG recordings [168]. Even though the work was carried out before the beginning of this PhD project, the algorithm was used as a basis for the signal processing tasks developed during this project. Therefore, the fundamental details will be presented in paragraph “4.2 Estimation of the time of closure of the cardiac valves”.

The mentioned algorithm was designed and validated on single-source PCG recordings. Goal of the signal processing phase of this PhD project is to define how to adapt the algorithm for use with the multiple available PCG signals recorded with the multi-sensor array. Two main approaches exist to tackle the problem: signal selection and signal combination. The first consists of identifying a single signal or a subset of signals that are the most suitable for the specific valve. The second involves using specific processing techniques, such as Blind Source Separation techniques, to combine the information carried by the recordings into one or multiple novel optimized signals. In this work a signal selection approach was tried out: the signal processing methods hereby described aim at selecting the most suitable subset of PCG signals from the 48 available channels and to use them for the estimation of the CTIs. This articulates in three tasks:

1. Reliably assessing the quality of each channel and discarding channels with a below-threshold signal quality.
2. Separating the channels into spatially coherent groups that could constitute auscultation areas.
3. Identifying the best auscultation area, i.e., the signal or subset of signals to be used for the estimate of the CTIs.

The designed methods will be described in detail in the next paragraphs, along with the results of their preliminary validation. As anticipated, the proposed pipeline is not the only possibility: some signal combination approaches were explored, as expanded at the end of this section, and may be object of future development.

4.2 Estimation of the time of closure of the cardiac valves

The two main heart sounds have long been considered in their totality: most heart sounds segmentation algorithms proposed in the literature focus on identifying the time instant of beginning, peak and end of the two heart sounds but do not take into consideration the fact that each heart sound is actually made up of

multiple components. In particular, the first heart sound (S1) is typically described as the sound generated by the closure of the atrioventricular valves, but the closure of the two atrioventricular valves (mitral and tricuspid) is not simultaneous. The same happens with the second heart sound (S2), where the split between the aortic and pulmonary components is even more relevant and correlated with the respiration phase and with some cardiac pathologies.

Being able to distinguish between the closure of the mitral and tricuspid components in S1 and between the closure of the aortic and pulmonary components in S2 is of key importance for the application of interest. In fact, as highlighted in paragraph “2.1.1 Brief pathophysiology of heart failure”, multiple phenotypes of HF exist, also depending on the pathophysiological path that led to the development of the syndrome. Heart failure can affect mainly the left or the right side of the heart (or both), which affects differently the time of closure of the valves of the left and right side. Moreover, from a technical point of view, the differentiation of the two components of the two main heart sounds increases the accuracy and the repeatability of the estimate.

In the past, some methods were proposed to distinguish the time of closure of the two heart sounds components, mainly devoted to the separation of the aortic and pulmonary components in the second heart sound and measure their split. In fact, the S2 split is expected to be correlated with the PAP which in turns is related to the development of pathologies such as Pulmonary Hypertension (PH) and CHF. Among the proposed methods, two main families can be identified:

- Methods aimed at identifying the instant of closure of the two overlapping cardiac valves as the peaks of the signal in some domain.
- Methods aimed at separating the acoustic waveforms emitted by respectively the closure of each heart valve.

To achieve the first goal, the most tested approaches were either based on the wavelets, and in particular on the identification of the peaks of the Continuous Wavelet Transform [169,170], or on the identification of the peaks on some representations of the signal in the time-frequency domain, and particularly on the Wigner-Ville Distribution [171–175]. Nevertheless, the two components overlap in both the time and the frequency domains, makes it very complicated to see two well-distinguishable peaks even in the time-frequency or wavelet domains. In fact, the performances of the mentioned approaches were not outstanding.

Better results were produced using the second family of methods. In this case, two sub-families can be distinguished. Some Authors proposed methods where the waveform corresponding to each of the two components was defined a priori and modeled by a known function. Goal of the method is to optimize the model's parameters. Proposed models include nonlinear transient chirps [176,177], Gaussian chirplets [178], windowed sinusoids [179]. Other Authors proposed methods where the waveform's model was not defined a priori, but extracted from the signal itself. In this concern, Gaussian Mixture Model was tested [180]. Tang et al. proposed a method based on the estimate of the aortic waveform through averaging and the pulmonary waveform through subtraction [181]. Renna et al. proposed a further improvement of Tang's approach employing alternating optimization of time and amplitude of the two waveforms [182].

For the application of interest, in the final version of the device, the algorithm for the estimation of the time of closure of the four cardiac valves should be embedded in the device itself. The goal is to provide the patient with a direct, straightforward, almost real-time feedback. For this purpose, lightweight algorithms are required. Even though model optimization algorithms have shown good performances in the past, they typically involve an iterative, computationally expensive optimization. With the purpose of finding a lighter solution to the problem, in our research group we explored an envelope-based approach. Envelope-based segmentation of the two main heart sounds was often described in the past, but was not applied independently to distinguish the heart sounds components.

We proposed an algorithm for the estimation of the time of closure of the four cardiac valves from a PCG recording by identifying the two main components of the two main heart sounds with an envelope-based approach. The method was published in MDPI Sensors journal with the title "A novel method for measuring the timing of heart sound components through digital phonocardiography" [168]. A summary of the fundamental aspects is presented in the following, starting with the flowchart proposed in Figure 30. Each block in the flowchart will be better detailed in the following paragraphs.

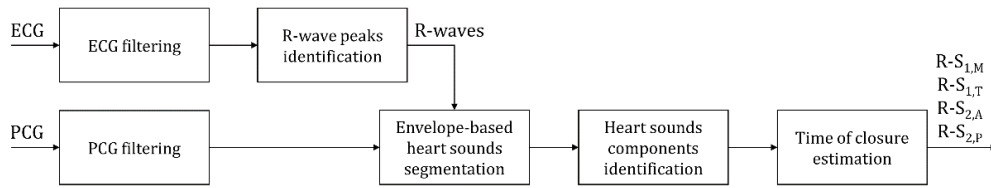


Figure 30: Flowchart of the algorithm for the estimation of the time of closure of the cardiac valves.

ECG filtering and R-wave peaks identification

For the application of interest, the ECG signal is not meant to be object of a morphological analysis but to be used as a time reference for the estimation of the time of closure of the cardiac valves. In this sense, the feature of interest is the QRS complex, which is a representation of the electrical activity corresponding to the ventricular depolarization. For the stated reasons, ECG filtering was designed to preserve the frequency components typical of the QRS complex while reducing the effect of high frequency noise as well as baseline wandering.

To achieve this goal, a band-pass filter was designed as the cascade of a high-pass filter with a cut-off frequency of 10 Hz and a low-pass filter with a cut-off frequency of 35 Hz. The high-pass filter was implemented in the form of a moving median filter with a 100-ms long moving window. The low-pass filter was implemented as a Finite Impulse Response (FIR) filter of order 250. It should be highlighted that the 125-sample delay introduced by the FIR filter was compensated to preserve the time relationship between the ECG and the PCG signals.

Even though in the literature the Q-wave is typically used as reference to compute the CTIs, the latter is not always easily recognizable from the clinical and technical point of view. To have a more robust reference, the R-wave peak was used in this work. The identification of the R-wave peaks within the filtered ECG signals was performed by means of a modified version of the well-known Pan-Tompkins algorithm [183]. The latter was selected because of its high sensitivity in front of a moderate computational cost. The algorithm involves applying to the filtered ECG a cascade of linear and nonlinear filters: derivative, point-wise squaring, moving average integration with a 150-ms-long moving window. The goal is to highlight the QRS complex within the recording and segment it. The peaks are then identified through a double-thresholding process, to increase the algorithm sensitivity and discard mis-identified peaks.

PCG filtering

PCG recordings are typically the object of a wide range of interferences: digital filtering is a key pre-processing step to decrease noise interference with the signal segmentation [184]. Noise contributions may be due to internal or external causes. Internal causes may be physiological, i.e., determined by the normal activity of other physiological districts (e.g., lung sounds), or pathological, such as heart murmurs and clicks generated by the heart itself in the presence of a CVD. External causes are related to the recording phase and may be generated by a wide range of situations, from ambient noises to relative motion at the interface between the microphone probe and the chest [184].

Given that a PCG recording involves the presence of multiple sounds, murmurs and clicks, PCG filtering should be customized depending on the application of interest. In this case, the two main heart sounds (S1 and S2) are the object of the analysis, therefore filtering aims at preserving their frequency content while reducing the effect of other internal or external sounds. For this purpose, a band-pass Infinite Impulse Response (IIR) filter with cut-off frequencies between 20 Hz and 100 Hz was used. Since there is not a complete agreement in the literature regarding the frequency boundaries of the two main heart sounds, the cut-off frequencies were defined by visual inspection of the Power Spectrum Density function of recordings from more than 70 healthy subjects. The IIR filter was implemented as 5th order Chebyshev I filter. Given that IIR filters do not guarantee a linear phase response, zero-phase filtering was carried out not to cause signal distortion in the time domain.

Heart sounds segmentation

PCG segmentation methods can be divided into methods which involve the use of a simultaneous ECG as reference and methods which do not. In this case, an ECG is available (and it is unavoidable to estimate the CTIs) and it can be used to simplify the segmentation step.

As anticipated, among the many proposed segmentation methods, in this work an envelope-based approach was selected because of the low computational cost, which is required to implement the algorithm on board the device, in the future. In particular, the envelope was computed using the second-order Shannon energy (SE), which was already attempted in the literature with good results in terms of sensitivity and specificity [185]. Higher orders of SE, capable of smoothing the envelope and reducing the effect of noise [186], were tested, but were found to

decrease the discriminative capability among two components of the same sound. Second order was considered as a good trade-off.

If x is the normalized filtered PCG signal, SE can be defined as follows:

$$SE = -\frac{1}{N} \sum_{i=1}^N x^2(i) \cdot \log x^2(i)$$

where N is the length of the moving window expressed in samples. Given that the sampling frequency of the recording system is 1 kHz, N was set to 20 samples, which is the expected duration of the closure of the valve. In literature, the integration window is typically shifted by 50% of its own duration [185]. Nevertheless, in this way, the original time resolution of 1 millisecond, suitable to correctly differentiate among different components, which are typically split by 10 to 30 milliseconds, is affected. For this reason, the components could not be distinguished in previous works based on the Shannon Energy envelope. In this work, instead, the integration window was shifted by one sample at a time to preserve a 1-ms time resolution. The SE envelope was standardized over a 1-second-long sliding window, devoted to ensure that changes in amplitude over the recording do not affect the standardization. In the end, the nonnegative samples were set to zero to obtain a nonnegative envelope.

Segmentation was performed using a double-thresholding approach on the signal envelope. First, an amplitude threshold on the envelope was used to gate the signal and identify the segments corresponding to a heart sound. The amplitude threshold was set to the 5% of the maximum SE value. Then, time thresholding was used to fix the segmentation, in two ways:

1. By removing false positives: if two segments are less than 20% of the RR interval apart, the one with the lowest SE is removed.
2. By joining together split segments: if two segments are less than 10% of the RR interval apart, they are joint together.

Heart sound components identification and time of closure estimation

The process of identifying the time of closure of the cardiac valves was performed in two steps. First, the signal segments identified in the previous steps are classified into:

1. S1, if the peak SE value of the segment falls within the -0.05% and the 20% of the cardiac cycle.
2. S2, if the peak SE value of the segment falls within the 30% and the 60% of the cardiac cycle.
3. None, otherwise.

Once the segments corresponding to S1 and S2 were identified, the problem of identifying the two components within each segment was faced. The problem is not naïve because the two components mostly overlap, and the separation is almost impossible to recognize in the time or frequency domain. Nevertheless, the split is visible in the SE envelope domain as a local minimum. Therefore, the identification of the two components was carried out by:

1. Locating the local minimum with the highest prominence
2. Locating the maximum of the envelope before the local minimum (mitral in S1, aortic in S2) and after the local minimum (tricuspid in S1, pulmonary in S2).

In the end, for each cardiac cycle, the time of closure of the cardiac valves is expressed as the latency of the identified components with respect to the R-wave peak. Therefore, the output of the algorithm is expressed in the form of the following parameters:

1. $R-S_{1,M}$: the average latency between the R-wave peak and the mitral component in the S1.
2. $R-S_{1,T}$: the average latency between the R-wave peak and the tricuspid component in the S1.
3. $R-S_{2,A}$: the average latency between the R-wave peak and the aortic component in the S2.
4. $R-S_{2,P}$: the average latency between the R-wave peak and the pulmonary component in the S2.

Figure 31 proposes a graphical representation of the temporal relationships of the defined parameters on the ECG, the PCG, and the PCG envelope.

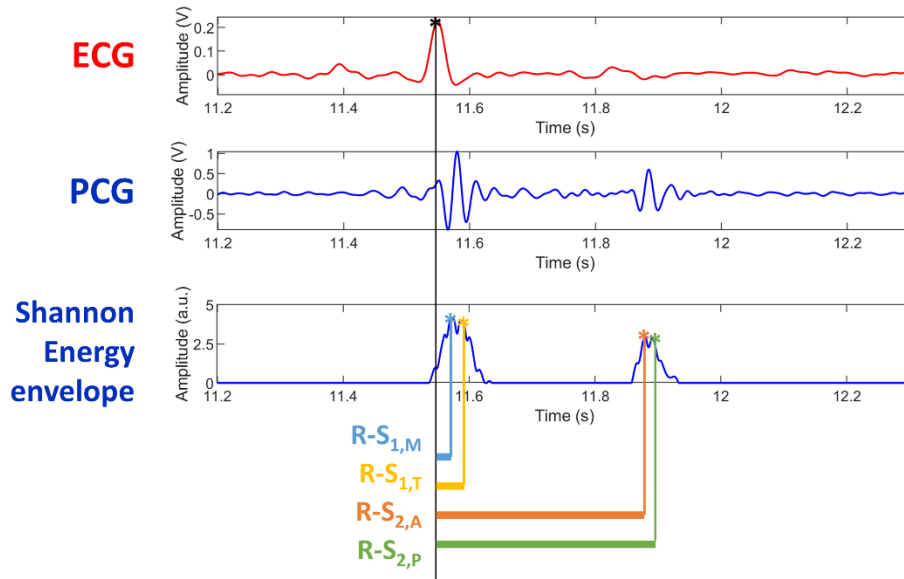


Figure 31: Graphical representation of the defined temporal parameters on the ECG, PCG, and PCG envelope signals.

Experimental validation

Validation was performed on single-source PCG recordings from healthy volunteers and included two phases. In a first phase, the sensitivity and specificity of the algorithm in the identification of the two main heart sounds was assessed separately for S1 and S2. The sensitivity was defined as the percentage of correctly detected heart sounds, taking as reference the detected R-wave peaks. This grounds on the assumption, manually verified, that the modified Pan-Tompkins algorithm could correctly detect all R-wave peaks. This is obviously not guaranteed in the broad population, but holds for the sample population used for the validation. The specificity was defined as the percentage of heartbeats where murmurs or noise were wrongly identified as heart sounds. In the overall, the sensitivity of detection was found as high as 99.6% for S1 and 98.9% for S2, 99.2% in total. The value is in line with the results obtained by previous works in the literature. Specificity was found equal to 100%, meaning that no murmur nor noise contribution of any kind was misclassified as a heart sound. In the second phase, the distribution of the estimated time of closure was evaluated and compared to expected values from the physiology and the literature. The values were found coherent to what expected from the literature and from the physiology of the cardiac cycle.

4.3 Assessment of the quality of PCG signals

As already highlighted, the quality of the PCG signal may vary noticeably. The quality may depend on the position of the stethoscope, but it may also be affected by the anatomical characteristics of the subject. In fact, a consistent layer of fat or the presence of breasts is expected to cause attenuation in the propagation of the acoustic vibrations, which in turn reflects into a lower intensity [152,187].

In this context, it is fundamental to determine how the quality of the signal affects the estimate of the time of closure of the cardiac valves. This is crucial to determine what are the constraints the algorithm is subjected to. Figure 32 proposes a comparison between a good-quality and a poor-quality signal. The two signals were acquired using the same recording system, from the same position of the chest, in similar conditions and they have both been digitally filtered. It is evident that extracting reliable information about the time of closure of the cardiac valves from the second is impossible.

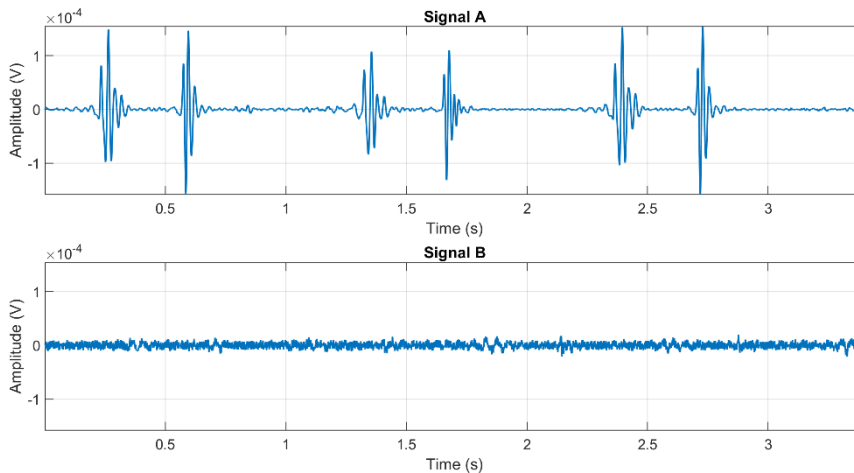


Figure 32: Comparison between a good-quality signal (A, with SNR = 31 dB) and a poor-quality signal (B, with SNR = 4 dB).

The question to be answered is: what minimum signal quality is required to be sure that the results of the designed algorithm guarantee the reliability of the estimate of the time of closure of the cardiac valves? The issue is particularly relevant in homecare applications, as the one proposed in this work. In a homecare context, recordings are performed by inexperienced users, such as the patient or a caregiver: the variety of possible situations decreasing the quality of the signals

may be relevant. Moreover, the patient is not capable of determining whether the recording is of sufficient quality or not. Therefore, an automated and robust method to assess the quality of the recordings is required. Besides, knowledge about the minimum requirements is needed to determine the range of applicability of the method.

In the latest decades, a few methods were previously proposed in the literature for the automatic assessment of PCG signals. The first approaches that were proposed grounded the quality assessment on the periodicity of the signal [188] or on the spectral matching using a low-noise beat as reference [189]. Afterwards, the proposed methods can be divided between heuristics-based and ML-based.

Concerning the heuristics family, most Authors grounded their quality analysis on a range of physiological or technical features extracted from the signal, that were sometimes combined into some evaluation criteria. Features were extracted from the time, frequency or time-frequency domains, and included the logarithmic energy of the signal, the power of noise over 700 Hz, the duration of the heart sounds segments, the root mean square of consecutive differences of the signal, the number of detected peaks over different moving windows, the zero crossing ratio [184,190,191].

ML-based methods typically aimed at classifying a recording as whether good quality or not, in a binary fashion. This interpretation is interesting because the output is easily understandable by both clinicians and inexperienced users. On the contrary, such an interpretation does not provide a numerical quality metric and is therefore much application dependent. ML-based methods typically consider a high number of features. Tested ML approaches included Neural Networks [192], Support Vector Machine [193], Logistic Regression [194], Convolutional Neural Networks [195] or ensemble classification using multiple of the above-mentioned techniques [196,197].

Despite the usefulness of these methodologies, their reliance on a wide range of features extracted from the signal, some of which have no clear physiological interpretation, can make it difficult for physicians to understand why a specific signal is not considered of sufficient quality. Additionally, the large number of features used may be affected by the presence of a pathological condition. Lastly, most of the proposed methods are computationally expensive and thus unsuitable to provide the user with a real-time feedback, as of interest for telemonitoring.

In this study, the use of a simple numerical metrics such as the Signal-to-Noise Ratio (SNR) is explored to obtain a straightforward yet reliable assessment of the quality of the signal. To achieve this, the robustness of the estimate of the time of closure of the cardiac valves against noise was studied. The analysis proposed in this paragraph was published in MDPI Sensors journal with the title “Automated Assessment of the Quality of Phonocardiographic Recordings through Signal-to-Noise Ratio for Home Monitoring Applications” [198].

4.3.1 Materials and methods

Quality assessment: the Signal-to-Noise Ratio

As anticipated, some methods were previously proposed in the literature for the assessment of the quality of a PCG signal. Most methods grounded the assessment on some features, extracted from the signal and reflecting its physiological characteristics, used to develop a ML algorithm or to build criteria.

Nevertheless, such an approach is not suitable for the application of interest. In fact, in this case, the quality assessment needs to be implemented on a wearable device to be used in a telemonitoring setting at the patient domicile. The evaluation of the quality is of key importance to give the user direct feedback in real time, so that, in case the quality is deemed insufficient to perform a reliable monitoring, the array can be re-positioned, and the recording can be performed again. In such a scenario, it is evident that a simple quality assessment algorithm is preferable so that it can be implemented directly onboard the recording system.

Here, a simple quality assessment solely based on the SNR of the PCG signal was explored. The SNR formula is based on elementary numerical computations and considers solely the level of noise in the signal, without depending on more complex characteristics that may change in case of pathology. We defined the SNR beat by beat and independently for each of the two heart sounds, i.e., two separate SNR values were computed for each heartbeat. Assuming that each heart sound is a quasi-periodic signal and that the additive noise is a stochastic process, we defined the SNR as:

$$SNR = 20 \log_{10} \frac{A_S}{4 \sigma_N}$$

where:

- A_S is a measure of the amplitude of the signal, i.e., the peak-to-peak amplitude of the heart sound of interest;
- $4\sigma_N$ is a measure of the amplitude of the noise, i.e., the 95% band of noise.

The definition of the two heart sounds and of the noise was performed by dividing the cardiac cycles in segments where each sound is expected to occur according to physiology. In particular:

- S1 segment: $[-0.05 \cdot RR; 0.2 \cdot RR]$
- S2 segment: $[0.3 \cdot RR; 0.6 \cdot RR]$
- Noise: $[0.7 \cdot RR; 0.85 \cdot RR]$

Figure 33 proposes a graphical representation of the definitions.

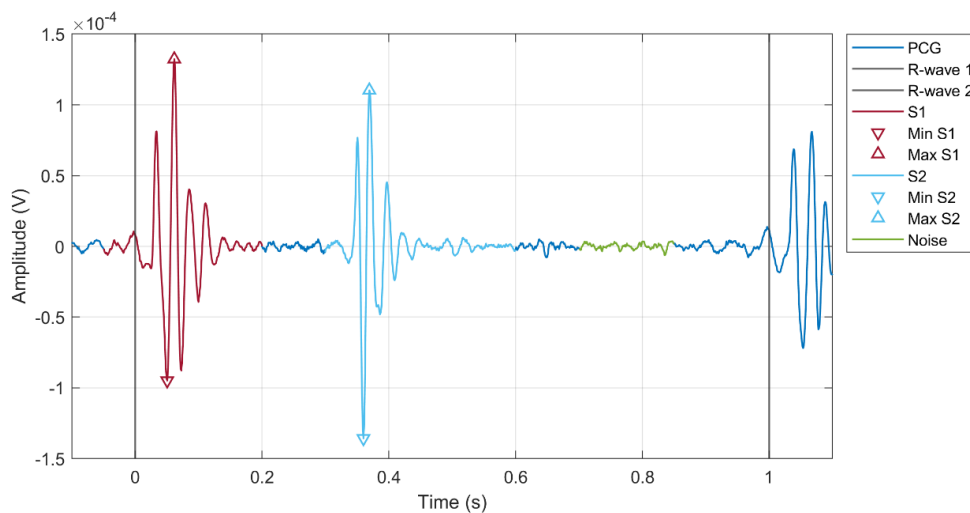


Figure 33: Definition of the intervals of the heartbeat corresponding to S1, S2 and the noise.

Rationale of the robustness analysis

Figure 34 proposes a flowchart of the methodology designed to assess the quality of a PCG recording and its effect on the estimate of the time of closure of the cardiac valves.

Real PCG recordings were used, performed on healthy subjects in a laboratory setting to ensure repeatable environmental conditions. Even so, the signals presented a wide range of quality levels, with a SNR ranging from 7 dB to 25 dB

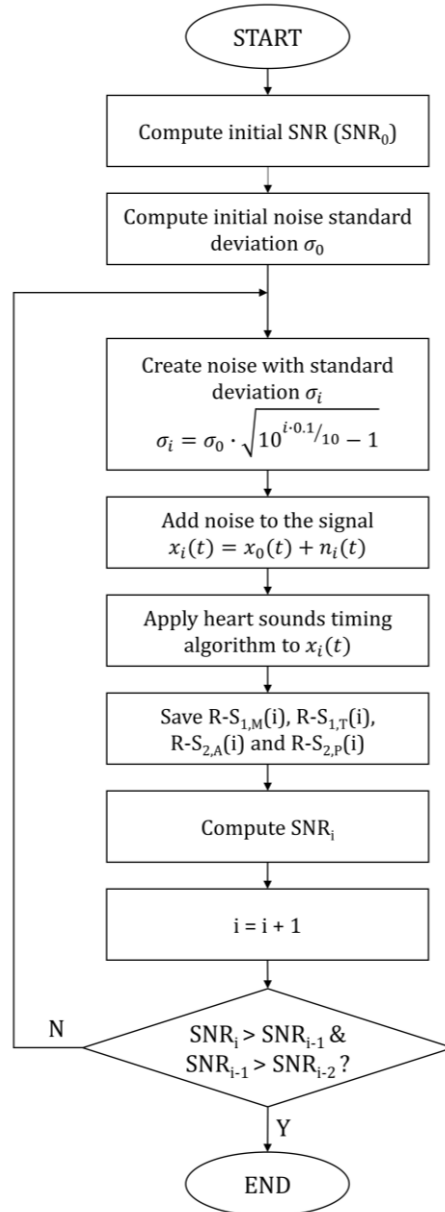


Figure 34: flowchart of the methodology for the assessment of the effect of the signal quality on the estimate of the time of closure of the cardiac valves.

before any digital filter is applied. Then, each recording was progressively corrupted with artificial noise to decrease its SNR in a controlled way.

At iteration i , the PCG signal object of analysis $x_i(t)$ can be modelled as:

$$x_i(t) = s(t) + n(t) + n_i(t)$$

where $s(t)$ is the original acoustic signal as emitted by the closure of the cardiac valves; $n(t)$ is the noise originally present in the recording; $n_i(t)$ is the noise that was artificially added at iteration i . The artificially added noise $n_i(t)$ was hypothesized to be modelled as a Gaussian white stochastic process. To confirm this point, the original noise $n(t)$ was analyzed. It was extracted from the original recordings as the segments between the 70% and the 85% of each cardiac cycle, when no heart sound is expected to occur, using the simultaneous R-wave peak as reference. We analyzed more than 16000 cardiac cycles, applied the Chi-square goodness of fit test ($\alpha = 0.05$) against the normal distribution and found that the null hypothesis could not be rejected in 84% of the heartbeats. Therefore, $n_i(t)$ was modelled as a white Gaussian noise with a standard deviation equal to:

$$\sigma_i = \sigma_0 \cdot \sqrt{10^{\frac{0.1 i}{10}} - 1}$$

With this formula, the SNR is set to progressively decrease by 0.1 dB steps. It should be highlighted that the computed SNR is accurate only if the heart sounds can be correctly identified within the signal. Therefore, when the quality of the signal is extremely poor, the SNR value stops monotonically decreasing. If the SNR does not decrease in two consecutive iterations, the stop condition is met.

At each iteration, the time of closure of each cardiac valve was estimated from $x_i(t)$ using the algorithm described in paragraph “4.2 Estimation of the time of closure of the cardiac valves”. Therefore, for each recording four arrays of time of closure values (each corresponding to a cardiac valve) were computed.

Evaluation of the results

The test presented in the previous paragraph was repeated 10 times for each signal, for robustness. In the end, all 10 arrays were resampled at fixed SNR values, maintaining a resolution of 0.1 dB, and the median array was computed.

Two kinds of analysis were carried out to define the minimum acceptable SNR value.

In the first place, the minimum acceptable SNR value was defined, valve by valve, as the first SNR value in decreasing order where the estimated time of closure of the valve of interest could be considered significantly different from the reference estimate, i.e., the estimate at the maximum available SNR, when no

artificial noise is added. An estimate was considered as significantly different if two conditions were met:

1. The estimate differs from the reference by at least 1 millisecond (resolution of the recording system).
2. A trend in the estimate is detected (by applying Wald–Wolfowitz runs test with $\alpha = 0.05$).

For reference, Figure 35 shows an example of the variation of the time of closure of the tricuspid valve over a set of 10 experiments, with the median curve highlighted, performed on a subject and the corresponding minimum acceptable SNR threshold.

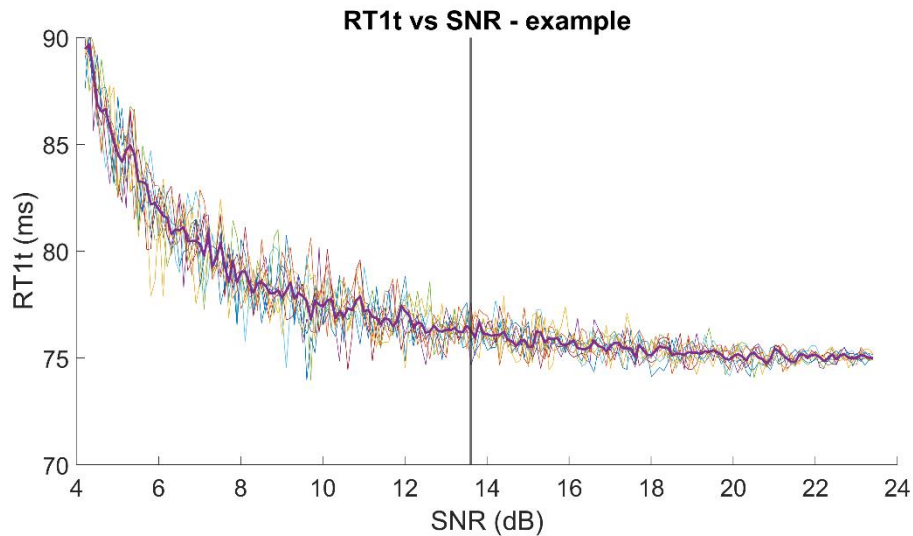


Figure 35: Variation of the time of closure of the tricuspid valve for one subject (10 experiments) in function of the SNR. The vertical line represents the minimum acceptable SNR value to obtain an estimate not significantly different from the reference.

The presented criterion ensures that the measurement error of the estimate is lower or equal to the resolution of the recording system. In other words, in the first analysis the minimum detectable error was considered as significant. Nevertheless, this is not always consistent with the requirements of the clinical application. In fact, most often, a more relaxed measurement uncertainty is sufficient in the clinical context.

Therefore, in a second phase, the analysis was repeated by considering as acceptable subsequently higher percentages of the reference estimate: 2.5%, 5%,

7.5%, 10%, 12.5%, 15%, 17.5%, 20%. In the end, for each valve, a curve of the minimum acceptable SNR value in function of the acceptable measurement uncertainty was built.

Testing population

The algorithm was tested (and the acceptable SNR values found) on a sample population counting 25 healthy subjects. Enrolled subjects were different in terms of biological sex (46% females), age (18 to 83 years), Body Mass Index (BMI, 17.7 kg/m² to 30.5 kg/m²). Therefore, the testing population could be considered representative of the overall population.

For convenience, 10-minute-long single-source recordings were used, carried out using a commercial system for the recording of biomedical signals (ReMotus™, It-MeD, Italy). The ReMotus™ system is suited to acquire up to four channels, simultaneously sampled at a sampling frequency of 1 kHz and converted by means of a 24-bit ADC. It ensures a 3-dB bandwidth spanning from DC to 262 Hz, suitable for the biomedical signals of interest. The system is fully isolated (CF type) to ensure the patient's safety. The recordings are performed through a PC, whom the system is connected via USB.

Among the four available channels, one was devoted to ECG recording and one to PCG recording. The first channel was equipped with an active probe for ECG recording with an input impedance of 1 GΩ and a 0-dB gain. Three disposable Ag/AgCl electrodes were employed and positioned over the subject's chest as to recreate a first standard lead, with the two active electrodes in the right and left subclavian areas, along the midclavicular lines, and the reference electrode over the right side of the subject's abdomen. The second channel was devoted to PCG recording and equipped with a custom designed microphone probe for the purpose. The microphone probe uses an electret condenser microphone sensor, as in the multi-sensor array, along with the required conditioning circuit. The PCB mounting the sensor and the electronics is housed into a rigid 3D-printed case shaped as a truncated cone, like a typical stethoscope head, to focus the acoustic waves on the sensor, located in the center. The position of the microphone probe over the subject's chest was not standardized, but the examiner decided the best location by visually inspecting the signal through the ReMotus™ computer interface, to ensure a sufficient signal quality. Figure 36 presents a picture of the system and of the custom designed microphone probe, along with a graphical representation of the positioning of the sensors over the chest.

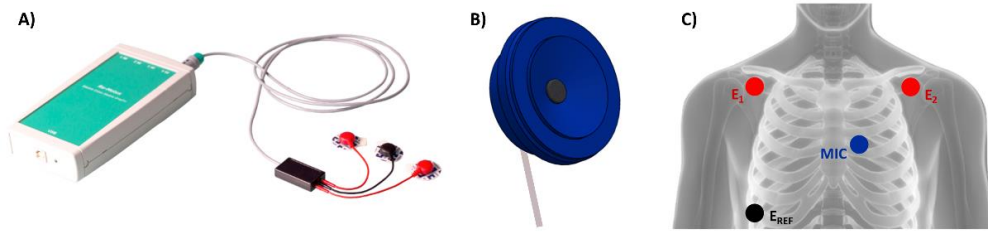


Figure 36: Recording system for the single-source recordings: A) ReMotus™, B) the custom realized microphone probe, C) the positioning of three electrodes and of the microphone probe over the chest.

Validation population

As anticipated, the acceptable SNR values in function of the measurement uncertainty were found, valve by valve, on the testing population. To validate the results, the publicly available PhysioNet CinC Challenge 2016 dataset [199] was employed. In particular, the recordings from the Massachusetts Institute of Technology (MIT) heart sound database were selected because the remaining recordings did not provide a simultaneous ECG. Only the “Normal” recordings, i.e., the recordings from patients with no history of cardiopathy, were used, in coherence with the testing population.

Among the 117 available recordings, only the signals with a starting SNR higher than the identified minimum acceptable SNR found in the testing phase were selected. For each of them, the robustness analysis was repeated, and a minimum acceptable SNR found accordingly. The sensitivity of the methodology and of the acceptable SNR values found in the testing phase was assessed by means of the percentage of recordings of the validation population featuring a minimum acceptable SNR lower or equal to our finding.

4.3.2 Experimental results

Figure 37 shows the plots of the time of closure of each of the four cardiac valves in function of the decreasing SNR. To enable a comparison among different subjects, the values were normalized with respect to the reference estimate, i.e., the estimated time of closure at the highest available SNR, before any artificial noise was added.

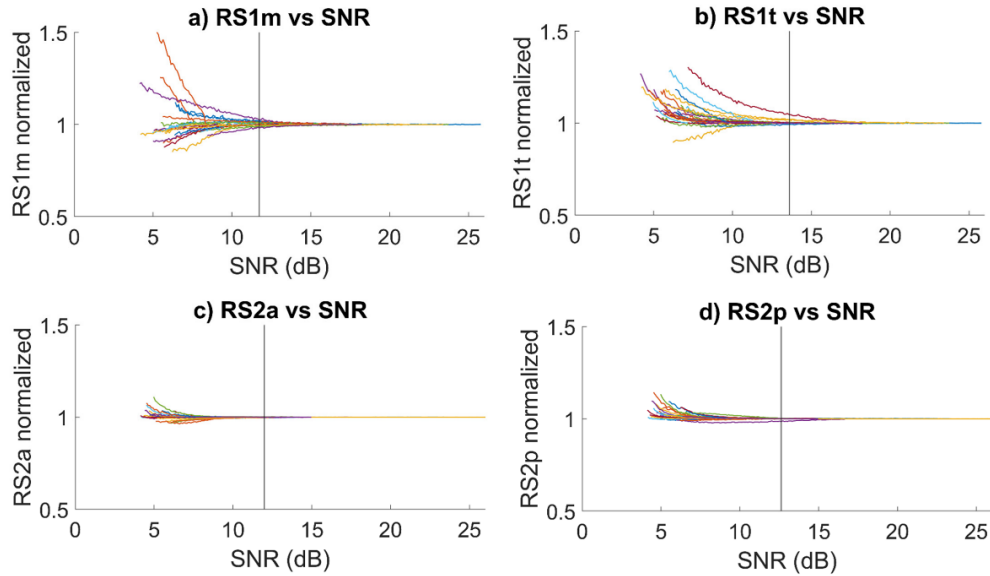


Figure 37: Time of closure of each cardiac valve in function of the SNR. The values are normalized with respect to the reference estimate for the purposes of comparison. Each line represents a different subject in the testing population. The black vertical lines represent the computed minimum acceptable SNR value.

For each subject, a minimum acceptable SNR value was computed for the four valves according to the above-described criteria. The detailed values are reported in [198]. In the end, the overall minimum acceptable SNR values were defined as the maximum values over the testing population (worst case). Their values are reported in Table 5.

Table 5: **Minimum acceptable SNR value for each cardiac valve.**

Heart valve	Min SNR (dB)
Mitral	12
Tricuspid	14
Aortic	12
Pulmonary	13

Results in Table 5 show that a PCG recording with a SNR equal to or higher than 14 dB is sufficient to estimate the time of closure of all four cardiac valves with an uncertainty lower than the time resolution of the recording system (1 millisecond). It should be highlighted that this is a technically relevant limit, but it may even be exaggerated when considering the clinical applicability of the method. In fact, the plots reported in Figure 37 show that in most cases, and mainly concerning the semilunar valves, the variability of the estimate is extremely small even below the estimated threshold. Nevertheless, the mentioned SNR values represent a solid technical limit that should put the user in a safe position.

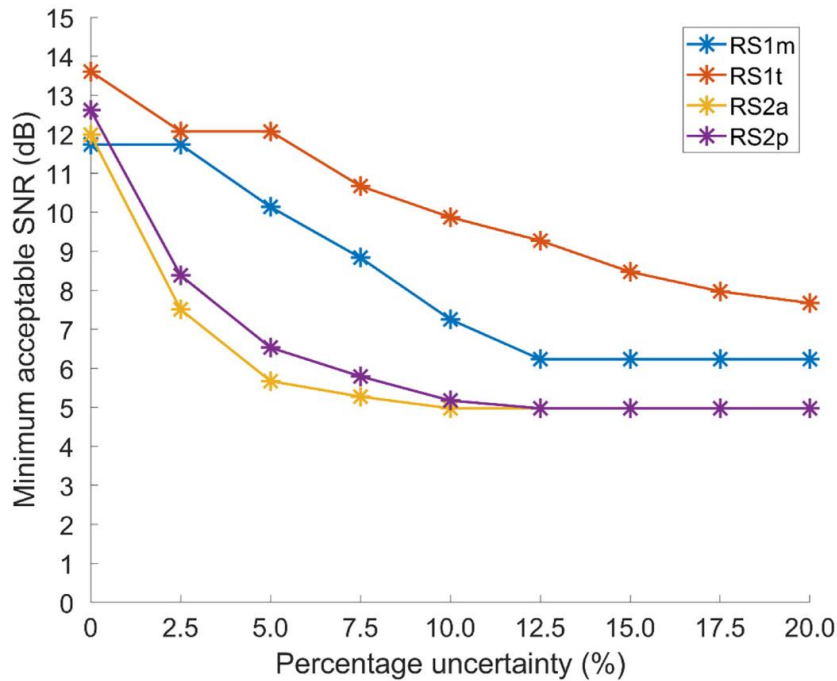


Figure 38: Minimum acceptable SNR in function of the acceptable measurement uncertainty for the four cardiac valves.

The second phase of the analysis considered different possible measurement uncertainties to evaluate their effect on the minimum acceptable SNR value. Figure 38 summarizes the obtained results.

It should be highlighted that also in this case the reported results represent the maximum over the testing population (worst case scenario). The decreasing curves confirm that the methodology is robust. It can also be inferred that the time of closure of the atrioventricular valves, extracted from S1, is more sensitive to noise than the time of closure of the semilunar valves, extracted from S2. This is coherent

with the fact that the time of closure of the semilunar valves is several times higher: percentage uncertainties over higher values produce a higher absolute error. Nevertheless, in clinics, percentage errors are typically more relevant than absolute ones. Moreover, the estimates on the left side of the heart are typically slightly more robust towards noise than their right counterpart. This may depend on the fact that the left heart components are typically wider in amplitude, due to the higher pressure gradients, and more easily recognizable.

The presented curves provide a useful tool to determine the acceptable signal quality depending on the application of interest. For example, if a 10% accuracy is sufficient, a SNR equal to 10 dB ensures a reliable estimate on all four cardiac valves.

In the end, Figure 39 presents the results of the validation phase, i.e., the sensitivity of the minimum acceptable SNR values found for the increasing percentage uncertainties. Each bar represents the percentage of recordings in the validation population that satisfied the corresponding percentage uncertainty when their SNR is decreased at the corresponding minimum acceptable SNR value.

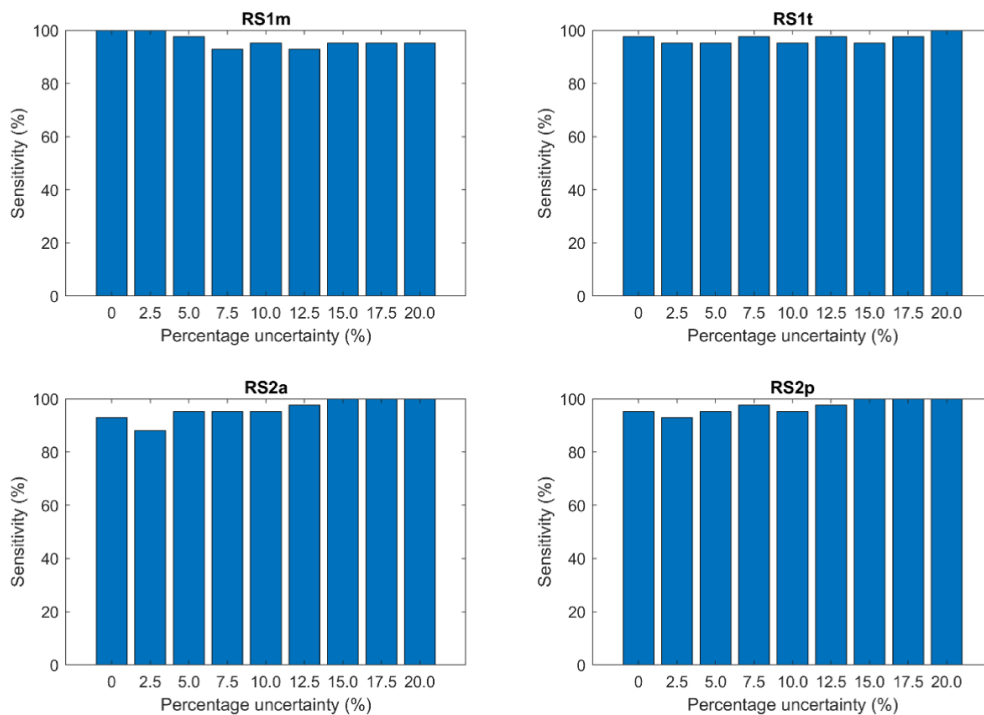


Figure 39: Sensitivity of the computed minimum acceptable SNR values over the validation population for the four cardiac valves.

As shown, the sensitivity of the found minimum acceptable SNR values is always higher than 90% for all uncertainties and all cardiac valves. This result is especially relevant when considering that the validation population was extracted from a dataset with different characteristics than what used in the testing population: different locations of the stethoscope, different recording conditions (from clinical contexts to extremely noisy domiciliary contexts), different types of subjects (children are included), different recording systems and users, different durations. It is possible to conclude that the proposed method is robust with respect to the sample population, the context, the recording system, the user, the duration of the recording and the location of the stethoscope.

4.3.3 Discussion

A couple of take-home messages can be derived from the results of the presented analysis.

In the first place, the presented results confirm that a simple numerical metrics such as the SNR is a robust option to describe the quality of the PCG signal. In fact, the curves in Figure 37 are monotonic and show that the error on the estimate is well inversely correlated with the SNR of the signal, as expected. This is extremely useful because:

1. The SNR is based on elementary numerical computations with a low computational complexity: therefore, it is apt to be embedded on the device and provide the user with automatic, real-time feedback on the signal quality.
2. The SNR has a technical rather than physiological meaning: its interpretation is not affected by the presence of a pathological condition.
3. The interpretation of the information provided by the SNR about the signal quality is straightforward and easily interpretable by clinicians but also by inexperienced users.

Concerning the minimum acceptable SNR values that were found and validated in this study, a few considerations can be made. Results show that a SNR equal to 14 dB on both heart sounds ensures an estimate with a measurement uncertainty as low as the time resolution of the recording system. This level of quality can easily be obtained by an expert user, with an average electronic stethoscope and in a clinical or laboratory setting. Nevertheless, the selection of the validation population proved that obtaining such quality in a domicile setting is not

straightforward. In fact, the MIT heart sounds dataset, where the validation population was extracted from, counted 117 recordings from various settings, including the patient's domicile: only the 39% of the recordings had a starting SNR higher than 14 dB, and was thus selected to build up the validation population. This confirms that the quality of the signal is an essential characteristic to be considered when moving PCG to home care applications.

As already highlighted the 14 dB limit should not be considered a limit in the strict sense, since higher uncertainties are typically considered acceptable in the clinical practice. In this concern, some considerations should be made to interpret the results of the proposed analysis in function of the application of interest, i.e., the telemonitoring of HF patients. For monitoring purposes, the acceptable uncertainty over the estimate is highly dictated by the order of magnitude of the physiological fluctuations that the CTIs are subjected to on a daily basis.

We investigated the latter point in a single-subject study that was presented at the “Convegno Nazionale di Bioingegneria” conference in June 2020 (Trieste, Italy). Details can be found in [200]. In this pilot study, simultaneous ECG and single-source PCG recordings were performed on the same subjects repeatedly for 25 consecutive days. The recordings were performed in supine position, within an hour from waking up, before breakfast and with the same experimental setup, with the goal of ensuring the highest possible repeatability of the experimental conditions, both from a physiological and an environmental point of view. The coefficients of variation (CV) of the estimates of the time of closure of the four cardiac valves were found equal to 8% for the mitral, 11% for the tricuspid, 2% for the aortic and 3% for the pulmonary [200].

Even though the study was performed of a single subject (due to the practical complexity of performing a long-term analysis on a wider population), thus limiting the generalizability of the results, it can be used to hypothesize the order of magnitude of the physiological fluctuations of the time of closure over the time in a simulated monitoring setting. If we consider the above-enunciated CVs as a measure of the acceptable uncertainty and we compare, valve by valve, with the curves in Figure 38, it can be derived that a SNR equal to 10 dB ensures a good enough estimate on all cardiac valves. It can also be observed that the CVs were found higher for S2 than for S1, but this results in a similar acceptable SNR for the two heart sounds.

In the overall, the presented study provided us, from one side, with a method to automatically assess the quality of the signals in a simple, computationally inexpensive and straightforward way, and, on the other side, with a quantitative interpretation of the metrics that enables a direct feedback on the suitability of the signal quality depending on the application of interest.

4.4 Spatial clustering of the signals

After having defined a robust method to assess the quality of the multi-source recordings, the next problem to be faced consists in identifying the best signal or group of signals to be used for the estimation of the time of closure of each cardiac valve. The most straightforward approach consists in simply selecting the signal with the highest SNR for the heart sound under analysis. This conceptually simulates what happens with single-source PCG: the expert user moves the electronic stethoscope over the thorax of the patient and manually selects a point where the signal quality is considered sufficient according to his/her expertise. The same can be achieved with multi-source PCG by selecting the signal with the highest SNR in the processing phase. Nevertheless, this approach may not be optimal when a high number of channels recorded at a high spatial resolution are available. Indeed, a higher amount of information can be used to improve the robustness of the estimate and its repeatability over the time.

Potential benefits may arise from selecting not the best auscultation point, i.e., the best signal, but the best auscultation area, i.e., the best subset of neighboring signals. Nevertheless, identifying coherent subsets of microphones for a given valve can be challenging when the recordings are made by inexperienced users, since the microphone placement on the chest may vary across recordings. In other words, selecting the best signal in a relevant auscultation area is not possible without dividing the channels in potential auscultation areas before. Therefore, the automated selection of the best auscultation area requires two processing steps:

1. Dividing the channels into groups that represent potential auscultation areas.
2. Selecting the best auscultation area as the group with the best characteristics according to some identified criteria.

The first step is the object of the study presented in this paragraph. It should be highlighted that this step of the processing pipeline is exploratory: no evidence

exists that selecting a subset of signals produces better results than selecting a single signal with optimal characteristics.

The question to be answered is: how to automatically divide the signals into spatially coherent groups with similar characteristics without having any knowledge about the spatial location of the array over the chest? Clustering may provide a suitable answer.

Clustering is a family of techniques aimed at dividing the items belonging to a dataset into groups, or *clusters*, based on their similarity. The similarity is measured using a relevant metric, whose definition depends on the characteristics of the dataset and the intended use of clustering. Clustering was often used in the literature for purposes such as Knowledge Discovery in Data, Identification of Frequent Patterns, and Data Mining [201,202]. In fact, its main advantage resides in its suitability for use on unlabeled datasets, i.e., datasets where no a priori information is available regarding which group each item is expected to belong to.

Typically, in the context of signal processing, clustering techniques are fed with a set of relevant features extracted from the signals. Some Authors used this approach for heart sounds segmentation in the past [203–210]. The choice for the relevant features strongly impacts the result of the clustering and must be wisely analyzed in the context of the application of interest. In this study, a novel approach was tested which performs clustering based on the signal itself and not on a set of features extracted from it. In fact, the signal waveforms were directly compared. To the best of the Author's knowledge, no previous study exists that uses clustering techniques to group PCG signals into coherent clusters according to their morphology.

The first challenge faced in this work consisted of defining an appropriate similarity measure to compare the morphology of the waveforms of different channels. Then, two possible clustering techniques were evaluated and compared:

1. Hierarchical clustering, and in particular agglomerative hierarchical clustering.
2. Partitional clustering, and in particular k-means.

More details about the implementation of the two methods for the purpose of dividing the PCG signals into groups, along with the methodology for their evaluation and comparison are presented in the next paragraphs. The study presented in this paragraph was presented at the 2022 IEEE International

Symposium on Medical Measurements and Applications (MeMeA) in June 2022 with the title “Comparison of Hierarchical and Partitional Clustering in Multi-Source Phonocardiography” [211].

4.4.1 Materials and methods

Rationale and similarity measure

The below-described methodology was applied on the 48-channel recordings performed using the presented multi-source array. Pre-processing involved the following steps:

1. ECG band-pass filtering (10 Hz to 35 Hz) and identification of the R-wave peaks using the modified Pan-Tompkins algorithm.
2. 48-channel PCG band-pass filtering (20 Hz to 100 Hz).
3. Segmentation of the 48-channel PCG into heartbeats, where the heartbeat i is defined, channel by channel, as the signal’s samples within the interval $]R_i - 100; R_{i+1} - 100]$.
4. Assessment of the signal quality using the SNR (as described in paragraph “4.3 Assessment of the quality of PCG signals”) and removal of channels with $\text{SNR} < 10$ dB.

As anticipated, the goal of clustering is to divide the elements of the dataset in groups: in this case, the elements to be grouped are the signals recorded by different microphones of the multi-sensor array. It should be highlighted that the number of signals to be clustered may be lower than 48, because some signals may have been discarded in the quality assessment phase of the preprocessing. The methodology is applied repeatedly to each heartbeat independently. Figure 40 presents an example of a set of signal segments the clustering is applied to.

For every heartbeat, two clustering methods, i.e., agglomerative hierarchical clustering and k-means, were employed to divide the good-quality signals into coherent groups. Although both methods are iterative, they differ in their approach to initialize and construct clusters: details are provided in the next paragraphs. The ultimate goal of both methods, however, is to group the elements into clusters that have low intra-cluster variability, indicating homogeneity, and high inter-cluster distance, indicating dissimilarity among clusters.

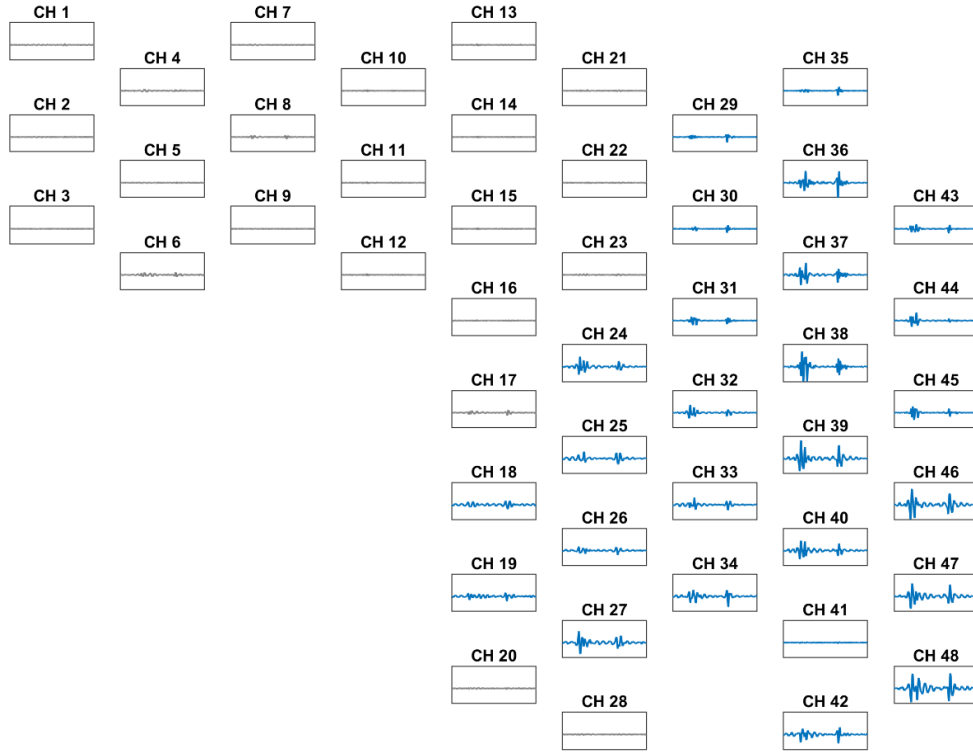


Figure 40: Single-heartbeat segments recorded by the 48 microphones of the multi-sensor array. The grey signals were classified as poor-quality (SNR < 10 dB) and discarded.

The most important parameter to be defined, equally for both approaches, is the similarity metrics. In this sense, we wanted to ground the similarity measure on the morphological characteristics of the signals. In this way, the signals are compared with each other directly, and not in terms of a set of extracted features as most typically done in the literature. The goal was to insert no constraint concerning the spatial relationship of the microphones the signals are recorded from in the clustering phase. Therefore, the definition of the similarity metrics was based on the correlation between two signal segments captured by different microphones. If x_i and x_j are two signal segments corresponding to the same heartbeat recorded by different microphones, the distance between them $d_{i,j}$ is calculated as:

$$d_{i,j} = 1 - \frac{(x_i - \bar{x}_i)(x_j - \bar{x}_j)'}{\sqrt{(x_i - \bar{x}_i)(x_i - \bar{x}_i)'} \sqrt{(x_j - \bar{x}_j)(x_j - \bar{x}_j)'}}$$

According to the proposed definition, $0 < d_{i,j} < 2$, where small values are associated with heartbeats with a similar morphology: in the extreme case, if $x_i = x_j$, then $d_{i,j} = 0$, i.e., their distance is at its minimum. It should be highlighted that the defined similarity metrics is independent on the scaling: if two signals have a similar morphology they will be associated with a low distance even if their amplitude is different. For the sake of comparison, Figure 41 shows the similarity between the same heartbeat recorded by three different channels and the corresponding distances.

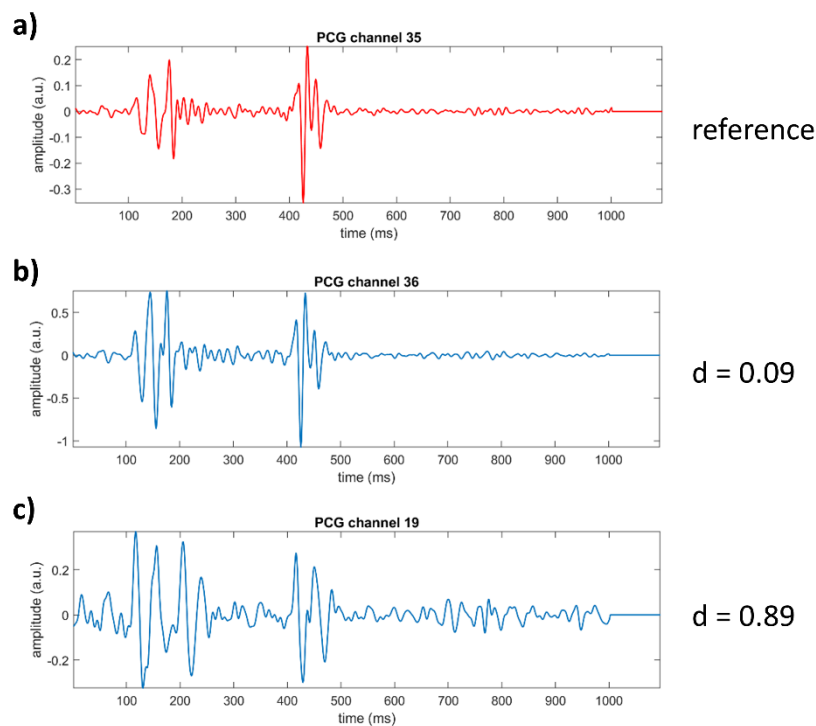


Figure 41: Comparison between the morphology of the same heartbeat recorded by different microphones. If the heartbeat a) is taken as reference, the heartbeat b) has a high similarity and therefore a low distance whereas the heartbeat c) has a low similarity and thus a high distance.

Agglomerative hierarchical clustering

In agglomerative hierarchical clustering, every element of the dataset initially represents a separate cluster. In each iteration, the two clusters that have the highest similarity metrics (or the smallest distance) are merged, until all elements belong to a single cluster. This process results in a hierarchical tree, called *dendrogram*, which can be cut at a certain level to obtain the final clusters. The appropriate cut level depends on the intended use of the clustering. One major advantage of

hierarchical clustering is that it requires minimal initial parameters and prior knowledge. The user only needs to set the similarity metrics, the linkage method for merging clusters, and the cut level. Additionally, this method is completely deterministic [201,212].

In this study, we used the defined distance as the similarity metrics and the "*complete linkage*" as the linkage method. The complete linkage uses the farthest distance between elements in different clusters to select the two clusters to be merged. This approach yields more compact groups and identifies outlier points [213]. The cut level was automatically set as the iteration in which the two farthest clusters were merged. For the sake of brevity, agglomerative hierarchical clustering will be referred to as "*dendrogram*" in the following.

K-means

The k-means algorithm is a popular unsupervised ML technique used for clustering the elements of a dataset into k groups, where k is a priori selected. The algorithm starts by randomly initializing k cluster centroids, which are the center points of each group. Then, each item is assigned to the cluster with the nearest centroid based on the similarity metric. The centroid of each cluster is then updated, typically as the mean of the elements assigned to that cluster. This process is repeated iteratively until the assignment of points to clusters no longer changes, or a specified maximum number of iterations is reached [201]. The result is k clusters, each with a centroid that represents the center of the group.

Despite its good performances in a variety of situations, the main limitation of k-means is that it requires the number of clusters k to be specified in advance, which can be challenging in some cases, depending on the clinical problem. Moreover, the algorithm has a stochastic nature: in fact, the final result may be influenced by the initial centroids, which are randomly defined. To increase the robustness of the methodology, the k-means algorithm is typically repeated more than once. In this study, k values between 5 and 10 were tried out, as suitable to identify a reasonable number of homogeneous areas. The algorithm was run 10 times for each k value and the result featuring the highest minimum inter-cluster distance was selected.

Experimental validation

The two clustering techniques were applied to multi-source recordings performed using the version of the array with homogeneously distributed microphones. This choice was dictated by the will of studying the distribution of

the selected areas without any constraint posed by a non-symmetrical distribution of the sensors. A dataset composed of 721 heartbeats, extracted from daily repeated recordings on a healthy volunteer, was employed for the testing. Both agglomerative hierarchical clustering and k-means were applied to each heartbeat belonging to the sample population, independently.

The analysis of the results included two phases. In the first phase, the agreement between the methods was assessed. Two tools were employed for this purpose, namely the contingency matrix and the Rand Index (RI). The contingency matrix was built by inserting in the cell with the coordinates (i, j) the number of elements that are clustered in cluster i by hierarchical clustering and in cluster j by k-means. If a is the number of pairs of elements that are clustered together by both approaches, b is the number of pairs of elements that are clustered separately by both approaches and n is the total number of elements of the dataset, the RI can be computed as [201]:

$$RI = \frac{a + b}{\binom{n}{2}}$$

According to its definition, the RI ranges from 0 to 1, with 0 corresponding to a complete disagreement and 1 corresponding to a complete agreement. The analysis was repeated twice:

1. By selecting the number of clusters using the dendrogram and then running k-means with the same k .
2. By selecting k using the k-means and then cutting the dendrogram to obtain the same number of clusters.

In the second phase, each clustering technique was evaluated on its own, using its optimal number of clusters. Three performance metrics were employed, namely:

- *VarIntra*: the maximum (worst case) intra-cluster variability, defined for each cluster as the average distance between elements belonging to the same cluster.
- *DistInter*: the minimum (worst case) inter-cluster distance, defined for each pair of clusters as the distance between their centroids, defined as the median of its elements.

- *SC*: Silhouette Coefficient, defined as the average of the silhouette values defined for an element i as:

$$s(i) = \frac{\min_{j \neq I} \frac{1}{N_{C_j}} \sum_{j \in C_j} d(i, j) - \frac{1}{N_{C_I} - 1} \sum_{j \in C_I, j \neq i} d(i, j)}{\max \left(\frac{1}{N_{C_I} - 1} \sum_{j \in C_I, j \neq i} d(i, j), \min_{j \neq I} \frac{1}{N_{C_j}} \sum_{j \in C_j} d(i, j) \right)}$$

where the first addend of the numerator represents the distance from the closest element belonging to a different cluster (measure of the inter-cluster distance) and the second addend is the average distance from the elements from the same cluster (measure of the intra-cluster variability). Silhouette value ranges from -1 to 1, where -1 represents a badly clustered element and 1 represents an optimally clustered element. Therefore, a SC close to 1 is associated to a good clustering, i.e., a clustering that ensures a good trade-off between VarIntra and DistInter.

4.4.2 Experimental results

Figure 42 proposes a graphical representation of the clustering obtained on the same randomly selected heartbeat using the two methodologies, i.e., the dendrogram and the k-means (10 repetitions). Each circle represents a microphone, and they are spatially distributed as in the physical array. Each color represents a cluster, and the blank circles represent discarded microphones, i.e., microphones whose recorded signal had a below-threshold SNR.

Concerning k-means, the clustering results varied to some degree across different repetitions, which is known to depend on the stochastic nature of the algorithm. In this study, the final k-means clustering was chosen based on the highest inter-cluster distance, which was found in the second repetition in the proposed example. Therefore, the result of the second repetition of k-means was compared against the result of the dendrogram by means of the contingency matrix and of the RI. The results are presented in Figure 43.

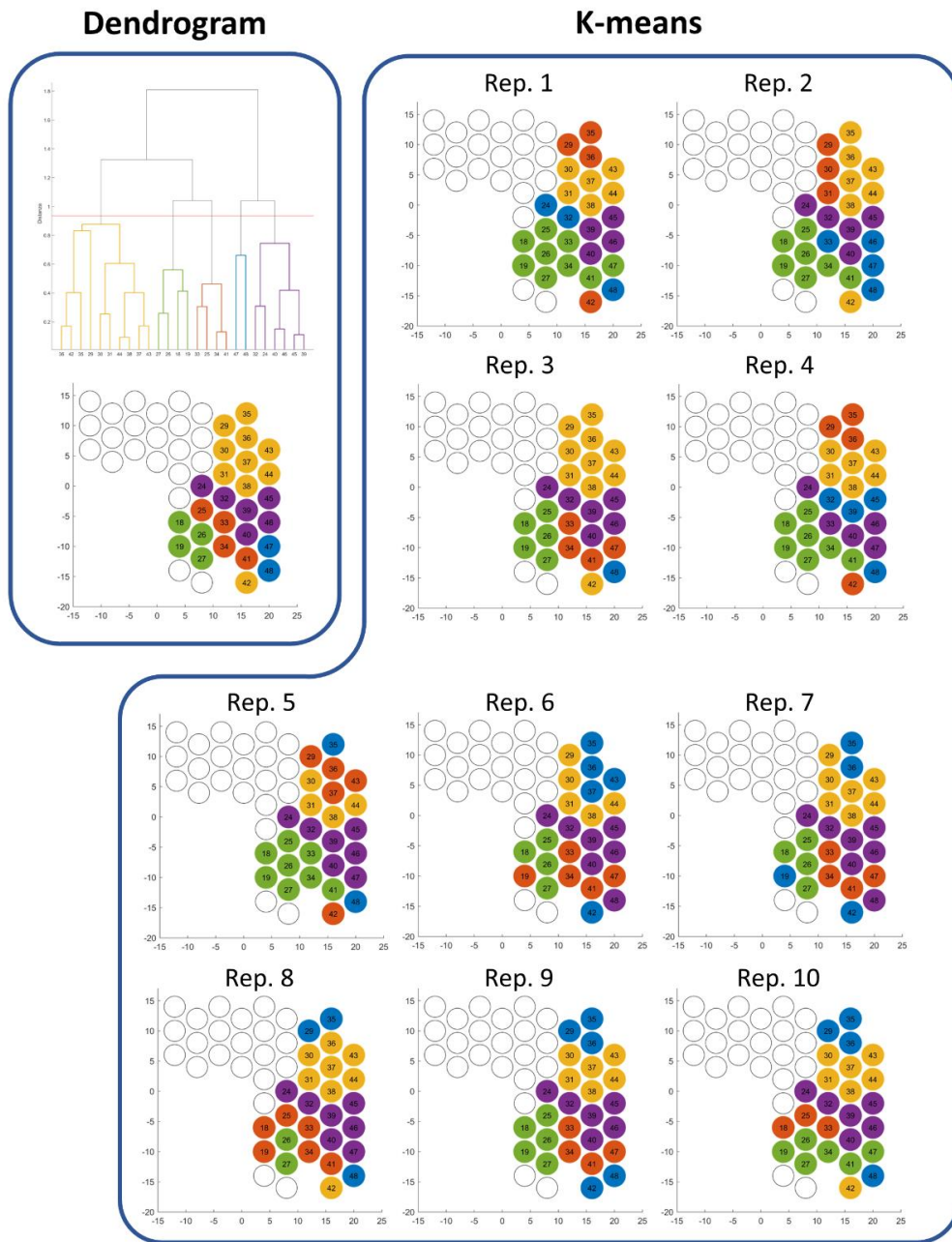


Figure 42: Example of comparison between the clustering obtained by agglomerative hierarchical clustering (dendrogram) and k-means over 10 different repetitions on the same heartbeat. Each circle represents a microphone, and the colors of the circles highlight the clusters. The white circles represent microphones whose signal's SNR was below threshold.

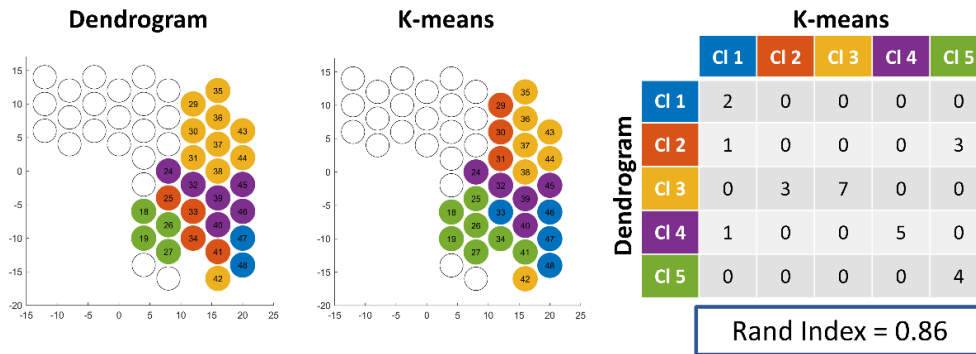


Figure 43: Example of the contingency matrix and the corresponding Rand Index for the clustering shown on the maps.

The contingency matrix proposes a detailed analysis of the agreement between the two methods, whereas the RI summarizes the agreement in a single value and enables the comparison among the heartbeats belonging to the sample population. Table 6 summarizes the mean and standard deviation of the RI obtained by either selecting the number of clusters using the dendrogram or by using the k-means.

Table 6: **Distribution of the Rand Index over the sample population.**

Heart valve	Rand Index	
	Mean	Std
Number of clusters selected through dendrogram	0.88	0.05
Number of clusters selected through k-means	0.84	0.06

In both cases, the RI was found higher than 0.7 for every heartbeat belonging to the sample population. This confirms that the agreement among the two approaches is good. The RI obtained when the dendrogram drives the selection of the optimal number of clusters is significantly higher when the Student’s *t*-test is applied with a significance level $\alpha = 0.05$ ($p < 0.001$). It was also observed that the optimal number of clusters selected through the two approaches is equal only in 26% of the heartbeats. The automatic cutting rule on the dendrogram selects a

higher number of clusters in the 70% of the cases, which may be considered a better choice in the context based on the RI results.

Figure 44 proposes three sets of boxplots comparing the two clustering approaches in terms of inter-cluster distance, intra-cluster variability and Silhouette Coefficient. The two approaches were applied with their own selected optimal number of clusters.

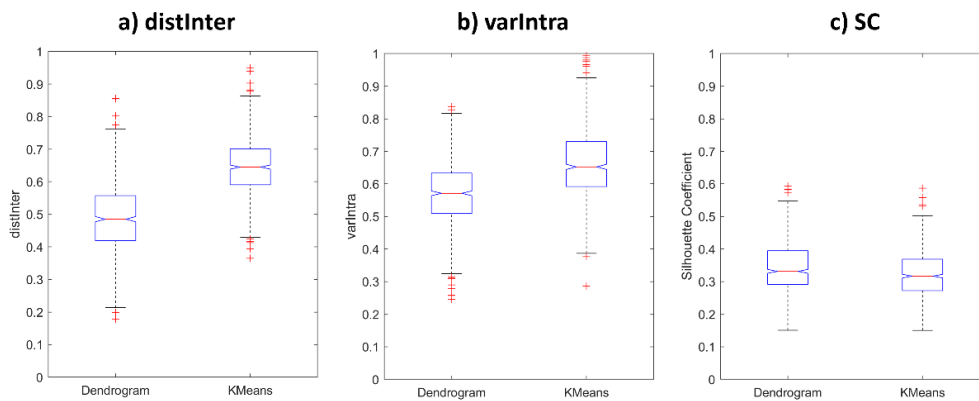


Figure 44: Comparison between the distribution of respectively a) the inter-cluster distance, b) the intra-cluster variability and c) the Silhouette Coefficient using hierarchical clustering (dendrogram) and k-means.

It can be observed that the hierarchical approach favors the minimization of the intra-cluster variability at the expense of the maximization of the inter-cluster distance, whereas the opposite happens with k-means. Nevertheless, the SC was found slightly (but significantly) higher for the dendrogram. The absolute value of the SC was found positive for all heartbeats in the sample population and for both approaches, which is associated to a good clustering.

4.4.3 Discussion

Even with a limited sample population, the presented results allow to make some interesting considerations regarding the suitability of clustering for the application of interest and regarding the method to perform it.

In the first place, the distribution of the channels in the clusters should be assessed from a spatial perspective. It should be reminded that no spatial constraint was inserted in the definition of the similarity metric: only the signal morphology was considered. In other words, the waveforms were compared to group the

channels into clusters. If the clustering works correctly, it can be expected that signals recorded by neighboring microphones have similar waveforms and will be clustered together. The results of both clustering approaches show that this actually happens: microphones belonging to the same cluster were typically located near each other, indicating spatial coherence. This confirms the significance of the results and provides an implicit validation of the similarity metrics and of the use of clustering for the purpose.

Concerning the comparison among the hierarchical and partitional clustering, a first take-home message from the experimental results resides in the agreement between the methods. The high agreement level that was found constitutes a validation, again, of the goodness of clustering. Little discrepancies may even be due to the stochastic nature of k-means: a similar level of agreement can be found when comparing different repetitions of the k-means algorithm over the same heartbeat.

Given the high level of agreement, both techniques should be considered reliable to divide the channels of a multi-source recordings into coherent groups. If one method needs to be chosen to be embedded in the overall processing pipeline, the choice should better fall on agglomerative hierarchical clustering. This is partly due to the experimental results, which show that the latter method allows for obtaining a slightly better trade-off between the homogeneity of the groups and their distance. But even if the results were absolutely equal, agglomerative hierarchical clustering should be selected because of its implicitly deterministic nature and because it does not require to determine the number of clusters a priori. Therefore, the use of agglomerative hierarchical clustering to divide channels into coherent groups looks to be reasonable in theory and supported by the presented experimental data.

4.5 Automatic identification of the best auscultation area

The last step of the proposed processing pipeline consists of deciding which of the identified subset of signals is to be selected as the most appropriate auscultation area for each of the four cardiac valves. This is not a naïve task since the decision may be based on different criteria.

Criteria may be based either on technical features of the signals, such as the average SNR, which we would like to maximize, or the variability of the SNR over the signals belonging to the same cluster, which we would like to minimize. Or may

be based on physiological hypotheses, such as that the time of closure should be minimized to minimize the propagation time in the chest, or that the variability of the time of closure in the same cluster should be minimized because it is unreasonable that close microphones pick up very different signals.

Even if all reasonable, the mentioned criteria may be conflicting, raising issues regarding which criterion should be prioritized. Instead of choosing a criterion, multiple criteria can be considered simultaneously by using Multi-Criteria Decision Analysis techniques. Multi-Criteria Decision Analysis (MCDA) is a branch of operation research that deals with decision making problems in complex environments, when conflicting criteria may be taken into account [214,215].

Having defined a set of sub-objectives from the main general objective, the first step in MCDA consists of translating them into criteria, i.e. measurable variables to be maximized or minimized. The MCDA algorithms work on an evaluation matrix E , defined as an A -by- C matrix, where A is the number of possible alternatives to choose among and C is the number of criteria. Each element of the evaluation matrix is the value of a certain criterion for a certain alternative.

Among the possible MCDA methods to evaluate the alternative against the mentioned criteria, Electre III [216] is particularly suitable for the application of interest. The latter is an aggregation method, meaning that it aims at globally aggregating the local information from the criteria to reach a decision. It is also an ordinal method, i.e., it builds on pairwise comparisons of alternatives (and not on an individual score). This allows for avoiding a total compensation among criteria (a very good score of one criterion does not compensate a very bad score of another one). What mentioned makes Electre III a suitable method to face the decision-making problem under analysis, from a theoretical point of view.

The use of MCDA in healthcare has been explored in the last decade in the context of clinical decision making, for both screening and treatment purposes [217]. Nevertheless, novel applications may arise by employing MCDA for automatic decision making, as required in telemonitoring.

The goal of the study presented in this paragraph is to test the use of a MCDA approach, using Electre III, against the use of single criteria for the selection of the cluster representing the best auscultation area. The study presented in this paragraph was presented at the 2022 Computing in Cardiology (CinC) conference in September 2022 entitled “Automatic Identification of the Best Auscultation Area

for the Estimation of the Time of Closure of Heart Valves through Multi-Source Phonocardiography” [218].

4.5.1 Materials and methods

Pre-processing

The same pre-processing as in paragraph “4.4 Spatial clustering of the signals” was carried out, involving the following steps:

1. ECG band-pass filtering (10 Hz to 35 Hz) and identification of the R-wave peaks using the modified Pan-Tompkins algorithm.
2. 48-channel PCG band-pass filtering (20 Hz to 100 Hz).
3. Segmentation of the 48-channel PCG into heartbeats, where the heartbeat i is defined, channel by channel, as the signal’s samples within the interval $]R_i - 100; R_{i+1} - 100]$.
4. Assessment of the signal quality using the SNR (as described in paragraph “4.3 Assessment of the quality of PCG signals”) and removal of channels with an SNR < 10 dB.
5. Agglomerative hierarchical clustering (as described in paragraph “4.4 Spatial clustering of the signals”).

The output of the pre-processing phase consists of, for each heartbeat and for each channel:

- A label which assigns the channel to a cluster.
- The SNR value of S1 and S2.
- The estimated time of closure for each cardiac valve.

Multi-criteria Decision Analysis

After having divided the channels into homogenous subsets, the next step is defining which cluster is to be used to estimate the time of closure of the four heart valves. What described in the following is repeated for each heart valve. The latency of the heart valve under analysis is generally referred to as $RS_{x,y}$ (with $\{x,y\} = \{1,M\}, \{1,T\}, \{2,A\}, \{2,P\}$).

The first step of MCDA is the definition of the sub-objectives to be translated into quantifiable criteria. In the application under analysis, we identified four sub-objectives to be considered for selecting the cluster:

- Sub-objective 1: to obtain an estimation as close as possible to the real time of closure of the heart valve, it is needed to minimize the time of propagation of the acoustic waves across the biological tissues.
- Sub-objective 2: to obtain a robust estimation, it is preferable to select a cluster where the estimated latencies are as similar as possible.
- Sub-objective 3: to obtain a technically reliable estimation, from the signal processing point of view, it is preferable to select a cluster containing good-quality signals.
- Sub-objective 4: to obtain a robust estimation also from the technical point of view, it is preferable to select a cluster where the quality of the signals is as similar as possible.

To apply MCDA, we translated the above-mentioned sub-objectives into four measurable criteria, which should be either minimized or maximized:

- Criterion 1: the average of the latency value estimated by each of the channels belonging to the cluster ($RS_{x,y}$). To be minimized.
- Criterion 2: the difference between the maximum and the minimum latency values estimated by channels belonging to the cluster (RS_{x,y_var}). To be minimized.
- Criterion 3: the average of the SNR values of the channels belonging to the cluster (SNR). To be maximized.
- Criterion 4: the difference between the maximum and the minimum SNR values of the channels belonging to the cluster (SNR_var). To be minimized.

The evaluation matrix was built using as alternatives to choose from the identified clusters and as criteria the four above-mentioned ones. Each element of the evaluation matrix is the value of a certain criterion for a certain alternative (for example, the value of the $RS_{x,y}$ latency for the cluster 1). Afterwards, Electre III method was applied to the defined evaluation matrix, heartbeat by heartbeat. The outcome of Electre III was the subset of signals to be selected according to the multiple criteria taken into account.

Experimental validation

The same sample population described in paragraph “4.4 Spatial clustering of the signals” was employed. As anticipated, the dataset was acquired on the same healthy volunteer over daily recordings. Instead of putting all the heartbeats

together, as in the previous study, the one-minute recordings were kept separate. The recordings were performed over 5 consecutive days, roughly at the same time (\pm one hour) and in a repeatable laboratory setting. The experimental protocol was defined as described to simulate, to some extent, the telemonitoring application of interest.

In this study we explored 3 possible decision approaches:

1. Maximization of the SNR, as an expression of the signal quality (technical criterion).
2. Minimization of the time of closure of each cardiac valve (physiological criterion).
3. The above-described approach based on MCDA, which allows us to consider all the described criteria simultaneously.

First, a visual evaluation of the results was performed by plotting the maps of the hits. For each recording and each approach, a map was realized where each circle represents a microphone, and the color of the circle represents the number of times that microphone was selected by each of the three decision approaches as part of the best auscultation area. In this way, insight about the dispersion of the selected microphones over the beats could be obtained. In fact, the selected best auscultation area was expected not to vary much over the heartbeats of the same recording.

Then, the time of closure estimated through three proposed approaches for the selection of the best auscultation areas were compared among each other and against the time of closure estimated by selecting the single signal with the highest SNR. The latter simulates a traditional single-source PCG approach, where an expert user selects the best auscultation point by moving around the electronic stethoscope over the expected auscultation areas until they find the best quality. The comparison was performed in terms of mean and standard deviation of the estimated time of closure.

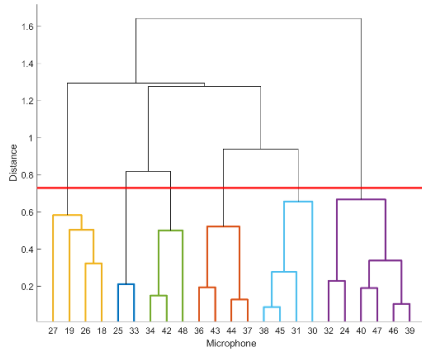
4.5.2 Experimental results

Before the aggregated results are presented, an overview of the individual results of the clustering and MCDA phase on a single, randomly selected heartbeat are proposed. The mitral valve was considered. For this purpose, Figure 45 shows:

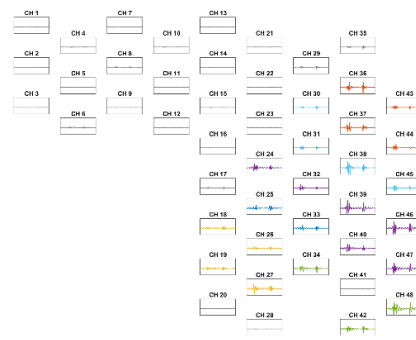
- A. The dendrogram obtained performing agglomerative hierarchical clustering on the above-threshold channels of the selected heartbeat.

- B. A map representing the spatial distribution of the signals divided into clusters.
- C. The resulting evaluation matrix, where in each cell there is the value of a specific criterion (on the rows) by each cluster (on the columns).
- D. The outranking matrix resulting from the application of Electre III, showing the obtained outranking relationship among each pair of clusters.
- E. The resulting distillation graph, which plots the rank of each cluster according to the ascending and descending distillation. The best cluster is the one on the top right corner on the main bisector.

A) Dendrogram



B) Map of the signals divided in clusters



C) Evaluation matrix

Criteria	Cl 1	Cl 2	Cl 3	Cl 4	Cl 5	Cl 6
$RS_{x,y}$ (ms)	18	25	24	25	32	43
$RS_{x,y \text{ var}}$ (ms)	3	7	3	5	4	22
SNR (dB)	13	17	15	17	19	15
SNR_{var} (dB)	2	3	5	4	0	6

D) Outranking matrix

	Cl 1	Cl 2	Cl 3	Cl 4	Cl 5	Cl 6
Cl 1	I	R	R	R	P-	P+
Cl 2	R	I	P-	P-	P-	P+
Cl 3	R	P+	I	R	P-	P+
Cl 4	R	P+	R	I	P-	P+
Cl 5	P+	P+	P+	P+	I	P+
Cl 6	P-	P-	P-	P-	P-	I

I = indifferent
P+ = outranks
P- = is outranked by
R = incomparable

E) Distillation graph

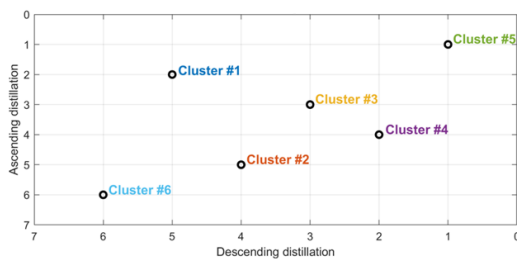


Figure 45: Results of the various phases of the proposed pipeline on a randomly selected heartbeat for the mitral valve: A) dendrogram, B) map of the signals divided in clusters, C) evaluation matrix, D) outranking matrix and E) distillation graph generated by Electre III.

Cluster number 5 was selected in the proposed example, which shows the best trade-off between the values of the criteria. As shown, the average time of closure is not minimized, but the selected cluster outranks all the other clusters due to the values of the other criteria. The minimization of the time of closure would be achieved by cluster number 1, but the latter has the smallest average SNR: the weirdly low time of closure may be due to an error in the estimate, given the severely lower quality of the signals belonging to the cluster. In this sense, cluster number 5 allows to obtain the best trade-off among the multiple criteria of interest.

Figure 46 presents the maps of the hits obtained for the three approaches on the recording performed on the first day of analysis. The mitral valve is considered.

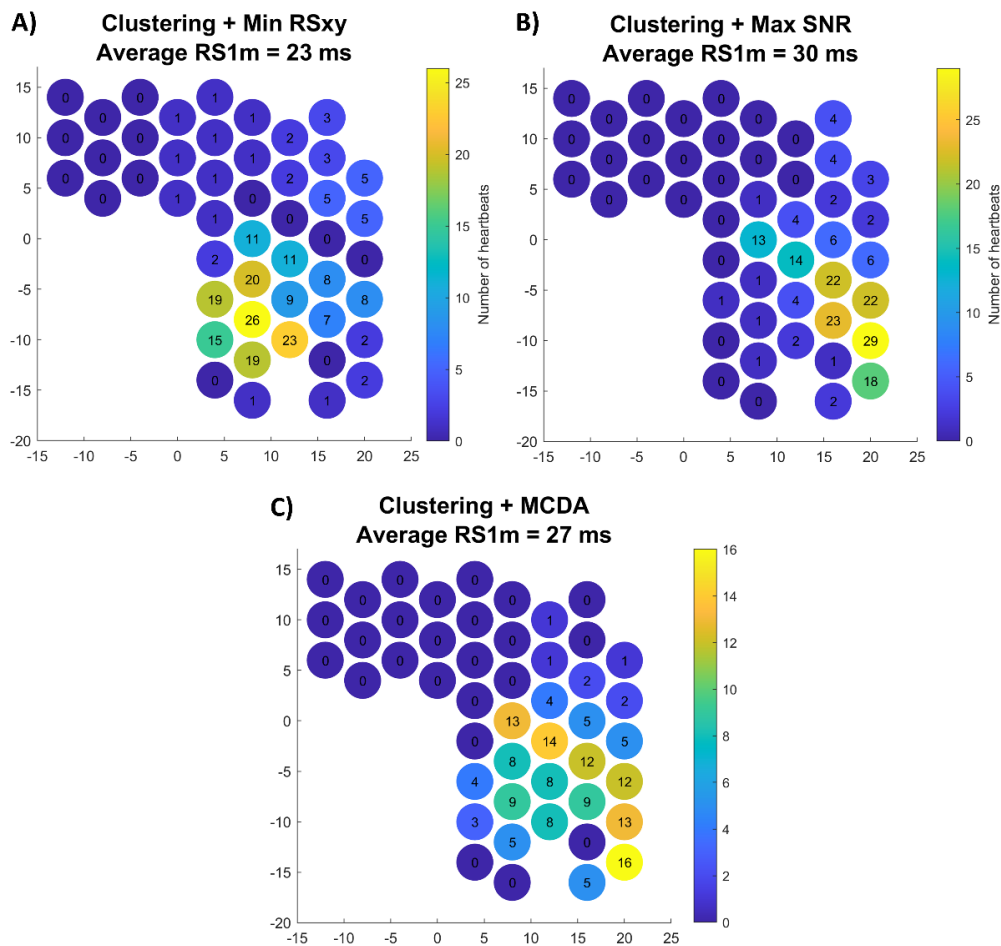


Figure 46: Maps of the hits for the mitral valve obtained on the recording performed on day 1 using the three approaches: A) minimum time of closure, B) maximum quality, C) MCDA.

It can be observed in the first two maps that the best quality criterion and the minimum time of closure criterion led to the selection of different auscultation areas. A disagreement between the criteria reinforces the idea that MCDA is a valuable tool to find the best trade-off among multiple involved criteria. In this case, it can be observed that the auscultation area selected through MCDA is most similar to what selected using the SNR approach (also due to the higher weight assigned to the quality criteria), but the final estimate is slightly lower, which is preferable. The maps also show that the dispersion of the values over the map is low, meaning that the selected area is coherent over the heartbeats.

In the end, the results of the proposed approach are presented, i.e., the comparison among the time of closure obtained by the three presented approaches against the simulated single-source approach. The resulting time of closure (mean and standard deviation band) are plotted in Figure 47, where each point of the time axis represents a consecutive recording day, as in a real telemonitoring application.

Results show that the standard deviation band of the three multi-source approaches is thinner, in every recording day, than the standard deviation band of the single-source approach. This proves that, independently on the approach for selecting the best auscultation area, multi-source PCG allows for obtaining a more stable and accurate estimate of the time of closure of the heart valves over the days.

When comparing the different approaches for the automatic selection of the best auscultation area, it can be observed that the maximum SNR approach leads to the most unstable estimates. On the other side, the estimates obtained through MCDA are coherent to what obtained selecting the cluster with the minimum time of closure, but are theoretically more robust.

4.5.3 Discussion

A first consideration to be made after observing the presented results is that the task of channel selection is definitely not naïve. Single-criterion approaches led to consistent definitions of the best auscultation area: the maps of hits proposed in Figure 46 show that the area is well defined in all proposed approaches, with a low spatial variability of the selected microphones. Given that the clusters were found to group together neighboring microphones, as inferred in paragraph “4.4 Spatial clustering of the signals”, this means that most often the same cluster was selected. This is relevant to conclude that the combination of clustering and cluster selection can produce consistent results across heartbeats. Nevertheless, the maps of hits also

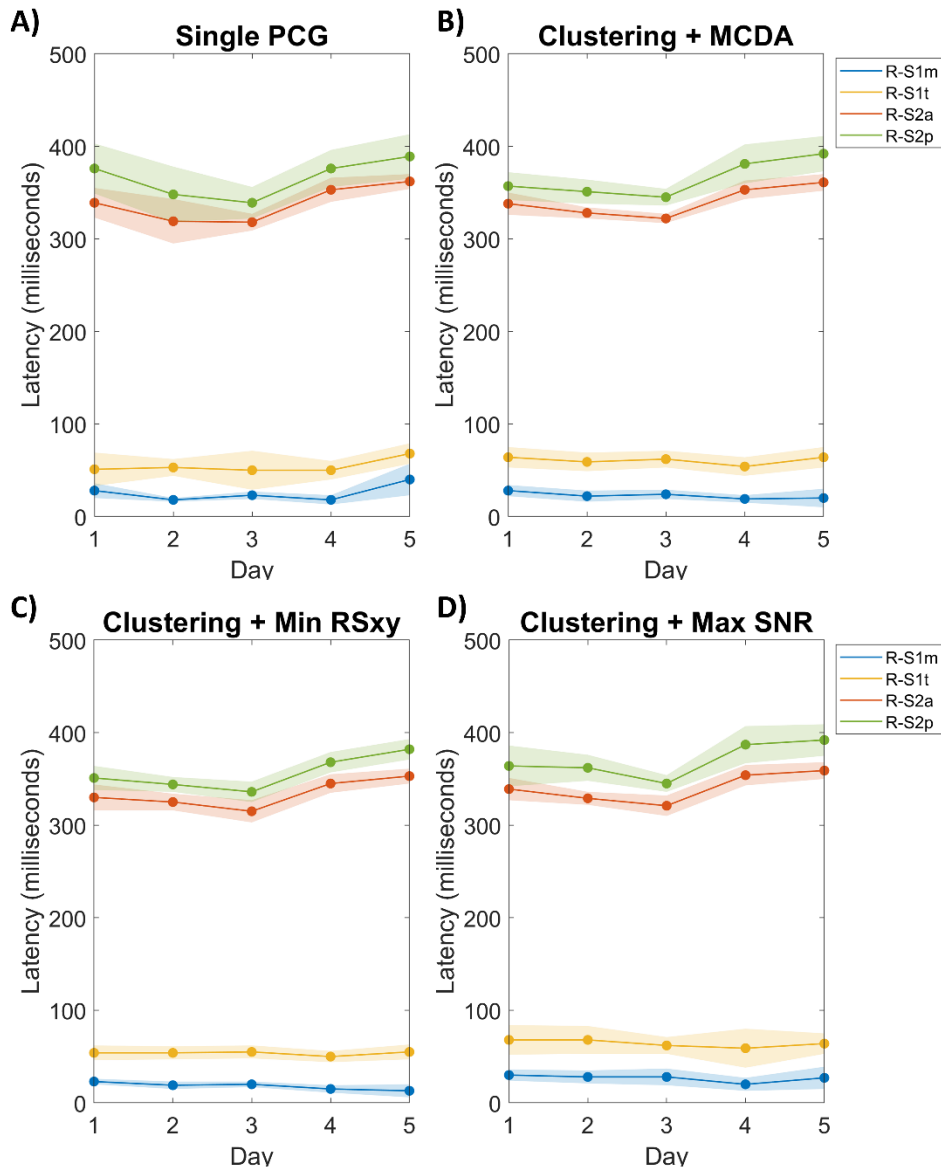


Figure 47: Comparison of the time of closure obtained through: A) the simulated single-source approach, B) the MCDA approach, C) the minimum time of closure approach, D) the maximum quality approach. The dots represent the mean value, the dashed area represents the standard deviation band over each recording.

show that single criteria may be conflicting, even if they are both quite reasonable. The experimental application of the designed pipeline shows that the reality is probably more complicated than the theory.

On a second level of analysis, the comparison between the single-source approach and the multi-source approach shows that selecting a subset of microphones instead of a single microphone improves the robustness of the estimate of the time of closure. This is true regardless of the method for the cluster selection. Keeping in mind that the maps of the hits show that signals from the same area are always selected, this proved more robust than selecting a single channel, which probably fluctuates more.

Concerning the comparison between single- and multi-criteria approaches, it should be first underlined that, from a clinical perspective, the most straightforward choice for the selection criterion would be the signal quality. This is associated to the clinical experience in the field of auscultation: the cardiologist typically moves around the stethoscope on the desired area to find the point where the most audible sound is heard. Nevertheless, results show that adding other criteria to the signal quality may be relevant to improve the robustness of the estimate: in fact, the estimate obtained by maximizing the SNR is the one that decreases the least the standard deviation of the estimate itself. It should be highlighted that a certain level of variability of the estimate is physiological, particularly on the right heart valves that are affected the most by respiration. Nevertheless, a higher variability using different methods is most probably associated to errors in the estimate. The lower variability obtained using MCDA instead of a SNR-based approach may suggest that inserting some physiological constraint may be helpful.

In the end, it should be highlighted that the presented results should be considered as preliminary. A thorough validation of the proposed approach on a wider sample population is required, not only to ensure that the MCDA approach works better than its single-criterion counterparts, but also to explore the use of different possible criteria and to optimize the definition of the Electre III parameters. A further criterion to be explored, for example, is the prominence of the split between the two components, which should be maximized to obtain the highest level of differentiability between them.

4.6 Signal selection or signal combination?

As anticipated in the Introduction to this section, two main approaches can be conceived to deal with multi-source recordings: signal selection and signal combination. This is true with a whatsoever number of available channels. With some decades of available channels, as in the proposed system, this is particularly relevant and even hybrid approaches could be designed.

The proposed signal processing pipeline explores a signal selection approach. Nevertheless, some explorative analysis on signal combination was carried out in the context of this project. In particular, the viability of a Blind Source Separation (BSS) approach was investigated.

Blind Source Separation is a family of techniques that are typically employed in acoustics to separate a number of source signals from a set of recordings performed on at different spatial positions. Each recording can be regarded to as a mixture of the source signals, that need to be identified and separated. The advantage of BSS technique is that they require no a priori knowledge about the sources, nor the geometry of the recording system, nor the mixture mechanism [220]. Some previous works explored the use of BSS techniques in the context of heart sounds, with two main goals: the separation of the heart sounds from lung sounds, for denoising purposes, and the separation of fetal heart sounds from maternal sounds. A few Authors previously explored the use of BSS to separate the contributions of different cardiac structures [221–224]. To the Author’s best knowledge, no previous work successfully separated the contribution of the left and right side of the heart to separately identify the two components of the two heart sounds via BSS.

To fill this gap, a preliminary study was conducted. The study was presented at the 2020 IEEE International Symposium on Medical Measurements and Applications (MeMeA) in June 2020 entitled “A Method for the Estimation of the Timing of Heart Sound Components Through Blind Source Separation in Multi-Source Phonocardiography” [225].

The study was conducted on 3-channel recordings performed on 12 healthy volunteers. The 3 microphones were located by an expert user on the pulmonary, tricuspid and mitral areas. The goal of using 3 channels instead of 48 was to reduce the complexity of the problem. Given that the maximum number of source signals that can be separated using BSS is equal to the number of available recordings, we aimed at separating three source signals:

- Contribution of the left side of the heart
- Contribution of the right side of the heart
- Contribution of noise

The rationale of the proposed approach is graphically summarized in Figure 48.

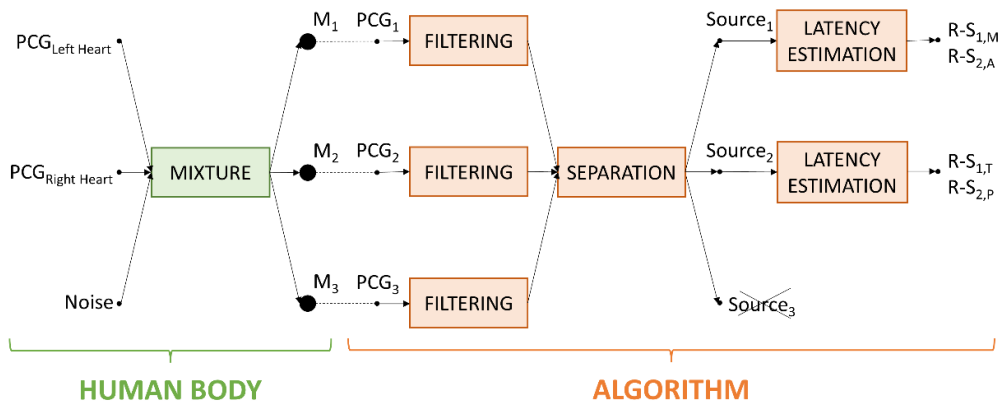


Figure 48: Rationale of the tested 3-channel BSS approach devoted to separate the contribution of the left and right sides of the heart to better identify the heart sounds components.

For the separation phase, Independent Component Analysis (ICA) was performed. The latter method consists of transforming the signals into a suitable statistical domain where the components are the most independent. Two different algorithms for ICA were tested, namely FastICA and Joint Approximation of Diagonalization of Eigenmatrices (JADE). The first is the most common ICA choice because it's highly efficient. It aims at maximizing the independence of the components by maximizing a measure of their non-gaussianity (kurtosis). JADE is based on the construction and diagonalization of a fourth-order cumulant tensor from the data. Further details can be found in [225].

Results were quite promising. First, the two algorithms provided consistent results. The application of one-way Analysis of Variance (ANOVA) resulted in a very high p-value for all cardiac valves, showing that the results were not statistically different. Moreover, a visual inspection of the separation of the components showed that the separated source signals were coherent to what expected from the analysis of the single-source recording. Figure 49 shows an example of what stated on a single heartbeat.

When compared against the single-source reference, the two BSS-based approaches proved a higher consistency with each other. Even though a thorough validation would be needed, this may be interpreted as a potential increased accuracy.

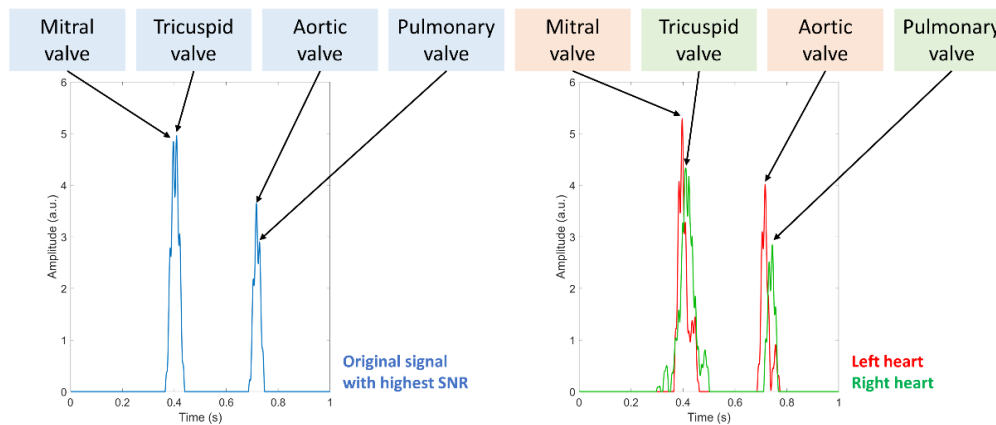


Figure 49: Comparison between the heart sounds components identified on a single-source signal against on separated source signals.

From what observed in the above-described preliminary study, a BSS-based approach may be promising. This is even more relevant when the problem is moved to a 48-channel space, where more source signals could be identified and thus the contributions of more anatomical structures separated. Nevertheless, besides being so appealing, BSS presents some challenges that need to be solved. A main conceptual issue regards the independence of the sources to be separated. In fact, even though the two overlapping sounds are generated by two distinct valves, i.e., two distinct anatomical structures, the mechanical processes that generate the two sounds are interacting: the contraction of each side of the heart is not completely independent on the other [182]. Moreover, the application of BSS techniques to a high number of recordings is definitely more challenging than its application to a few simultaneous recordings: the level of complexity of source separation is way higher when the number of sources is increased and should be properly dealt with.

In the overall, it can be stated that the exploration of both a signal selection and a signal combination approach can open to novel interesting processing possibilities devoted to increase the robustness of the estimate of the time of closure of the cardiac valves for multi-source PCG recordings at a high spatial resolution. A combination of the two approaches may be of interest when a high number of channels is available, as with the designed multi-sensor array.

Chapter 5

Pre-clinical validation

5.1 Introduction

A fundamental stage of every novel biomedical device is its clinical validation. In fact, even if thorough evidence exists in the literature that the approach the device grounds on is solid, nothing replaces the experimental evidence of its functioning on the target patients. Nevertheless, clinical validation is to be considered the last stage of the validation process: before going to the clinics, every novel approach should prove its functioning in a pre-clinical setting.

The multi-sensor system proposed in this work grounds on two main assumptions that need to be validated in a pre-clinical validation phase.

The first assumption is related to the physiological aspect of the project. Based on the literature review presented in paragraph “2.3.2 Cardiac Time Intervals and Heart Failure”, it was hypothesized that the monitoring of the CTIs, extracted from ECG-PCG noninvasive recordings, can be used as a surrogate of the monitoring of the intracardiac pressures. Nevertheless, this assumption must be verified. In fact, both the aspects, i.e., the designed multi-sensor array, and the signal processing pipeline, may impact the predictive value of the extracted parameters.

To validate this first assumption, the correlation between the features extracted from the signals and the intracardiac pressures must be assessed. Before clinically validating this point on patients affected by HF, a pre-clinical validation was

performed in this work on an animal model. The advantage of the employment of animals is the possibility of designing a reversible experiment that involves actively triggering changes in the intracardiac pressures, which would not be feasible in humans. A detailed description of the experimental protocol, the analysis that was carried out and the experimental results is presented in paragraph “5.2 Validation on animal model”.

The second assumption is related to the technical aspect of the project. As explained in paragraph “3.1 Conceptualization of the array”, the multi-sensor array was specifically designed with the purpose of enabling the application of PCG in a homecare scenario, which is not ensured by traditional single-source systems. This translates into a usability test: the multi-sensor array must prove to be usable directly by its target users, i.e., the patient or (most often) a caregiver.

Before designing a more complex experimental protocol to clinically validate the usability of the system by its target users in a real home monitoring setting, a pre-clinical validation on healthy subjects in a simulate laboratory environment was carried out. In fact, to give the system to real patients, a further re-engineering step is required: the actual prototype still requires a computer for the recording, which is not straightforward for all users. The most critical aspect of the usability concerns the positioning of the array of the chest: this feature can be verified on healthy subjects in a laboratory setting without losing generalizability. A detailed description of the experimental protocol, the analysis that was carried out and the experimental results, are presented in paragraph “5.3 Validation on healthy subjects”.

5.2 Validation on animal model

As anticipated, a validation of the physiological hypothesis the proposed approach grounds on, i.e., the hypothesis that the monitoring of the intracardiac pressures can be performed noninvasively thanks to the heart sounds, was carried out by means of an animal study. This study, presented in this paragraph, was conducted during a 5-month visiting period of the author at the CardioTech research group, Department of Health Science and Technology, Aalborg University (DK), under the supervision of Prof. Samuel Emil Schmidt. The experimental protocol was designed Prof. Schmidt and conducted at the Aalborg University Hospital under the supervision of Dr. Benedict Kjærgaard.

The following paragraphs provide details about the conceptualization and the design of the experimental protocol and about the analysis conducted on the gathered experimental data. The experimental protocol and its efficacy to produce reversible PAP changes in the animals were presented by Prof. Samuel Emil Schmidt at the 2022 Computing in Cardiology (CinC) conference in September 2022 with the title “Porcine model for validation of noninvasive estimation of pulmonary artery pressure”. They will be summarized in the next paragraphs. The processing phase is still ongoing: the results obtained by recording the heart sounds using the multi-sensor array should be considered as preliminary.

5.2.1 Motivation for the animal model

As motivated in paragraph “2.2 Monitoring of heart failure patients: state of the art”, CardioMEMS™ by Abbott (Chicago, Illinois, US) is currently the gold standard device for the monitoring of patients affected by HF. The CardioMEMS™ hemodynamic monitor is a miniaturized pressure sensor implanted in the pulmonary artery. Therefore, CardioMEMS™ monitoring grounds on the monitoring of the PAP. The availability of a noninvasive alternative to CardioMEMS™, i.e., a system capable of noninvasively monitor the PAP, is appealing.

The use of heart sounds to monitor the status of decompensation of the patients affected by HF grounds on the assumption that changes in the intracardiac pressures affect the time of closure of the cardiac valves. As shown in paragraph “2.3.2 Cardiac Time Intervals and Heart Failure”, a fair amount of experience was gained over the years within the scientific community about the correlation between the CTIs and the functionality of the heart, but further validation is needed concerning the correlation between the CTIs and the intracardiac pressures.

When the focus is placed on PAP, the analysis of S2 is of particular interest. In fact, S2 is generated by the closure of the aortic and pulmonary valves: if changes in the PAP occur, they are expected to primarily affect the pulmonary component of S2, and thus to provoke changes in the S2 split, i.e. the time separation between the aortic component (A2) and the pulmonary component (P2). In particular, a raise in the PAP is expected to be associated with a prolongation of the S2 split. In a previous study, Xu et al. investigated the problem in a porcine animal model and found a strong correlation between the split of S2, normalized with respect to cardiac cycle, and the systolic and mean PAP [226]. Their experimental protocol

was designed to change the PAP level to three different levels (normal, moderate PH, severe PH) [226].

In this work, the experimental protocol was designed with the scope of enabling a controlled, continuous, and reversible modification of the intracardiac pressures of the animal. This is dictated by two main reasons. On the ethical side, a reversible experiment allows the investigator to repeat the experiment multiple times on the same animal and thus reduces the number of animals that are required to obtain sufficient data to demonstrate the scientific hypothesis. On the technical side, a reversible experiment provides the possibility of tracking both the ascending and descending phase of the intracardiac pressure. Indeed, both phases may be interesting from a monitoring point of view, to track both the worsening and the recovery of the HF-patient from an acute episode. Moreover, the possibility of monitoring the PAP in a continuous fashion is novel and closer to the real-life scenario.

5.2.2 Experimental protocol

Experimental setup

The experimental protocol was developed for use on a porcine model. The latter choice was dictated by the fact that the pig has the most similar cardiovascular system to the human and is therefore the typical choice for cardiovascular animal studies. The protocol was applied to Danish Landrace pigs (also known as Danish bacon). The pigs were anesthetized and mechanically ventilated throughout the experiment.

Two catheters were employed for the recording of the intracardiac pressures. Arterial catheterization provided the measurement of the systemic blood pressure measured in the aorta. A Swan-Ganz catheter was used for the monitoring of the pressure in the heart. As anticipated, the goal of the study consists of determining the correlation between the S2 split and the PAP. Nevertheless, placing the tip of the catheter inside the PA is not fully convenient in this case: in fact, the Swan-Ganz catheter would need to be inserted through the pulmonary valve, and thus it would affect its closure and the generated S2. To work this issue around, the tip of the catheter was placed in the RV. As it can be observed in Figure 7 (which represents the pressures in the left side of the heart, but the same relative relationships exist on the right side), in the systolic phase of the cardiac cycle the pressure in the PA equals the pressure in the RV. Therefore, the systolic RV pressure (RVPs) can be used as a surrogate for the systolic PA pressure (PAPs).

In the overall, the following vital signs were monitored throughout the experiment and visualized on the surgical monitor:

- Heart rate (HR)
- Systolic pressure in the aorta (SBP)
- Diastolic pressure in the aorta (DBP)
- Systolic pressure in the RV (RVPs)
- Diastolic pressure in the RV (RVPd)
- Oxygen saturation (SpO₂)

The values for each vital sign were automatically recorded every 10 seconds, i.e., with a 0.1 Hz sampling frequency.

The experiment was first designed with the scope of extracting the S2 split from SCG recordings. For the purpose, two triaxial accelerometers were employed: one located over the fourth intercostal space next to the sternum (IC4) and one over the lower border of the sternum. The two triaxial accelerometer signals were recorded through an iWrox™ commercial system for the recording of biomedical signals, with a sampling frequency of 5 kHz. A simultaneous ECG was recorded.

For the testing of the multi-sensor array presented in this work, the accelerometers were removed, and the multi-sensor array was placed on the thorax of the animal. The dimensions of the array were not optimized for the shape and dimensions of the chest of a pig, but the flexibility of the array enabled its adaptation to the animal. The contact between the animal skin and the multi-sensor array was ensured by means of an elastic band. Figure 50 proposes a graphical representation of the experimental setup, both in the original setup with the two accelerometers and in the modified setup with the multi-sensor array.

Provocation of pulmonary hypertension

Two types of experiment were designed to provoke PH, using two different kinds of triggers. Both triggers were aimed at causing PH acting on some physiological mechanisms, but they are meant to provoke a different systemic reaction. In this way, the change in the PAP is not always associated with the same changes in the other vital signs.

The first kind of experiment was based on the provocation of a condition of *hypoxemia* in the animal. The latter was obtained through a mechanism known as hypoxic pulmonary vasoconstriction, that was triggered through nitrogen

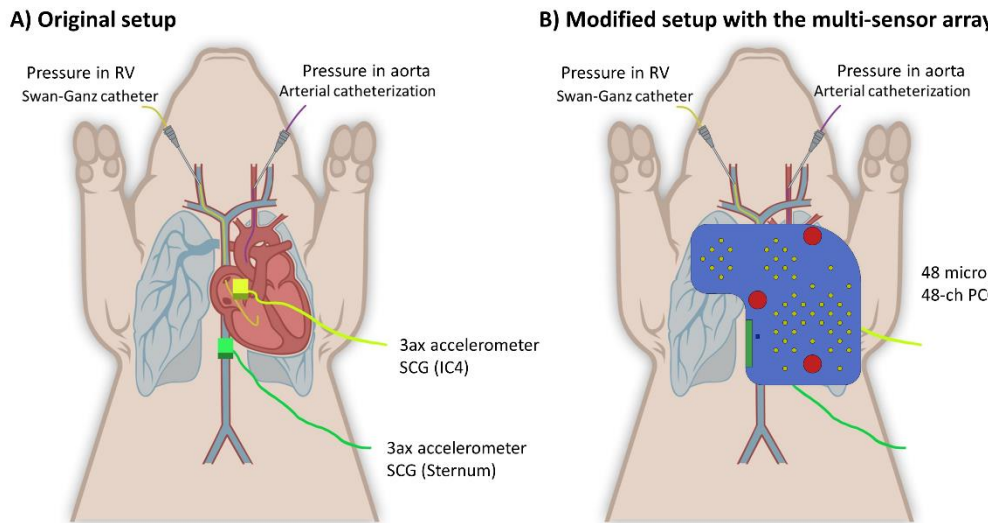


Figure 50: Graphical presentation of the experimental setup, in its original conceptualization (A) and adapted for the validation of the multi-sensor array (B).

asphyxiation: the oxygen supply through the ventilator was replaced by nitrogen. From a physiological perspective, a low oxygen concentration in the inspired air causes localized vasoconstriction of the pulmonary capillaries at an alveolar level, devoted to divert the blood to areas of the lungs characterized by a higher ventilation [227]. An increased pressure at pulmonary capillaries level reflects in the PA and provokes a rise in the PAP.

The second kind of experiment was based on the provocation of a condition of *hypercapnia* in the animal. In this case, the condition was obtained by means of carbon dioxide asphyxiation: the oxygen supply was replaced by CO_2 and the CO_2 absorber was removed, to further increase the CO_2 concentration and its effect. The physiological mechanism at the base of the hypercapnic pulmonary vasoconstriction is similar to what described for hypoxemia, and, again, results in an increase of the PAP [228].

In both types of experiment, the trigger was removed, i.e., normal oxygen supply was provided again through the ventilator and, in case it was removed, the CO_2 absorber was put back in place, when either the RVPs reached a plateau or in case of severe arrhythmias. In both cases, the cardiovascular system of the animal was expected to return to the baseline condition after a proper amount of time.

For each animal, the following experimental protocol was executed:

1. *Baseline*. A 1-minute recording was performed before any trigger was provided.
2. *Hypoxemia*. While recording, the hypoxemic trigger was provided and kept until the RVPs reached a plateau or severe arrhythmias arose. Then the trigger was removed and the recording was continued until the animal was again in a stable condition.
3. *Hypercapnia*. While recording, the hypercapnic trigger was provided and kept until the RVPs reached a plateau or severe arrhythmias arose. Then the trigger was removed and the recording was continued until the animal was again in a stable condition.

Hypoxemia and hypercapnia experiments were repeated iteratively, always waiting until the animal was back to a stable condition, until the Clinical Supervisor decided that the baseline condition was compromised.

5.2.3 Sample population and efficacy of the model

The experimental protocol was executed on 11 Danish Landrace pigs. Pigs with a weight of around 30 kg were selected for the study. Three pigs were used for the SCG experiment alone, whereas 8 pigs were also equipped with the designed multi-sensor array. As anticipated, in each experiment, either SCG or multi-source PCG was recorded.

A total number of 71 experiments were carried out. Among them, 58 were included in the sample population: in the remaining experiments, no increase in the RVPs was observed when the trigger was applied. The recordings were almost equally divided between hypoxemia and hypercapnia experiments (30 vs 28). Among the 58 available experiments, heart sounds were recorded using the triaxial accelerometers in 42 recordings and using the designed multi-sensor array in 16 recordings.

As a first analysis, the effect of the triggers on the monitored physiological variables was assessed, partly to verify that the rise in the PAP occurs as expected, partly to determine the effect on the other physiological variables that could affect the timing of the cardiac valves, such as the heart rate and the systolic blood pressure. Figure 51 presents the relative variations of the heart rate, the SBP, the RVPs and the SpO2 in function of the elapsed time from the start of the trigger.

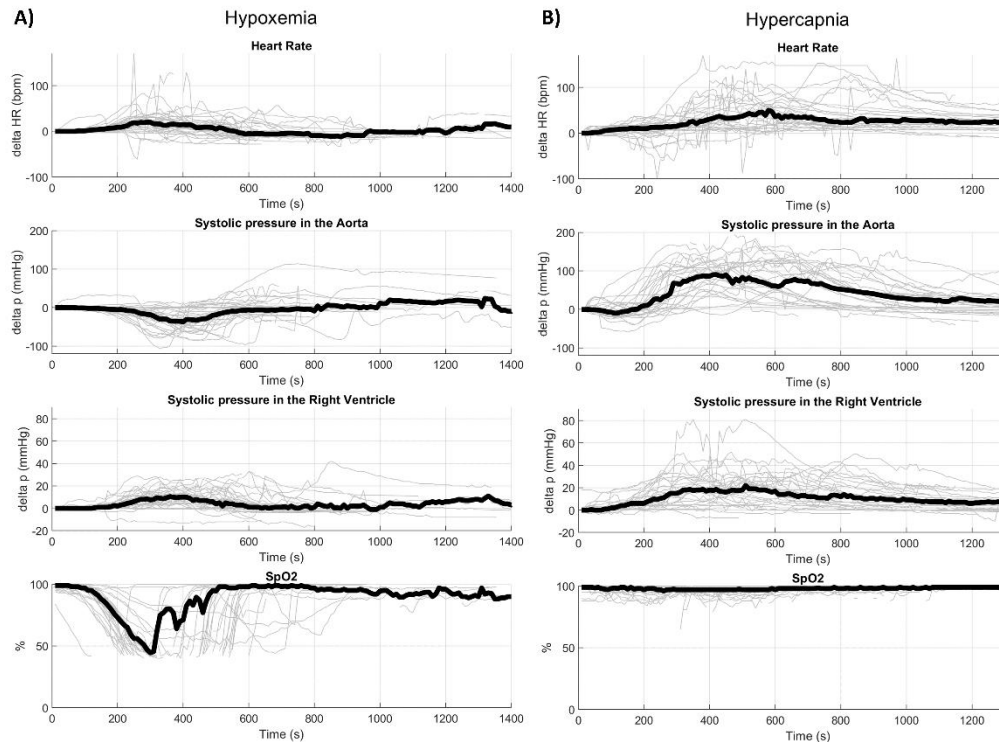


Figure 51: Changes produced in the monitored physiological parameters when the hypoxemic trigger (A) or the hypercapnic trigger (B) is applied.

It can be observed that both triggers provoke a consistent rise in the RVPs and in the HR, but the effect of the hypercapnic is stronger than that of the hypoxemic triggers. On the contrary, a diverse effect was observed on the SBP: the hypoxemic trigger was followed by a decrease in the SBP, whereas the hypercapnia caused the SBP to strongly increase. This is an interesting effect from the perspective of the correlation analysis: the effect of the pressures in the pulmonary circuit and in the systemic circuit can be differentiated and the changes in the S2 split can be more safely associated with the changes of the correct pressure. Concerning the SpO₂, the trend confirms that the trigger provoked the expected effect in terms of oxygen saturation: the hypoxemic trigger actually causes hypoxemia, as the severe decrease in SpO₂ confirms, whereas the hypercapnic trigger does not. Table 7 presents the values of the HR, the RVPs and the SBP for the baseline (i.e., the first recorded value), and the peak of the trigger (i.e., the maximum value of the RVPs) for both the hypoxemic and the hypercapnic triggers.

Table 7: Comparison of the baseline and peak values of the monitored physiological variables, both in hypoxemic and hypercapnic experiments.

Physiological variable	Hypoxemia		Hypercapnia	
	Baseline	Peak	Baseline	Peak
HR (bpm)	76 ± 15	105 ± 29	72 ± 20	123 ± 46
RVPs (mmHg)	29 ± 10	48 ± 12	28 ± 10	61 ± 21
SBP (mmHg)	124 ± 19	112 ± 27	127 ± 22	224 ± 67

Even though the trend of the physiological variables is repeatable over the experiments, even across different animals, the variability is high. If on one side this strengthens the validity of the results of the correlation analysis (if obtained), on the other side it complicates the analysis because a different combination of the physiological variables may provoke a different effect on the heart sounds.

In the end, the repeatability of the experiments was verified by checking if the baseline values over subsequent experiments performed on the same animal were significantly different or not. The values were found not to be significantly different for HR, RVPs, and SBP.

5.2.4 Correlation between S2 split and PAP

For the purposes of this work, only the analysis of the experiments performed using the multi-source array is presented in this paragraph. The analysis involved 16 experiments, carried out over 8 pigs. Among them, 9 hypoxemic and 7 hypercapnic experiments are described. The methods of analysis and the preliminary results over the reduced sample population are presented in the next paragraphs.

Methods

Given the complexity of the experiments, which involved the combined effect of the variations of multiple physiological variables, a first-level analysis involved the visual inspection of the recordings. Afterwards, a quantitative correlation analysis was carried out.

Given that no morphological analysis is typically performed on the heart sounds, because no clear interpretation exists on the waveform of the sounds, the visual inspection was not performed directly on signals. Instead, a 200-millisecond-long segment containing the S2 was first segmented from the signal, to create a N-by-M matrix where N is the number of heartbeats and M is 200 samples. The matrix was then visualized as an image, with the heartbeats of the recording on the x-axis and the time of the S2 segments on the y-axis. This method found inspiration from what described in [181].

For a better visualization of the changes in the S2 split, the S2 segments were visualized both before and after alignment. In fact, the latency of S2 with respect to the QRS complex is strongly influenced by the heart rate, which is not constant over time during the experiment. Since the focus of this analysis is on the changes in the S2 split, the variability of the $RS_{2,A}$ and $RS_{2,P}$ timing may be misleading. The alignment was performed by computing the cross-correlation between each segment and the median segment and compensating for the delay estimated as the maximum of the cross-correlation function.

The changes in the heart sounds were visually compared to the changes in the physiological variables, and to RVPs in particular.

As a second-level analysis, the quantitative correlation between the S2 split of the heart sounds and the corresponding RVPs, used as a surrogate for the PAP, was computed. To estimate the S2 splits, the signal processing pipeline described in section “**Error! Reference source not found.**” was applied to the recordings. The S2 split was defined, beat-by-beat, as the time difference between the located aortic component and the located pulmonary component. The RVPs value corresponding to each beat was computed by interpolation of the monitored RVPs signal. In the end, a S2 split value and a RVPs value were available for each heartbeat. Both arrays were low-pass filtered by applying a moving average of 60 heartbeats to highlight the trend.

The correlation analysis was first performed on three levels: experiment-by-experiment, animal-by-animal, and in the overall. The goals are different. The overall analysis is interesting to understand if a single linear model can describe the relationship between PAP and S2 split in general, from a physiological point of view. This would be extremely interesting for generalization purposes: nevertheless, it's also especially challenging given the multitude of other physiological variables potentially involved. On the other side, the experiment-by-

experiment analysis and the animal-by-animal analysis are more related to the final scope, i.e., the monitoring of the PAP over the time. In fact, it can be hypothesized that each subject is characterized by a different combination between the baseline PAP and the baseline S2 split. Given that the monitoring is patient-wise, the relative changes of the physiological variables within the same subject are more important than the absolute variable of the parameters.

Correlation was estimated by means of the Pearson correlation coefficient.

Preliminary results

Figure 52 shows an example of the visual inspection phase performed on a single experiment. The matrices of the S2 segments, realized as described above, are represented in the form of images. Both the S2 segments and their envelope are shown, before and after the alignment step. The figure also shows the trend of the S2 split estimated from the signal and the monitored RVPs.

It should be noted that the proposed example shows a very good match between the S2 split and the RVPs, corresponding to a Pearson correlation coefficient as high as 0.93. In other cases, the relationship between the two is less visible, and the variability of the S2 segments is much higher. In the proposed example, instead, the progressive separation of the aortic and pulmonary components of S2 at the rise of the RVPs is clearly recognizable. Even though the separation is visible in the S2 segments, the use of the Shannon Energy envelope strongly highlights the components. It should be highlighted that the aortic component is stronger in amplitude and in energy than the pulmonary, as expected, and that the pulmonary component is more affected by the respiration.

Figure 53 presents a graphical representation of the Pearson correlation coefficients, with their confidence intervals, for every experiment where the multi-sensor array was employed and the best channel was selected.

In the vast majority of the experiments, the estimated S2 split was found to be strongly correlated with the RVPs, i.e., with the PAP. Only one experiment resulted in a negative correlation and one experiment in a weak positive correlation: these cases should be object of further analysis in the future to understand if the changes of other physiological variables played a role. A median Pearson correlation coefficient as high as 0.71 was found.

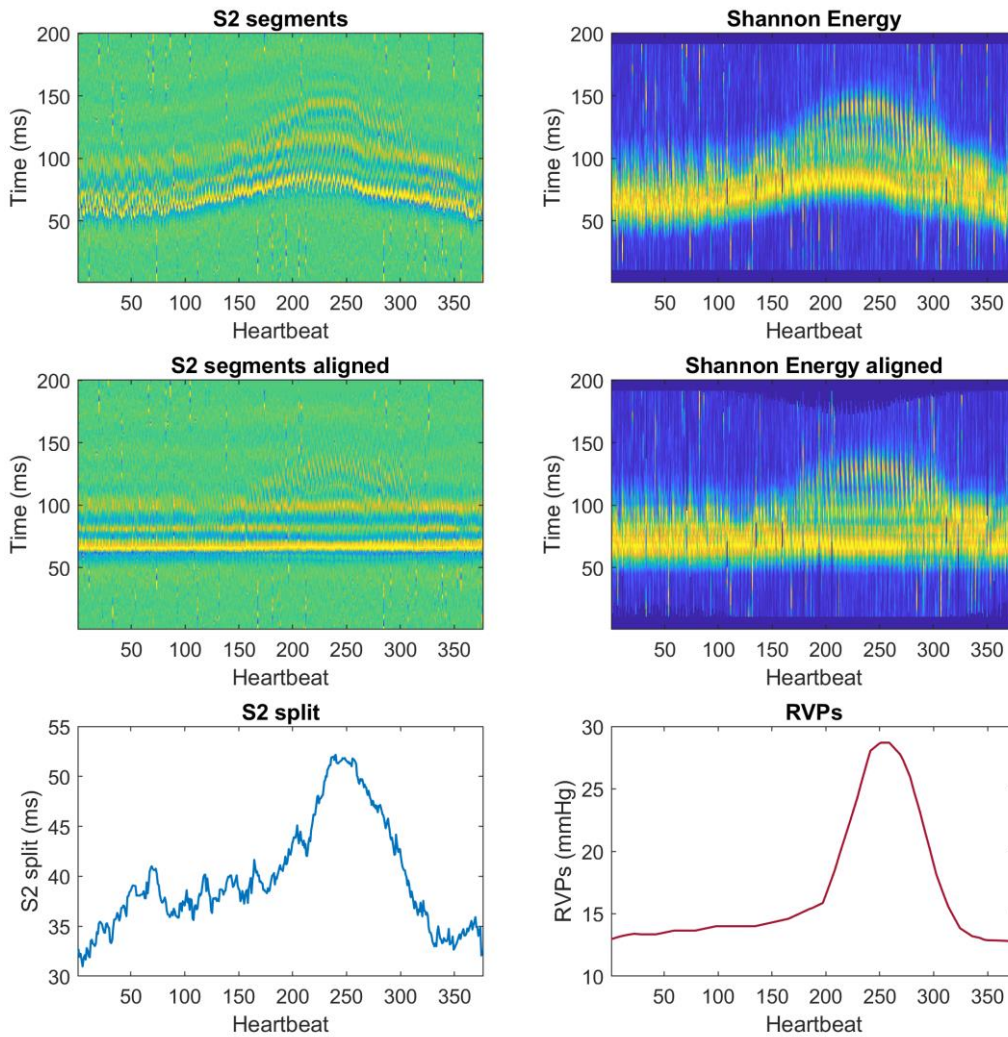


Figure 52: Example for a single experiment. Representation by images of the S2 segments, before and after alignment, and their envelope. Comparison between the resulting S2 split and the monitored RVPs.

Concerning the pig-by-pig analysis, Figure 54 presents a pig-by-pig comparison between the estimated S2 split and the corresponding RVPs. On each pig, one to three experiments were performed with the multi-sensor array.

A qualitative analysis of the plots confirms that in every pig the changes in the S2 split are consistent with the changes in the RVPs, i.e., in the PAP. Nevertheless, the S2 split is characterized by a much higher variability, which decreases the

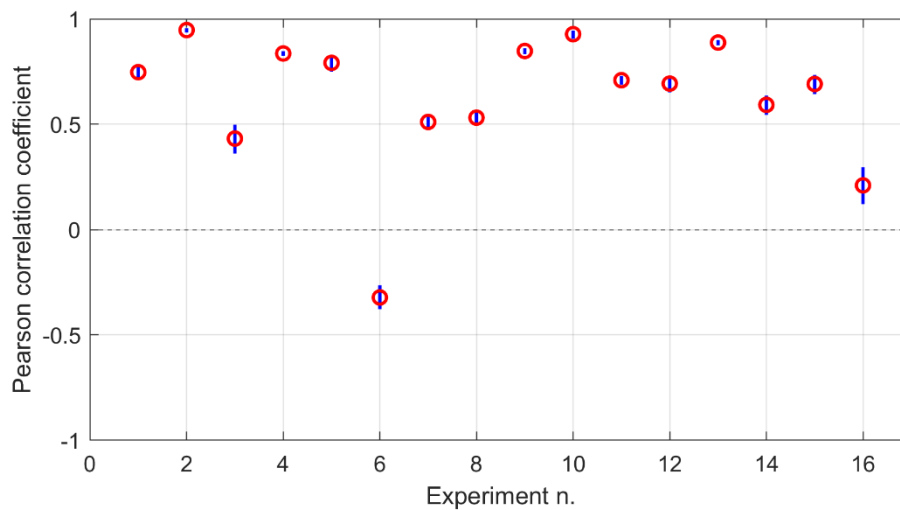


Figure 53: Correlation coefficient between S2 split and RVPs of each recording. The red circles represent the estimated R, whereas the blue lines represent the confidence interval.

correlation between the variables. This suggests that the correlation is present, but the S2 split estimate can be improved. The median Pearson correlation coefficient was found equal to 0.68, which is not significantly lower than what obtained in the experiment-by-experiment analysis.

Table 8 reports the correlation coefficient found in the three levels of the analysis: the median correlation coefficient of the experiment-by-experiment phase, the median correlation coefficient of the pig-by-pig phase and the overall correlation coefficient.

Table 8: Correlation coefficient obtained in the three phases of analysis.

	Single experiments (median)	Single animals (median)	Overall
Pearson correlation coefficient	0.71	0.68	0.23

It can be observed that the overall correlation is weak. This can be explained by the fact that each pig has a different combination of baseline PAP and baseline S2 split, as it can be observed in Figure 54.

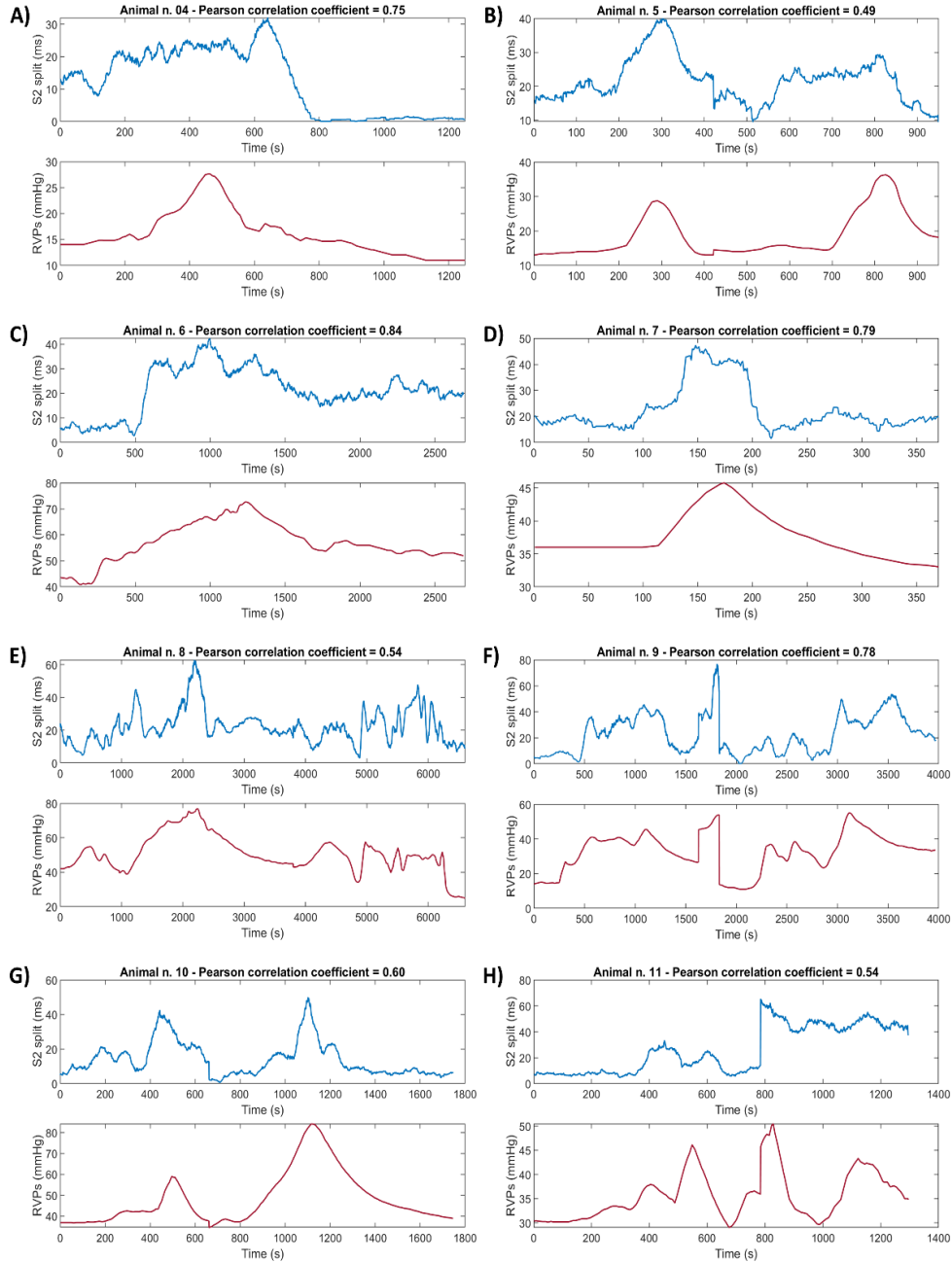


Figure 54: Pig-by-pig comparison between the S2 split and the RVPs over time. Each panel represents the physiological variables of a different pig.

Discussion

As anticipated, the results presented in this paragraph are to be considered as preliminary: if on one side they confirm the physiological hypothesis that a correlation exists between the timing of the heart sounds and the intracardiac pressures, on the other side a multitude of further research questions arise from the presented analysis.

A first point of focus regards the complexity of the experiment and thus of the analyses that can be done. Both the hypoxemic and hypercapnic triggers provoke extreme physiological states in the animal. If this results, on one side, on strong and steady variations of the PAP, which is beneficial to study its effect on the heart sounds, it also causes extreme variations in the heart rate and in the systemic blood pressure (among the others). This also results from the visual inspection of the images constructed by stacking the S2 segments and their envelopes: the variations in the heart sounds over the recording are clearly recognizable, but not always as easy explained as in the case of the example proposed in Figure 52.

Therefore, even if at this stage the correlation of the S2 split and the PAP was assessed, a more complex model of the changes in the time of closure of the four cardiac valves (and particularly of the semilunar valves, which are mostly affected by changes at the pulmonary level) including the changes of multiple physiological variables may be required. This will be the object of future work.

From the presented results, it can be derived that a positive correlation exists between the split of the aortic and pulmonary components in S2 and the PAP on the same subject. In other words, a rise in the PAP delays the closure of the pulmonary valve with respect to the closure of the aortic valve. This is coherent to what expected from physiology and what suggested from previous studies [226]. Nevertheless, the relationship between the S2 split and the PAP over the general population is not easily derived: if the correlation is strong when comparing values recorded on the same subject, even across different recordings and different experiments (hypoxemic or hypercapnic), this does not hold when values recorded on different animals are put together. This is mainly due to the fact that baseline S2 split and PAP values are different across different animals.

The presented finding does not limit the applicability of the approach in home care telemonitoring: since the monitoring is performed independently on each subject, a personalized ground truth could be constructed when the subject is in a verified compensated state and relative variations with respect to the ground truth

could be recognized from the S2 split, according to the presented results. Nevertheless, the existence of a general correlation should not be excluded: a further analysis of the impact of the other physiological variables may provide a better insight into the matter.

From the technical point of view, the interpretation of the results is threefold. On one hand, the existence of a strong correlation in the vast majority of the recordings proves that the processing pipeline leads to reasonable estimates of the time of closure of the cardiac valves. On the other hand, the trend in the S2 split is affected by a higher variability than the trend in the RVPs, which is expected to be the result of errors in the estimates on some heartbeats. This suggests that the separation of the two components, which is the most critical processing phase, can still be improved. On a third level, the comparison between the visual inspection of the heart sounds and the trends of the extracted heart sounds components may be an interesting validation tool: for example, in experiment number 6 (Figure 53) the correlation coefficient was found to be negative, but the trend in the S2 split was found to be consistent with the changes in the heart sounds that could be visualized in the images. This tells us that the reason of the negative correlation should not be searched for in the estimation algorithm, but in the physiological domain.

In conclusion, the above-presented preliminary results confirm that a positive correlation exists between some time features extracted from the heart sounds and some intracardiac pressures. This constitutes, to some extent, a validation of the hypothesis this work grounds on. On the other side, the analysis can be extended and opens to the construction of a more complex model of the effect of the changes of some physiological variables (and their combination) on the time of closure of the four cardiac valves.

5.3 Validation on healthy subjects

As anticipated, the pre-clinical validation on healthy subjects was designed with the purpose of validating the usability of the multi-sensor array by inexperienced users. This translates, as a primary goal, in validating that the multi-sensor array can be successfully positioned over the chest of a subject by someone with no clinical nor technical knowledge about auscultation. As a secondary goal, the device should ensure a good fit on the broadest possible population. Indeed, the device was designed as a noninvasive alternative to invasive hemodynamic monitors: the main advantage resides in enlarging the pool of at-risk patients that can benefit from the monitoring.

The validation was carried out at the Polito^{BIO}Med Lab at Politecnico di Torino. It was articulated in two phases: in the first, the usability was assessed on the multi-source PCG recordings alone; in the second, the results obtained with the multi-source PCG approach was compared to what obtained through the traditional single-source approach. Details about the experimental protocols and the performed analyses are the object of the next paragraphs.

5.3.1 Experimental protocol

To achieve the goal, volunteers were enrolled for the experiment with the following exclusion criteria:

- Medical or technical education in the field of auscultation
- Declared presence or history of cardiovascular diseases.

The goal of the first exclusion criterion was to ensure that the volunteers could be considered inexperienced with respect to auscultation, and in particular with respect to the correct positioning of the stethoscope over the chest. On the other side, the second exclusion criterion was meant to limit the experiment to healthy subjects, to ensure that no pathological conditions affect the analysis and to obtain a baseline for the quality and the CTIs.

The experimental protocol simulated a real-life home monitoring scenario, where a caregiver performs the recording on a patient. For this purpose, volunteers were enrolled in couples. Upon their arrival, the volunteers were thoroughly explained the scope and methods of the experiment and asked to sign an informed consent. Then, in each couple, volunteers were randomly labelled as Subject A and Subject B.

First, Subject A was assigned the role of the patient and Subject B the role of the caregiver. The experiment articulated in three phases:

Phase 1: Multi-source PCG recording by inexperienced user. The volunteer-caregiver was asked to read a simple set of instructions on how to use multi-sensor array. Figure 55 shows the instructions paper.

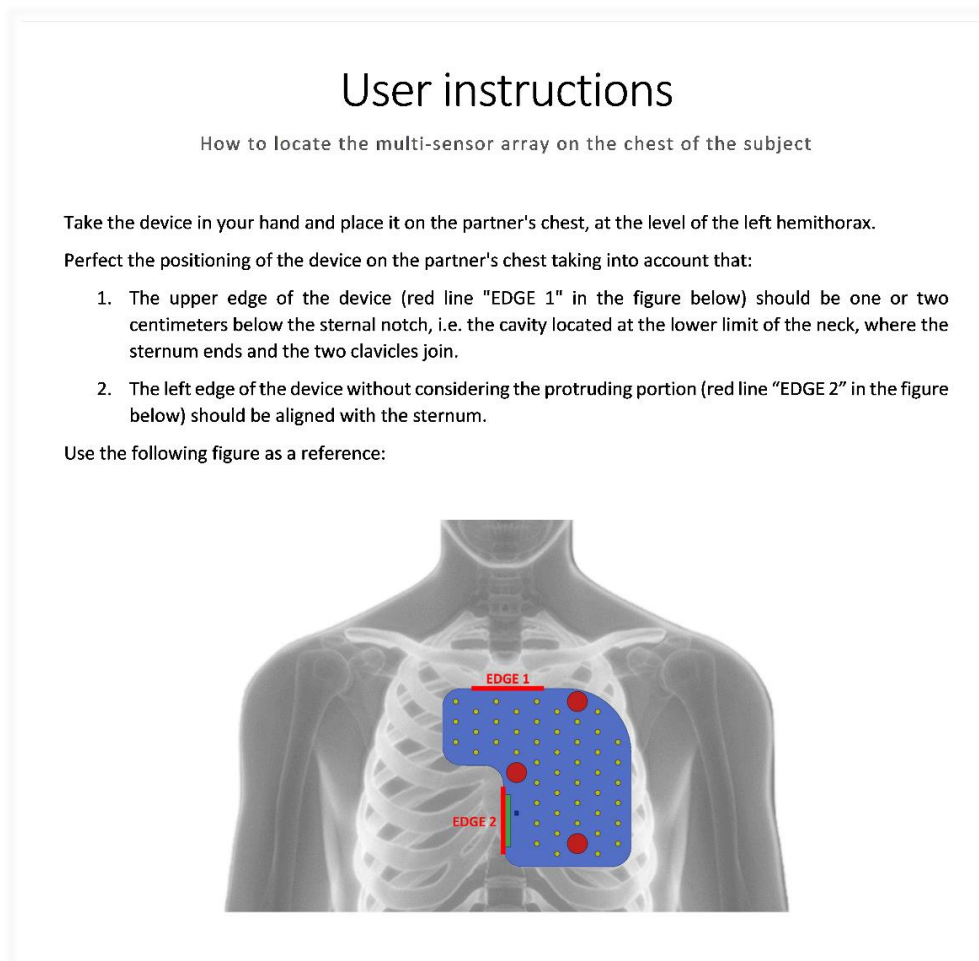


Figure 55: Instructions provided to the volunteer-caregiver on how to locate the multi-sensor array on the chest of the volunteer-patient.

In the meanwhile, height, weight, and thoracic circumference of the volunteer-patient were measured by the investigator. Then, the volunteer-patient was asked to lay on an examination table in a supine position with a bare thorax. When the volunteer-caregiver was ready, he/she was asked to locate the multi-sensor array on the volunteer-patient and to fix it with an elastic band. No feedback whatsoever was given by the investigators. A 5-minute recording was then performed. The volunteer-patient was asked to stay still and quiet throughout the recording and to breath normally.

Phase 2: Single-source PCG recording (left heart) by expert user. An investigator, acting the role of the expert user, removed the multi-sensor array from

the chest of the volunteer-patient and set up the single-source system. The ReMotus™ system described in paragraph “4.3 Assessment of the quality of PCG signals” was employed. The investigator placed three Ag/AgCl disposable electrodes to recreate a first standard lead. The two active electrodes were located in the left and right sub-clavicular areas, along the mid-clavicular lines, whereas the reference electrode was located on the right side of the abdomen. Two microphone probes were located over the:

1. Mitral area: fifth left intercostal space, along the mid-clavicular line.
2. Aortic area: second right intercostal space, next to the border of the sternum.

A 5-minute recording was performed in this setting.

Phase 3: Single-source PCG recording (right heart) by expert user. The investigator changed the positions of the microphone probes and located them over the:

1. Tricuspid area: fourth left intercostal space, next to the border of the sternum.
2. Pulmonary area: second left intercostal space, next to the border of the sternum.

A 5-minute recording was performed in this setting.

Figure 56 compares the positioning of the sensors in the three phases of the experiment and the traditional auscultation areas.

At the end, the roles were reversed: Subject A was assigned the role of the caregiver and Subject B was assigned the role of the patient. The three above-described phases were repeated with the same modalities. In the end, for each subject, the following signals were available:

- One 5-minute 48-channel PCG recording at high spatial resolution.
- Four 5-minute single-channel PCG recordings, each one optimized for a different cardiac valve.

The described experimental protocol was approved by the Research Ethics Committee of Politecnico di Torino (protocol number 16863/2021).

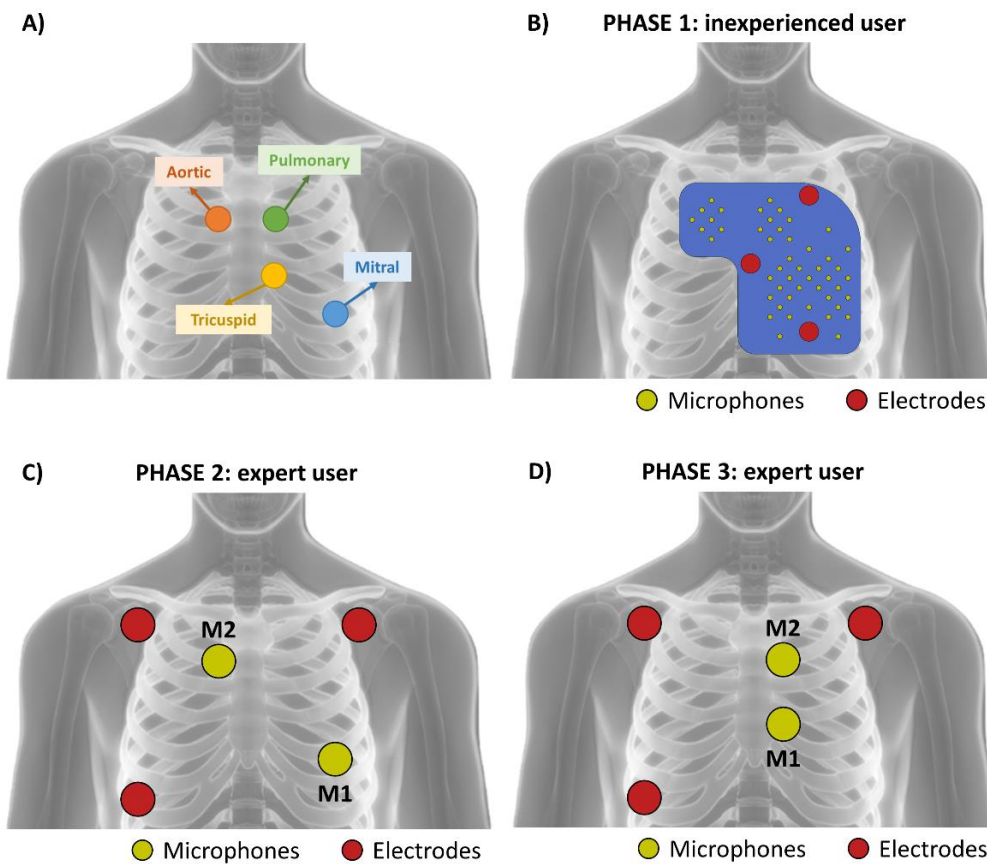


Figure 56: Comparison between the traditional auscultation areas (A) and the positioning of the sensors in the three phases of the experimental protocol (B-D).

Sample population

Forty-two volunteers were enrolled in the study to constitute the sample population. The subjects were heterogeneous in terms of biological sex (50% females) and body shape. The body shape was described in terms of Body Mass Index (BMI) and thoracic circumference. Figure 57 presents the distribution of BMI and thoracic circumference in the sample population, in function of the gender.

5.3.2 Validation of usability

The validation of usability is of fundamental importance because it determines whether the designed multi-sensor array achieves the primary goal it was designed for. The usability articulates in two different analyses:

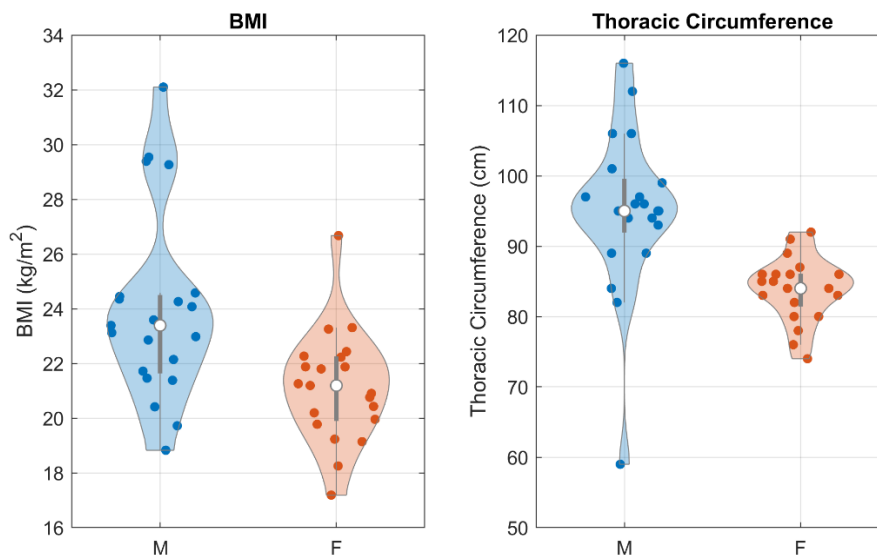


Figure 57: Violin plots of the distributions of respectively BMI and thoracic circumference, differentiating the biological sex, over the sample population.

1. Usability by inexperienced users.
2. Usability on a wide range of body types.

The first analysis is aimed at determining whether the multi-sensor array enables users with no technical nor clinical experience, as the patient or a caregiver, to record signals apt to estimate the CTIs for monitoring purposes. The second analysis is aimed at determining if the characteristics of the chest of the subject affect the quality of the recordings and thus limit the target population of the device. This is required for every wearable device. The usability on a wide range of body types should not be taken for granted: it is reasonable to hypothesize that factors like the presence of breasts or the presence of a thick interposed layer of fat or muscular tissue could increase the filtering effect of the biological tissues and in turn cause a decreased intensity of the vibrations produced by the closure of the cardiac valves on the skin. What stated was also suggested by previous studies in the field of heart sounds analysis [152,187].

The next paragraphs will provide details about the method of analysis and the experimental results, along with their discussion. Part of the analysis presented in this paragraph was accepted for poster presentation at the VIII Congress of the National Group of Bioengineering (GNB) entitled “Usability of a multi-sensor array for the application of electro-phonocardiography in home care”.

Rationale and methods

For the first goal, the usability of the device was defined as the capability of inexperienced users of carrying out a recording through the device which can be used to reliably estimate the CTIs. This translates into a quality assessment of the recording, which requires to be classified as good quality for the purpose of estimating the time of closure of the four cardiac valves.

It was found in the study presented in paragraph “4.3 Assessment of the quality of PCG signals” that a SNR higher than 13 dB for S1 and 14 dB for S2 ensures an absolute error on the estimate lower than the temporal resolution of the recording system (1 millisecond) [198]. Therefore, it can be stated that if an inexperienced user can obtain a recording with a SNR higher than 13 dB for S1 and 14 dB for S2, the said recording can be reliably used to estimate the CTIs. Therefore, the usability of the multi-sensor array was evaluated as the percentage of multi-source recordings with an above-threshold SNR for both S1 and S2.

At the first level of analysis, the best SNR of each recording was considered to demonstrate that at least one good single-channel recording could be achieved by all inexperienced volunteers. The percentage of recordings with the best SNR higher than the thresholds was computed for this purpose. The analysis was conducted on both raw and filtered PCG signals. Filtered signals were obtained from raw signals by means of a band-pass IIR Chebyshev II filter between 20 Hz and 100 Hz.

A second-level analysis involved assessing the percentage of channels with an above-threshold SNR, recording by recording. If a high number of channels present a good quality even in recordings performed by inexperienced user, this could give an insight into the possibility of differentiating the auscultation areas in a home monitoring. In the end, the spatial distribution of the SNR over the chest across the subjects was visually inspected to investigate the consistence with the expected auscultation areas.

For the second goal, the usability of the device was defined as the possibility of obtaining good-quality recordings on a broad population, regardless of their body type. For this scope, the body shape of the subject was described in terms of:

- Biological sex (categorical variable, male or female).
- BMI (continuous variable, expressed in kg/m^2).
- Thoracic circumference (continuous variable, expressed in cm).

The correlation between the SNR of respectively S1 and S2 and each of the above-defined descriptors of the body shape was evaluated. The correlation was computed by means of the point biserial correlation for categorical variables (biological sex) and by means of Pearson correlation coefficient for continuous variables (BMI and thoracic circumference). If a correlation is found, a regression line is computed with the scope of defining the limits of applicability of the device.

Results

Concerning the usability by inexperienced users, Figure 58 shows the boxplots of the distribution of the best SNR for respectively S1 and S2, in respectively the raw and filtered recordings.

The two distributions (raw and filtered) provide a different kind of information. An above-threshold SNR on the raw recordings confirms that the subject could perform a good quality recording, regardless of the goodness of the signal processing. Even in case the quality of the original recordings was low, an above-threshold SNR on the filtered signals ensures that the features of interest can be reliably extracted provided that appropriate signal processing is performed.

In the tested sample population, all recordings achieved an above-threshold SNR on both heart sounds even before any digital filtering was applied. As a result, 100% of the inexperienced users could successfully perform the task of recording the heart sounds on a peer by means of the multi-sensor array. If the filtered signals are taken into consideration, the average best SNR was found as high as 24 dB for both heart sounds, which proves that excellent-quality recordings are achievable in a telemonitoring context.

When considering the different channels independently, the average percentage of channels resulting in an above-threshold SNR was found to be 55% for S1 and 64% for S2. The difference is consistent with the slightly higher values of the SNR of S2 resulting from the distributions in Figure 58. It can be stated that on average more than half of the available channels can be used for further processing. This in turn enables the use of both signal selection and signal combination techniques on multi-source recordings: in fact, it can be hypothesized that some good-quality signals are available in each of the forecasted auscultation areas.

As a confirmation of what stated, Figure 59 presents a graphical mapping of the percentage of recordings where respectively the SNR of S1 is higher than the SNR of S2 and the other way round. In other words, the map in panel A shows a

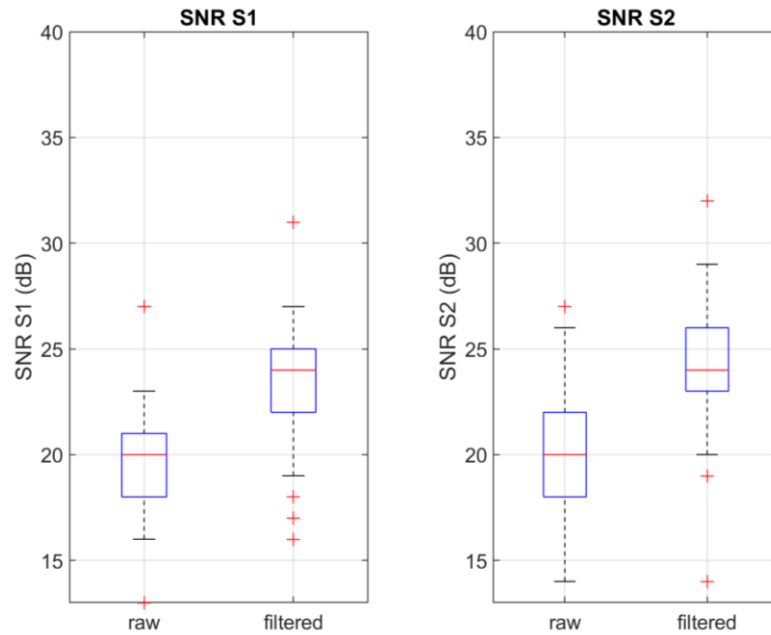


Figure 58: Boxplots of the distributions of the SNR of S1 and S2 over the sample population, before and after filtering.

higher intensity on the channels where the S1 is prevalent, whereas the map in panel B shows a higher intensity on the channels where the S2 is prevalent.

It can be observed that the channels presenting the highest quality on S1 are located in the lower side of the left lower side of the map, which is consistent with the expected positioning of the device over the chest. In fact, the mentioned area of the map corresponds to the mitral and tricuspid auscultation areas. On the contrary, the highest quality on S2 is found in the channels in the upper side of the array, corresponding to the aortic and pulmonary valves.

Concerning the effect of the characteristics of the chest, Figure 60 shows the scatter plots of the SNR of respectively S1 and S2 in function of each of the three descriptors of the body type, namely BMI, thoracic circumference and gender.

Table 9 includes the correlation coefficients that were found between the SNR of respectively S1 and S2 and each of the three descriptors of the body type. The values in brackets represent the confidence interval of the correlation coefficient. The * highlights the correlation coefficients that were found statistically significant ($\alpha = 0.05$).

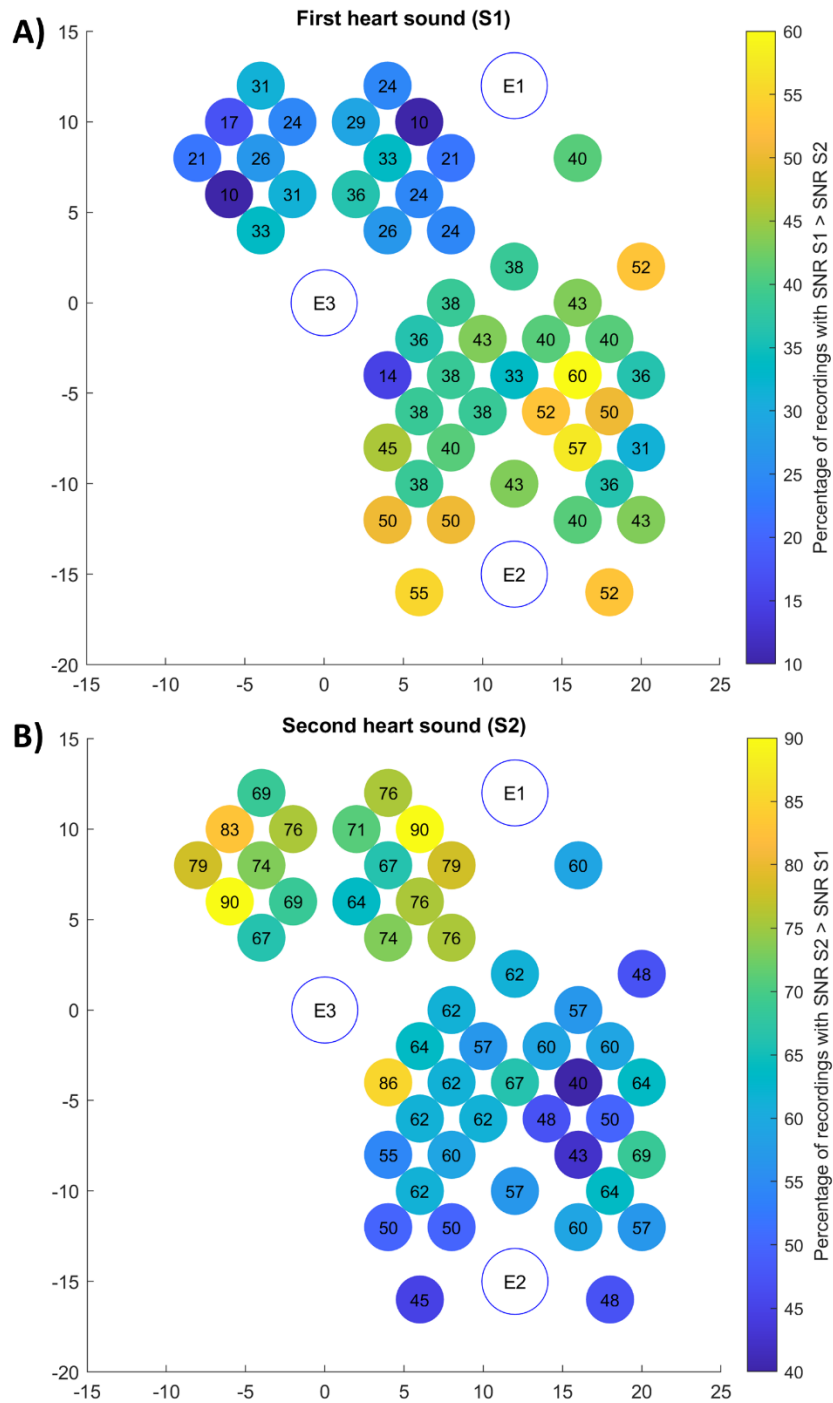


Figure 59: Maps of the percentage of recordings belonging to the sample population with respectively A) the SNR of S1 higher than the SNR of S2 and B) the SNR of S2 higher than the SNR of S1. Each circle represents a microphone, the color represents the percentage according to the colorbar.

Table 9: Correlation coefficients between the SNR of S1 and S2 and the descriptors of the body type.

Descriptor of the body type	Correlation against SNR S1	Correlation against the SNR S2
Sex	0.00 (-0.30 – 0.31)	0.35 * (0.06 – 0.60)
BMI	-0.03 (-0.33 – 0.28)	-0.53 * (-0.72 - -0.27)
Thoracic circumference	-0.16 (-0.44 – 0.15)	-0.48 * (-0.68 – -0.21)

Results show that no correlation is present between the signal quality of S1 and the characteristics of the chest of the subject. On the contrary, a weak to moderate correlation was found between the quality of S2 and the biological sex, the BMI and the thoracic circumference. In particular, a wider thorax and a higher BMI (which are most typically found in male subjects) seem to be associated with a lower quality of S2. To further investigate the effect of body shape in the real-life applicability of the multi-sensor array, we used a linear regression model to predict the threshold of respectively BMI and thoracic circumference that would theoretically lead to an under-threshold SNR for S2. Table 10 reports the results.

Table 10: Linear regression of the SNR of S2 against BMI and thoracic circumference.

Linear regression	SNR S2 vs BMI	SNR S2 vs thoracic circumference
Regression coefficient	-0.35 dB/kg/m ²	-0.08 dB/cm
Intercept	28.14 dB	26.85 dB
Predicted value of the anatomical feature @ SNR S2 = 14 dB	39.88 kg/m ²	171 cm

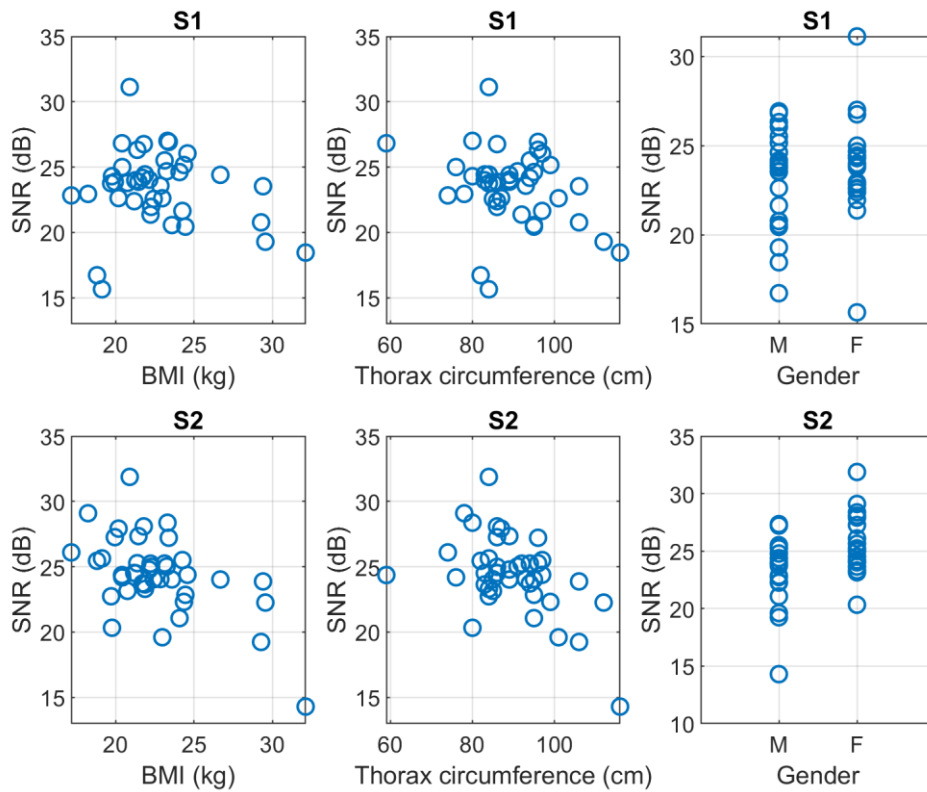


Figure 60: Scatter plots of the SNR of S1 and S2, in function of the BMI, the thoracic circumference and the biological sex, respectively.

The resulting predicted values for BMI and thoracic circumference, respectively equal to 39.88 kg/m^2 and 171 cm , are extreme values. As a reference, a BMI of 40 kg/m^2 determines the threshold for class 3 obesity, which affects less than the 2% of the population in developed countries [229].

Discussion

The results of the validation of the usability of the device can be considered extremely promising to demonstrate that the approach proposed in this work can overcome the limits of traditional PCG for the use by the patient or a caregiver in a domicile setting. From the results of the analysis on the usability by inexperienced users, it is possible to conclude that the multi-sensor array achieves its primary goal, i.e., obtaining a PCG signal of good to excellent quality even if the device is positioned by a user with no clinical nor technical skills. This is by itself a validation of the designed multi-sensor array for the purposed goal.

A more thorough analysis of the spatial distribution of the recordings according to their quality shows that not only naïve users can successfully record heart sounds from a peer by means of the array, but also that a high number of good-quality signals is achievable and that the positioning is consistent to the instructions. Therefore, the multi-sensor array not only enables inexperienced users to gain the same information that an expert user would gain through a traditional single-source system but also to gain access to a greater insight.

In other words, the multi-sensor array successfully achieves its primary goal but goes further and allows a real multi-source analysis, even when inexperienced users perform the recording. In this sense, the array opens to completely new possibilities of analysis that could be of use not only in domiciliary monitoring but also in an ambulatory setting.

The applicability to a broad population is a secondary key requirement for the final application. It should be highlighted that design decisions were made with the scope of ensuring the ergonomics of the device, from the dimensions to the flexibility of the pad. Nevertheless, the success of the proposed approach had to be experimentally evaluated.

The experimental results confirmed that good-quality signals could be recorded from every subject belonging to the sampling population, regardless the presence of breasts, the BMI, and the thoracic circumference. A difference was found among S1 and S2: the quality of S1 was not affected by the body type, whereas the quality of S2 was. A weak to moderate correlation was found between the quality of S2 and the descriptors of the anatomy of the chest. This may be due to physiological reasons, besides to the propagation of the acoustic waves: in fact, a condition of overweight or obesity can produce a higher load on the cardiac output, which affects the closure of the semilunar valves more directly than the atrioventricular ones.

The regression analysis showed that the theoretical limits on the BMI and thoracic circumference that would cause the quality of S2 to become too poor for a reliable estimate of the time of closure of the aortic and pulmonary valves are extreme. It should be highlighted that, given that the correlation is not strong, the regression analysis should be performed on a wider population for robustness. Nevertheless, if the found limits hold, they would limit the applicability of the device to the 98% of the population, when it comes to the anatomy of the thorax.

The possibility of using the multi-sensor array on the broadest possible population is a key factor to increase its value. In fact, the monitoring of the CTIs through ECG and multi-source PCG was first proposed as a noninvasive alternative to invasive hemodynamic sensors such as CardioMEMS™. The greatest value of the noninvasive approach against its invasive counterpart resides in the possibility of reaching a wider at-risk population: to achieve this goal successfully, the multi-sensor array should not be constrained to be used on an “optimal” body type, but should be usable regardless the characteristics of the chest of the patient. In the worst case, if such constraints exist, they should be quantified so that the use of the multi-sensor array can properly be inserted in the clinical pathway of the patients only if they can effectively benefit from its use.

From the experimental results of this phase of the analysis, it can be concluded that the multi-sensor array enables inexperienced volunteers to record signals of sufficient quality for the estimate of the CTIs regardless of their anatomical characteristics. This is a fundamental preliminary confirmation that the multi-sensor array is worth testing in a real home monitoring setting and with at-risk patients for HF, which should be the next validation step.

5.3.3 Validation against single-source PCG

The validation against a single-source PCG system is used, in this work, as a gold standard for comparison. Single-source PCG cannot be considered a gold standard in the broad sense for the estimate of the CTIs: echocardiography and cardiac catheterization are currently used for the purpose in clinics. Nevertheless, the goal of this work is to propose a system that can replace single-source PCG in a home care setting: the question that this validation phase is aimed at answering is not whether PCG is a valid method to estimate the CTIs against the gold standard (cardiac catheterization, echocardiography) or not, but whether the proposed multi-source PCG approach enables the use of PCG by inexperienced users against the traditional single-source PCG approach, performed by an expert user by locating the well-known auscultation areas. In this sense, single-source PCG can be used as a gold standard for the purposes of this analysis.

The comparison between the single-source PCG performed by an expert user and the multi-source PCG performed by an inexperienced user was analyzed in two phases:

1. The quality of the signals obtained through each system was compared.

2. The time of closure of the four cardiac valves estimated through each system was compared. As a final analysis, the main CTIs were computed and compared.

The next paragraphs will describe the methods of the analysis and the experimental results obtained on the sample population, along with their discussion.

Rationale and methods

First, the quality of the multi-source recordings performed by inexperienced users was compared against the quality of the single-source recordings performed by expert users over the four traditional auscultation areas.

To achieve the purposed goal, the microphones of the array were divided in four areas, according to the theoretical auscultation areas. This choice was made after having experimentally confirmed that the distribution of the signal quality over the channels was consistent with the expected auscultation areas, as shown in paragraph “5.3.2 Validation of usability”. Figure 61 shows the correspondence between each auscultation area and its associated microphones.

From each area, the microphone with the highest SNR was selected, to simulate what the expert user physically does when he/she positions the stethoscope over the chest. For each cardiac valve, the SNR of the single-source signal was statistically compared against the SNR of the selected microphone in the multi-source recording using a paired Student’s t -test ($\alpha = 0.05$).

Then, the times of closure of each cardiac valve were extracted from the single-source and multi-source PCG recordings. The single-source recordings were processed using the method described in [168] and summarized in paragraph “4.2 Estimation of the time of closure of the cardiac valves”. Four single-source recordings were performed, one on each auscultation area: the time of closure of each cardiac valve was extracted from the signal recorded over the corresponding auscultation area. In the end, for each cardiac valve, an array containing its time of closure for each recorded heartbeat was obtained. The multi-source recordings were processed using the full pipeline described in chapter “**Error! Reference source not found.**”, where the channels are divided in potential auscultation areas through clustering and the best auscultation area is selected by means of MCDA. Also in this case, an array containing the time of closure of each cardiac valve for each recorded heartbeat was available in the end.

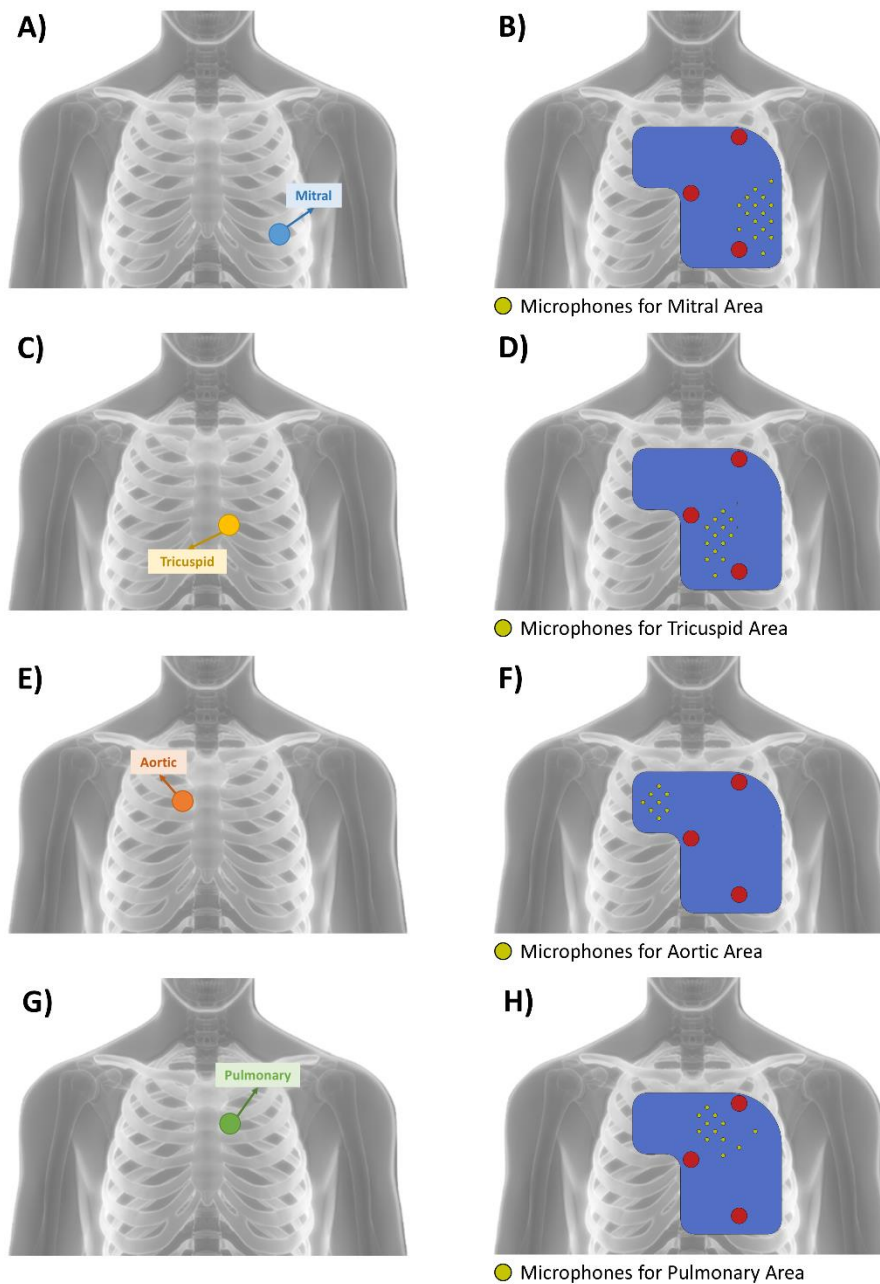


Figure 61: Comparison between the positioning of the single-source stethoscope over the four auscultation areas (A, C, E, G) and the corresponding microphones in the multi-sensor array (B, D, F, H).

The comparison between the series of results could not be performed directly, because it was found that the heart rate was not stable across the recordings. In fact, a physiological relaxation took place along the experiment and caused a decrease

in the heart rate over the time. The effect of heart rate was compensated by considering the normalized time of closure. The latter was obtained by dividing the real time of closure by the corresponding RR interval and corresponds to the percentage of the cardiac cycle. To obtain the corresponding value in milliseconds, which is needed to estimate the CTIs from the time of closure, the normalized time of closure estimated through the single-source system was multiplied by the average RR interval obtained with the multi-source system.

The comparison between the time of closure of the cardiac valves obtained through the two approaches was carried out by computing on three levels, for each cardiac valve:

1. The two distributions were compared through the rank-sum Wilcoxon test ($\alpha = 0.05$) to check if they were statistically different.
2. The Pearson correlation coefficient between the distributions was computed.
3. The Root Mean Squared Error and the Normalized Root Mean Squared Error between the distributions were estimated to quantify the difference among the estimates.

In the end, the following CTIs were computed:

- EMAT: difference between the time of closure of the mitral valve and the Q wave in the ECG.
- cEMAT: EMAT divided by the RR interval.
- LVST: difference between the time of closure of the aortic valve and the time of closure of the mitral valve.
- EMAT/LVST: ratio between EMAT and LVST.

For each CTI, the two distributions were compared through the rank-sum Wilcoxon test ($\alpha = 0.05$) to check if they are statistically different.

Results

The first analysis investigates the compared quality of S1 and S2 obtained through the single-source and multi-source systems, optimized for each cardiac valve. Figure 62 presents the boxplots of the distribution of the SNR values for each auscultation area.

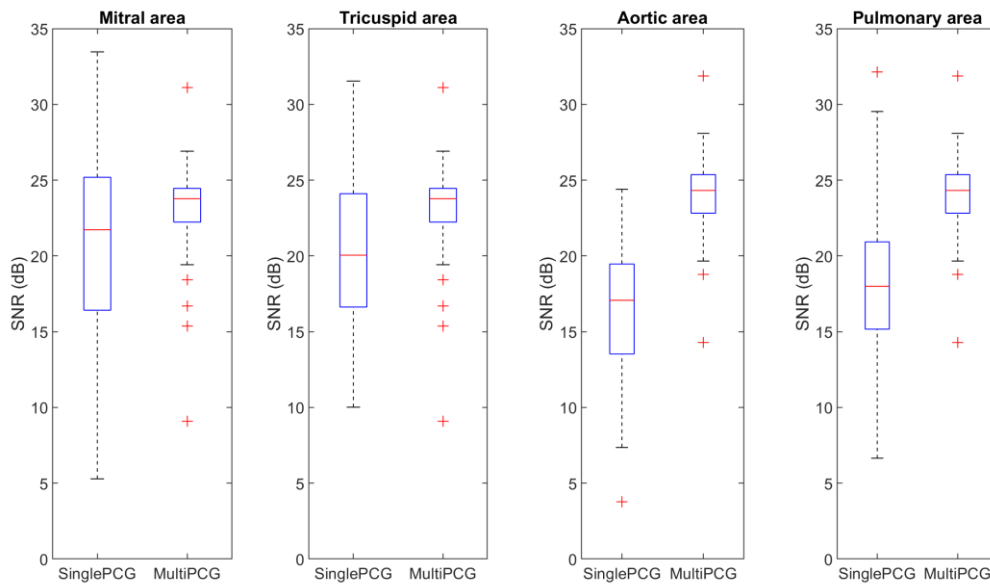


Figure 62: Boxplots of the distribution of the SNR of respectively the single-source and the multi-source recordings for each cardiac valve.

Complementarily, Table 11 presents a comparison between the average SNR over the sample population for each cardiac valve. The table also reports the p-value of the Student's t -test applied to each comparison: the * highlights the comparisons which resulted as statistically different.

Table 11: **Average SNR of the signals obtained by the two systems optimized for each auscultation area.**

Cardiac valve	Single-source SNR (dB)	Multi-source SNR (dB)	Student's t -test p-value
Mitral	21.4	21.8	0.59
Tricuspid	21.0	22.9	0.008 *
Aortic	17.1	18.1	0.19
Pulmonary	18.9	22.4	< 0.001 *

The average SNR was found to be statistically different only for the valves of the right side of the heart. In this case, the SNR obtained using the multi-sensor array was found statistically higher by 1.9 dB for the tricuspid and 3.5 dB for the pulmonary valve. In the case of the mitral and aortic valves, instead, the two systems were found equivalent with respect to the signal quality.

Concerning the time of closure of the four cardiac valves, Figure 63 (panels A to D) presents a plot of the distribution of the estimated values subject-wise. The lines represent the mean of the distribution for each subject whereas the shaded area represents the standard deviation. Panel E presents the mean values in the form of a scatter plot: theoretically, the points should lie on the bisector.

The plots show the corrected mean value for the single-source PCG, i.e., the value corrected by the heart rate. The results presented in Figure 63 qualitatively show that the two systems provide comparable results. The results of the statistical comparison of the values obtained through the systems are presented in Table 12.

Table 12: Results of the statistical comparison between the time of closure of each cardiac valve obtained through single-source and multi-source PCG.

Cardiac valve	p-value Wilcoxon test	Pearson coefficient	RMSE (ms)	NRMSE
Mitral	0.92	0.60	9	0.19
Tricuspid	0.04	0.66	14	0.16
Aortic	0.29	0.93	17	0.07
Pulmonary	0.47	0.88	20	0.07

The results of the Wilcoxon test show that the time of closure of the mitral, aortic, and pulmonary valves are not statistically different when estimated using single-source and multi-source PCG. On the contrary, the time of closure of the tricuspid valve was found to be significantly different, even though the p-value is at the limits of the confidence level. A moderate to strong correlation was found for the atrioventricular valves, whereas a very strong correlation was found for the

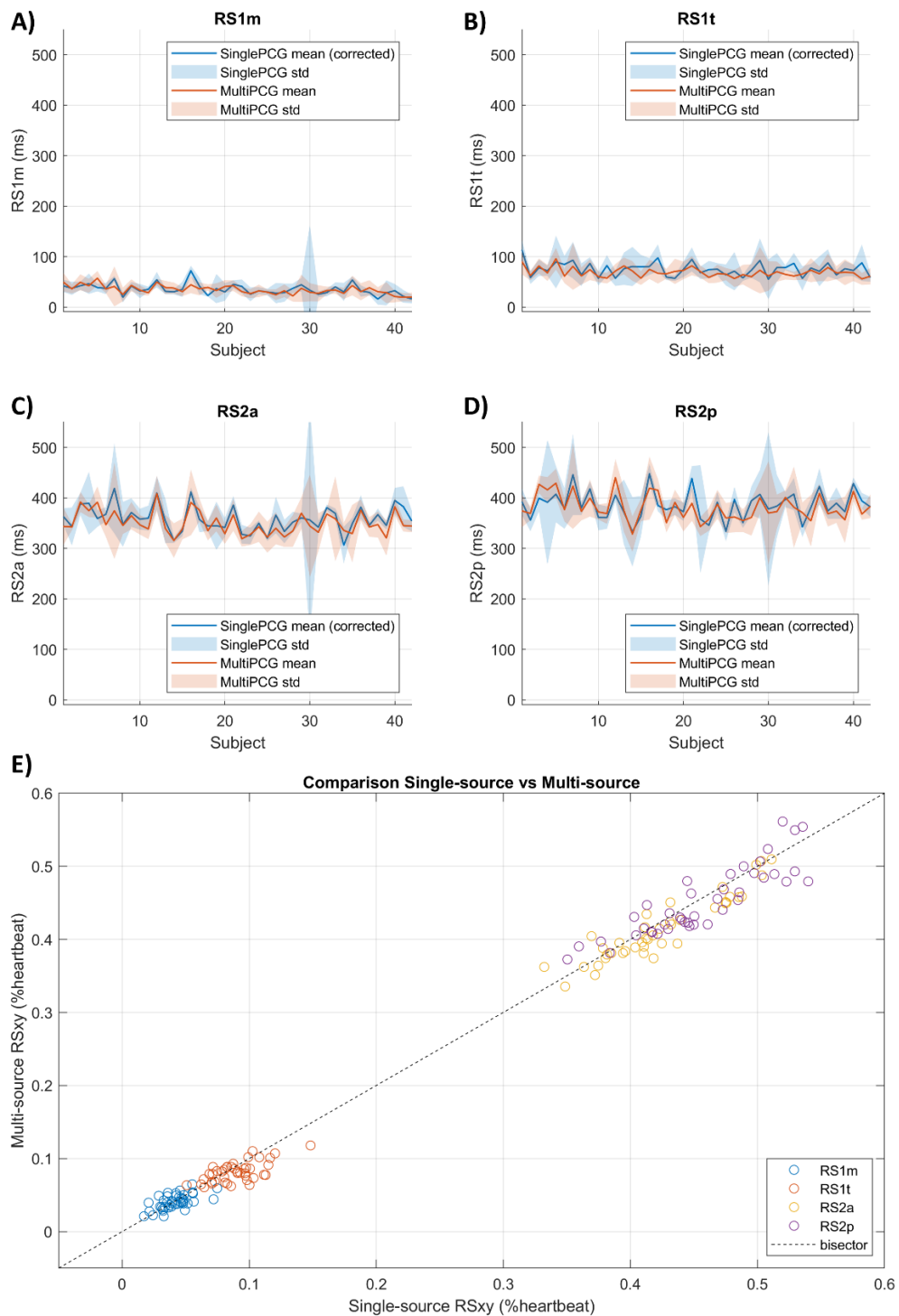


Figure 63: Plots of the time of closure of each cardiac valve estimated by single-source PCG recordings performed by an expert user in the traditional auscultation areas and by multi-source PCG recordings performed by inexperienced users through the described multi-sensors array.

semilunar valves. The NRMSE was found to be higher for the atrioventricular valves than for the semilunar valves.

In the end, Figure 64 presents the boxplots of the CTIs obtained on the sample population using each of the two systems. The horizontal lines represent the thresholds that were found in the literature search presented in paragraph “2.3.2 Cardiac Time Intervals and Heart Failure” to determine the normality ranges, and are equal to:

- $EMAT < 100$ ms.
- $cEMAT < 0.15$.
- $LVST > 270$ ms.
- $EMAT/LVST < 0.4$.

The green areas represent the normality ranges, the red area the ranges where the value of the CTI is associated with an impairment of the cardiac functionality.

Given that the presence of an existing or previous condition of cardiopathy was considered an exclusion criterion for the enrollment of the subjects, it is expected that all CTIs follow within the normality ranges. The experimental results confirm this assumption. The statistical comparison of the two distributions resulted, for all CTIs, in a p-value higher than the significance level.

Discussion

The experimental results of the comparison between the single-source system used by an expert user on the four traditional auscultation areas and the multi-source system used by an inexperienced user complete with the processing pipeline are definitely encouraging.

From the point of view of the signal quality, the comparison between the systems proves the success of the proposed multi-source approach. In fact, even though the multi-source recordings were performed by inexperienced users, they demonstrated an equal or higher quality than their single-source counterpart, recorded by an expert user. It should also be highlighted that the average SNR obtained by the two systems is slightly higher than the average SNR obtained on a publicly available dataset (PhysioNet CinC Challenge 2016 [199] – recordings from training set “a” from the MIT), which was found equal to 17 dB for S1 and 15 dB for S2. This confirms that the proposed system has characteristics in line with the state of the art.

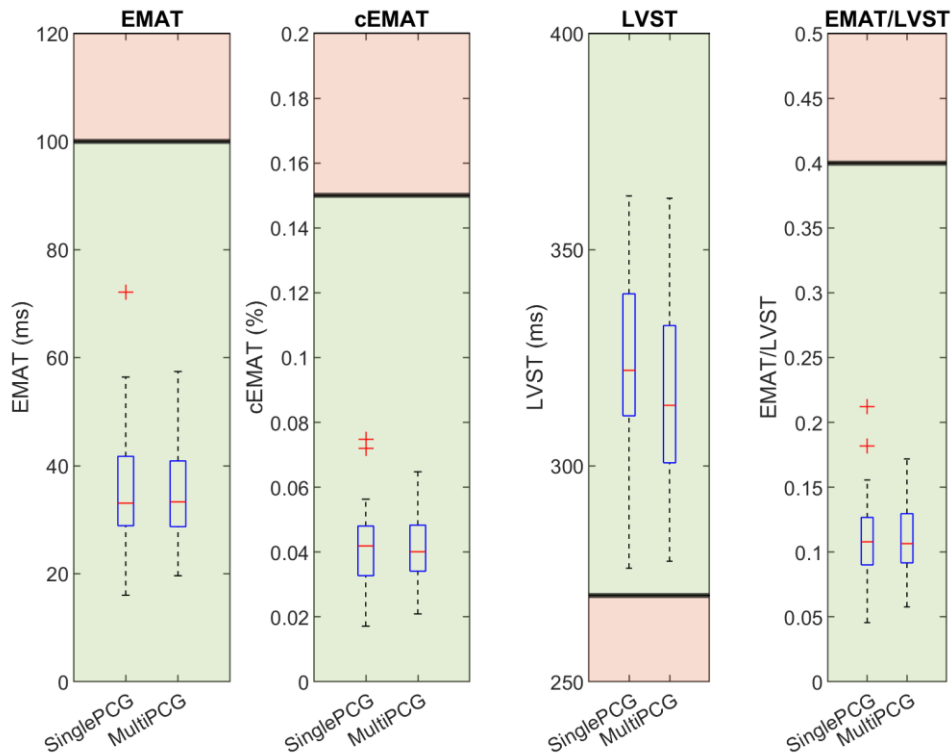


Figure 64: Boxplots of the CTIs estimated by the single-source and multi-source PCG recordings. The horizontal lines represent the thresholds proposed in the literature to distinguish a normal vs abnormal cardiac functionality. The green area represents the normality area.

The experimental results show that the multi-sensor array is superior to the single-source system regardless of the skills of the user. In this sense, it could be interesting to evaluate the use of the device even in an ambulatory setting or in an emergency department. In fact, it was proved in previous studies that the auscultation performed by a general clinical practitioner or by a physician with a different specialty is not equivalent to the auscultation performed by a cardiologist [230]. The availability of the proposed multi-sensor array could simplify the procedure of obtaining good-quality recordings regardless the specialty of the clinical practitioner in charge, in an efficient way: the four cardiac valves could be auscultated simultaneously, thus shortening the duration of the exam, and without the need of expert staff.

Concerning the estimate of the time of closure of the four cardiac valves, the experimental results show that mostly consistent results could be obtained through the two systems. The statistical comparison between the distributions highlighted

that only the estimate of the time of closure is significantly different, even though the p-value was found to be at the limit of the confidence level, suggesting a borderline situation. The result is not surprising and is coherent with the physiology of the two heart sounds: if the closure of the semilunar valves is the sole contribution to S2, the generation of S1 is more complex and most often more than two contributors can be hypothesized (for example the opening of the aortic valve is known to contribute to the generation of the sound to some extent). This can mask the tricuspid component, which is lower in amplitude than the mitral. From a technical point of view, this translates to a higher difficulty in accurately identifying and separating the tricuspid component.

A very strong correlation was found on the semilunar valves: this demonstrates that the method works very well when it comes to separating the components of S2. The correlation is present but lighter in the case of the atrioventricular valves. This is mainly linked to the difficulties in correctly detecting the tricuspid component of S1: sometimes the latter can influence the detection of the mitral component since the two are performed together. A similar finding was derived from the NRMSE, which was found to be significantly higher for the atrioventricular valves than for the semilunar.

It should be noted that reasonable CTIs can be extracted from the recordings performed using either approach, since all CTIs were found to lie in the normality range, as expected. Moreover, the distributions were found not to be statistically different for all the CTIs.

The analysis on the signal quality combined with the analysis of the quantification of the error in the estimate proves that there is room for an improvement of the algorithm for the identification of the two components of the heart sounds. This is particularly relevant for S1. In fact, even though good quality recordings can be obtained by either system, the partial agreement between them can be attributed to a partially diverse detected components in the heart sounds. As anticipated in the introduction to paragraph “4.2 Estimation of the time of closure of the cardiac valves”, some other approaches for the identification of the time of closure of the cardiac valves exist and could be tested in the future. Nevertheless, the separation of the components of the heart sounds is still an open problem in the scientific community.

5.3.4 Final remarks

The pre-clinical validation of the multi-sensor array on a population of healthy individuals proposed in this paragraph led to some important take-home messages.

On one side, the analysis of the usability proved that inexperienced users can successfully use the array to obtain a good-quality PCG recording, even without technical or clinical experience with auscultation. The latter results were obtained in a simulated home-care scenario: the promising findings found in this phase suggest that the analysis can be repeated in a real-life home setting with real patients for clinical validation. On the other hand, successfully testing the device on a population featuring a variety of different body types is highly encouraging to hypothesize that the proposed monitoring approach can broaden the target population, to include not only patients already affected by HF but also at-risk patients, with no restrictive limits regarding the physical characteristics. From this point of view, the multi-sensor array proved to achieve the goals it was designed for, at least in a pre-clinical phase.

When it comes to comparing the proposed system against the “*gold standard*” single-source PCG recording performed on the traditional auscultation areas by an expert user, the experimental results are slightly more controversial. The quality of the recordings obtained by inexperienced users through the array was found to be equal or higher than the quality obtained by an expert user through the traditional system. This can be regarded as further proof of the suitability of the designed array for telemonitoring in a homecare setting.

Concerning the extraction of the CTIs, the preliminary results presented in this paragraph show that the estimates obtained by the two systems are consistent but can be improved. This is hypothesized to be related to the algorithm for the separation of the components of the heart sounds: since the quality of the recordings is comparable, no clue exists that the reason is to be searched in the hardware part of the project. On the contrary, the separation of the components is known to be a critical aspect in the PCG processing panorama. Nevertheless, the sample population acquired in this work can serve as basis to optimize the algorithms in the future.

Chapter 6

Conclusions

6.1 Resume of the project

The project described in this work had an ambitious goal: to move a step further in the noninvasive monitoring of patients at-risk for decompensation episodes of heart failure. The goal is described as ambitious because it aims at reducing the mortality of one of the most burdensome diseases in the developed countries. From this perspective, the approach presented in this work has a clear clinical relevance and finds straightforward applicability in the clinical domain.

The proposed solution for the noninvasive home monitoring of the status of heart failure patients grounds on three main assumptions:

1. Pathophysiology confirms that the first changes before an acute episode can be detected in the intracardiac pressures and occur weeks before the episode.
2. Evidence exists in the literature that the changes in the intracardiac pressures reflect in changes in the timing of the opening and closure of the cardiac valves, which may be noninvasively monitored through heart sounds.
3. Heart sounds cannot be easily recorded in a home care context because inexperienced users such as the patient or a caregiver have difficulties

in correctly positioning the stethoscope over the right auscultation areas.

An approach based on multi-source PCG was designed. The approach involved both the design of a novel wearable device to record the biomedical signals of interest and the design of the signal processing pipeline to extract the features of interest from the signals. The proposed multi-sensor array aims at enabling the recording of the heart sounds by inexperienced users by shifting the problem of finding a good auscultation point from the recording phase to the processing phase. This was obtained through a flexible pad mounting a high number of microphones at a high spatial resolution along with custom algorithms to assess the quality of the signals, estimate the time of closure of the cardiac valves, divide the channels into consistent groups, and automatically determine the best auscultation area.

Two independent pre-clinical validations were carried out. On one side, an animal study was conducted to verify the physiological hypothesis of the project, i.e., that the timing of the cardiac valves can be used as a surrogate for the monitoring of the intracardiac pressures. Specifically, the study was aimed at assessing the correlation between the split of the second heart sound and the pressure in the pulmonary artery. On the other hand, an experimental analysis on healthy volunteers was conducted to verify the technical hypothesis of the project, i.e., that multi-source PCG at high spatial resolution enables the recording of heart sounds by inexperienced users.

6.2 Take-home messages

First and foremost, the proposed multi-sensor array proved to achieve its primary goal, i.e., to overcome the limits of traditional PCG and enable the recording of heart sounds in a home care setting without the need for an expert user. As a wearable device, its ergonomics ensured, on one hand, a straightforward positioning by naïve users, and on the other hand, a successful use on a wide population without strict limitations concerning the body type and the morphology of the chest. In this sense, the multi-sensor array has a straightforward clinical applicability and has the potentiality of broadening the target monitored population with respect to its invasive counterpart.

Multi-source PCG at a high spatial resolution can be considered as a promising approach not only to bring the recording of heart sounds to the patient's domicile, but also to gain access to a greater insight into the hemodynamics of the heart,

difficult to obtain otherwise using biomedical signals. It can be deemed that the use of multi-source PCG, even when performed by inexperienced users, may open to novel possibilities of analysis in the future by evaluating not only the time variability of heart sounds but also their spatial variability.

The extraction of the information about the timing of the closure of the cardiac valves from the heart sounds could effectively be performed, even by means of computationally light methods that could be embedded on the device itself. Nevertheless, the separation of the contributions of the two components of each heart sounds confirmed to be a delicate processing step that is worth further study in the future.

In the end, the physiological hypothesis the project grounds on, i.e., that the changes in the timing relationships between the time of closure of the cardiac valves could be used a surrogate for the changes of the intracardiac pressures, could be validated to some extent. The availability of a dataset where the heart sounds and the intracardiac pressures are monitored simultaneously while physiological triggers are applied to change the latter opens to interesting novel possibilities of analysis that could improve our understanding of the effect of the hemodynamics of the heart on cardiac sounds and improve its clinical relevance.

6.3 Limitations of the work

As already highlighted over the text, the proposed work presents some limitations.

First, the algorithms for signal processing require improvement to some extent. As already highlighted, the separation of the components of the two heart sounds is critical and the experimental results suggest that it does not work properly on all heartbeats. The main limitation to the improvement of the algorithm resides in the difficulty of finding a proper method for the validation of the correct identification of the instant of closure of the cardiac valves. A good gold standard may be a simultaneous echocardiographic examination, but it's complex to obtain given the positioning of the device on the chest.

Concerning the design of the multi-sensor array, the main limitation resides in the fact that the device is at a prototypal stage and must be connected to a computer to record the signals. Even though the usability of the device was demonstrated from the positioning point of view, the same cannot be said on the entire system. In fact, not all patients or caregivers may have an available computer or be capable of

using it. The author was fully aware of this limitation since the conceptualization of the device, but decided to develop a computer-based prototype as an intermediate step in the technological transfer of the solution to enable a first validation of the multi-sensor array.

In the end, the validation of the array was performed only in a pre-clinical fashion and with a limited sample population, both in case of the animal study and in case of the study on healthy volunteers. The work requires a clinical validation on pathological subjects (both with HF and with different comorbidities, to analyze their effect) to prove its clinical effectiveness.

6.4 Future developments

Both the promising experimental results and the highlighted limitations contribute to define the future developments of the project. In fact, the project proved, on one side, its potential for solving the aimed clinical problem if some technical issues are solved and a further validation is carried out.

From the signal processing perspective, the two novel datasets that were acquired during the project (the animal dataset and the healthy subjects' dataset) constitute an invaluable new resource for the optimization of the algorithms. In fact, modifications can be applied to the algorithms and their effect on the trends in the pig recordings and on the consistency with the single-source recordings assessed for validation. The focus will be on the algorithm for the separation of the heart sounds components and on the algorithm for the identification of the best auscultation area (the MCDA parameters need to be further optimized). Moreover, as already highlighted, further analysis of the combined effect of different physiological variables on the cardiac timing will be carried out on the animal dataset.

On the device side, two main future developments are foreseen. First, the use of the MIMU, already embedded in the sensor but unused at date, will be explored to analyze (and in case compensate for) the effect of the posture, to automatically recognize the motion artifacts and to monitor the respiration of the subject. Second, and most importantly, a new stand-alone prototype will be designed to embed the entire system on the flexible pad. This project already won a new Proof of Concept funding (PoC Instrument 2022-2024 – Transition track – by Compagnia di Sanpaolo).

The new stand-alone device will enable a clinical validation on patients affected by heart failure in a real home monitoring setting. The latter is a further future objective of the project and will provide a real validation of the efficacy of the proposed approach for its purposed application.

List of publications

Papers

- **Giordano, N.**, & Knaflitz, M. (2019). A novel method for measuring the timing of heart sound components through digital phonocardiography. *Sensors*, 19(8), 1868. <https://doi.org/10.3390/s19081868>
- Checcucci, E., Rosati, S., De Cillis, S., Vagni, M., **Giordano, N.**, Piana, A., ... & Porpiglia, F. (2021). Artificial intelligence for target prostate biopsy outcomes prediction the potential application of fuzzy logic. *Prostate Cancer and Prostatic Diseases*, 1-4. <https://doi.org/10.1038/s41391-021-00441-1>
- **Giordano, N.**, Rosati, S., & Knaflitz, M. (2021). Automated Assessment of the Quality of Phonocardiographic Recordings through Signal-to-Noise Ratio for Home Monitoring Applications. *Sensors*, 21(21), 7246. <https://doi.org/10.3390/s21217246>
- Checcucci, E., Rosati, S., De Cillis, S., **Giordano, N.**, Volpi, G., Granato, S., ... & Porpiglia, F. (2023). Machine-Learning-Based Tool to Predict Target Prostate Biopsy Outcomes: An Internal Validation Study. *Journal of Clinical Medicine*, 12(13), 4358. <https://doi.org/10.3390/jcm12134358>
- **Giordano, N.**, Rosati, S., Balestra, G., & Knaflitz, M. (2023). A Wearable Multi-Sensor Array Enables the Recording of Heart Sounds in Homecare. *Sensors*, 23(13), 6241. <https://doi.org/10.3390/s23136241>

Chapters

- **Giordano, N.**, Rosati, S., Valeri, F., Borchiellini, A., & Balestra, G. (2021). Simulation of the Impact on the Workload of the Enlargement of the Clinical Staff of a Specialistic Reference Center. In *Public Health and Informatics* (pp. 605-609). IOS Press. <https://doi.org/10.3233/SHTI210242>

Proceedings

- **Giordano, N.**, & Knaflitz, M. (2019, July). Multi-source signal processing in phonocardiography: Comparison among signal selection and signal

enhancement techniques. In *2019 41st Annual International Conference of the IEEE Engineering in Medicine and Biology Society (EMBC)* (pp. 6689-6692). IEEE. <https://doi.org/10.1109/EMBC.2019.8856725>

- **Giordano, N.**, & Knaflitz, M. (2020, June). A Method for the Estimation of the Timing of Heart Sound Components Through Blind Source Separation in Multi-Source Phonocardiography. In *2020 IEEE International Symposium on Medical Measurements and Applications (MeMeA)* (pp. 1-6). IEEE. <https://doi.org/10.1109/MeMeA49120.2020.9137315>
- **Giordano, N.**, Rosati, S., Valeri, F., Borchiellini, A., & Balestra, G. (2020, June). Agent-Based Modeling and Simulation of Care Delivery for Patients with Thrombotic and Bleeding Disorders. In *MIE* (pp. 1193-1194). <https://doi.org/10.3233/shti200358>
- Vagni, M., **Giordano, N.**, Balestra, G., & Rosati, S. (2021, June). Comparison of different similarity measures in hierarchical clustering. In *2021 IEEE International Symposium on Medical Measurements and Applications (MeMeA)* (pp. 1-6). IEEE. <https://doi.org/10.1109/MeMeA52024.2021.9478746>
- Checcucci, E., Rosati, S., De Cillis, S. T., Vagni, M., **Giordano, N.**, Piana, A., ... & Porpiglia, F. (2021, September). Fuzzy logic algorithms artificial intelligence for target prostate biopsy: outcomes prediction study. In *The Journal of Urology, proceeding of the AUA Annual Meeting 2021*, 206(Supplement 3), e462-e462. <https://doi.org/10.1097/JU.0000000000002023.01>
- Rosati, S., **Giordano, N.**, Checcucci, E., De Cillis, S., Porpiglia, F., & Balestra, G. (2021). Decision Support System for Target Prostate Biopsy Outcome Prediction: Clustering and FP-Growth Algorithm for Fuzzy Rules Extraction. In *SMARTERCARE@ AI* IA* (pp. 85-90). <https://www.doi.org/10.48448/k1q3-e576>
- **Giordano, N.**, Rosati, S., Knaflitz, M., & Balestra, G. (2022, June). Comparison of Hierarchical and Partitional Clustering in Multi-Source Phonocardiography. In *2022 IEEE International Symposium on Medical Measurements and Applications (MeMeA)* (pp. 1-6). IEEE. <https://doi.org/10.1109/MeMeA54994.2022.9856547>
- **Giordano, N.**, Rosati, S., Knaflitz, M., Balestra, G. (2022, September). Key Aspects to Teach Medical Device Software Certification. In *Digital Professionalism in Health and Care: Developing the Workforce, Building*

the Future: Proceedings of the EFMI Special Topic Conference 2022 (Vol. 298, p. 159). IOS Press. <https://doi.org/10.3233/SHTI220928>

- **Giordano, N.**, Balestra, G., Ghislieri, M., Knaflitz, M., Rosati, S. (2022, September). Automatic Identification of the Best Auscultation Area for the Estimation of the Time of Closure of Heart Valves through Multi-Source Phonocardiography. In *2022 Computing in Cardiology (CinC)*.

Patents

- Knaflitz, M., **Giordano, N.** Dispositivo multi-sensore per la prevenzione dello scompenso cardiaco. Filed in Italy with the identification number 102020000014428 on 17/06/2020.

References

- [1] Arrigo M, Jessup M, Mullens W, Reza N, Shah AM, Sliwa K, et al. Acute heart failure. *Nat Rev Dis Prim* 2020;6. <https://doi.org/10.1038/s41572-020-0151-7>.
- [2] McDonagh TA, Metra M, Adamo M, Gardner RS, Baumbach A, Böhm M, et al. 2021 ESC Guidelines for the diagnosis and treatment of acute and chronic heart failure. *Eur Heart J* 2021;42:3599–726. <https://doi.org/10.1093/eurheartj/ehab368>.
- [3] Klabunde RE. *Cardiovascular Physiology Concepts*. 2012.
- [4] Kemp CD, Conte J V. The pathophysiology of heart failure. *Cardiovasc Pathol* 2012;21:365–71. <https://doi.org/10.1016/j.carpath.2011.11.007>.
- [5] New York Heart Association and Criteria Committee and Dolgin M. *Nomenclature and criteria for diagnosis of diseases of the heart and great vessels*. 1994.
- [6] Heidenreich PA, Bozkurt B, Aguilar D, Allen LA, Byun JJ, Colvin MM, et al. 2022 AHA/ACC/HFSA Guideline for the Management of Heart Failure: A Report of the American College of Cardiology/American Heart Association Joint Committee on Clinical Practice Guidelines. vol. 145. 2022. <https://doi.org/10.1161/CIR.0000000000001063>.
- [7] Gheorghide M, De Luca L, Fonarow GC, Filippatos G, Metra M, Francis GS. Pathophysiologic targets in the early phase of acute heart failure syndromes. *Am J Cardiol* 2005;96:11–7. <https://doi.org/10.1016/j.amjcard.2005.07.016>.
- [8] Fuster V, Harrington RA, Narula J, Eapen ZJ. *Hurst's the Heart*. McGraw-Hill Medical; 2011.
- [9] Libby P, Bonow RO, Mann DL, Tomaselli GF, Bhatt D, Solomon SD, et al. *Braunwald's Heart Disease A Textbook of Cardiovascular Medicine*. Elsevier Health Sciences; 2021.
- [10] Maisel A, Mueller C, Adams K, Anker SD, Aspromonte N, Cleland JGF, et al. State of the art: Using natriuretic peptide levels in clinical practice. *Eur J Heart Fail* 2008;10:824–39. <https://doi.org/10.1016/j.ejheart.2008.07.014>.

- [11] Yoo B-S. Clinical Significance of B-type Natriuretic Peptide in Heart Failure. *J Lifestyle Med* 2014;4:34–8. <https://doi.org/10.15280/jlm.2014.4.1.34>.
- [12] Trabelsi I, Msolli MA, Sekma A, Fredj N, Dridi Z, Bzeouich N, et al. Value of systolic time intervals in the diagnosis of heart failure in emergency department patients with undifferentiated dyspnea. *Int J Clin Pract* 2020;74:1–7. <https://doi.org/10.1111/ijcp.13572>.
- [13] Southworth MR. Treatment options for acute decompensated heart failure. *Am J Health Syst Pharm* 2003;60 Suppl 4:7–15. https://doi.org/10.1093/ajhp/60.suppl_4.s7.
- [14] Matsue Y, Damman K, Voors AA, Kagiya N, Yamaguchi T, Kuroda S, et al. Time-to-Furosemide Treatment and Mortality in Patients Hospitalized With Acute Heart Failure. *J Am Coll Cardiol* 2017;69:3042–51. <https://doi.org/10.1016/j.jacc.2017.04.042>.
- [15] Braunwald E. Shattuck lecture—cardiovascular medicine at the turn of the millennium. *N Engl J Med* 1997;337:1360–9. <https://doi.org/10.1056/NEJM199711063371906>.
- [16] Vos T, Abajobir AA, Abbafati C, Abbas KM, Abate KH, Abd-Allah F, et al. Global, regional, and national incidence, prevalence, and years lived with disability for 328 diseases and injuries for 195 countries, 1990–2016: A systematic analysis for the Global Burden of Disease Study 2016. *Lancet* 2017;390:1211–59. [https://doi.org/10.1016/S0140-6736\(17\)32154-2](https://doi.org/10.1016/S0140-6736(17)32154-2).
- [17] Conrad N, Judge A, Tran J, Mohseni H, Hedgecott D, Crespillo AP, et al. Temporal trends and patterns in heart failure incidence: a population-based study of 4 million individuals. *Lancet* 2018;391:572–80. [https://doi.org/10.1016/S0140-6736\(17\)32520-5](https://doi.org/10.1016/S0140-6736(17)32520-5).
- [18] Roger VL. Epidemiology of Heart Failure: A Contemporary Perspective. *Circ Res* 2021;128:1421–34. <https://doi.org/10.1161/CIRCRESAHA.121.318172>.
- [19] Savarese G, Lund LH. Global public health burden of heart failure. *Card Fail Rev* 2017;3:7. <https://doi.org/10.15420/cfr.2016:25:2y>.
- [20] van Riet EE, Hoes AW, Wagenaar KP, Limburg A, Landman MA, Rutten FH. Epidemiology of heart failure: the prevalence of heart failure and ventricular dysfunction in older adults over time. A systematic review. *Eur J Heart Fail* 2016;18:242–252. <https://doi.org/https://doi.org/10.1002/ejhf.483>.

- [21] Ceia F, Fonseca C, Mota T, Morais H, Matias F, De Sousa A, et al. Prevalence of chronic heart failure in Southwestern Europe: The EPICA study. *Eur J Heart Fail* 2002;4:531–9. [https://doi.org/10.1016/S1388-9842\(02\)00034-X](https://doi.org/10.1016/S1388-9842(02)00034-X).
- [22] Ponikowski P, Anker SD, AlHabib KF, Cowie MR, Force TL, Hu S, et al. Heart failure: preventing disease and death worldwide. *ESC Hear Fail* 2014;1:4–25. <https://doi.org/10.1002/ehf2.12005>.
- [23] Lloyd-Jones DM, Larson MG, Leip EP, Beiser A, D’Agostino RB, Kannel WB, et al. Lifetime risk for developing congestive heart failure: The Framingham Heart Study. *Circulation* 2002;106:3068–72. <https://doi.org/10.1161/01.CIR.0000039105.49749.6F>.
- [24] Tubaro M, Vranckx P, Price S, Vrints C, Bonnefoy E. The ESC textbook of intensive and acute cardiovascular care. vol. 15. Oxford University Press; 2021.
- [25] Farmakis D, Parissis J, Lekakis J, Filippatos G. Acute Heart Failure: Epidemiology, Risk Factors, and Prevention. *Rev Española Cardiol (English Ed)* 2015;68:245–8. <https://doi.org/10.1016/j.rec.2014.11.004>.
- [26] Gerber Y, Weston SA, Redfield MM, Chamberlain AM, Manemann SM, Jiang R, et al. Contemporary Appraisal of the Heart Failure Epidemic, 2000–2010. *Circulation* 2014;130:A15685–A15685. <https://doi.org/10.1001/jamainternmed.2015.0924>.
- [27] Cook C, Cole G, Asaria P, Jabbour R, Francis DP. The annual global economic burden of heart failure. *Int J Cardiol* 2014;171:368–76. <https://doi.org/10.1016/j.ijcard.2013.12.028>.
- [28] Tsao CW, Aday AW, Almarzooq ZI, Alonso A, Beaton AZ, Bittencourt MS, et al. Heart Disease and Stroke Statistics-2022 Update: A Report From the American Heart Association. vol. 145. 2022. <https://doi.org/10.1161/CIR.0000000000001052>.
- [29] Heidenreich PA, Albert NM, Allen LA, Bluemke DA, Butler J, Fonarow GC, et al. Forecasting the impact of heart failure in the united states a policy statement from the american heart association. *Circ Hear Fail* 2013;6:606–19. <https://doi.org/10.1161/HHF.0b013e318291329a>.
- [30] Hamatani Y, Iguchi M, Ikeyama Y, Kunugida A, Ogawa M, Yasuda N, et al. Prevalence, Temporal Change, and Determinants of Anxiety and Depression in Hospitalized Patients With Heart Failure. *J Card Fail* 2022;28:181–90. <https://doi.org/10.1016/j.cardfail.2021.07.024>.

- [31] Zile MR, Bennett TD, St. John Sutton M, Cho YK, Adamson PB, Aaron MF, et al. Transition from chronic compensated to acute d compensated heart failure: Pathophysiological insights obtained from continuous monitoring of intracardiac pressures. *Circulation* 2008;118:1433–41. <https://doi.org/10.1161/CIRCULATIONAHA.108.783910>.
- [32] Adamson PB. Pathophysiology of the transition from chronic compensated and acute decompensated heart failure: New insights from continuous monitoring devices. *Curr Heart Fail Rep* 2009;6:287–92. <https://doi.org/10.1007/s11897-009-0039-z>.
- [33] Singh B, Russell SD, Cheng A. Update on device technologies for monitoring heart failure. *Curr Treat Options Cardiovasc Med* 2012;14:536–49. <https://doi.org/10.1007/s11936-012-0192-7>.
- [34] Mcalister FA, Youngson E, Kaul P, Ezekowitz JA. Early follow-up after a heart failure exacerbation. *Circ Hear Fail* 2016;9:1–9. <https://doi.org/10.1161/CIRCHEARTFAILURE.116.003194>.
- [35] Mhanna M, Beran A, Nazir S, Al-Abdouh A, Barbarawi M, Sajdeya O, et al. Efficacy of remote physiological monitoring-guided care for chronic heart failure: an updated meta-analysis. *Heart Fail Rev* 2022;27:1627–37. <https://doi.org/10.1007/s10741-021-10176-9>.
- [36] Hafkamp FJ, Tio RA, Otterspoor LC, de Greef T, van Steenberg GJ, van de Ven ART, et al. Optimal effectiveness of heart failure management — an umbrella review of meta-analyses examining the effectiveness of interventions to reduce (re)hospitalizations in heart failure. vol. 27. Springer US; 2022. <https://doi.org/10.1007/s10741-021-10212-8>.
- [37] Page MJ, McKenzie JE, Bossuyt PM, Boutron I, Hoffmann TC, Mulrow CD, et al. The PRISMA 2020 statement: An updated guideline for reporting systematic reviews. *Int J Surg* 2021;88. <https://doi.org/10.1016/j.ijvsu.2021.105906>.
- [38] Mohebbali D, Kittleson MM. Remote monitoring in heart failure: Current and emerging technologies in the context of the pandemic. *Heart* 2021;107:366–72. <https://doi.org/10.1136/heartjnl-2020-318062>.
- [39] Lewin J, Ledwidge M, O’Loughlin C, McNally C, McDonald K. Clinical deterioration in established heart failure: What is the value of BNP and weight gain in aiding diagnosis? *Eur J Heart Fail* 2005;7:953–7. <https://doi.org/10.1016/j.ejheart.2005.06.003>.
- [40] Zhang J, Goode KM, Cuddihy PE, Cleland JGF. Predicting hospitalization

- due to worsening heart failure using daily weight measurement: Analysis of the Trans-European Network-Home-Care Management System (TEN-HMS) study. *Eur J Heart Fail* 2009;11:420–7. <https://doi.org/10.1093/eurjhf/hfp033>.
- [41] Goldberg LR, Piette JD, Walsh MN, Frank TA, Jaski BE, Smith AL, et al. Randomized trial of a daily electronic home monitoring system in patients with advanced heart failure: The Weight Monitoring in Heart Failure (WHARF) trial. *Am Heart J* 2003;146:705–12. [https://doi.org/10.1016/S0002-8703\(03\)00393-4](https://doi.org/10.1016/S0002-8703(03)00393-4).
- [42] Lyng P, Persson H, Hgg-Martinell A, Hgglund E, Hagerman I, Langius-Eklf A, et al. Weight monitoring in patients with severe heart failure (WISH). A randomized controlled trial. *Eur J Heart Fail* 2012;14:438–44. <https://doi.org/10.1093/eurjhf/hfs023>.
- [43] Cleland JGF, Louis AA, Rigby AS, Janssens U, Balk AHMM. Noninvasive home telemonitoring for patients with heart failure at high risk of recurrent admission and death: The Trans-European Network-Home-Care Management System (TEN-HMS) study. *J Am Coll Cardiol* 2005;45:1654–64. <https://doi.org/10.1016/j.jacc.2005.01.050>.
- [44] Dar O, Riley J, Chapman C, Dubrey SW, Morris S, Rosen SD, et al. A randomized trial of home telemonitoring in a typical elderly heart failure population in North West London: Results of the Home-HF study. *Eur J Heart Fail* 2009;11:319–25. <https://doi.org/10.1093/eurjhf/hfn050>.
- [45] Mortara A, Pinna GD, Johnson P, Maestri R, Capomolla S, La Rovere MT, et al. Home telemonitoring in heart failure patients: The HHH study (Home or Hospital in Heart Failure). *Eur J Heart Fail* 2009;11:312–8. <https://doi.org/10.1093/eurjhf/hfp022>.
- [46] Scherr D, Kastner P, Kollmann A, Hallas A, Auer J, Krappinger H, et al. Effect of home-based telemonitoring using mobile phone technology on the outcome of heart failure patients after an episode of acute decompensation: Randomized controlled trial. *J Med Internet Res* 2009;11:1–12. <https://doi.org/10.2196/jmir.1252>.
- [47] Weintraub A, Gregory D, Patel AR, Levine D, Venesy D, Perry K, et al. A Multicenter Randomized Controlled Evaluation of Automated Home Monitoring and Telephonic Disease Management in Patients Recently Hospitalized for Congestive Heart Failure: The SPAN-CHF II Trial. *J Card Fail* 2010;16:285–92. <https://doi.org/10.1016/j.cardfail.2009.12.012>.
- [48] Koehler F, Winkler S, Schieber M, Sechtem U, Stangl K, Böhm M, et al.

- Impact of remote telemedical management on mortality and hospitalizations in ambulatory patients with chronic heart failure: The telemedical interventional monitoring in heart failure study. *Circulation* 2011;123:1873–80. <https://doi.org/10.1161/CIRCULATIONAHA.111.018473>.
- [49] Seto E, Leonard KJ, Cafazzo JA, Barnsley J, Masino C, Ross HJ. Mobile phone-based telemonitoring for heart failure management: A randomized controlled trial. *J Med Internet Res* 2012;14:1–14. <https://doi.org/10.2196/jmir.1909>.
- [50] Blum K, Gottlieb SS. The effect of a randomized trial of home telemonitoring on medical costs, 30-day readmissions, mortality, and health-related quality of life in a cohort of community-dwelling heart failure patients. *J Card Fail* 2014;20:513–21. <https://doi.org/10.1016/j.cardfail.2014.04.016>.
- [51] Dendale P, De Keulenaer G, Troisfontaines P, Weytjens C, Mullens W, Elegeert I, et al. Effect of a telemonitoring-facilitated collaboration between general practitioner and heart failure clinic on mortality and rehospitalization rates in severe heart failure: the TEMA-HF 1 (TElemonitoring in the MAnagement of Heart Failure) study. *Eur J Heart Fail* 2012;14:333–40.
- [52] Vuorinen AL, Leppänen J, Kaijanranta H, Kulju M, Heliö T, Van Gils M, et al. Use of home telemonitoring to support multidisciplinary care of heart failure patients in Finland: Randomized controlled trial. *J Med Internet Res* 2014;16. <https://doi.org/10.2196/jmir.3651>.
- [53] Kraai I, de Vries A, Vermeulen K, van Deursen V, van der Wal M, de Jong R, et al. The value of telemonitoring and ICT-guided disease management in heart failure: Results from the IN TOUCH study. *Int J Med Inform* 2015;85:53–60. <https://doi.org/10.1016/j.ijmedinf.2015.10.001>.
- [54] Ong MK, Romano PS, Edgington S, Harriet U, Auerbach AD, Black JT, et al. Effectiveness of remote patient monitoring after discharge of hospitalized patients with heart failure: the better effectiveness after transition - Heart Failure (BEAT-HF) randomized clinical trial. *JAMA Intern Med* 2016;176:310–8. <https://doi.org/10.1001/jamainternmed.2015.7712.Effectiveness>.
- [55] Rahimi K, Nazarzadeh M, Pinho-Gomes AC, Woodward M, Salimi-Khorshidi G, Ohkuma T, et al. Home monitoring with technology-supported management in chronic heart failure: A randomised trial. *Heart* 2020;106:1573–8. <https://doi.org/10.1136/heartjnl-2020-316773>.
- [56] Koehler F, Koehler K, Deckwart O, Prescher S, Wegscheider K, Kirwan BA,

- et al. Efficacy of telemedical interventional management in patients with heart failure (TIM-HF2): a randomised, controlled, parallel-group, unmasked trial. *Lancet* 2018;392:1047–57. [https://doi.org/10.1016/S0140-6736\(18\)31880-4](https://doi.org/10.1016/S0140-6736(18)31880-4).
- [57] Adamson PB, Smith AL, Abraham WT, Kleckner KJ, Stadler RW, Shih A, et al. Continuous autonomic assessment in patients with symptomatic heart failure: Prognostic value of heart rate variability measured by an implanted cardiac resynchronization device. *Circulation* 2004;110:2389–94. <https://doi.org/10.1161/01.CIR.0000139841.42454.78>.
- [58] La Rovere MT, Pinna GD, Maestri R, Mortara A, Capomolla S, Febo O, et al. Short-term heart rate variability strongly predicts sudden cardiac death in chronic heart failure patients. *Circulation* 2003;107:565–70. <https://doi.org/10.1161/01.CIR.0000047275.25795.17>.
- [59] Kumar PS, Rai P, Ramasamy M, Varadan VK, Varadan VK. Multiparametric cloth-based wearable, SimpleSense, estimates blood pressure. *Sci Rep* 2022;12:1–11. <https://doi.org/10.1038/s41598-022-17223-x>.
- [60] Bekfani T, Fudim M, Cleland JGF, Jorbenadze A, von Haehling S, Lorber A, et al. A current and future outlook on upcoming technologies in remote monitoring of patients with heart failure. *Eur J Heart Fail* 2021;23:175–85. <https://doi.org/10.1002/ejhf.2033>.
- [61] Yu CM, Wang L, Chau E, Chan RHW, Kong SL, Tang MO, et al. Intrathoracic impedance monitoring in patients with heart failure: Correlation with fluid status and feasibility of early warning preceding hospitalization. *Circulation* 2005;112:841–8. <https://doi.org/10.1161/CIRCULATIONAHA.104.492207>.
- [62] Heist EK, Herre JM, Binkley PF, Van Bakel AB, Porterfield JG, Porterfield LM, et al. Analysis of different device-based intrathoracic impedance vectors for detection of heart failure events (from the detect fluid early from intrathoracic impedance monitoring study). *Am J Cardiol* 2014;114:1249–56. <https://doi.org/10.1016/j.amjcard.2014.07.048>.
- [63] Van Veldhuisen DJ, Braunschweig F, Conraads V, Ford I, Cowie MR, Jondeau G, et al. Intrathoracic impedance monitoring, audible patient alerts, and outcome in patients with heart failure. *Circulation* 2011;124:1719–26. <https://doi.org/10.1161/CIRCULATIONAHA.111.043042>.
- [64] Abraham WT, Compton S, Haas G, Foreman B, Canby RC, Fishel R, et al. Intrathoracic Impedance vs Daily Weight Monitoring for Predicting

- Worsening Heart Failure Events: Results of the Fluid Accumulation Status Trial (FAST). *Congest Hear Fail* 2011;17:51–5. <https://doi.org/10.1111/j.1751-7133.2011.00220.x>.
- [65] Böhm M, Drexler H, Oswald H, Rybak K, Bosch R, Butter C, et al. Fluid status telemedicine alerts for heart failure: A randomized controlled trial. *Eur Heart J* 2016;37:3154–63. <https://doi.org/10.1093/eurheartj/ehw099>.
- [66] Lütjhe L, Vollmann D, Seegers J, Sohns C, Hasenfuß G, Zabel M. A randomized study of remote monitoring and fluid monitoring for the management of patients with implanted cardiac arrhythmia devices. *Europace* 2015;17:1276–81. <https://doi.org/10.1093/europace/euv039>.
- [67] Domenichini G, Rahneva T, Diab IG, Dhillon OS, Campbell NG, Finlay MC, et al. The lung impedance monitoring in treatment of chronic heart failure (the LIMIT-CHF study). *Europace* 2016;18:428–35. <https://doi.org/10.1093/europace/euv293>.
- [68] Conraads VM, Tavazzi L, Santini M, Oliva F, Gerritse B, Yu CM, et al. Sensitivity and positive predictive value of implantable intrathoracic impedance monitoring as a predictor of heart failure hospitalizations: The SENSE-HF trial. *Eur Heart J* 2011;32:2266–73. <https://doi.org/10.1093/eurheartj/ehr050>.
- [69] Amir O, Ben-Gal T, Weinstein JM, Schliamsner J, Burkhoff D, Abbo A, et al. Evaluation of remote dielectric sensing (ReDS) technology-guided therapy for decreasing heart failure re-hospitalizations. *Int J Cardiol* 2017;240:279–84. <https://doi.org/10.1016/j.ijcard.2017.02.120>.
- [70] Abraham WT, Perl L. Implantable Hemodynamic Monitoring for Heart Failure Patients. *J Am Coll Cardiol* 2017;70:389–98. <https://doi.org/10.1016/j.jacc.2017.05.052>.
- [71] Ritzema J, Troughton R, Melton I, Crozier I, Doughty R, Krum H, et al. Physician-directed patient self-management of left atrial pressure in advanced chronic heart failure. *Circulation* 2010;121:1086–95. <https://doi.org/10.1161/CIRCULATIONAHA.108.800490>.
- [72] Bourge RC, Abraham WT, Adamson PB, Aaron MF, Aranda JM, Magalski A, et al. Randomized Controlled Trial of an Implantable Continuous Hemodynamic Monitor in Patients With Advanced Heart Failure. The COMPASS-HF Study. *J Am Coll Cardiol* 2008;51:1073–9. <https://doi.org/10.1016/j.jacc.2007.10.061>.
- [73] Adamson PB, Gold MR, Bennett T, Bourge RC, Stevenson LW, Trupp R, et

- al. Continuous Hemodynamic Monitoring in Patients With Mild to Moderate Heart Failure: Results of the Reducing Decompensation Events Utilizing Intracardiac Pressures in Patients With Chronic Heart Failure (REDUCEhf) Trial. *Congest Hear Fail* 2011;17:248–54. <https://doi.org/10.1111/j.1751-7133.2011.00247.x>.
- [74] Abraham WT, Adamson PB, Bourge RC, Aaron MF, Costanzo MR, Stevenson LW, et al. Wireless pulmonary artery haemodynamic monitoring in chronic heart failure: A randomised controlled trial. *Lancet* 2011;377:658–66. [https://doi.org/10.1016/S0140-6736\(11\)60101-3](https://doi.org/10.1016/S0140-6736(11)60101-3).
- [75] Mullens W, Sharif F, Dupont M, Rothman AMK, Wijns W. Digital health care solution for proactive heart failure management with the Cordella Heart Failure System: results of the SIRONA first-in-human study. *Eur J Heart Fail* 2020;22:1912–9. <https://doi.org/10.1002/ejhf.1870>.
- [76] Perl L, Meerkin D, D'amario D, Avraham B Ben, Gal T Ben, Weitsman T, et al. The V-LAP System for Remote Left Atrial Pressure Monitoring of Patients With Heart Failure: Remote Left Atrial Pressure Monitoring. *J Card Fail* 2022;28:963–72. <https://doi.org/10.1016/j.cardfail.2021.12.019>.
- [77] Varma N, Epstein AE, Irimpen A, Schweikert R, Love C. Efficacy and safety of automatic remote monitoring for implantable cardioverter-defibrillator follow-up: The lumos-t safely reduces routine office device follow-up (TRUST) trial. *Circulation* 2010;122:325–32. <https://doi.org/10.1161/CIRCULATIONAHA.110.937409>.
- [78] Landolina M, Perego GB, Lunati M, Curnis A, Guenzati G, Vicentini A, et al. Remote monitoring reduces healthcare use and improves quality of care in heart failure patients with implantable defibrillators: The evolution of management strategies of heart failure patients with implantable defibrillators (EVOLVO) study. *Circulation* 2012;125:2985–92. <https://doi.org/10.1161/CIRCULATIONAHA.111.088971>.
- [79] Boriani G, Da Costa A, Quesada A, Ricci R Pietro, Favale S, Boscolo G, et al. Effects of remote monitoring on clinical outcomes and use of healthcare resources in heart failure patients with biventricular defibrillators: results of the MORE-CARE multicentre randomized controlled trial. *Eur J Heart Fail* 2017;19:416–25. <https://doi.org/10.1002/ejhf.626>.
- [80] Whellan DJ, Ousdigian KT, Al-Khatib SM, Pu W, Sarkar S, Porter CB, et al. Combined Heart Failure Device Diagnostics Identify Patients at Higher Risk of Subsequent Heart Failure Hospitalizations. Results From PARTNERS HF (Program to Access and Review Trending Information and Evaluate Correlation to Symptoms in Patients With Hear. *J Am Coll Cardiol*

- 2010;55:1803–10. <https://doi.org/10.1016/j.jacc.2009.11.089>.
- [81] Hindricks G, Taborsky M, Glikson M, Heinrich U, Schumacher B, Katz A, et al. Implant-based multiparameter telemonitoring of patients with heart failure (IN-TIME): A randomised controlled trial. *Lancet* 2014;384:583–90. [https://doi.org/10.1016/S0140-6736\(14\)61176-4](https://doi.org/10.1016/S0140-6736(14)61176-4).
- [82] Tajstra M, Sokal A, Gadula-Gacek E, Kurek A, Wozniak A, Niedziela J, et al. Remote supervision to decrease hospitalization rate (RESULT) study in patients with implanted cardioverter-defibrillator. *Europace* 2020;22:769–76. <https://doi.org/10.1093/europace/euaa072>.
- [83] Sardu C, Santamaria M, Rizzo MR, Barbieri M, di Marino M, Paolisso G, et al. Telemonitoring in heart failure patients treated by cardiac resynchronisation therapy with defibrillator (CRT-D): the TELECARD Study. *Int J Clin Pract* 2016;70:569–76. <https://doi.org/10.1111/ijcp.12823>.
- [84] Morgan JM, Kitt S, Gill J, McComb JM, Andre Ng G, Raftery J, et al. Remote management of heart failure using implantable electronic devices. *Eur Heart J* 2017;38:2352–60. <https://doi.org/10.1093/eurheartj/ehx227>.
- [85] Hansen C, Loges C, Seidl K, Eberhardt F, Tröster H, Petrov K, et al. INvestigation on Routine Follow-up in CONgestive HearT FAilure Patients with Remotely Monitored Implanted Cardioverter Defibrillators SysTems (InContact). *BMC Cardiovasc Disord* 2018;18:1–12. <https://doi.org/10.1186/s12872-018-0864-7>.
- [86] Cowie MR, Sarkar S, Koehler J, Whellan DJ, Crossley GH, Tang WHW, et al. Development and validation of an integrated diagnostic algorithm derived from parameters monitored in implantable devices for identifying patients at risk for heart failure hospitalization in an ambulatory setting. *Eur Heart J* 2013;34:2472–80. <https://doi.org/10.1093/eurheartj/eht083>.
- [87] Boehmer JP, Hariharan R, Devecchi FG, Smith AL, Molon G, Capucci A, et al. A Multisensor Algorithm Predicts Heart Failure Events in Patients With Implanted Devices: Results From the MultiSENSE Study. *JACC Hear Fail* 2017;5:216–25. <https://doi.org/10.1016/j.jchf.2016.12.011>.
- [88] Ahmed FZ, Sammut-Powell C, Kwok CS, Tay T, Motwani M, Martin GP, et al. Remote monitoring data from cardiac implantable electronic devices predicts all-cause mortality. *Europace* 2022;24:245–55. <https://doi.org/10.1093/europace/euab160>.
- [89] Pedretti RFE, Curnis A, Massa R, Morandi F, Tritto M, Manca L, et al. Proportion of patients needing an implantable cardioverter defibrillator on

- the basis of current guidelines: Impact on healthcare resources in Italy and the USA. Data from the ALPHA study registry. *Europace* 2010;12:1105–11. <https://doi.org/10.1093/europace/euq106>.
- [90] Dehkordi P, Khosrow-Khavar F, Di Rienzo M, Inan OT, Schmidt SE, Blaber AP, et al. Comparison of Different Methods for Estimating Cardiac Timings: A Comprehensive Multimodal Echocardiography Investigation. *Front Physiol* 2019;10:1–11. <https://doi.org/10.3389/fphys.2019.01057>.
- [91] Lewis RP, Rittgers SE, Forester WF, Boudoulas H. A Critical Review of the Systolic Time Intervals. *Circulation* 1977;56:146–58.
- [92] Tavakolian K. Systolic Time Intervals and New Measurement Methods. *Cardiovasc Eng Technol* 2016;7:118–25. <https://doi.org/10.1007/s13239-016-0262-1>.
- [93] Shah SJ, Michaels AD. Hemodynamic correlates of the third heart sound and systolic time intervals. *Congest Heart Fail* 2006;12 Suppl 1:8–13. <https://doi.org/10.1111/j.0889-7204.2006.05767.x>.
- [94] Roos M, Toggweiler S, Zuber M, Jamshidi P, Erne P. Acoustic cardiographic parameters and their relationship to invasive hemodynamic measurements in patients with left ventricular systolic dysfunction. *Congest Heart Fail* 2006;12 Suppl 1:19–24. <https://doi.org/10.1111/j.1527-5299.2006.05769.x>.
- [95] Weissler AM, Harris WS, Schoenfeld CD. Systolic Time Intervals in Heart Failure in Man. *Circulation* 1968;37:149–59. <https://doi.org/10.1161/01.CIR.37.2.149>.
- [96] Guyton AC, Hall JE. *Textbook of Medical Physiology*. 11th ed. Pennsylvania: Elsevier Health Sciences; 2015.
- [97] Thalmayer A, Zeising S, Fischer G, Kirchner J. A robust and real-time capable envelope-based algorithm for heart sound classification: Validation under different physiological conditions. *Sensors (Switzerland)* 2020;20. <https://doi.org/10.3390/s20040972>.
- [98] Paiva RP, Carvalho P, Couceiro R, Henriques J, Antunes M, Quintal I, et al. Beat-to-beat systolic time-interval measurement from heart sounds and ECG. *Physiol Meas* 2012;33:177–94. <https://doi.org/10.1088/0967-3334/33/2/177>.
- [99] Sørensen K, Schmidt SE, Jensen AS, Søggaard P, Struijk JJ. Definition of Fiducial Points in the Normal Seismocardiogram. *Sci Rep* 2018;8:1–11. <https://doi.org/10.1038/s41598-018-33675-6>.

- [100] Işilay Zeybek ZM, Racca V, Pezzano A, Tavanelli M, Di Rienzo M. Can Seismocardiogram Fiducial Points Be Used for the Routine Estimation of Cardiac Time Intervals in Cardiac Patients? *Front Physiol* 2022;13:1–11. <https://doi.org/10.3389/fphys.2022.825918>.
- [101] Shandhi MMH, Semiz B, Hersek S, Goller N, Ayazi F, Inan OT. Performance Analysis of Gyroscope and Accelerometer Sensors for Seismocardiography-Based Wearable Pre-Ejection Period Estimation. *IEEE J Biomed Heal Informatics* 2019;23:2365–74. <https://doi.org/10.1109/JBHI.2019.2895775>.
- [102] Shandhi MMH, Semiz B, Hersek S, Goller N, Ayazi F, Inan OT. Performance Analysis of Gyroscope and Accelerometer Sensors for Seismocardiography-Based Wearable Pre-Ejection Period Estimation. *IEEE J Biomed Heal Informatics* 2019;23:2365–74. <https://doi.org/10.1109/JBHI.2019.2895775>.
- [103] Cieslak M, Ryan WS, Babenko V, Erro H, Rathbun ZM, Meiring W, et al. Quantifying rapid changes in cardiovascular state with a moving ensemble average. *Psychophysiology* 2018;55. <https://doi.org/10.1111/psyp.13018>.
- [104] Carvalho P, Paiva RP, Couceiro R, Henriques J, Antunes M, Quintal I, et al. Comparison of systolic time interval measurement modalities for portable devices. *2010 Annu Int Conf IEEE Eng Med Biol Soc EMBC'10* 2010:606–9. <https://doi.org/10.1109/IEMBS.2010.5626642>.
- [105] Salvi P, Grillo A, Tan I, Simon G, Salvi L, Gao L, et al. Systolic time intervals assessed from analysis of the carotid pressure waveform. *Physiol Meas* 2018;39. <https://doi.org/10.1088/1361-6579/aad51b>.
- [106] Buxi D, Hermeling E, Mercuri M, Beutel F, Van Der Westen RG, Torfs T, et al. Systolic Time Interval Estimation Using Continuous Wave Radar with On-Body Antennas. *IEEE J Biomed Heal Informatics* 2018;22:129–39. <https://doi.org/10.1109/JBHI.2017.2731790>.
- [107] Zhang X, Zhang L, Wang K, Yu C, Zhu T, Tang J. A rapid approach to assess cardiac contractility by ballistocardiogram and electrocardiogram. *Biomed Tech* 2018;63:113–22. <https://doi.org/10.1515/bmt-2015-0204>.
- [108] Inan OT, Etemadi M, Wiard RM, Kovacs GTA, Giovangrandi L. Non-invasive measurement of Valsalva-induced hemodynamic changes on a bathroom scale ballistocardiograph. *Proc 30th Annu Int Conf IEEE Eng Med Biol Soc EMBS'08 - "Personalized Healthc through Technol* 2008:674–7. <https://doi.org/10.1109/iembs.2008.4649242>.

- [109] Chan GSH, Middleton PM, Celler BG, Wang L, Lovell NH. Automatic detection of left ventricular ejection time from a finger photoplethysmographic pulse oximetry waveform: Comparison with Doppler aortic measurement. *Physiol Meas* 2007;28:439–52. <https://doi.org/10.1088/0967-3334/28/4/009>.
- [110] Chan W, Woldeyohannes M, Colman R, Arand P, Michaels AD, Parker JD, et al. Haemodynamic and structural correlates of the first and second heart sounds in pulmonary arterial hypertension: An acoustic cardiography cohort study. *BMJ Open* 2013;3:1–10. <https://doi.org/10.1136/bmjopen-2013-002660>.
- [111] Kaneko T, Tanaka A, Jojima K, Yoshida H, Yajima A, Asaka M, et al. Relationship between Cardiac Acoustic Biomarkers and Pulmonary Artery Pressure in Patients with Heart Failure. *J Clin Med* 2022;11. <https://doi.org/10.3390/jcm11216373>.
- [112] Wang M, Hu Y, Guo B, Tang H. Simulation of Acute Pulmonary Hypertension in Beagle Dogs: Correlation Analysis Between Phonocardiogram and Right Ventricular Blood Pressure. *Int Heart J* 2022;63:612–22. <https://doi.org/10.1536/ihj.21-676>.
- [113] Shapiro M, Moyers B, Marcus GM, Gerber IL, McKeown BH, Vessey JC, et al. Diagnostic Characteristics of Combining Phonocardiographic Third Heart Sound and Systolic Time Intervals for the Prediction of Left Ventricular Dysfunction. *J Card Fail* 2007;13:18–24. <https://doi.org/10.1016/j.cardfail.2006.09.009>.
- [114] Efstratiadis S, Michaels AD. Computerized Acoustic Cardiographic Electromechanical Activation Time Correlates With Invasive and Echocardiographic Parameters of Left Ventricular Contractility. *J Card Fail* 2008;14:577–82. <https://doi.org/10.1016/j.cardfail.2008.03.011>.
- [115] Moyers B, Shapiro M, Marcus GM, Gerber IL, McKeown BH, Vessey JC, et al. Performance of phonoelectrocardiographic left ventricular systolic time intervals and B-type natriuretic peptide levels in the diagnosis of left ventricular dysfunction. *Ann Noninvasive Electrocardiol* 2007;12:89–97. <https://doi.org/10.1111/j.1542-474X.2007.00146.x>.
- [116] Wen YN, Lee APW, Fang F, Jin CN, Yu CM. Beyond auscultation: Acoustic cardiography in clinical practice. *Int J Cardiol* 2014;172:548–60. <https://doi.org/10.1016/j.ijcard.2013.12.298>.
- [117] Kosmicki DL, Collins SP, Kontos MC, Zuber M, Kipfer P, Attenhofer Jost C, et al. Noninvasive Prediction of Left Ventricular Systolic Dysfunction in

- Patients With Clinically Suspected Heart Failure Using Acoustic Cardiography. *Congest Hear Fail* 2010;16:249–53. <https://doi.org/10.1111/j.1751-7133.2010.00191.x>.
- [118] Zuber M, Kipfer P, Attenhofer Jost C. Systolic dysfunction: correlation of acoustic cardiography with Doppler echocardiography. *Congest Hear Fail* 2006;12 Suppl 1:14–8. <https://doi.org/10.1111/j.0889-7204.2006.05768.x>.
- [119] Roos M, Toggweiler S, Jamshidi P, Zuber M, Kobza R, Meier R, et al. Noninvasive Detection of Left Ventricular Systolic Dysfunction by Acoustic Cardiography in Cardiac Failure Patients. *J Card Fail* 2008;14:310–9. <https://doi.org/10.1016/j.cardfail.2007.12.004>.
- [120] Cheng HM, Yu WC, Sung SH, Wang KL, Chuang SY, Chen CH. Usefulness of systolic time intervals in the identification of abnormal ventriculo-arterial coupling in stable heart failure patients. *Eur J Heart Fail* 2008;10:1192–200. <https://doi.org/10.1016/j.ejheart.2008.09.003>.
- [121] Hsu HCSCP, Chen PCC. Systolic time intervals revisited : correlations with N-terminal pro-brain natriuretic peptide in a community population 2005:256–63. <https://doi.org/10.1007/s00380-005-0844-6>.
- [122] Thompson B, Drazner MH, Dries DL, Yancy CW. Systolic Time Ratio by Impedance Cardiography to Distinguish Preserved vs Impaired Left Ventricular Systolic Function in Heart Failure. *Congest Hear Fail* 2008;14:261–5. <https://doi.org/10.1111/j.1751-7133.2008.00001.x>.
- [123] Constantino J, Hu Y, Lardo AC, Trayanova NA. Mechanistic insight into prolonged electromechanical delay in dyssynchronous heart failure: A computational study. *Am J Physiol - Hear Circ Physiol* 2013;305:1265–73. <https://doi.org/10.1152/ajpheart.00426.2013>.
- [124] Burkhoff D, Bailey G, Gimbel JR. Characterization of cardiac acoustic biomarkers in patients with heart failure. *Ann Noninvasive Electrocardiol* 2020;25:1–10. <https://doi.org/10.1111/anec.12717>.
- [125] Orter S, Möstl S, Bachler M, Hoffmann F, Mayer CC, Kaniusas E, et al. A comparison between left ventricular ejection time measurement methods during physiological changes induced by simulated microgravity. *Exp Physiol* 2022;107:213–21. <https://doi.org/10.1113/EP090103>.
- [126] Wang S, Lam YY, Liu M, Fang F, Wang J, Shang Q, et al. Acoustic cardiography helps to identify heart failure and its phenotypes. *Int J Cardiol* 2013;167:681–6. <https://doi.org/10.1016/j.ijcard.2012.03.067>.

- [127] Zhang J, Liu WX, Lyu SZ. Predictive Value of Electromechanical Activation Time for In-Hospital Major Cardiac Adverse Events in Heart Failure Patients. *Cardiovasc Ther* 2020;2020. <https://doi.org/10.1155/2020/4532596>.
- [128] Zhang J, Liu W. Cardiac cycle time-corrected electromechanical activation time greater than 15% is an independent risk factor for major adverse cardiovascular events in chronic heart failure outpatients. *Pakistan J Med Sci* 2022;38:456–61. <https://doi.org/10.12669/pjms.38.3.4500>.
- [129] Chao TF, Sung SH, Cheng HM, Yu WC, Wang KL, Huang CM, et al. Electromechanical activation time in the prediction of discharge outcomes in patients hospitalized with acute heart failure syndrome. *Intern Med* 2010;49:2031–7. <https://doi.org/10.2169/internalmedicine.49.3944>.
- [130] Shitara J, Kasai T, Murata N, Yamakawa N, Yatsu S, Murata A, et al. Temporal changes of cardiac acoustic biomarkers and cardiac function in acute decompensated heart failure. *ESC Hear Fail* 2021;8:4037–47. <https://doi.org/10.1002/ehf2.13492>.
- [131] Sung SH, Huang CJ, Cheng HM, Huang WM, Yu WC, Chen CH. Effect of Acoustic Cardiography-guided Management on 1-year Outcomes in Patients With Acute Heart Failure. *J Card Fail* 2020;26:142–50. <https://doi.org/10.1016/j.cardfail.2019.09.012>.
- [132] Wen YN, Lee APW, Fang F, Jin CN, Yu CM. Beyond auscultation: Acoustic cardiography in clinical practice. *Int J Cardiol* 2014;172:548–60. <https://doi.org/10.1016/j.ijcard.2013.12.298>.
- [133] Dillier R, Zuber M, Arand P, Erne S, Erne P. Assessment of systolic and diastolic function in asymptomatic subjects using ambulatory monitoring with acoustic cardiography. *Clin Cardiol* 2011;34:384–8. <https://doi.org/10.1002/clc.20891>.
- [134] Collins SP, Lindsell CJ, Kontos MC, Zuber M, Kipfer P, Jost CA, et al. Bedside prediction of increased filling pressure using acoustic electrocardiography. *Am J Emerg Med* 2009;27:397–408. <https://doi.org/10.1016/j.ajem.2008.03.014>.
- [135] Erath JW, Wanczura P, Wranicz J, Linke A, Rohrer U, Scherr D. Influence of decompensated heart failure on cardiac acoustic biomarkers: impact on early readmissions. *ESC Hear Fail* 2020;7:4198–205. <https://doi.org/10.1002/ehf2.13045>.
- [136] Giordano N, Knaflitz M. Multi-source signal processing in

- phonocardiography: Comparison among signal selection and signal enhancement techniques*. Proc. Annu. Int. Conf. IEEE Eng. Med. Biol. Soc. EMBS, IEEE; 2019, p. 6689–92. <https://doi.org/10.1109/EMBC.2019.8856725>.
- [137] Bao X, Deng Y, Gall N, Kamavuako EN. Analysis of ECG and PCG time delay around auscultation sites. BIOSIGNALS 2020 - 13th Int Conf Bio-Inspired Syst Signal Process Proceedings; Part 13th Int Jt Conf Biomed Eng Syst Technol BIOSTEC 2020 2020:206–13. <https://doi.org/10.5220/0008942602060213>.
- [138] Fontecave-Jallon J, Fojtik K, Rivet B. Is there an Optimal Localization of Cardio-microphone Sensors for Phonocardiogram Analysis? 2019 41st Annu Int Conf IEEE Eng Med Biol Soc 2019:3249–52. <https://doi.org/10.1109/embc.2019.8857681>.
- [139] Cheng X, Feng S, Li Y, Gui G. Research on parallel compressive sensing and application of multi-channel synchronous acquisition of heart sound signals. IEEE Access 2019;7:30033–41. <https://doi.org/10.1109/ACCESS.2019.2900446>.
- [140] Nunes D, Leal A, Couceiro R, Henriques J, Mendes L, Carvalho P, et al. A low-complex multi-channel methodology for noise detection in phonocardiogram signals. Proc Annu Int Conf IEEE Eng Med Biol Soc EMBS 2015;2015-Novem:5936–9. <https://doi.org/10.1109/EMBC.2015.7319743>.
- [141] Pasha S, Lundgren J, Ritz C. Multi-channel electronic stethoscope for enhanced cardiac auscultation using beamforming and equalisation techniques. Eur Signal Process Conf 2021;2021-Janua:1289–93. <https://doi.org/10.23919/Eusipco47968.2020.9287636>.
- [142] Pathak A, Samanta P, Mandana K, Saha G. Detection of coronary artery atherosclerotic disease using novel features from synchrosqueezing transform of phonocardiogram. Biomed Signal Process Control 2020;62:102055. <https://doi.org/10.1016/j.bspc.2020.102055>.
- [143] Samanta P, Pathak A, Mandana K, Saha G. Classification of coronary artery diseased and normal subjects using multi-channel phonocardiogram signal. Biocybern Biomed Eng 2019;39:426–43. <https://doi.org/10.1016/j.bbe.2019.02.003>.
- [144] Liu T, Li P, Liu Y, Zhang H, Li Y, Jiao Y, et al. Detection of coronary artery disease using multi-domain feature fusion of multi-channel heart sound signals. Entropy 2021;23. <https://doi.org/10.3390/e23060642>.

- [145] Saeidi A, Almasganj F, Shojaeifard M. Automatic cardiac phase detection of mitral and aortic valves stenosis and regurgitation via localization of active valves. *Biomed Signal Process Control* 2017;36:11–9. <https://doi.org/10.1016/j.bspc.2017.03.005>.
- [146] Saeidi A, Almasganj F. Cardiac valves disorder classification based on active valves appearance periodic sequences tree of murmurs. *Biomed Signal Process Control* 2020;57:101775. <https://doi.org/10.1016/j.bspc.2019.101775>.
- [147] Radziewsky N, Papyan S, Kushnir I, Gat M, Kushnir A, Sagie A, et al. Estimation of left ventricular function using a novel acoustic-based device. *Eur J Clin Invest* 2012;42:402–10. <https://doi.org/10.1111/j.1365-2362.2011.02596.x>.
- [148] Paiva RP, Sapata T, Henriques J, Quintal I, Baptista R, Gonçalves L, et al. Multi - Channel Audio - based Estimation of the Pre - Ejection Period 2015:5932–5.
- [149] Zhang X, Maddipatla D, Narakathu BB, Bazuin BJ, Atashbar MZ. Development of a Novel Wireless Multi-Channel Stethograph System for Monitoring Cardiovascular and Cardiopulmonary Diseases. *IEEE Access* 2021;9:128951–64. <https://doi.org/10.1109/ACCESS.2021.3111778>.
- [150] Guo B, Tang H, Xia S, Wang M, Hu Y, Zhao Z. Development of a Multi-Channel Wearable Heart Sound Visualization System. *J Pers Med* 2022;12. <https://doi.org/10.3390/jpm12122011>.
- [151] Voin V, Oskouian RJ, Loukas M, Tubbs RS. Auscultation of the heart: The Basics with Anatomical Correlation. *Clin Anat* 2017;30:58–60. <https://doi.org/10.1002/ca.22780>.
- [152] Lee DH, Seo JH, Mittal R. Quantifying the Effect of Body Habitus on Cardiac Auscultation Via Computational Hemoacoustics. *J Biomech Eng* 2023;145:1–8. <https://doi.org/10.1115/1.4055513>.
- [153] Lange RA, Katz J, McBride W, Moore DM, Hillis LD. Effects of supine and lateral positions on cardiac output and intracardiac pressures. *Am J Cardiol* 1988;62:330–3. [https://doi.org/10.1016/0002-9149\(88\)90240-8](https://doi.org/10.1016/0002-9149(88)90240-8).
- [154] Wang H, Gao X, Shi Y, Wu D, Li C, Wang W. Effects of trunk posture on cardiovascular and autonomic nervous systems: A pilot study. *Front Physiol* 2022;13:1–12. <https://doi.org/10.3389/fphys.2022.1009806>.
- [155] Fois M, Maule SV, Giudici M, Valente M, Ridolfi L, Scarsoglio S.

- Cardiovascular Response to Posture Changes: Multiscale Modeling and in vivo Validation During Head-Up Tilt. *Front Physiol* 2022;13:1–20. <https://doi.org/10.3389/fphys.2022.826989>.
- [156] Arnott PJ, Pfeiffer GW, Tavel ME. Spectral analysis of heart sounds: Relationships between some physical characteristics and frequency spectra of first and second heart sounds in normals and hypertensives. *J Biomed Eng* 1984;6:121–8. [https://doi.org/10.1016/0141-5425\(84\)90054-2](https://doi.org/10.1016/0141-5425(84)90054-2).
- [157] Walker HK, Hall WD, Hurst JW. *Clinical methods: the history, physical, and laboratory examinations*. Butterworth Publishers; 1990.
- [158] Fuedner M. *Microphones*. INC; 2020. <https://doi.org/10.1016/B978-0-12-817786-0.00048-7>.
- [159] Ramasamy S, Balan A. Wearable sensors for ECG measurement: a review. *Sens Rev* 2018;38:412–9. <https://doi.org/10.1108/SR-06-2017-0110>.
- [160] Fu Y, Zhao J, Dong Y, Wang X. Dry electrodes for human bioelectrical signal monitoring. *Sensors (Switzerland)* 2020;20:1–30. <https://doi.org/10.3390/s20133651>.
- [161] Pani D, Achilli A, Bonfiglio A. Survey on Textile Electrode Technologies for Electrocardiographic (ECG) Monitoring, from Metal Wires to Polymers. *Adv Mater Technol* 2018;3:1800008. <https://doi.org/10.1002/admt.201800008>.
- [162] Galli A, Montree RJH, Que S, Peri E, Vullings R. An Overview of the Sensors for Heart Rate Monitoring Used in Extramural Applications. *Sensors* 2022;22:1–29. <https://doi.org/10.3390/s22114035>.
- [163] Meziane N, Webster JG, Attari M, Nimunkar AJ. Dry electrodes for electrocardiography. *Physiol Meas* 2013;34. <https://doi.org/10.1088/0967-3334/34/9/R47>.
- [164] Gan Y, Vauche R, Pons JF, Rahajandraibe W. Dry Electrode Materials for Electrocardiographic Monitoring. 2018 25th IEEE Int Conf Electron Circuits Syst ICECS 2018 2019:645–6. <https://doi.org/10.1109/ICECS.2018.8617992>.
- [165] Bergey GE, Squires RD, Sipple WC. Electrocardiogram Recording with Pasteless Electrodes. *IEEE Trans Biomed Eng* 1971;BME-18:206–11. <https://doi.org/10.1109/TBME.1971.4502833>.
- [166] Joutsen AS, Kaappa ES, Karinsalo TJ, Vanhala J. Dry electrode sizes in

- recording ECG and heart rate in wearable applications 2018:735–6. <https://doi.org/10.1007/978-981-10-5122-7>.
- [167] Winter BB, Webster JG. Driven-Right-Leg Circuit Design 1983:62–6.
- [168] Giordano N, Knaflitz M. A novel method for measuring the timing of heart sound components through digital phonocardiography. *Sensors (Switzerland)* 2019;19:1–16. <https://doi.org/10.3390/s19081868>.
- [169] Thiyagaraja SR, Vempati J, Dantu R, Sarma T, Dantu S. Smart phone monitoring of second heart sound split. 2014 36th Annu Int Conf IEEE Eng Med Biol Soc EMBC 2014 2014:2181–4. <https://doi.org/10.1109/EMBC.2014.6944050>.
- [170] Debbal SM, Bereksi-Reguig F. Automatic measure of the split in the second cardiac sound by using the wavelet transform technique. *Comput Biol Med* 2007;37:269–76. <https://doi.org/10.1016/j.compbiomed.2006.01.005>.
- [171] Sang B, Wen H, Gupta P, Shokouhmand A, Khan S, Puma JA, et al. Detection of Normal and Paradoxical Splitting in Second Heart Sound (S2) using a Wearable Accelerometer Contact Microphone. *Proc IEEE Sensors* 2022;2022-October:5–8. <https://doi.org/10.1109/SENSORS52175.2022.9967056>.
- [172] Andreev VG, Gramovich V V., Krasikova M V., Korolkov AI, Vyborov ON, Danilov NM, et al. Time–Frequency Analysis of The Second Heart Sound to Assess Pulmonary Artery Pressure. *Acoust Phys* 2020;66:542–7. <https://doi.org/10.1134/S1063771020050012>.
- [173] Barma S, Chen BW, Man KL, Wang JF. Quantitative Measurement of Split of the Second Heart Sound (S2). *IEEE/ACM Trans Comput Biol Bioinforma* 2015;12:851–60. <https://doi.org/10.1109/TCBB.2014.2351804>.
- [174] Djebbari A, Bereksi-Reguig F. Detection of the valvular split within the second heart sound using the reassigned smoothed pseudo Wigner-Ville distribution. *Biomed Eng Online* 2013;12:1–21. <https://doi.org/10.1186/1475-925X-12-37>.
- [175] Yildirim I, Ansari R. A robust method to estimate time split in second heart sound using instantaneous frequency analysis. *Annu Int Conf IEEE Eng Med Biol - Proc* 2007:1855–8. <https://doi.org/10.1109/IEMBS.2007.4352676>.
- [176] Xu J, Durand LG, Pibarot P. Extraction of the aortic and pulmonary components of the second heart sound using a nonlinear transient chirp signal model. *IEEE Trans Biomed Eng* 2001;48:277–83.

- <https://doi.org/10.1109/10.914790>.
- [177] Muramatsu S, Takamatsu S, Itoh T. Separation of Aortic and Pulmonary Components from Second Heart Sounds without an Assumption of Statistical Independence. *Sensors Mater* 2022;34:2723–34. <https://doi.org/10.18494/SAM3738>.
- [178] Popov B, Sierra G, Durand LG, Xu J, Pibarot P, Agarwal R, et al. Automated extraction of aortic and pulmonary components of the second heart sound for the estimation of pulmonary artery pressure. *Annu Int Conf IEEE Eng Med Biol - Proc* 2004;26 II:921–4. <https://doi.org/10.1109/iembs.2004.1403310>.
- [179] Sæderup RG, Hoang P, Winther S, Bøttcher M, Struijk J, Schmidt S, et al. Estimation of the second heart sound split using windowed sinusoidal models. *Biomed Signal Process Control* 2018;44:229–36. <https://doi.org/10.1016/j.bspc.2018.04.006>.
- [180] Renna F, Coimbra M. Source Separation of the Second Heart Sound Using Gaussian Mixture Models. *2019 Comput Cardiol Conf* 2019;45:1–4. <https://doi.org/10.22489/cinc.2019.236>.
- [181] Tang H, Chen H, Li T. Discrimination of aortic and pulmonary components from the second heart sound using respiratory modulation and measurement of respiratory split. *Appl Sci* 2017;7:1–16. <https://doi.org/10.3390/app7070690>.
- [182] Renna F, Plumbley MD, Coimbra M. Source Separation of the Second Heart Sound via Alternating Optimization. *Comput Cardiol (2010)* 2021;2021-Sept:2021–4. <https://doi.org/10.23919/CinC53138.2021.9662814>.
- [183] Pan J, Tompkins WJ. A Real-Time QRS Detection Algorithm. *IEEE Trans Biomed Eng* 1985;BME-32:230–6. <https://doi.org/10.1109/TBME.1985.325532>.
- [184] Mubarak Q ul A, Akram MU, Shaukat A, Hussain F, Khawaja SG, Butt WH. Analysis of PCG signals using quality assessment and homomorphic filters for localization and classification of heart sounds. *Comput Methods Programs Biomed* 2018;164:143–57. <https://doi.org/10.1016/j.cmpb.2018.07.006>.
- [185] Liang H, Lukkarinen S, Hartimo I. Heart sound segmentation algorithm based on heart sound envelopogram. *Comput Cardiol* 1997;24:105–8. <https://doi.org/10.1109/cic.1997.647841>.
- [186] Saini M. Proposed Algorithm for Implementation of Shannon Energy

- Envelope for Heart Sound Analysis 2016;7109:15–9.
- [187] Larsen BS, Winther S, Bølttcher M, Nissen L, Struijk J, Schmidt SE. Correlations of first and second heart sounds with Age, Sex, and Body Mass Index. *Comput Cardiol* (2010) 2017;44:1–4. <https://doi.org/10.22489/CinC.2017.141-408>.
- [188] Li T, Tang H, Qiu T, Park Y. Best subsequence selection of heart sound recording based on degree of sound periodicity. *Electron Lett* 2011;47:841–3. <https://doi.org/10.1049/el.2011.1693>.
- [189] Kumar D, Carvalho P, Antunes M, Paiva RP, Henriques J. Noise detection during heart sound recording using periodicity signatures. *Physiol Meas* 2011;32:599–618. <https://doi.org/10.1088/0967-3334/32/5/008>.
- [190] Naseri H, Homaeinezhad MR. Computerized quality assessment of phonocardiogram signal measurement-acquisition parameters. *J Med Eng Technol* 2012;36:308–18. <https://doi.org/10.3109/03091902.2012.684832>.
- [191] Grzegorzczuk I, Solinski M, Leppek M, Perka A, Rosinski J, Rymko J, et al. PCG classification using a neural network approach. *Comput Cardiol* (2010) 2016;43:1129–32. <https://doi.org/10.22489/cinc.2016.323-252>.
- [192] Zabihi M, Rad AB, Kiranyaz S, Gabbouj M, Katsaggelos AK. Heart sound anomaly and quality detection using ensemble of neural networks without segmentation. *Comput Cardiol* (2010) 2016;43:613–6. <https://doi.org/10.22489/cinc.2016.180-213>.
- [193] Springer DB, Brennan T, Zuhlke LJ, Abdelrahman HY, Ntusi N, Clifford GD, et al. Signal quality classification of mobile phone-recorded phonocardiogram signals. *ICASSP, IEEE Int Conf Acoust Speech Signal Process - Proc* 2014;6:1335–9. <https://doi.org/10.1109/ICASSP.2014.6853814>.
- [194] Springer DB, Brennan T, Ntusi N, Abdelrahman HY, Zühlke LJ, Mayosi BM, et al. Automated signal quality assessment of mobile phone-recorded heart sound signals. *J Med Eng Technol* 2016;40:342–55. <https://doi.org/10.1080/03091902.2016.1213902>.
- [195] Chakraborty D, Bhattacharya S, Thakur A, Gosthipaty AR, Datta C. Feature Extraction and Classification of Phonocardiograms using Convolutional Neural Networks. *2020 IEEE Int Conf Converg Eng ICCE 2020 - Proc* 2020:275–9. <https://doi.org/10.1109/ICCE50343.2020.9290565>.
- [196] Shi K, Schellenberger S, Michler F, Steigleder T, Malessa A, Lurz F, et al.

- Automatic Signal Quality Index Determination of Radar-Recorded Heart Sound Signals Using Ensemble Classification. *IEEE Trans Biomed Eng* 2020;67:773–85. <https://doi.org/10.1109/TBME.2019.2921071>.
- [197] Grooby E, He J, Kiewsky J, Fattahi D, Zhou L, King A, et al. Neonatal Heart and Lung Sound Quality Assessment for Robust Heart and Breathing Rate Estimation for telehealth Applications. *IEEE J Biomed Heal Informatics* 2020;2194:1–12. <https://doi.org/10.1109/JBHI.2020.3047602>.
- [198] Giordano N, Rosati S, Knaflitz M. Automated assessment of the quality of phonocardiographic recordings through signal-to-noise ratio for home monitoring applications. *Sensors* 2021;21. <https://doi.org/10.3390/s21217246>.
- [199] Liu C, Springer D, Li Q, Moody B, Juan RA, Chorro FJ, et al. An open access database for the evaluation of heart sound algorithms. *Physiol Meas* 2016;37:2181–213. <https://doi.org/10.1088/0967-3334/37/12/2181>.
- [200] Giordano N, Knaflitz M. Single-subject analysis of the variability of the latency of heart sounds over 25-day period. *Convegno Naz Di Bioingegneria* 2020:119–22.
- [201] Rokach L, Maimon O. Clustering Methods. *Data Min. Knowl. Discov. Handb.*, Springer US; 2005, p. 321--352. https://doi.org/10.1007/0-387-25465-X_15.
- [202] Duda R, Hart P. Pattern classification. John Wiley & Sons; 2006.
- [203] Tsai WH, Sue SH. Unsupervised clustering of heart sound recordings for cardiac auscultation database indexing. *J Inf Sci Eng* 2014;30:1655–68. <https://doi.org/10.1688/JISE.2014.30.5.20>.
- [204] Yang X, Fu W, Wang Y, Ding J, Wei C. Heart sound clustering based on supervised kohonen network. *Appl Mech Mater* 2012;138–139:1115–20. <https://doi.org/10.4028/www.scientific.net/AMM.138-139.1115>.
- [205] Tseng YL, Ko PY, Jaw FS. Detection of the third and fourth heart sounds using Hilbert-Huang transform. *Biomed Eng Online* 2012;11:1–13. <https://doi.org/10.1186/1475-925X-11-8>.
- [206] Tang H, Li T, Qiu T, Park Y. Segmentation of heart sounds based on dynamic clustering. *Biomed Signal Process Control* 2012;7:509–16. <https://doi.org/10.1016/j.bspc.2011.09.002>.
- [207] Safara F, Doraisamy S, Azman A, Jantan A. Heart sounds clustering using a

- combination of temporal, spectral and geometric features. *Comput Cardiol* (2010) 2012;39:217–20.
- [208] Syed Z, Leeds D, Curtis D, Nesta F, Levine RA, Gutttag J. Acoustical Cardiac Signals. *IEEE Trans Biomed Eng* 2007;54:651–62.
- [209] Amit G, Gavriely N, Intrator N. Cluster analysis and classification of heart sounds. *Biomed Signal Process Control* 2009;4:26–36. <https://doi.org/10.1016/j.bspc.2008.07.003>.
- [210] Choi S, Jiang Z, Kim I, Park C. Cardiac Sound Characteristic Waveform with Data Clustering Technique 2007:1596–600.
- [211] Giordano N, Rosati S, Knaflitz M, Balestra G. Comparison of Hierarchical and Partitional Clustering in Multi-Source Phonocardiography. 2022 IEEE Int Symp Med Meas Appl MeMeA 2022 - Conf Proc 2022. <https://doi.org/10.1109/MeMeA54994.2022.9856547>.
- [212] Murtagh F, Contreras P. Algorithms for hierarchical clustering: An overview. *Wiley Interdiscip Rev Data Min Knowl Discov* 2012;2:86–97. <https://doi.org/10.1002/widm.53>.
- [213] Kaufman L, Rousseeuw PJ. Finding groups in data: an introduction to cluster analysis. John Wiley & Sons; 2009.
- [214] Belton V, Stewart T. Multiple Criteria Decision Analysis: an integrated approach. Springer Science & Business Media; 2002.
- [215] Tsoukiàs A. From decision theory to decision aiding methodology. *Eur J Oper Res* 2008;187:138–61. <https://doi.org/10.1016/j.ejor.2007.02.039>.
- [216] Figueira JR, Greco S, Roy B, Słowiński R. An Overview of ELECTRE Methods and their Recent Extensions. *J Multi-Criteria Decis Anal* 2013;20:61–85. <https://doi.org/10.1002/mcda.1482>.
- [217] Gongora-Salazar P, Rocks S, Fahr P, Rivero-Arias O, Tsiachristas A. The Use of Multicriteria Decision Analysis to Support Decision Making in Healthcare: An Updated Systematic Literature Review. *Value Heal* 2022;26:780–90. <https://doi.org/10.1016/j.jval.2022.11.007>.
- [218] Giordano "Noemi, Balestra G, Ghislieri M, Knaflitz M, Rosati" S. Automatic Identification of the Best Auscultation Area for the Estimation of the Time of Closure of Heart Valves through Multi-Source Phonocardiography. 2022 *Comput Cardiol Conf* 2022;49:1–4. <https://doi.org/10.22489/cinc.2022.088>.

- [219] Figueira J, Roy B. Determining the weights of criteria in the ELECTRE type methods with a revised Simos' procedure. *Eur J Oper Res* 2002;139:317–26. [https://doi.org/10.1016/S0377-2217\(01\)00370-8](https://doi.org/10.1016/S0377-2217(01)00370-8).
- [220] Qian Y min, Weng C, Chang X kai, Wang S, Yu D. Past review, current progress, and challenges ahead on the cocktail party problem. *Front Inf Technol Electron Eng* 2018;19:40–63. <https://doi.org/10.1631/FITEE.1700814>.
- [221] Nigam V, Priemer R. A dynamic method to estimate the time split between the A2 and P2 components of the S2 heart sound. *Physiol Meas* 2006;27:553–67. <https://doi.org/10.1088/0967-3334/27/7/001>.
- [222] Geethu RS, Krishnakumar M, Pramod K V., George SN. Source Separation of Heartbeat Sounds for Effective E-Auscultation. *J Inst Eng Ser B* 2016;97:69–75. <https://doi.org/10.1007/s40031-015-0186-4>.
- [223] Tong Z, Qader IA, Abu-Amara F. Heart Sound Separation Using Fast Independent Component Analysis. *Proc - 2015 Int Conf Dev ESystms Eng DeSE 2015* 2016:3–6. <https://doi.org/10.1109/DeSE.2015.38>.
- [224] Yang X, Pan J, Zhang Z, Fang L, Ji Y, Fan Y, et al. Analyzing the phonocardiogram of ASD-patient based on independent component analysis. *Int Conf Signal Process Proceedings, ICSP 2006*;1:6–9. <https://doi.org/10.1109/ICOSP.2006.344449>.
- [225] Giordano N, Knaflitz M. A Method for the Estimation of the Timing of Heart Sound Components Through Blind Source Separation in Multi-Source Phonocardiography. *IEEE Med. Meas. Appl. MeMeA 2020 - Conf. Proc.*, 2020. <https://doi.org/10.1109/MeMeA49120.2020.9137315>.
- [226] Xu J, Durand LG, Pibarot P. A new, simple, and accurate method for non-invasive estimation of pulmonary arterial pressure. *Heart* 2002;88:76–80. <https://doi.org/10.1136/heart.88.1.76>.
- [227] Tarry D, Powell M. Hypoxic pulmonary vasoconstriction. *BJA Educ* 2017;17:208–13. <https://doi.org/10.1093/bjaed/mkw076>.
- [228] Kregenow DA, Swenson ER. The lung and carbon dioxide : implications for permissive and therapeutic hypercapnia 2002:6–11. <https://doi.org/10.1183/09031936.02.00400802>.
- [229] Czernichow S, Renuy A, Rives-Lange C, Carette C, Airagnes G, Wiernik E, et al. Evolution of the prevalence of obesity in the adult population in France, 2013–2016: the Constances study. *Sci Rep* 2021;11:2013–6.

<https://doi.org/10.1038/s41598-021-93432-0>.

- [230] Vukanovic-Criley JM, Criley S, Warde CM, Boker JR, Guevara-Matheus L, Churchill WH, et al. Competency in Cardiac Examination Skills in Medical Students, Trainees, Physicians, and Faculty. *Arch Intern Med* 2006;166:610–6. <https://doi.org/10.1001/archinte.166.6.610>.